Real-time HV OHTL sag monitoring system based on Power Line Carrier signal behaviour

Wernich de Villiers

December 2005

Supervisor: Professor J.H. Cloete

Dissertation presented for the Degree of Doctor of Philosophy in Electrical Engineering at the University of Stellenbosch.

UNIVERSITEIT·STELLENBOSCH·UNIVERSITY

jou kennisvennoot·your knowledge partner

Declaration

I, the undersigned, hereby declare that the work contained in this dissertation is my own original work and that I have not previously in its entirety or in part submitted it at any university for a degree.

W de Villiers: _____

Date: _____

Summary

A new method of measuring the change in the average height of phase conductors above the ground plane of High Voltage (HV) Overhead Transmission Lines (OHTLs) was discovered in 1999, at Stellenbosch University. The new method, called Power Line Carrier–Sag (PLC-SAG), measures average overhead conductor height variations in real-time by exploiting high frequency signal propagation characteristics on the existing PLC system.

The novelty of the newly discovered PLC-SAG system naturally led to a thorough testing and investigation of the technique. This thesis explains the methodology used to produce unique experimental data, which has indeed proven that the average height of an OHTL can be tracked very accurately via the PLC-SAG technique for continuous periods.

As the experiments on two live 400 kV transmission lines in South Africa were being undertaken, a serious concern regarding the new technique arose. Major HV Station impedance variations seemed to influence the PLC system and clouded the interpretation of PLC-SAG recorded data. Such HV Station impedance variations typically occur only a few times per year.

A new Power Line Carrier Impedance (PLC-IMP) technique was then discovered, by which these changes could be monitored. No structural changes to the existing PLC-SAG system were required for this technique. This was seen as a major breakthrough in the presented study. Not only does this newly established technique make it possible to develop a stable PLC-SAG system, but also a potential real-time condition monitor application. Its use on PLC systems has been proposed to the main Power Utility in South Africa.

Opsomming

‘n Nuwe metode om die veranderinge in die gemiddelde hoogte bo grondvlak van die fasegeleiers van hoogspanning oorhoofse transmissielyne te meet is in 1999 by die Universiteit Stellenbosch ontdek. Hierdie uitvindsel staan bekend as die Power Line Carrier Sag (PLC-SAG) metode en dit meet veranderinge in oorhoofse geleier hoogte intyds deur benutting van die eienskappe van hoëfrekwensie sein voortplanting op die bestaande hoogspanning oorhoofse transmissielyne.

Die nuutuitgevonde PLC-SAG stelsel is natuurlik onderworpe aan deeglike toetsing en ondersoek van die tegniek. Hierdie proefskrif verduidelik die metodiek gebruik, waarvolgens unieke eksperimentele data verkry is wat bewys dat die gemiddelde hoogte van ‘n hoogspannings oorhoofse transmissielyn inderdaad baie akkuraat gemeet kan word, oor lang ononderbroke tydperke.

Tydens die eksperimente en ondersoek op twee lewendige 400kV transmissielyne in Suid Afrika is ‘n ernstige probleem gewaar wat die vatbaarheid van die tegniek in gevaar gestel het. Groot verskille in impedansie by hoogspanningstasies beïnvloed die hoogspanning oorhoofse transmissielyn stelsel en versteur die interpretasie van die PLC-SAG data wat opgeneem is. Sulke groot impedansie verskille kom tipies slegs ’n paar keer per jaar by ‘n stasie voor.

‘n Tweede nuwe tegniek, die sogenoemde Powerline Carrier Impedance (PLC-IMP) tegniek, is toe ontdek wat hierdie veranderinge kan monitor en dus die intydse hoogspannings oorhoofse transmissielyne impedansie metings moontlik maak. Geen struktuurverandering van die bestaande PLC-SAG stelsel is nodig vir gebruik van die PLC-IMP tegniek nie, en dit word beskou as ‘n groot deurbraak in die studie wat hier aangebied word.

Hierdie tegniek het teweeggebring nie slegs ‘n stabiele PLC-SAG stelsel nie, maar ‘n potensiële intydse monitor vir gebruik op hoogspannings oorhoofse transmissielyn stelsels. Die tegniek is voorgestel aan die grootste kragvoorsiener in Suid Afrika vir gebruik op hul stelsels.

Acknowledgements

Soli Deo Gloria

I am greatly indebted to my supervisor, Prof JH Cloete, for sharing his expertise, for giving guidance and for his ever-present optimism. I would also especially like to thank Eskom/TAP, particularly Mr A Burger and Mr DC Smith as well as Prof LM Wedepohl. Furthermore I would also like to thank the following people for their support and help:

From Eskom Transmission Telecommunications: Frans Venter, Piet Lubbe, Drikus de Wet, Errol Wright, Tony Pereira and Ashley van der Poel.

From Trans Africa Projects TAP/Eskom: Johan Cloete, Dr D Muftic, Pieter Pretorius, Nick Kruger, Hein Pienaar and Sarel Cloete.

From Stellenbosch University: Prof HC Reader, Dr RG Urban and Anita van der Spuy.

The financial assistance of the Department of Labour (DoL), Harry Crossley Scholarship and TAP/Eskom towards this research is hereby acknowledged. Opinions expressed and conclusions arrived at, are those of the author and are not necessarily to be attributed to the DoL.

Finally, special thanks to my wife, family and friends for their continuous support.

Table of contents

List of Figures

List of photographs

Chapter 1

Introduction and background

1.1 Introduction

The Power Line Carrier-Sag (PLC-SAG) system measures average overhead conductor height variations in real-time. Knowledge of the average conductor height variation can be used in Ampacity control systems.

The PLC-SAG system is fundamentally based on the theory of Natural Modes in Multi Conductor Transmission Lines [1]. The Monitoring PLC-SAG tones are uniquely coupled via the existing Power Line Carrier (PLC) infrastructure to the overhead transmission line. These coupled PLC-SAG tones distribute into natural modes, which propagate to the remote station. At the remote station these tones are decoupled and analysed to extract information about the physical height of the overhead conductor.

The reader is further introduced to the research topic in Subsection 1.2, which gives more background about Ampacity, available Ampacity systems, history of the PLC-SAG system and comparisons between PLC-SAG and other Ampacity systems.

The author has done a theoretical study [2] on the PLC-SAG technique, with accompanying preliminary experiments. The goals of the research presented (Subsection 1.3) in this thesis, were to thoroughly test the PLC-SAG technique and to further develop the system for implementation.

These goals were achieved by designing and implementing PLC-SAG monitoring systems onto two Over Head Transmission Lines (OHTLs). The PLC-SAG system measures the average height of the OHTL conductor, and in order to test the system a unique direct OHTL conductor height experiment was planned and executed. From these experiments the performance of the PLC-SAG system was quantified and areas of concern were identified.

Subsection 1.4 describes the thesis layout and highlights the new key contributions.

1.2 Ampacity systems

1.2.1 Introduction and literature review of Ampacity systems

The ampacity of an OHTL is defined as the maximum current flowing in an OHTL that is consistent with safe operation [3].

Regulation [4] requires that transmission lines must be operated safely at all times. The primary limitation on OHTL ampacity is maintaining the design sags of the line under all operating conditions.

Environmental factors (for example temperature, wind and solar radiation) contribute, together with the current in the conductor, to the extent to which the transmission line conductor sags. Conservative Electrical Power companies would assume worst-case values for the environmental factors in order to determine the maximum current that will ensure safe operation. This rating is called the static ampacity rating [3] of the OHTL. In the competitive markets and fast growing demand which some Electrical Power companies are experiencing, it is not practical to operate the power grid on static ampacity ratings. By

monitoring the environmental effects, or the real-time sag of the transmission line, the current rating of the OHTL could be increased without compromising safety. This is called dynamic ampacity rating [3]. For example: On a cold winter day the ampacity rating will be higher than on a hot summer day, because more current can be transferred on a cold day before exceeding the sag limitations.

For Real Time dynamic line rating systems, continuous monitoring of OHTL conditions is needed. Parameters that could be monitored are current, weather related factors, conductor temperature and conductor sag. There are a number of operational systems, which each use either one or a combination of the mentioned parameters. For example:

- Real Time Thermal Rating System (RTTRS) [5] – Monitors the temperature of the conductor
- ATLAS [6] – Monitors the ambient temperature
- Tension Monitoring System [7] – Monitors the sag via a strain gauge
- LINEAMPS [8] – Monitors weather conditions
- RETMOS [9] - Monitors weather conditions and sag conditions

Due to the nature of dynamic ampacity control, most of the above systems incorporate some statistical techniques to compute the final estimated ampacity of the transmission line.

The author, in collaboration with Prof JH Cloete [2][9][10], invented a unique ampacity system called PLC-SAG. The history of the PLC-SAG initiative and subsequent developments will be discussed in the following section. This is done in order to put the research presented in this document in perspective.

1.2.2 History of the fundamental idea on which PLC-SAG is based

Prof LM Wedepohl (Emeritus Dean of Applied Science University of British Columbia) visited the University of Stellenbosch (US) during early 1999. Prof Wedepohl had discussions with Prof JH Cloete of the Department of Electrical & Electronic Engineering, sharing his experience on PLCs and a phenomenon called modal cancellation [1]. The phenomenon was a function of the average conductor height.

Later that same year the author suggested the investigation of ampacity and the possibility of monitoring sag through high frequency effects to Prof Cloete. The discussion with Prof Cloete then guided the author to thoroughly investigate the modal cancellation phenomenon which had been mentioned by Prof Wedepohl.

The author completed an undergraduate project in 1999 [10] with the initial simulations, which confirmed that there is an expected relationship between PLC-signal attenuation and OHTL conductor sag.

The main goal of the author's MScEng degree (2000-2001) [2] was to develop a detailed simulation program to explore the concept in more detail.

Due to extremely favourable results from the simulations and preliminary single tone experiments, it was decided to continue the work on PLC-SAG Ampacity.

The research presented in this thesis was the detailed continuation of the author's MScEng investigations with more emphasis on thorough evaluation and practical system development.

Mr A Burger, a senior engineer at TAP (Trans Africa Project, a subdivision of ESKOM enterprises) and his colleagues supported the continuation of the work with financial and manpower resources during 2003 and 2004. Mr DC Smith, a Corporate Consultant at Eskom transmission, and the Transmission Technology Department – Power Telecommunication section which also supported the work with equipment and skilled human resources from the start of the research. The research was integrated with TAP's existing RETMOS [9] ampacity research program.

1.2.3 Comparison of PLC-SAG with other Ampacity techniques

The ampacity systems mentioned in Subsection 1.2.1 only estimate the sectional sag in general, therefore numerous sensors are needed to monitor the average sag of the whole transmission line. The unique technical advantage of the PLC-SAG ampacity system is the fact that the average value of the sag is measured. This is a key distinguishing feature of the method.

The PLC-SAG system also has a significant competitive advantage in terms of installation and operating costs. The aforementioned methods use one or more loggers, which are installed on towers, conductors or near the OHTL. The logged information must then be transmitted from the loggers, which are typically in the middle of the transmission line, to the relevant substation. Due to the fact that these loggers are likely to be in a rural area, data transmission and maintenance becomes problematic, unreliable and very expensive.

By contrast, the PLC-SAG system uses mainly the existing PLC infrastructure. The Power Utility presently maintains this system. Only a few hardware components have to be added to the existing PLC system to

realize ampacity control; no data have to be transmitted to the substation and due to the sheltered environment of the substation, minimal maintenance is required.

The main disadvantage of the PLC-SAG system is that it depends on the existence of a PLC system. PLC systems are commonly installed on high voltage transmission line networks and less commonly on the distribution networks.

The fact that the average sag is measured can also be seen as a disadvantage if the PLC-SAG ampacity system is the only ampacity technique installed onto a particular OHTL. However, on a relatively short OHTL a stand-alone PLC-SAG system may be adequate in many cases.

The fact that the average sag is measured by use of a completely different measuring technique is an advantage, especially when the technique is used with a complementary technique which measures only the sectional sag, which makes it possible to utilize different technologies on the same transmission line and thus increase the confidence levels of the system operators.

The RETMOS system [9] is ESKOM's (main electrical power company in South Africa) Real Time ampacity monitoring system. The PLC-SAG technique is already recognized as one of the three fundamental techniques in the RETMOS system, which is still under development.

1.3 The goals of this study

The goals of the study were to thoroughly test the PLC-SAG technique and to further develop the technique for implementation in the field.

1.3.1 PLC-SAG system development

In [2] a preliminary single tone test was used to evaluate the performance of the PLC-SAG system. The PLC-SAG system in this study was further developed to a multi-tone monitoring system.

During the execution of the evaluation process (Section 1.3.2) the PLC-SAG system developed. The two biggest developments were:

1- Calibration procedure for the PLC-SAG system via direct height measurement
2- PLC Impedance monitoring (PLC-IMP) [12] technique, which is essential for the reliable operation of the PLC-SAG system.

These developments will be explained in more detail.

1.3.2 PLC-SAG evaluation

The methodology used in [2] to test the single tone PLC-SAG system was compared against another Ampacity system, which uses current and weather factors to compute the Ampacity on one OHTL. The problem with this other technique is that the Ampacity system is based on assumptions and does not produce an exact value. It is therefore very difficult to compare the systems, because the exact values are unknown.

After some consideration it was decided to perform a dedicated unique experiment to test the performance of the PLC-SAG system. Due to the fact that the PLC-SAG system measures the average height of the whole transmission line, it was decided to measure the height of the OHTL conductor directly at three well-spaced locations. By comparing the results

from the direct height experiment with the results from the PLC-SAG system the level of accuracy of the system could be determined.

These experiments were done on two live 400 kV OHTLs in South Africa.

1.4 Thesis layout and original contributions

1.4.1 Chapter 2: The Power Line Carrier (PLC) system

The existing PLC system is introduced by describing its functionality in the power network and the working of the individual PLC components. The characteristics of PLC signal propagation can be understood by studying the theory of Natural Modes [1]; therefore the theory of Natural Modes is discussed, with emphasis on the physical interpretation of the theory.

The Stellenbosch PLC signal attenuation simulation program, which is based on the theory of natural modes, will be described. The average ground resistance at PLC frequencies can be singled out as one of the parameters that is very difficult to determine for accurate simulations. A new simulation and measurement methodology was utilised to estimate the average ground resistance more accurately.

Original contribution

- A methodology to estimate the average ground resistance between substations or PLC-SAG installation points at PLC frequencies.

1.4.2 Chapter 3: Simulation of the two case studies and frequency allocation of the PLC-SAG monitoring tones

Two case studies were identified on which the PLC-SAG systems were evaluated. The first case study was on a short, un-transposed OHTL in the Western Cape (Koeberg-Acacia 400 kV line 1) and the second installation was on a long transposed OHTL in Mpumalanga (Kriel-Tutuka 400 kV line 1).

A simulation methodology was created for PLC-SAG systems. The methodology comprises:

i) Computing the default simulation condition for the specific OHTL
ii) Simulation of different coupling configurations and
iii) Exploring the best coupling configuration in detail.

Frequencies were allocated for the PLC-SAG monitoring tones. A general criterion for PLC-SAG frequency allocations was established.

Original contributions

- A simulation methodology for PLC-SAG systems
- A methodology for selecting the PLC-SAG monitoring frequencies.

1.4.3 Chapter 4: PLC-SAG experimental installations

Two unique multi-tone experimental systems were designed and installed on the Eskom transmission network in South Africa. The PLC-SAG experimental installations on the two OHTLs were very similar, and only the details of the latest installation are discussed.

Original contribution

- Development of a multi tone stand-alone PLC-SAG system

1.4.4 Chapter 5: Direct height measurements

A first of its kind, direct height measurement experiment was designed, planned and executed, which proved the predicted relationship between average sag and PLC-SAG tone attenuation.

The average height of the whole transmission line was estimated via the three direct height measurements repeatedly taken simultaneously over two days with a laser measurement device.

Original contribution

- Direct height measurement procedure that estimates the average conductor height of the whole transmission line. The procedure forms part of the calibration process.

1.4.5 Chapter 6: PLC-SAG system evaluation and calibration

The results of simulations (Chapter 3), the stand-alone PLC-SAG installations (Chapter 4) and direct height measurements (Chapter 5) are compared in this chapter. The results compare very well and therefore prove that the PLC-SAG system is indeed practical and has the necessary accuracy.

The calibration process of the PLC-SAG system is described.

Original contributions

- Comprehensive, convincing experimental evidence that the technique works as claimed: i.e. that there is extremely strong correlation between the monitored signal levels and conductor sag.
- A calibration methodology to calibrate the PLC-SAG attenuation to indicate the height of the transmission line.

1.4.6 Chapter 7: PLC-SAG impedance monitoring system

While studying the performance of the stand-alone experiments, a step-like phenomenon was noted in the received level of the PLC-SAG monitoring tones. It was determined that this effect was due to the station impedance variation, which resulted in the noted step attenuation. This effect resulted in a PLC-SAG calibration problem.

A new method was therefore invented, which can monitor the PLC system impedance in real time. This breakthrough in the research not only potentially solves the mentioned calibration problem, but may also lead to spin-off products in the future.

Original contribution

- It was determined that the correlation between attenuation measured by the PLC-SAG system and the conductor sag, may be unacceptably reduced due to sudden changes in the impedance presented to the PLC system by the terminating station buses.
- A new technique was invented to monitor the station impedance in real time. The technique is seen as a breakthrough in the study, as it potentially solves the PLC-SAG calibration problem.

1.4.7 Chapter 8: Conclusions

The main findings of the research are discussed and future research activity is proposed. The newly integrated PLC-SAG and PLC-IMP system is proposed as a feasible Ampacity system.

1.5 Conclusion

From the literature review, it was found that Ampacity based systems are not a new concept and that a large number of such systems had been designed and installed due to the increasing worldwide demand for electrical energy.

A new ampacity system called 'PLC-SAG' with distinguishing properties was discovered in 1999.

The aim of the presented research was to further develop the PLC-SAG method and to thoroughly evaluate the technique. The thesis layout is discussed in this chapter and the key original contributions are highlighted.

References:

[1] **Wedepohl, L.M.**, The Theory of Natural Modes in Multi-Conductor Transmission Systems*, unpublished lecture notes, Westbank, British Columbia, Canada, 10 January 1999.*

[2] **De Villiers, W.**, *Prediction and measurement of Power Line Carrier signal attenuation and fluctuation*, MScEng Thesis, University of Stellenbosch, November 2001.

[3] **A.K. Deb,** Powerline Ampacity System - Theory, modelling and Applications, CRC Press LLC, London, 2000.

[4] **South Africa, Occupational Health and Safety Act and Regulations,** Data 9000, No 85, Section 15 – Clearances of power lines, Published by Data Dynamics, 1993.

[5] **M.W. Davis**, "A new thermal rating approach: The real time thermal rating system for strategic overhead conductor transmission lines PART 1", Transact. on Power Apparatus and Systems, Vol. PAS-96, No. 3, May/June 1977, pp. 803 – 809.

[6] **W.J. Steeley, B. L. Norris, A.K. Deb**, "Ambient temperature corrected dynamic transmission line rating at two PG&E locations", Transact. on Power Delivery, Vol. 6, No. 3, July 1991, pp. 1234 – 1242.

[7] **T.O. Seppa**, "Accurate ampacity determination: temperature – sag model for operational real time ratings", IEEE Transact. on Power Delivery, Vol. 10, No. 3, July 1994, pp. 1460 – 1470.

[8] **A.K. Deb**, "Object-Oriented Expert System Estimates Line Ampacity ", IEEE Computer Applications in Power, Vol. 8, No 3, 1995, pp. 30 – 35.

[9] **A. Burger**, The RETMOS system, unpublished internal ESKOM handbook for the RETMOS system, Midrand, Johannesburg, South Africa, 2004.

[10] **W. de Villiers**, *An investigation into overhead feeder ampacity control*, BEng project report, Department of Electrical & Electronic Engineering at University of Stellenbosch, 5 November 1999.

[11] **SOUTH AFRICAN PATENT 2002/4105:** Ampacity and sag monitoring of Overhead power transmission lines.

[12] **SOUTH AFRICAN PROVISIONAL PATENT 2004/8736:** Impedance monitoring system and method.

Chapter 2

The Power Line Carrier (PLC) system

2.1 Introduction

The Power Line Carrier (PLC) system will be discussed in Section 2.2 as background, followed by the associated theory of Natural Modes (Section 2.3). Emphasis is put on the practical understanding of the eigenvectors and eigenvalues of a transmission line.

The PLC-SAG simulation model will be described in Section 2.4. The average ground resistance between two stations is not commonly known at PLC frequencies. To cover all possibilities, a wide spread of simulations are usually performed with different ground resistivity values. A new contribution is made in Section 2.5 to the overall PLC simulation methodology in order to improve the estimation of the average ground resistivity between two stations.

2.2 Overview of the PLC system [1]

A Power Line Carrier (PLC) link operates by transmitting signals in the frequency range 50-500 kHz over a High Voltage (HV) Overhead Transmission Line (OHTL), while the line is still carrying the normal 50 Hz current. The PLC signal is not dependent on the 50 Hz current, therefore the PLC system remains operational even if the line is out of commission, providing there are no working earths on the line. Through

the use of the coupling equipment the PLC signal can be injected and retrieved from the OHTL. PLC transmission constitutes the basic system of communication of many power utility companies. PLC is typically used for transmitting data, speech and protection signals.

Six main components of the PLC system as shown in Figure 2.1 will now be described: Overhead Transmission Line (OHTL), Line Trap (LT), Coupling Capacitor (CC) or Capacitor Voltage Transformer (CVT), Line Matching Equipment (LME), Phase Combiner (also known as a Hybrid and is only used for coupling to more than one phase) and the Carrier (a transceiver).

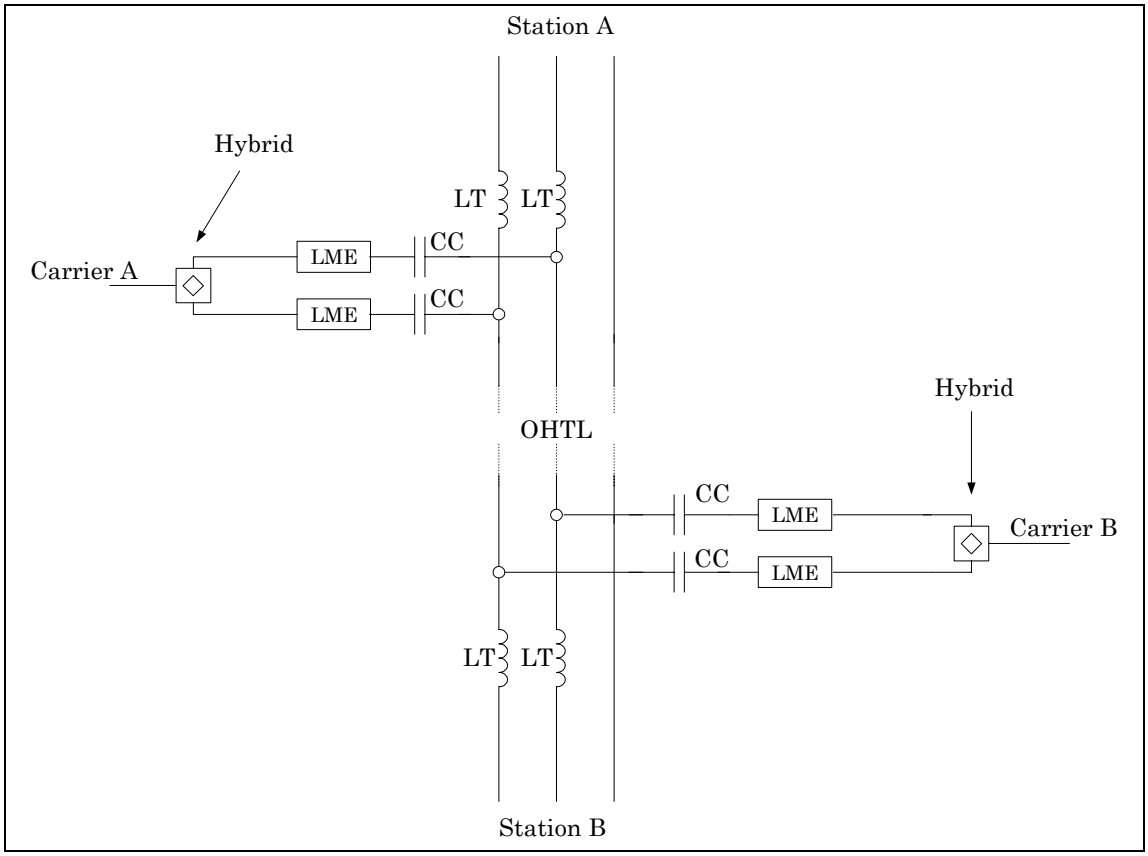

Figure 2.1 Simplified PLC system between two Stations

The LT, CC (or CVT) and the LME are located in the High Voltage (HV) yard of the Station, as indicated by Photograph 2.1. The Carrier and Hybrid are normally located in the relay room.

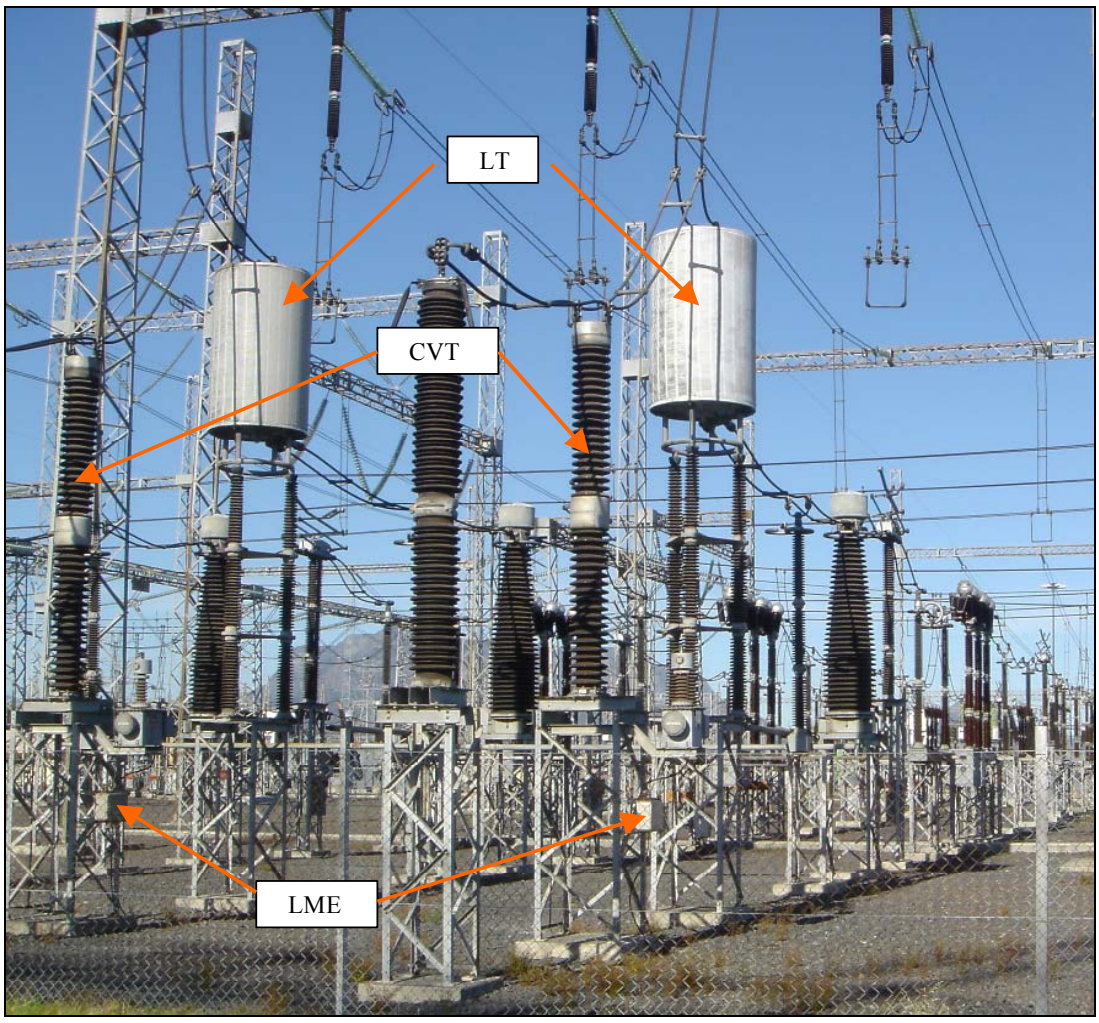

Photograph 2.1 Line Trap (LT), Capacitor Voltage Transformer (CVT) and Line Matching Equipment (LME)

The main function of each of the six mentioned components in the framework of the PLC system will now be briefly discussed.

The carrier is the main communication device. All the various types of signal, for example speech and teleprotection, are transmitted by the local carrier and received at the remote carrier.

The power of the communication signal from the carrier is then split by the hybrid at the local station to drive the two phases and excite the desired OHTL natural modes of propagation. The received power at the remote station is then re-combined via the remote hybrid (Figure 2.1).

The Line Matching Equipment (LME) matches the impedance of the PLC system to the impedance of the High Voltage OHTL network together with the other coupling equipment, for maximum signal power transfer to the OHTL phases.

The low voltage, high frequency carrier signal is then coupled onto the high voltage OHTL via a Coupling Capacitor (CC) or Capacitive Voltage Transformer (CVT).

The Line Trap (LT) is a filtering device and is located on the OHTL on the station side of the CC connection to the OHTL. The LT prevents the coupled signal from being shorted out in the Station by providing high impedance in the PLC frequency band. Therefore, the PLC signal energy is channelled to propagate along the OHTL towards the remote station.

Finally, the OHTL acts like a wave-guide for PLC signals. This can be seen as part of the transmission path where the PLC signals are guided in their propagation. The physical dimensions of the line are thus crucial, because they influence the propagation properties of the coupled signal. This effect is exploited in this thesis to measure the average height of the conductors.

The theory of Natural Modes [2], describes OHTL PLC signal propagation characteristics and will be discussed in the following section.

2.3 The theory of natural modes [2][3][4][5]

The attenuation of the PLC signal can be subdivided into two components:

i) The attenuation due to the transmission line, including the effect of ground resistivity.

ii) The attenuation due to the coupling system.

The latter is relatively simple to compute and is well described, but the former is more complex. Wedepohl's "Theory of Natural Modes" [2][3][4][5] will be introduced to calculate the line attenuation. This is done by first explaining the eigenvectors and eigenvalues of an OHTL.

2.3.1 Voltage propagation matrix

The impedance and admittance matrixes of a specific OHTL are a function of the OHTL geometry, the specific conductors configuration used and the ground resistance. The product of the impedance matrix and the admittance matrix defines the voltage propagation matrix squared (P), as shown in Equation 2.1.

$$[\mathrm{P}] = ZY \qquad 2.1$$

The voltage propagation matrix squared can also be expressed (Equation 2.2) by its eigenvalues (λ) and eigenvectors (E_v).

$$P = E_v \lambda E_v^{-1} \qquad 2.2$$

A better understanding of this powerful formulation can be gained if it is interpreted as follows. The eigenvectors contain the direction of the vectors or the fixed "physical part" of the solution. The eigenvalues describe the variable or dynamic characteristics of the solution.

A physical interpretation of the eigenvalues (λ) and eigenvectors (E_v) will be given in terms of the natural modes in a multi-conductor system.

2.3.2 Eigenvectors of the voltage propagation matrix

The modal matrix of the system relates to the eigenvectors and is fixed because of physical geometry. The modes are called the natural modes of a multi-conductor system. For a flat configuration transmission line the 'Clarke vector' (Equation 2.3) is a very good approximation of the natural modes.

$$E_v \approx Clarke\_Vector = \begin{bmatrix} \frac{1}{2} & 1 & 1 \\ -1 & 0 & 1 \\ \frac{1}{2} & -1 & 1 \end{bmatrix} \qquad 2.3$$

The three Columns of Equation 2.3 describes the natural modes for a flat OHTL configuration, which are known respectively as the "least attenuated mode" (Column 1), "the differential mode" (Column 2) and the "most attenuated mode" (Column 3).

Any voltage matrix coupled to the OHTL will be distributed in its natural modes and will propagate along the OHTL. The distribution of a coupled voltage matrix in its natural modes will now be further explained by an example.

Example: Standard differential coupling between the Outer phase and the Centre phase at the local station to the Outer phase and Centre phase at the remote station.

Figure 2.2 represents a transmission line with three phases, which describes a coupling configuration in general terms for a flat transmission line configuration.

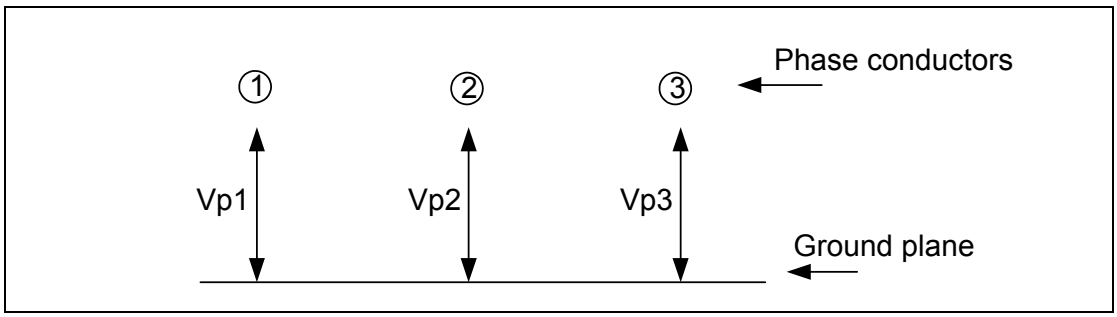

Figure 2.2 Coupling notation (Vp1,Vp2,Vp3) on a flat configuration OHTL

The standard coupling configuration (called differential coupling) of a PLC system which has coupling equipment on two phases (Figure 2.1), can be expressed as (Equation 2.4):

$$V_a = \begin{bmatrix} V_{p1} \\ V_{p2} \\ V_{p3} \end{bmatrix} = \begin{bmatrix} -1 \\ 1 \\ 0 \end{bmatrix} \qquad 2.4$$

Where

$V_a =$ Voltage vector at location or station a

$V_{pN} =$ Voltage on phase N

Let Subscript 'a' be the position along the transmission line where the local station is, 'b' the position along the transmission line where the remote station is and 'x' any position along the OHTL.

The coupled voltage matrix will distribute in its natural modes as follows (Equation 2.5):

$$V_a = A_1 \begin{bmatrix} E_v(1,1) \\ E_v(2,1) \\ E_v(3,1) \end{bmatrix} + A_2 \begin{bmatrix} E_v(1,2) \\ E_v(2,2) \\ E_v(3,2) \end{bmatrix} + A_3 \begin{bmatrix} E_v(1,3) \\ E_v(2,3) \\ E_v(3,3) \end{bmatrix} \quad 2.5$$

By substituting Equation 2.3 and Equation 2.4 in Equation 2.5, the distribution vector '*A*' can be computed to be:

$$\begin{aligned} A_1 &= -0.5 \\ A_2 &= -0.5 \\ A_3 &= 0 \end{aligned} \quad 2.6$$

To conclude the example, Figure 2.3 shows a graphical representation of the modal distribution for a signal which was coupled differentially onto the Outer phase (P1) and Centre phase (P2).

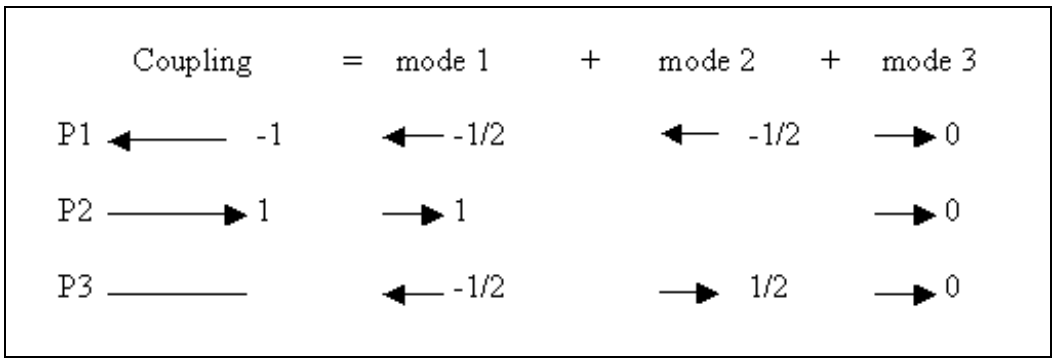

Figure 2.3 Graphical representation of the Modal distribution for a differentially coupled signal

The total power coupled onto the OHTL via a specific coupling configuration will distribute between the abovementioned natural modes. The standard coupling configuration (Equation 2.4) will excite 75% of mode 1 (least attenuated mode) 25% of mode 2 and 0% of mode 3 on a flat OHTL as in Figure 2.2.

The attenuation characteristics of the modes will be described in the following section.

2.3.3 Eigenvalues of the voltage propagation matrix

The eigenvalues describe the dynamic characteristics of the different natural modes (eigenvectors) of the system. Thus, the attenuation and phase retardation of modes are associated with the eigenvalues.

The attenuation constant (α) and phase velocity (β) can be computed by taking the square root of the eigenvalue of mode i (Equation 2.7):

$$\sqrt{\lambda_i} = \alpha_i + j\beta_i = \gamma_i \qquad 2.7$$

The typical modal attenuations for a flat transmission line are plotted in Figure 2.4 to provide the reader with a framework for comparison of the different attenuation constants.

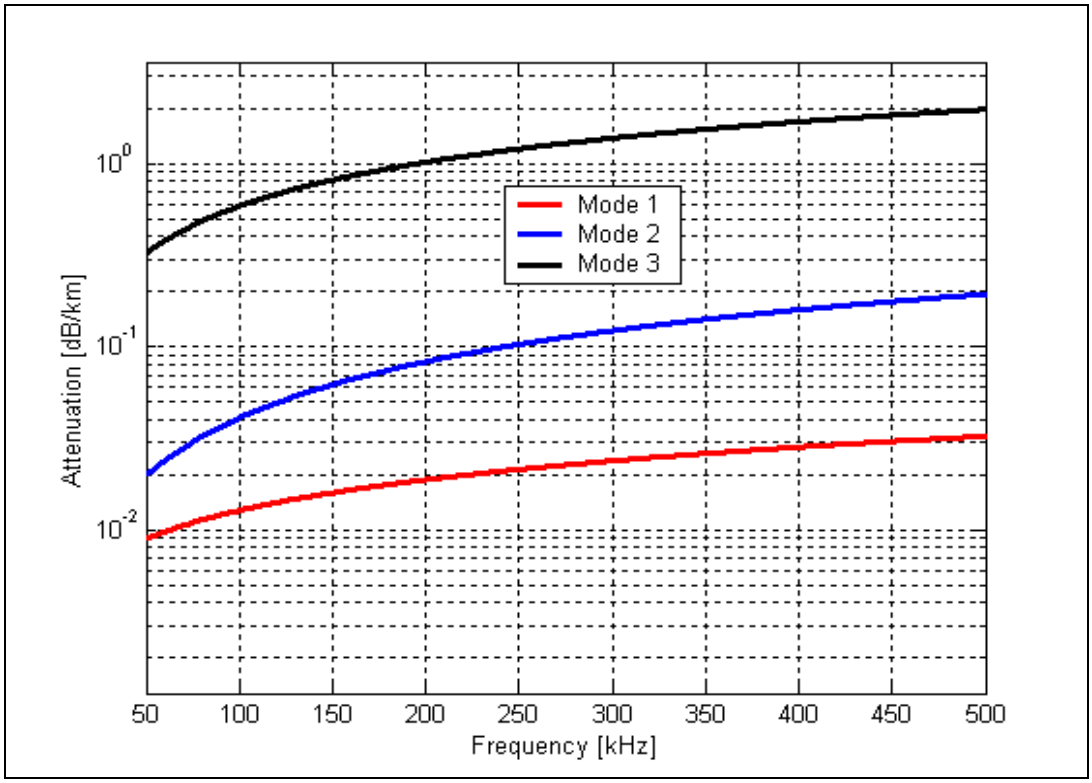

Figure 2.4 Typical attenuation constants for the different modes. (9 m-phase spacing, 19.6 m conductor height, twin dinosaur phase conductor type and 300 ohm-meter ground resistance)

From Figure 2.4, it is clear why mode 1 is called the least attenuated mode and mode 3 the most attenuated mode or the ground mode.

2.3.4 Multi-Conductor Wave equation

The voltage propagation matrix squared was defined in Equation 2.2. The voltage propagation matrix can now be defined as (Equation 2.8)

$$\Gamma = E_v \gamma E_v^{-1} \qquad 2.8$$

where

$\gamma = \sqrt{\lambda}$ (Modal propagation constant)

The multi-Conductor wave equation can now be expressed as (Equation 2.9)

$$V_x = e^{(-\Gamma x)}V_a + e^{(\Gamma x)}V_b \qquad 2.9$$

where V_x is the voltage on the transmission line $x = 0$ away, V_a is the coupled voltage at $x = 0$ and V_b is the reflected wave. For simplicity let us assume a very long transmission line, which will result in $V_b \approx 0$. Equation 2.9 can then be expressed by its natural modes or eigenvalues as [3]

$$V_x = E_v e^{-\gamma x} E_v^{-1} V_a \qquad 2.10$$

Finally, for a flat transmission line, we can express Equation 2.10 by using the Clarks vectors (Equation 2.3) and the Voltage distribution as:

$$V_x = \begin{bmatrix} -\frac{1}{2} & 1 & 1 \\ 1 & 0 & 1 \\ -\frac{1}{2} & -1 & 1 \end{bmatrix} \begin{bmatrix} e^{-\gamma_1 x} & 0 & 0 \\ 0 & e^{-\gamma_2 x} & 0 \\ 0 & 0 & e^{-\gamma_3 x} \end{bmatrix} \left(\begin{bmatrix} -\frac{1}{2} & 1 & 1 \\ 1 & 0 & 1 \\ -\frac{1}{2} & -1 & 1 \end{bmatrix} \right)^{-1} \begin{bmatrix} V_{p1} \\ V_{p2} \\ V_{p3} \end{bmatrix} \qquad 2.11$$

Choose a voltage V_a to be equal to column 'k' of the eigenvoltage (E_v) vector matrix, thus coupling a particular natural mode. Then Equation 2.11 simplifies to Equation 2.12:

$$V_x = e^{-\gamma_k x} E_{v(k)} \qquad 2.12$$

This is a significant result and proves that the sending end voltage $E_{v(k)}$ retains its distribution, which is being multiplied by a scalar factor $e^{-\gamma_{(k)} x}$. This is similar to a transmission line with one propagation constant. It is for this reason that the various γ are known as modal propagation

constants, the columns of $E_{v(k)}$ are known as the modal voltage vectors and the theory is known as the "theory of natural modes" [2].

In the next section the simulation program that was developed at Stellenbosch University will be discussed, with the emphasis on developing a model. The specific definitions of the model that relate the average height of an OHTL conductor to the signal propagation characteristics of PLC-SAG tones will also be discussed in detail.

2.4 PLC – SAG model development

The goal of the PLC-SAG simulation model is twofold.

The first goal of the model is to perform a sensitivity analysis. It is important to assess the phenomenon of PLC-SAG tone variation due to conductor height variations and whether these variations are prominent enough on the relevant OHTL.

The model is not accurate enough to relate the measured attenuation directly to conductor height, due to inaccuracies of input parameters (such as ground resistivity), assumptions and station impedance uncertainties. An on-site calibration procedure, which will be discussed in Chapter 6, was developed to achieve the needed accuracy.

The second goal was to identify possible faulty components on the existing operational PLC system. On short lines components, such as the tuning unit of a line trap, could be faulty without influencing the system. This is because the losses in the system are not significant due to the shortness of the transmission line. The system could thus be fully functional under normal conditions without the power utility being aware of the faulty component (or components) except under line fault conditions.

The high-level simulation model for the PLC-SAG system is shown in Figure 2.5. The computational part [2][3][4][5] of the model was implemented and verified by the author, and formed part of his MScEng project [7]. The model was further developed in this current study by adding a database interface and by making the specific parameters easily changeable. These additions were necessary to simplify the process of PLC-SAG installations.

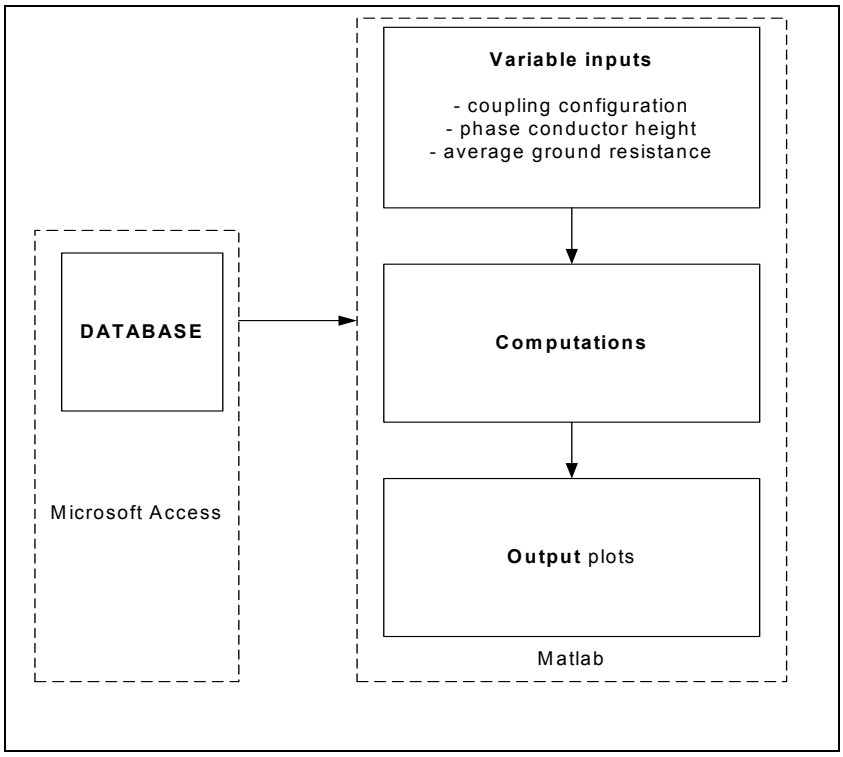

Figure 2.5 High level representation of the simulation model

The block diagram in Figure 2.5 will be discussed in more detail in the following sections. It will also be applied to two case studies in the following chapter. Some frequently used terminology in the model will first be explained.

2.4.1 Model definitions

The relevant terminology describing the geometry of an Overhead Transmission Line's (OHTL) is important, seen in the context of this study. Although some of the terms may seem obvious, the author feels that it is important to define those terms, which will be frequently used in this thesis. As indicated in Figure 2.6 the following terms can be defined as:

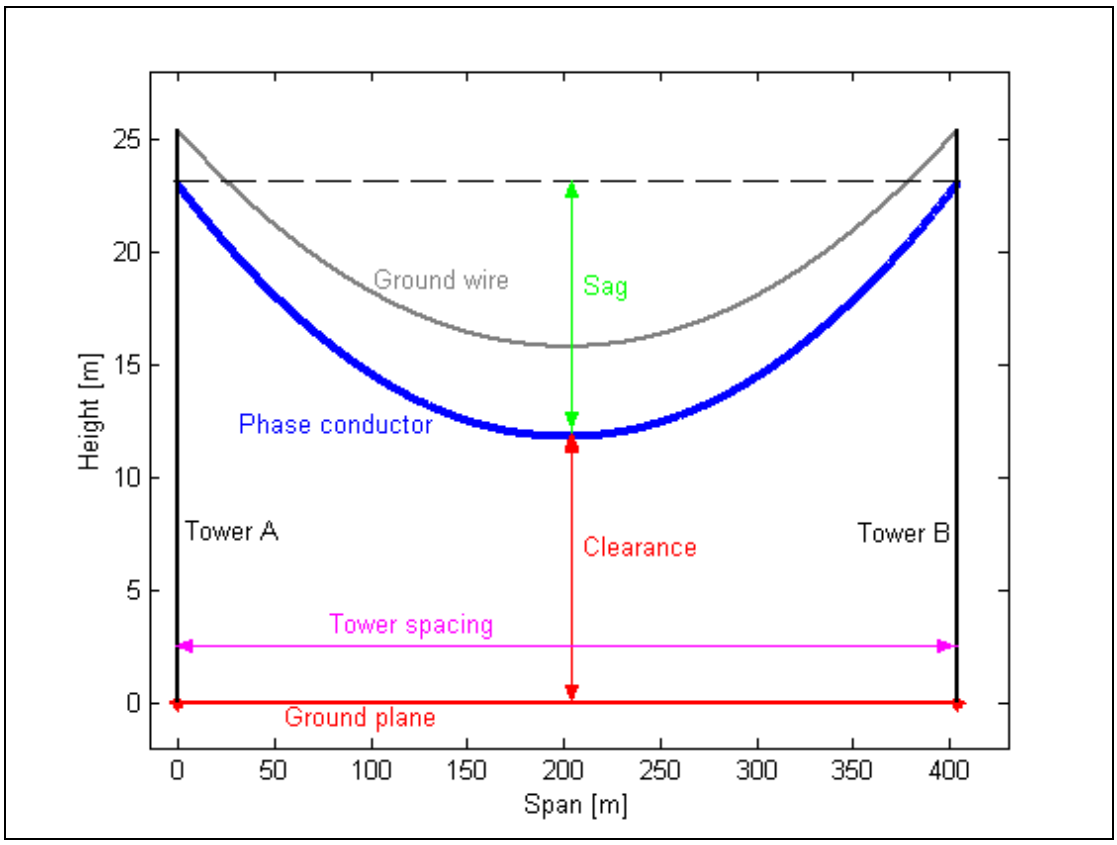

Figure 2.6 Defining an Overhead Transmission Line (OHTL) span between two adjacent towers for a special case (equal attachment height and horizontal ground)

Sag: The maximum vertical difference between a conductor and a straight line between supports. The sag of the phase conductor is shown in Figure 2.6

Clearance: The minimum distance between the phase conductor and the ground plane. According to the Occupational Health and Safety (OHS) Act [1] in South Africa the minimum clearance of a 400 kV OHTL is 8.1m. The minimum distance between the ground plane and the phase conductor is not necessarily in the middle of the span.

Equivalent Span: Because the PLC-SAG method measures the average height variation of the whole transmission line, the transmission line will be described in terms of its equivalent span. The equivalent span is the span that represents all the individual spans of the transmission line. Some textbooks also refer to it as the ruling span. In the context of this thesis the two parameters that describe the equivalent span are the tower spacing and the attachment height.

The tower spacing of the equivalent span (L_e) is defined as [9]:

$$L_e = \sqrt{\frac{L_1^3 + L_2^3 + L_3^3 + \ldots + L_n^3}{L_1 + L_2 + L_3 + \ldots + L_n}} \qquad 2.13$$

where

L_e = equivalent span
L_i = tower spacing of each individual span
n = total number of spans

The attachment heights of the phase conductor and the ground wire, for the equivalent span, can be computed by analysing the tower dimensions.

Average conductor height: One of the assumptions of the model is that it uses the average conductor height to do simulations. The average conductor height is, as the name indicates, the average height of the conductor of the equivalent span above a flat horizontal ground plane.

$$h_{ave} = \frac{1}{L_e}\int_0^{L_e} h(x)dx \qquad (2.14)$$

where

Le = Length of the span as shown in Figure 2.7.

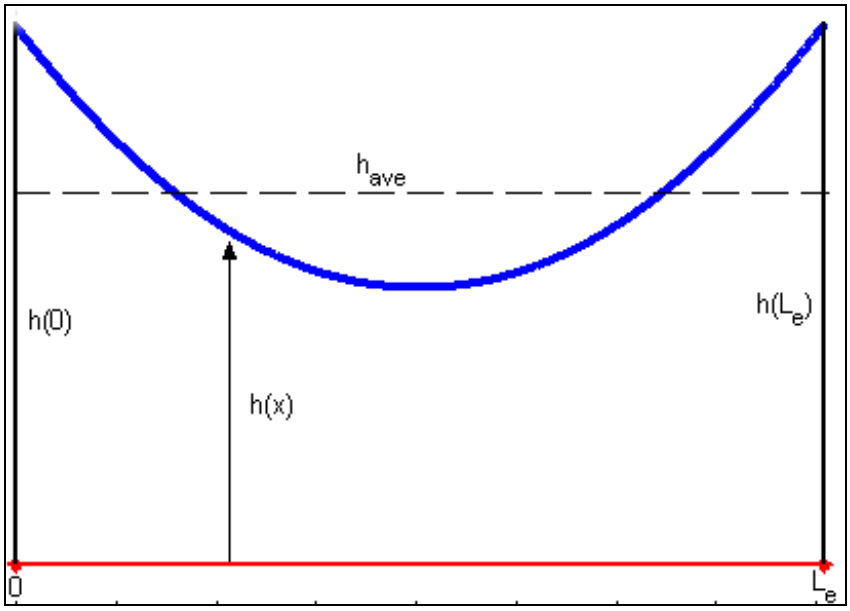

Figure 2.7 Average conductor height

The average ground wire height is defined in a similar manner.

Default Simulation Condition: The average heights of the Equivalent span of the phase conductor and ground wire, when tensioned to have a catenary constant [9] of 2100 m and 1800 m respectively. These values of the catenary constant are adopted from an in-house rule[1] in ESKOM (the main power utility in South Africa).

[1] Personal communication with Mr P Marais, Head Structural Engineer of TAP (Trans-Africa Projects, a division of ESKOM) dated 2004/07/13

With the definitions cleared, the high level model will be discussed in two sections; the database (Left-hand side of Figure 2.5) and the Matlab simulations options (middle of Figure 2.5)

2.4.2 Database (Microsoft Access, left-hand side of Figure 2.5)

Figure 2.8 shows the Microsoft database input format, which is used to store the information used by the model. The database is linked to a conductor database, which contains all the parameters for the listed conductor types. The user can therefore select the relevant phase and ground conductors quickly and easily.

The geometrical positions Y in Figure 2.8 (the average heights of the phase conductor and ground wire) are defined in the framework of the Equivalent Span and Default Simulation Condition as discussed. The other transmission line related parameters are quite easily understood in the Microsoft Access input data form.

The PLC system is described in its most elementary state (lower right-hand corner in Figure 2.8). This information is not compulsory, as provision is made in the main Matlab simulation program to include losses associated with coaxial cable and more detailed PLC information. These losses are normally fixed. The transmission line losses are more important because they contain information needed to monitor the height variation of the OHTL conductor.

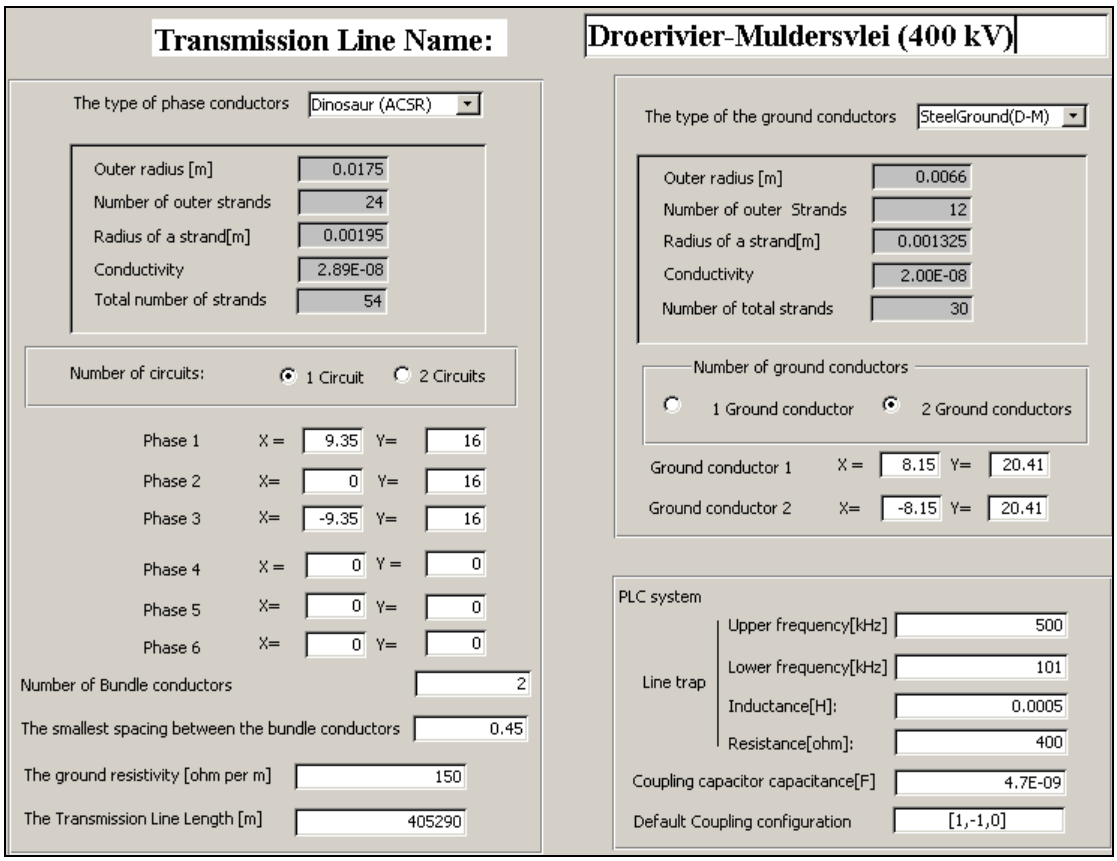

Figure 2.8 Input parameters for the Microsoft Database

In general, the information input format shown in Figure 2.8 is adequate to describe most of the attributes of the transmission line needed for simulations. If the transmission line is transposed or the conductor type is changed, the same format can be completed registering the changes. The Matlab simulation program will combine the user specified database form (if more than one format is needed to describe the system) to simulate the whole transmission line.

2.4.3 Input/Output ranges and (Matlab) GUI

There are three main inputs that can be easily varied in the new PLC-SAG model.

- Coupling configurations

- Conductor height variation
- Ground resistivity

The output of the simulation is the required attenuation for PLC frequencies (50 kHz – 500 kHz). This is represented in a graphical format (simulations are performed in the following chapter) but is also saved in a matrix format for extended data processing.

The three input parameters will now be discussed, followed by the Graphical User Interface (GUI).

Different coupling configurations

The standard coupling configuration (called differential coupling) for a PLC system, which has coupling equipment on two phases, can be expressed as Equation 2.4.

If the transmission line is not transposed then the same coupling configuration is used to decouple signals from the transmission line. This coupling configuration relates to the specific installation shown in Figure 2.1. Coupling equipment is installed on two of the phases. The hybrid in Figure 2.1 not only divides the PLC signal into two paths, but also introduces a 180-degree phase shift, thus the sign difference between Vp1 and Vp2. The decoupling vector at the remote station would be the same as the coupling vector shown in Equation 2.4.

From Section 2.3 it is evident that different propagation modes are energized in different ratios, dependent on the initial coupling configuration. The standard differential coupling configuration is chosen to ensure robust operation for the PLC system. However, the attenuation variation of a PLC signal coupled in this way is not very sensitive for determining the height of the conductor as may be expected.

Phase conductor height variation

For each coupling configuration the average phase conductor height must be varied to identify the "best" coupling configuration, with "best" meaning the coupling arrangement which is most sensitive to average height variations.

From previous simulations [7] it is evident that height variation of the ground wire does not influence the PLC-SAG tone attenuation significantly for a flat transmission line configuration. Therefore the height of the earth wire can be kept fixed during the simulations.

Ground resistance

The quality of the simulations is limited to the accuracy of the input parameters. One of the most difficult input parameters to estimate is the average ground resistance. A new technique to improve the estimation of the ground resistance has been developed and will be discussed in a subsequent section.

GUI (Graphical User Interface)

All the above-mentioned parameters can easily be changed for exploration simulations. A snapshot of the simulation program output is shown in Figure 2.9. Before the additions were made it was very cumbersome and time consuming to perform a range of simulations (Chapter 3). The GUI was also developed in Matlab. As mentioned before, the results of the simulation program are also saved in a file. This feature was very useful in a research environment. For example, the simulation data in the file can be incorporated together with measured values to perform comparisons in another program.

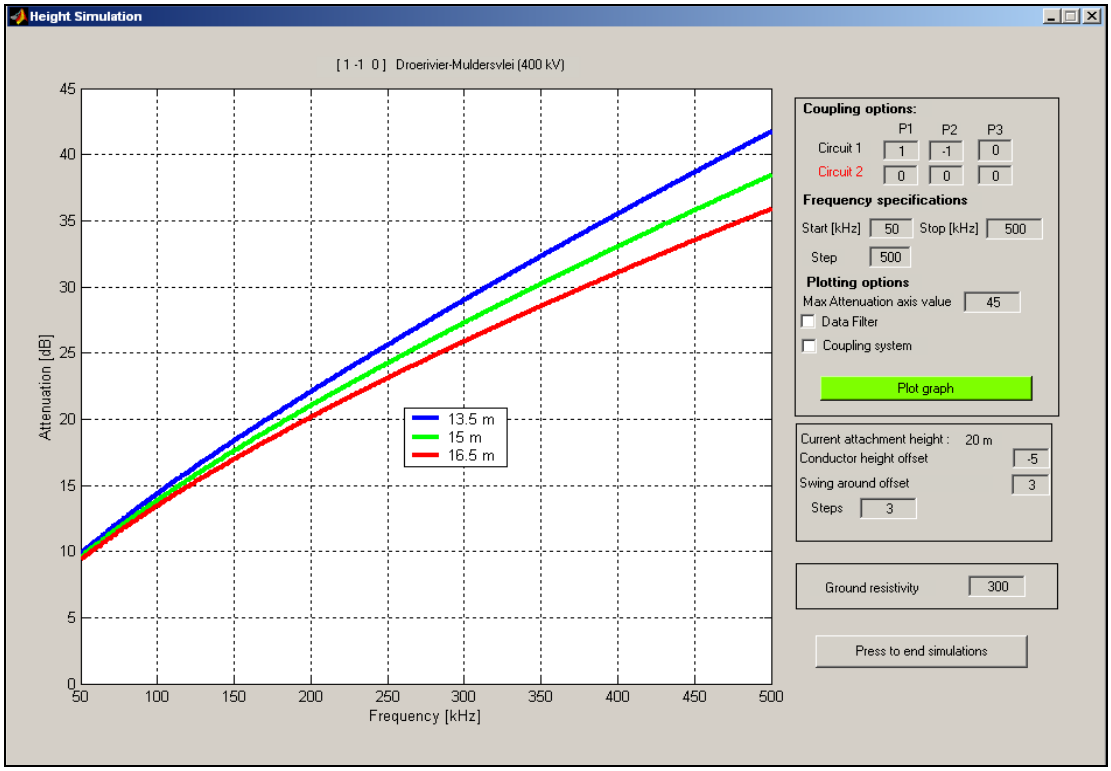

Figure 2.9 Snapshot of the PLC-SAG simulation program output display

2.5 New average ground resistance estimation technique for PLC signal attenuation simulations

2.5.1 Introduction

As mentioned before, the ground resistance is a difficult parameter to determine accurately. The theory behind the new technique for estimation of the average ground resistivity will be discussed in Subsection 2.5.2. The theory will then be applied on the Kriel-Tutuka PLC-link (Subsection 2.5.3) to estimate a ground resistivity value. The only other two attempts, using different techniques, to measure the average ground resistance over a large distance in South Africa was published by Vice in 1954 [9] and by ESKOM [11] in 1987. The technique that Vice used will be discussed in

Subsection 2.5.4. The results of the two different techniques, Vice's technique and the new technique, will also be compared.

2.5.2 Theory

The average error over the measurement frequency range between a measured and a simulated attenuation for a specific coupled signal is defined in, Equation 2.15:

$$SimError_a = \frac{\sum_{n=1}^{N}\left(MeasAtt_a(f_n) - SimAtt_a(f_n)\right)}{N} \qquad 2.15$$

where

$MeasAtt_a$ = The measured attenuation at different frequency points (f_n) for a specific coupling configuration "a".

$SimAtt_a$ = Simulated attenuation at the same frequency points (f_n) as the measured attenuation for a specific coupling configuration "a".

The biggest uncertainty in the Simulation model is the average ground resistance. Although the OHTL conductor height is also generally not known exactly when the measurements are performed, data on the OHTL and knowledge of the system made it possible to compute the average height under normal conditions. Therefore, a fair estimation of the OHTL average height can be made. It is common practice to do simulations from 10 Ω-m up to 1000 Ω-m ground resistivity because of the great uncertainty which exists.

Equation 2.16 can be rewritten as a function of ground resistivity:

$$SimError_a(GR(m)) = \frac{\sum_{n=1}^{N}\left(MeasAtt_a(f_n) - SimAtt_a(f_n, GR(m))\right)}{N} \qquad 2.16$$

where:

$GR(m) = 10,...,1000\ \Omega - \text{m for m} = 1,....,\text{M}$

A range of simulations can then be performed to search for the ground resistivity (GR), which will minimize the error in Equation 2.16. Assuming that there are no faults in the PLC system, the danger in this approach is that changing the ground resistivity (GR) could mask another error in the simulation program. To minimize this possibility, the same process can be repeated for the different coupling configurations that produce a unique attenuation response. This means that propagation modes are energized in different ratios, which would result in different attenuations (Section 2.3). Let us assume five different unique coupling configurations ("a" to "e"), which can be practically measured on a PLC system. The best ground resistivity can then be identified as the ground resistivity, which produces the minimum error between the measurements and the simulations:

$$C(m) = \sum_{coupling=a}^{e} SimError_{coupling}(GR(m))$$

$$\text{then} \qquad 2.17$$

$$GR_{best} = GR(m) \text{ such that C(m)} \leq \text{C(n) where n} \neq \text{m}$$

The following section will test this technique in practice as it was applied on the Kriel-Tutuka OHTL.

2.5.3 Simulations and average ground resistivity for the PLC link between Kriel power station and Tutuka power station.

The technique comprises 4 steps:

1) Identify the practical number of unique coupling configurations for the specific PLC system
2) Simulate the relevant attenuation for a spectrum of ground resistivity values (More details about the line and simulation process is given in Chapter 3)

3) Measure all the associated attenuation graphs
4) Compare the measurements and simulations to identify the best ground resistivity.

The applied steps will now be discussed:

Step 1: Identify unique coupling configurations:

Figure 2.10 outlines the Kriel-Tutuka link, which is subdivided into seven sections. A detailed description of the Kriel-Tutuka tranmission line is given in Chapter 3 and Appendix A. It can be noted that PLC coupling equipment is installed on the blue and white phases and that the transmission line is transposed once.

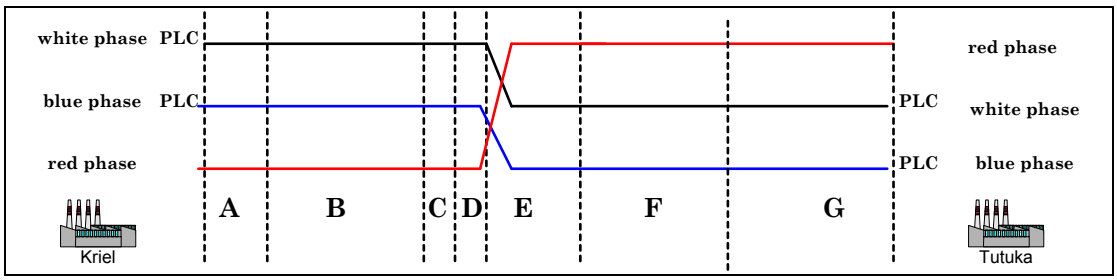

Figure 2.10 Kriel-Tutuka OHTL

Studying the specific line in the light of the theory identified five easily measurable unique coupling configurations:

1) Standard insertion loss (combined)

$$V_{Kriel} = \begin{pmatrix} 1 \\ -1 \\ 0 \end{pmatrix}, V_{Tutuka} = \begin{pmatrix} 0 \\ 1 \\ -1 \end{pmatrix} \qquad 2.18$$

2) Outer phase to Outer phase

$$V_{Kriel} = \begin{pmatrix} 1 \\ 0 \\ 0 \end{pmatrix}, V_{Tutuka} = \begin{pmatrix} 0 \\ 0 \\ 1 \end{pmatrix} \quad 2.19$$

3) Centre phase to Centre phase

$$V_{Kriel} = \begin{pmatrix} 0 \\ 1 \\ 0 \end{pmatrix}, V_{Tutuka} = \begin{pmatrix} 0 \\ 1 \\ 0 \end{pmatrix} \quad 2.20$$

4) Centre phase to Outer phase

$$V_{Kriel} = \begin{pmatrix} 0 \\ 1 \\ 0 \end{pmatrix}, V_{Tutuka} = \begin{pmatrix} 0 \\ 0 \\ 1 \end{pmatrix} \quad 2.21$$

5) Outer phase to Centre phase

$$V_{Kriel} = \begin{pmatrix} 1 \\ 0 \\ 0 \end{pmatrix}, V_{Tutuka} = \begin{pmatrix} 0 \\ 1 \\ 0 \end{pmatrix} \quad 2.22$$

Step 2: Simulations

With all the detailed information of the OHTL (Appendix A) the signal attenuation can be simulated for the different coupling configurations and the spectrum of ground resistances. The average height of the conductor is calculated for the default simulation condition as explained in Section 2.4.1. Figure 2.11 shows the attenuation for the five different coupling configurations for a ground resistance of 50 $\Omega - m$.

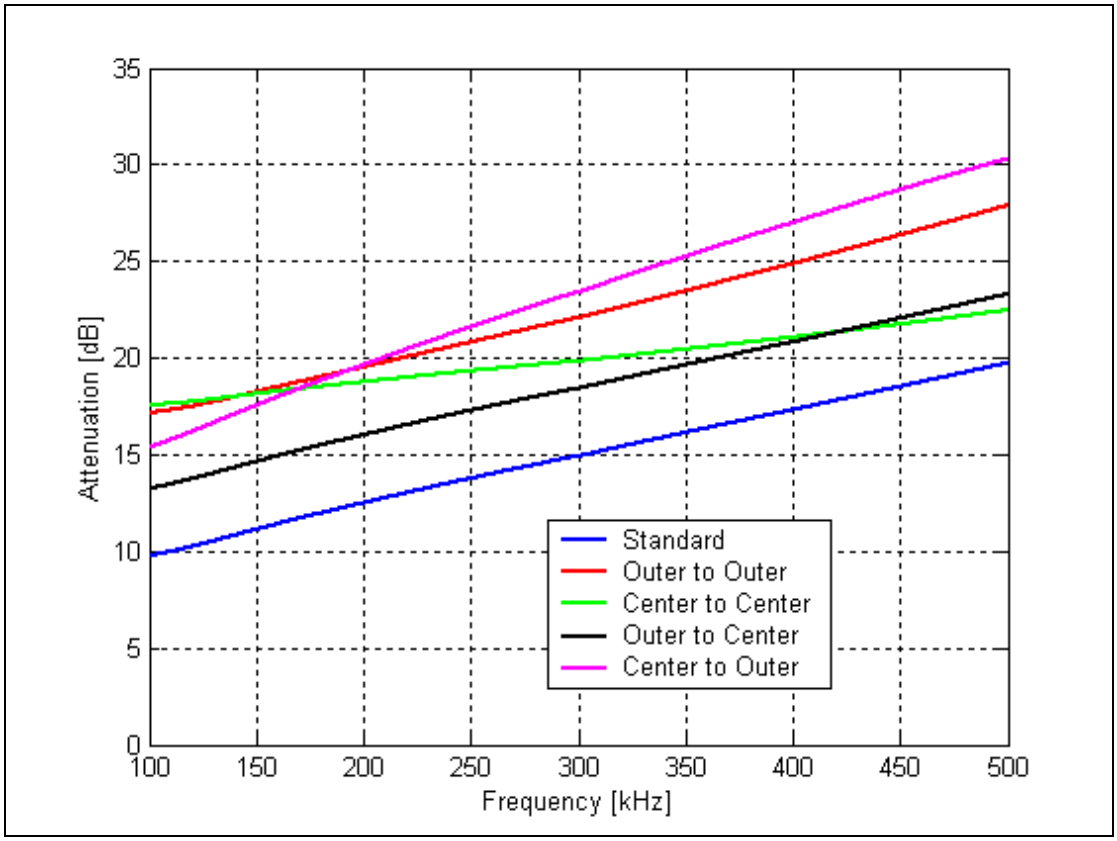

Figure 2.11 Different simulated attenuations on the Kriel-Tutuka transmission line for 50 ohm-meter ground resistance

Step 3: Measurements

The difficulty in performing the attenuation measurement is to get the necessary permission and the skilled PLC technicians to do the measurement. The operational PLC carrier system needs to be deactivated for these specific measurements, but no outage is required. Where the PLC system could not be switched off, a reduced number of coupling configurations had to be considered.

Two PLC technicians are needed, one on each side, with a transmit/receive instrument. Standard insertion loss or attenuation measurements can be performed for the different coupling configurations, transmitting from one station and measuring at the remote station. The estimated time per measurement is roughly 30 min per coupling configuration.

The measurement results of all the different coupling configurations will be presented in the following section.

Step 4: Comparison and identification of the best ground resistance value

This step is started by doing simulations from 10 Ω-m to 1000 Ω-m.

Table 2.1 shows the errors as defined in Equation 2.17. The least average error (Equation 2.18) and the associated resistance are presented in bold type in the table. Only resistivity values from 50 Ω−m to 100 Ω−m are shown in Table 2.1.

Table 2.1 Ground resistivity errors for differed coupling configurations

Ground resistivity (ohm-metre)	50	60	70	**80**	90	100
Standard configuration	2.199641	1.920269	1.681415	1.474366	1.321156	1.152466
Outer phase to Outer phase	1.515003	1.443741	1.400946	1.488166	1.68877	2.041184
Centre phase to Centre phase	4.038622	4.032896	4.033539	4.038473	4.046318	4.226727
Outer phase to Centre phase	2.367882	2.094308	1.860129	1.662253	1.492668	1.249736
Centre phase to Outer phase	1.654107	1.576879	1.633531	1.820509	2.167821	2.760368
Average error	2.355051	2.213619	2.121912	**2.096754**	2.143347	2.286096

The measurement and the simulations are shown in Figure 2.12 to Figure 2.16 for an average ground resistivity of 80 Ω−m.

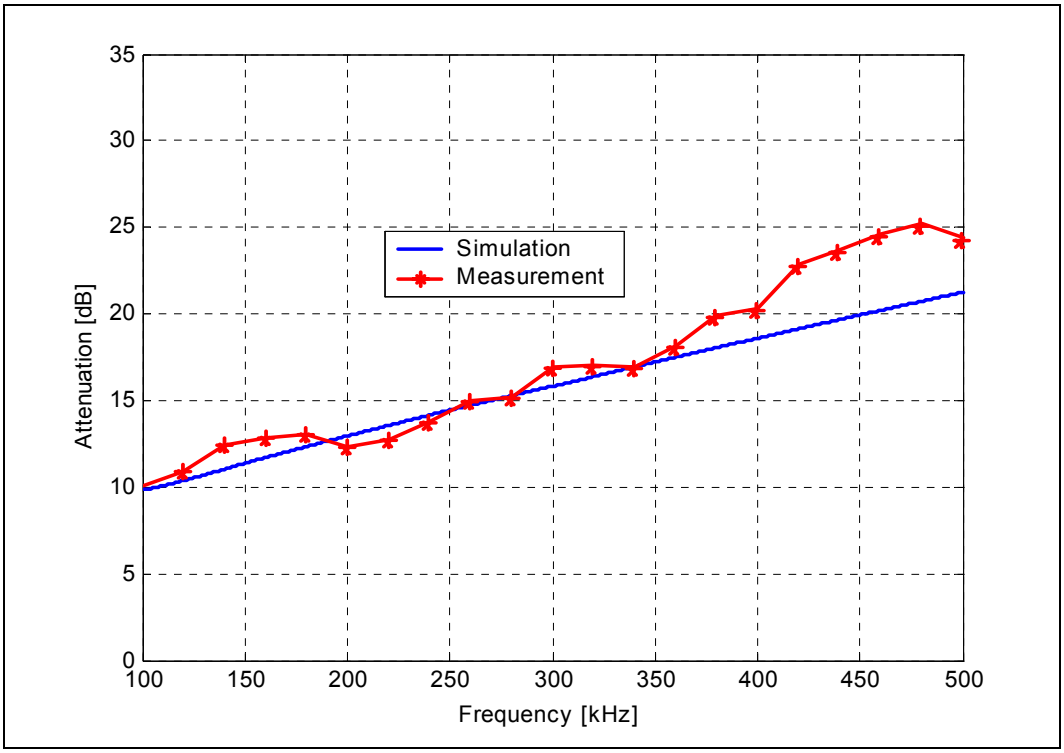

Figure 2.12 Measurement and simulation for standard coupling configurations (Equation 2.19)

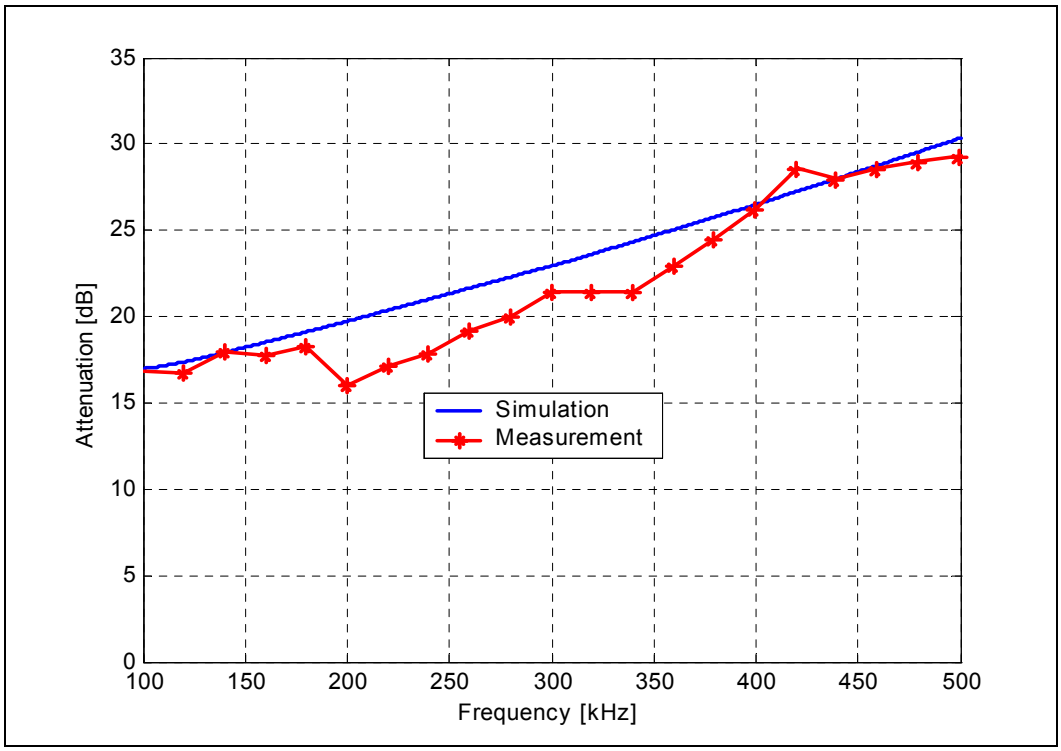

Figure 2.13 Measurement and simulation for outer phase to outer phase (Equation 2.20)

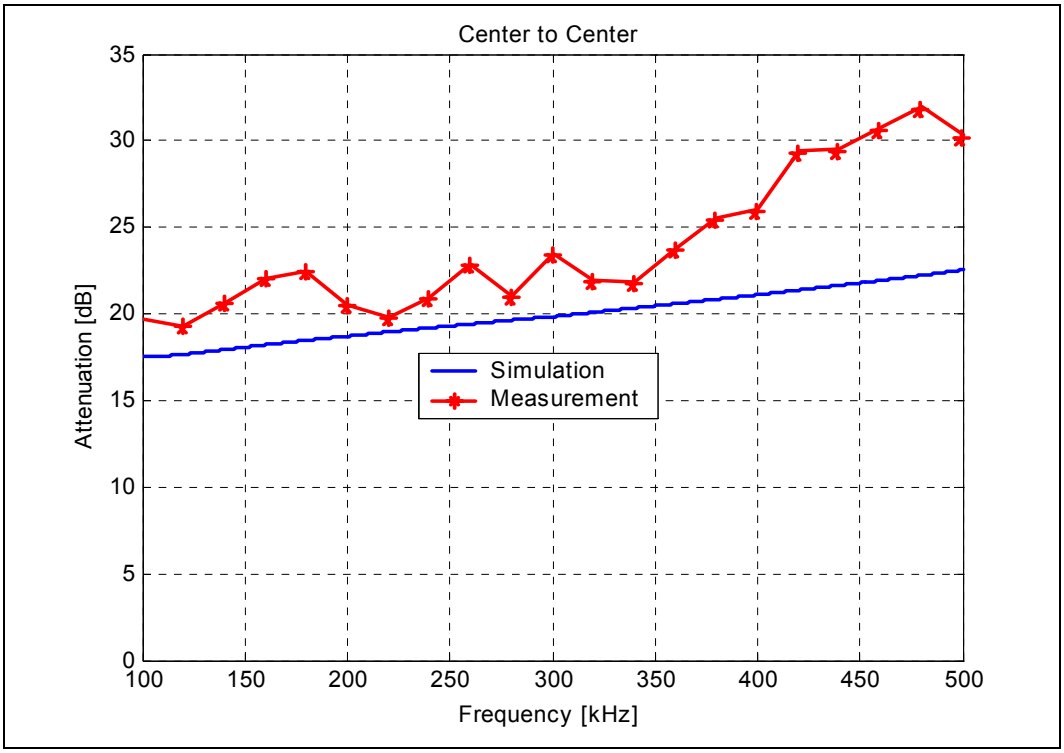

Figure 2.14 Measurement and simulation for centre phase to centre phase (Equation 2.20)

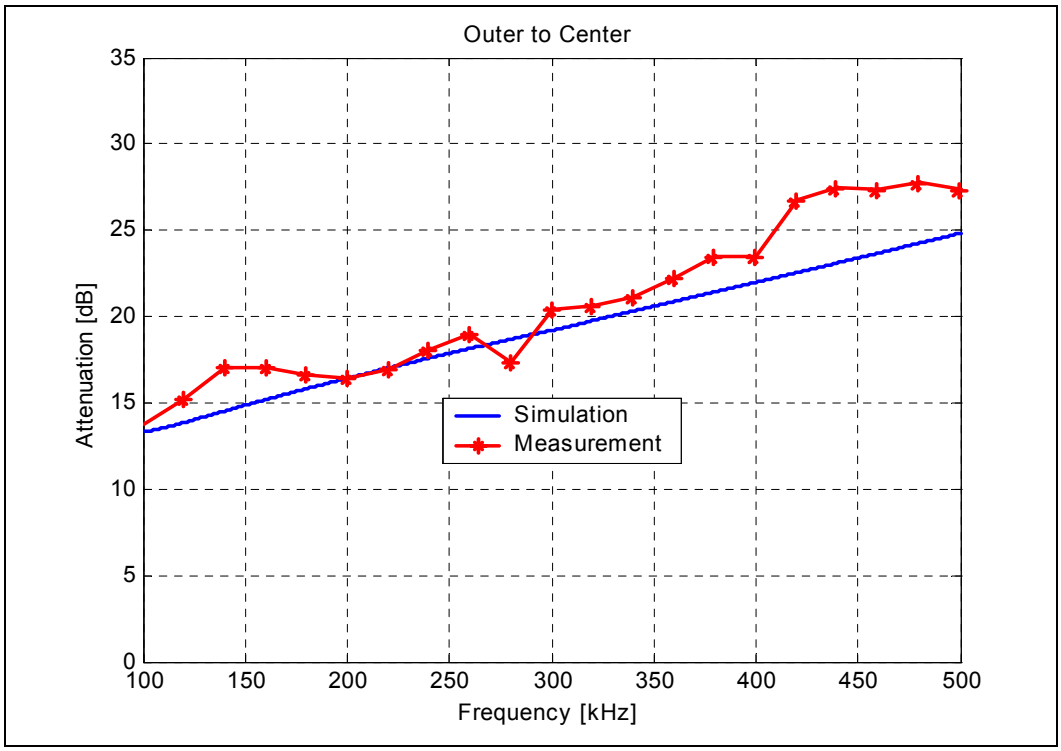

Figure 2.15 Measurement and simulation for outer phase to centre phase (Equation 2.21)

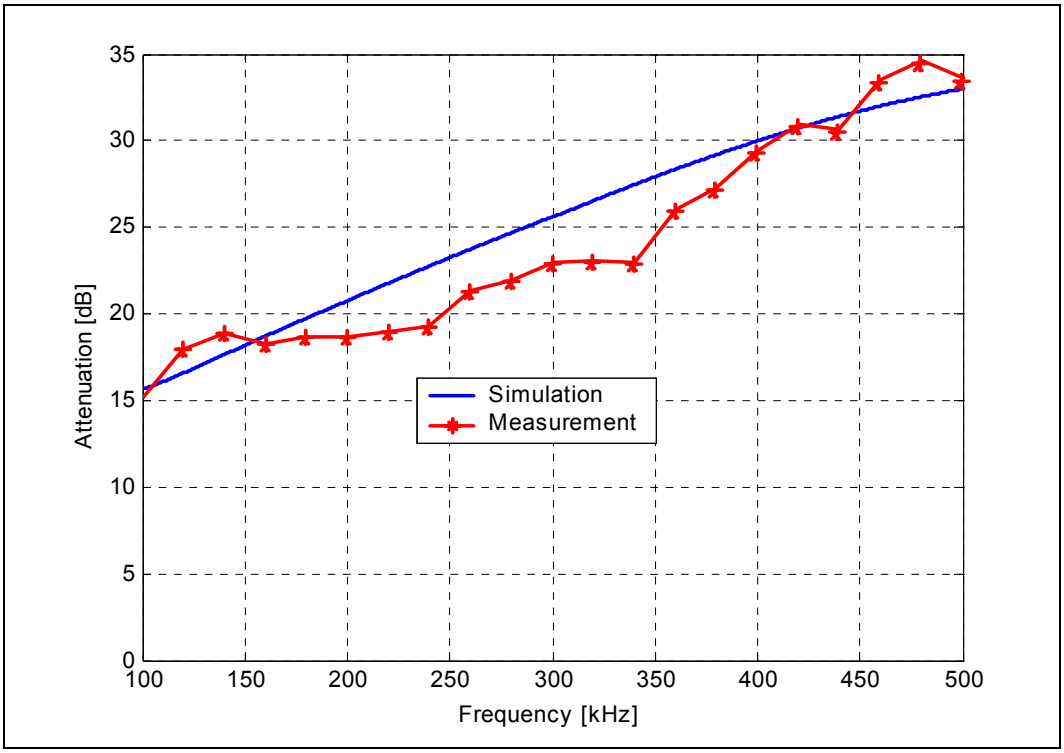

Figure 2.16 Measurement and simulation for centre phase to outer phase (Equation 2.22)

This is a remarkably good result, measured and simulated for a transposed transmission line that consists of seven different sections. The centre phase to centre phase simulation indicates the biggest average error of 4.04 dB and the standard coupling configuration the smallest error of 1.47 dB. The biggest error could be due to the station impedance uncertainty.

2.5.4 Comparing the technique with other techniques

The only other attempt to determine the average ground resistance over a long distance at PLC frequencies in South Africa was done by R.W. Vice between 1950 and 1952 [9]. From this survey, a ground conductivity map of South Africa was created. The ground resistance was determined by

analysing its effect on ground wave propagation between two distant antennas. According to the survey, the area in the vicinity of the location of the Kriel-Tutuka transmission line has an average ground resistance between 50 and 58 $\Omega-\mathrm{m}$. This compares well with the determined 80 Ω/m via the PLC technique, when considered in the framework of the wide range (10 Ω/m to 1000 Ω/m) of the ground resistance. An important difference between the two techniques is that Vice [9] determined the ground's resistance only at 500 kHz, whereas the PLC technique is applied over the PLC frequency range (100 kHz – 500 kHz).

2.6 Conclusion

Some background about the PLC system and the associated theory of natural modes is given. The eigenvector and eigenvalues are described in the context of signal propagation on an OHTL.

Terms used in the PLC-SAG model, which will be used consistently throughout the thesis, are discussed. Additional changes were made to the simulation program as described in [7], to ensure that it was tailor made for PLC-SAG related simulations.

A PLC technique to estimate the average ground resistance was created. This is a new contribution to the simulation model and was successfully done and evaluated.

References:

[1] **D.C. Smith,** *PLC system engineering and practical application,* unpublished notes, for one-day short course, University Stellenbosch, 1999.

[2] **L.M. Wedepohl**, The Theory of Natural Modes in Multi-Conductor Transmission Systems*, unpublished lecture notes, Westbank, British Columbia, Canada, 10 January 1999.*

[3] **Wedepohl, L.M.** "Applecation of Matrix Methods to the Solution of Travelling Wave Phenomena in Polyphase Systems", Proc. IEE, Vol. 110, Dec. 1963, p. 2200-2212. (13 Pages)

[4] **Galloway, R.H., Shorrocks, W.B., Wedepohl, L.M.** "Calculations of Electrical Parameters for Short and Long Polyphase Transmission Lines", Proc. IEE, Vol. 111, No. 12, Dec.1964, p. 2051-2059. (9 pages)

[5] **Wedepohl, L.M.** "Electrical Characteristics of Polyphase Transmission System, With Special Reference to Boundary Value Calculations at Power Line Carrier Frequencies", Proc. IEE, Vol. 112, No. 11, Nov. 1965, p.2103-2112. (10 pages)

[6] **F.Eggimann, W.Senn** and **K. Morf**, "The Transmission Characteristics of High-Voltage Lines at Carrier Frequencies", Brown Boveri Review 8-77, pp. 449-459.

[7] **De Villiers, W.**, *Prediction and measurement of Power Line Carrier signal attenuation and fluctuation*, MScEng Thesis, University of Stellenbosch, November 2001.

[8] **Occupational Health and Safety Act** of South Africa, Section 15: Clearances of power lines, 1993.

[9] **Turan Gönen**, *Electric power transmission system engineering – Analysis and Design*, John Wiley and Sons, New York, 1988.

[10] **R.W. Vice, "**A survey of ground wave propagation conditions in South Africa**",** The Transactions of the S.A. Institute of Electrical Engineers, April 1954, pp. 139-159

[11] **A.F. Pollard,** "Power Line Carrier and teleportation Design for Eskom's 765 kV system", ESKOM open Conference on EHV transmission systems, MegaWatt Park in South Aftrica, 23 Nov 1987.

Chapter 3

Simulation of the two case studies and frequency allocation of the PLC-SAG monitoring tones

3.1 Introduction

The two case studies of two transmission lines on which the PLC-SAG experimental systems were installed will be introduced. Simulations will be performed on the case studies and frequencies will be allocated for the PLC-SAG monitoring tones.

The first case study on which the PLC-SAG experiment was installed was the 400 kV transmission line between Koeberg Power Station and Acacia Sub Station, which is located in the Western Cape and is 31.318 km long. This line is considered a typical OHTL.

The second case study was done on the 400 kV transmission line between Kriel Power Station and Tutuka Power Station. This line is located in Mpumalanga and is 99.17 km long. The line is transposed once and has seven different sections due to previous changes made to the OHTL. This line is not classified as a typical OHTL and was chosen as an extreme case, in order to test the PLC-SAG system.

In this thesis the abbreviation 'KA' will be used to refer to the 400 kV transmission line between Koeberg Power Station and Acacia Sub Station

and ‘KT’ will be used when referring to the 400 kV transmission line between Kriel Power Station and Tutuka Power Station.

After more detail on the two case studies has been introduced in Section 3.2, simulations will be performed in Section 3.3 using the simulation program as described in the previous chapter. The PLC signal attenuation will be simulated for different coupling configurations and at different conductor heights above the ground. Five different coupling configurations were explored, from which the best coupling configuration was selected.

To explore the expected PLC signal level variations (simulated in this chapter) as a function of conductor height, a multi-tone experiment was proposed on each of the two case studies. After consultation with ESKOM it was concluded that 10 tones could be coupled and decoupled on each of the lines in the case studies. The frequency allocation process of the ten tones will be discussed in this chapter (Section 3.4), as it relates closely to the simulations presented. In Chapter 4 the physical hardware implementation of the experiment will be discussed.

3.2 Locations of the two OHTL sites

3.2.1 General

Two OHTLs in South Africa were chosen on which to install PLC-SAG systems. The most important criterion for an OHTL to be a candidate for PLC-SAG Ampacity control is that it should have an operational PLC system installed.

The KA line was chosen because it was a short (31.318 km), non-transposed flat horizontal OHTL and conveniently close to Stellenbosch University. The second transmission line had to be selected with more

care. After consultation with ESKOM, it was concluded that KT would be ideal as it is a long (99.17 km) transposed flat horizontal transmission line. It is a complex line, since it is a combination of two transmission lines and can therefore be classified as a non-standard OHTL.

The two transmission lines will now be discussed. More detailed information about the OHTL and the associated PLC system can be found in Appendix A.

3.2.2 Case Study 1: Koeberg-Acacia (KA)

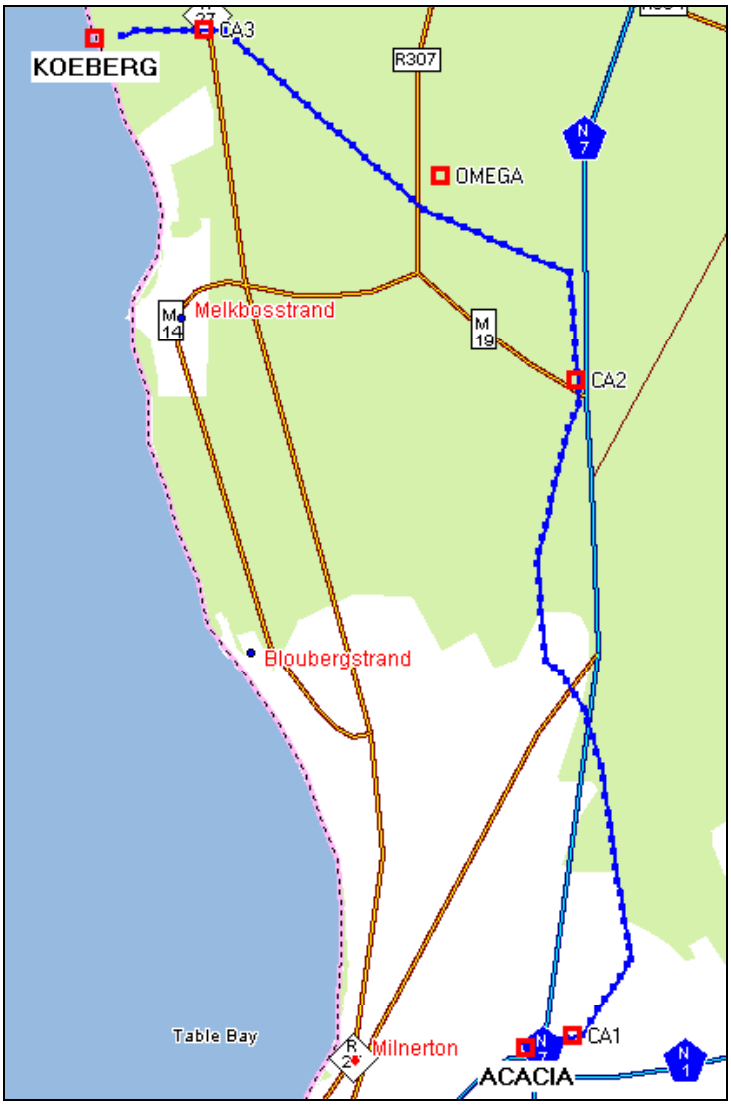

Figure 3.1 Map of Koeberg-Acacia OHTL

In Figure 3.1, the KA OHTL is presented as the blue dotted line between Acacia Sub Station and Koeberg Power Station. The KA OHTL runs semi parallel to the Atlantic Ocean coastline. A standard Twin "Dino" Aluminium Conductor Steel Reinforced (ACSR) bundle conductor configuration is used as the phase conductor. Steel conductors are commonly used as ground conductors, which are also called earth wires. Because this transmission line is located near the Western Cape coast, the earth wire is also an ACSR type conductor. Steel conductors rust severely in the harsh coastal environment of the Cape.

The complete line can be presented as one continuous section. The properties describing the section (Section A) are tabled in Table 3.1.

Table 3.1 Properties of the Koeberg-Acacia transmission line

Section	A
Length	31.318 km
Phase Conductors	2 Dino
Ground conductor	Tiger
Outer Phase to Outer Phase spacing of tower	18 m
Earth wire to earth wire spacing of tower	16.6 m

The OHTL that forms part of the second case study will be discussed in the following section.

3.2.3 Case Study 2: Kriel-Tutuka (KT)

Figure 3.2 is a map showing the 400 kV transmission line (thick blue line) between Kriel Power Station (PS) and Tutuka PS. It can be mentioned that the transmission line is routed via Zeus substation (very close to CA2 but not indicated on the map). The reason for being routed via Zeus is that the Kriel-Tutuka transmission line is a combination of the previously existing Kriel-Zeus and the Zeus-Tutuka transmission lines. Closer to

Tutuka PS one can note another sharp bend in the route of the transmission line. This is due to the surrounding underground coal mines.

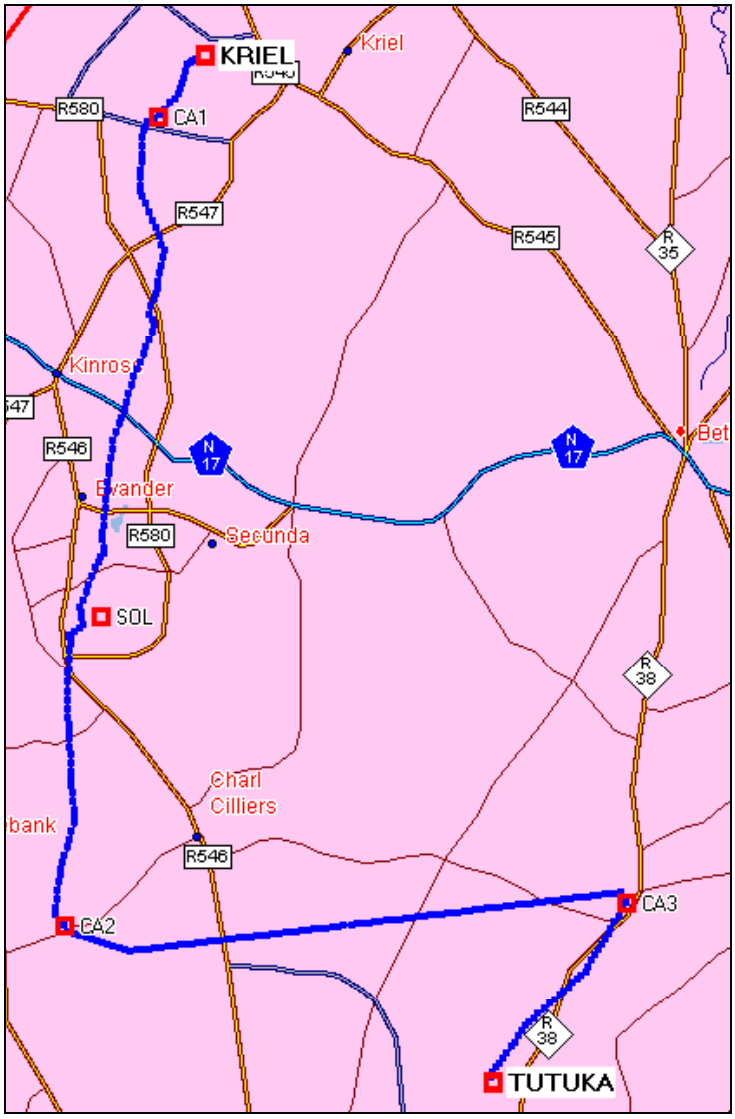

Figure 3.2 Map of Kriel-Tutuka OHTL

.

As a result of the combination of the lines and of changes made over the years, the KT OHTL is quite complex and can best be described by dividing the line up into seven sections (Figure 3.3). The key properties of these sections are given in Table 3.2.

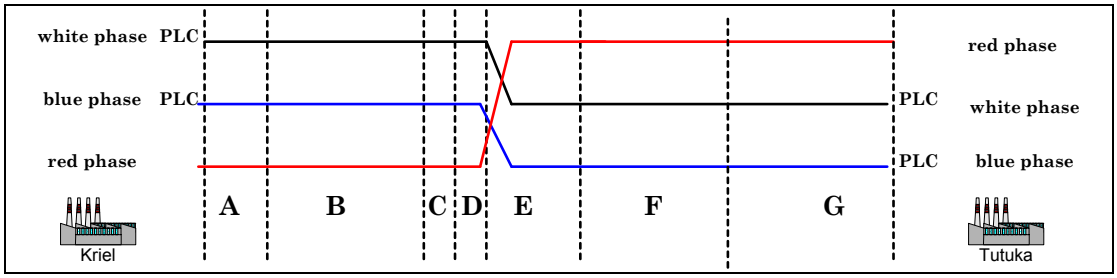

Figure 3.3 Seven sections of the OHTL

Table 3.2 Properties of the different sections of the Kriel-Tutuka transmission line

Section	A	B	C	D	E	F	G
Length [km]	4.79	29.994	0.701	0.3168	16.772	33.097	13.504
Phase Conductors	3 Dino	4 Zebra	3 Dino	2 Bull	4 Zebra	2 Dino	2 Dino
Ground conductor for steel (Number of strands/Size of strands [mm])	19/2.65	19/2.65	19/2.65	No ground conductor	19/2.65	19/2.65	19/2.65
Phase to Phase spacing of tower [m]	10	8.5	10	10	8.5	9.4	9.4
Earth wire to earth wire spacing of tower [m]	17.5	14.26	17.5	n.a.	14.26	11.2	16.6

The transposition of the OHTL can be noted between Section D and Section E. It can further be noted that the transmission line has one transposition and a short underpass section that is without any earth wires. This transposition complicates the PLC signal propagation and makes the transmission line a challenge in testing the PLC-SAG technique.

3.3 Simulations

3.3.1 General

The simulation program and associated theory used are discussed in the previous chapter. In this section the simulation program is applied to the two case studies. The simulation methodology will be discussed step by step.

The first step is to compute the ruling span of the transmission line, in order to define the default simulation condition (Chapter 2.4.1). Once this has been accomplished the phase conductor sag can be moved higher and lower around the default sag value and the associated average conductor height can be calculated. It is recommended that a lookup table be created which indicates the relationship between sag and the average conductor height for the ruling span.

The second step is to perform PLC-SAG tone attenuation simulations for two scenarios, namely: i) the default simulation condition and ii) a simulation condition where the phase conductor has sagged two meters below the default conditions. These simulations can be done for different coupling configurations, as explained in Chapter 2. The simulations will indicate which coupling configuration is sensitive to conductor height variation and show the uniformity of the change in the frequency band.

The final simulation step is to focus on the best coupling configuration as identified in the previous step and then to change the conductor height in smaller steps.

These three steps will now be applied to the two different case studies.

3.3.2 Case 1: Koeberg-Acacia

Step 1: Calculating the default simulation condition

The attachment height of the phase conductor is a function of the type of tower used for the transmission line. The attachment height of the conductor is 19.6 m for the KA OHTL[2]. The attachment height of the earth wire can then, in turn, be computed by further studying the tower dimensions used on this specific OHTL. The vertical spacing between the phase conductor and the earth wire is 5.55 m and therefore the attachment height for the earth wire is 25.15 m.

The tower spacing of the equivalent, or ruling span, can be computed by using Equation 2.13 in Chapter 2. Column seven in Table A.1 of Appendix A provides the individual lengths (L_e) needed. The tower spacing of the ruling span for KA was calculated as 347.36 m.

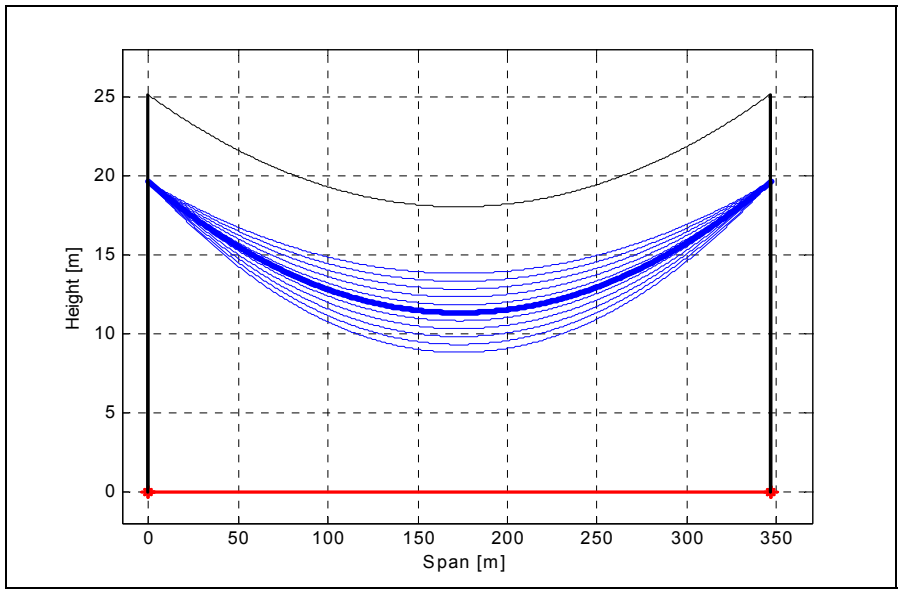

Figure 3.4 Ruling span of Koeberg-Acacia OHTL (Table 3.3)

[2] Email correspondence with Mr DC Smith, ESKOM Corporate Consultant: Telecommunications, dated 1 March 2001

Figure 3.4 plots the height versus distance between the equivalent tower spacing of the ruling span for KA. The thick blue curve represents the phase conductor between the two black 'towers' for the default simulation condition (Chapter 2) as it is plotted for a catenary constant of 2100. The earth wire is plotted with a catenary constant of 1800. Figure 3.4 also shows how the phase conductor height is changed around the default height value. Table 3.3 specifies the relationship between sag and the average conductor height for the ruling span. Row 6 in Table 3.3 represents the default simulation condition (Thick blue curve in Figure 3.4) whereas row 1 represents the height of the conductor if sagged 2.5 m less than the default condition. Row 11 in Table 3.3 represents a heavily sagged conductor, with a clearance of 9.105 m above a flat horizontal ground plane.

Table 3.3 Average value of conductor height for Koeberg-Acacia ruling span

	Sag	Average conductor height	Comments
1	5.7946	15.73703946	
2	**6.2946**	**15.40371476**	
3	6.7946	15.07039006	
4	**7.2946**	**14.73706537**	
5	7.7946	14.40374067	
6	**8.2946**	**14.07041597**	Default condition
7	8.7946	13.73709128	
8	**9.2946**	**13.40376658**	
9	9.7946	13.07044188	
10	**10.295**	**12.73711719**	Dotted curves in Fig 3.5 (2 m sag)
11	10.795	12.40379249	

The next step is to explore the PLC signal attenuation for different coupling conditions. The default simulation condition will be used in these simulations.

Step 2: Exploring different coupling configurations

The five different coupling configurations, as specified in Chapter 2, are explored. Only the attenuation of the transmission line is simulated and taken into consideration, as the attenuation due to the PLC coupling equipment is not expected to vary. The ground resistance is estimated to be 150 ohm meter, applying the PLC - ground resistance technique as described in Chapter 2 for only one coupling configuration.

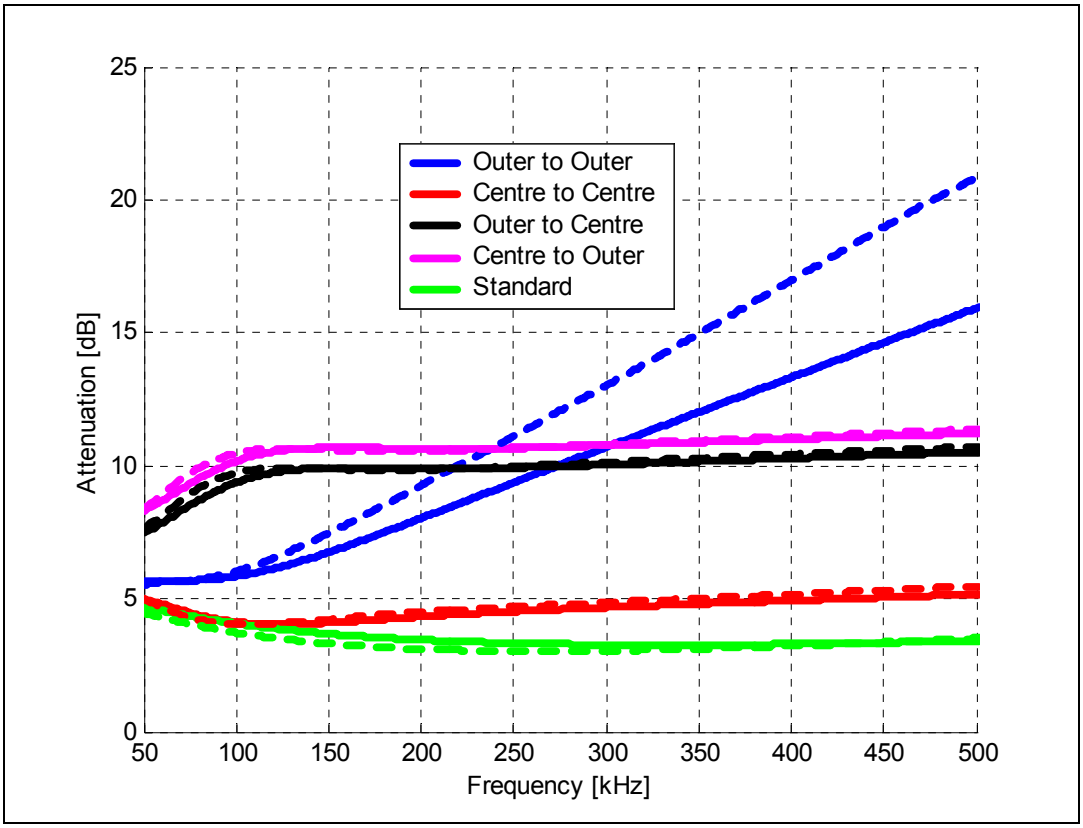

Figure 3.5 Koeberg-Acacia default simulation condition for the various coupling configurations (solid line) and two meter sagged conductor (dotted line). Ground resistivity equals 150 ohm meter.

It is quite remarkable to note that the only coupling configuration that shows a strong relationship between the phase conductor height and the signal attenuation is the Outer phase to Outer phase coupling configuration. The reason for this is because at the injection point the excitation amplitude of the mode 2 (differential mode) component is bigger that mode 1 (least attenuation) component for the coupling configuration. But mode 2 attenuates faster than mode 1, so for some length of the line, the amplitude of the two modes will be equal. The phases of the two modes are also different and if the phase different is approximately 180° the two modes will cancel out. This phenomenon is called modal cancellation. Although for the particular line complete modal cancellation occurs outside the PLC frequency range, the interaction between the two modes is strong within the band, leading to a practical observable effect.
Existing coupled PLC signals ('standard' in Figure 3.5 and where the energy in mode 1 is more than mode 2) are not sensitive for height variation, which means that the normal coupled PLC signals are not significantly influenced by external factors like the height of the phase conductors.

It is also worthy of note that the attenuation difference between the two simulation conditions for the Outer phase to Outer phase condition varies essentially uniformly and monotonically over the frequency range 100 kHz to 500 kHz. In the next step the Outer phase to Outer phase coupling will be explored in more detail, as this coupling configuration is most suitable for the PLC-SAG system.

Step 3: More detailed simulations on the best coupling configuration

More detailed simulation was done, to explore the predicted attenuation variation for height variation in the phase conductors. Figure 3.6 shows five different average height conditions, which relate to the bold rows in Table 3.3.

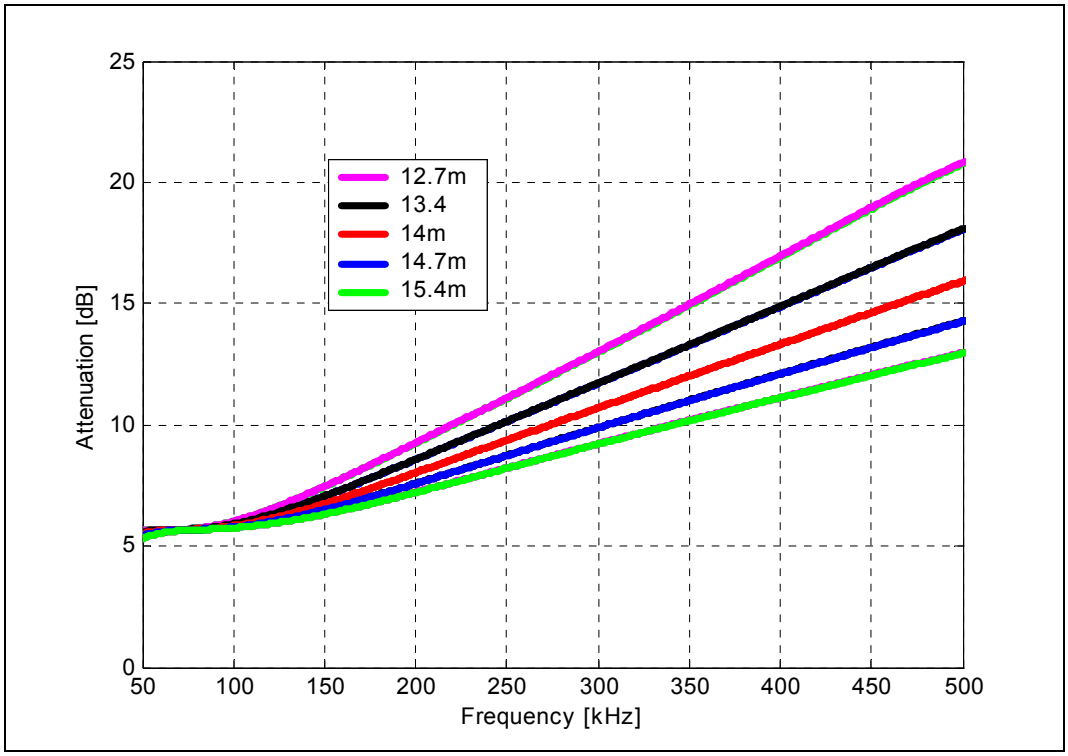

Figure 3.6 Expected PLC-SAG tone variation with average height for Outer phase to Outer phase coupling on Koeberg-Acacia OHTL

In Figure 3.6 it can be noted that the attenuation variation range increases as the frequency increases. A total variation of 5 dB can be noted at 350 kHz for an average conductor height variation of 2.7m. More detailed discussions about the mathematical relationship between attenuation and average conductor height will be given in Chapter 6.

The same three simulation steps will now be applied to the KT OHTL.

3.3.3 Case Study 2: Kriel-Tutuka

Step 1: Calculating the default simulation condition

Figure 3.7 shows the ruling span (404 m) and the attachment height (Phase conductor = 23 m and earth wire = 25.4 m). The information needed for these calculations is shown in Appendix A. A clear difference

can be noted in the attachment height of the earth wire compared to the KA case. This is due to the different type of OHTL tower used. As in the previous simulations, the thick blue line represents the default simulation condition as defined in Chapter 2. Table 3.4 shows the relationships between the average conductor height and the sag of the KT ruling span.

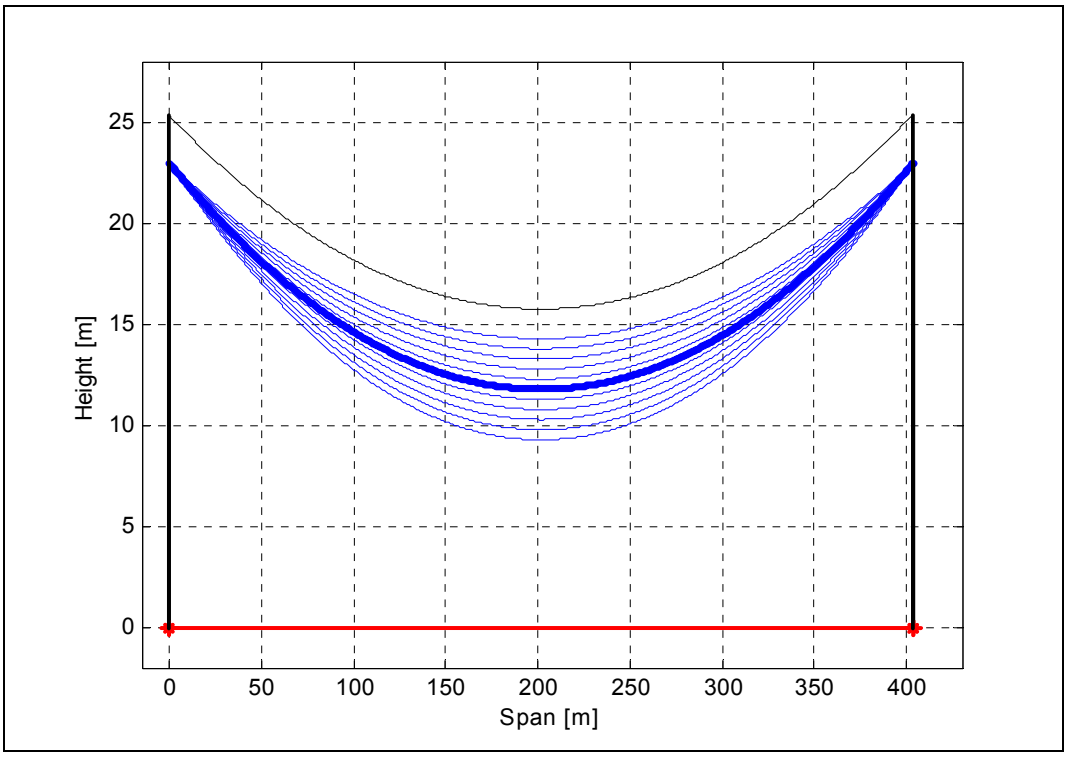

Figure 3.7 Ruling span of Kriel-Tutuka transmission line

Table 3.4 Average value of conductor height for the Kriel-Tutuka ruling span

	Sag	Average conductor height	Comments
1	8.7	17.2	
2	**9.2**	**16.9**	
3	9.7	16.5	
4	**10.2**	**16.2**	
5	10.7	15.9	
6	**11.2**	**15.5**	Default condition
7	11.7	15.2	
8	**12.2**	**14.9**	
9	12.7	14.5	
10	**13.2**	**14.2**	Dotted curves in Fig 3.8
11	13.7	13.9	

Step 2: Exploring different coupling configurations

The results of the different coupling configurations in Figure 3.8 for KT OHTL differ greatly from similar simulations for KA OHTL. The main reason for the difference is that all the configurations indicate some dependence on average conductor height, which fact is due to the transposition in the KT line.

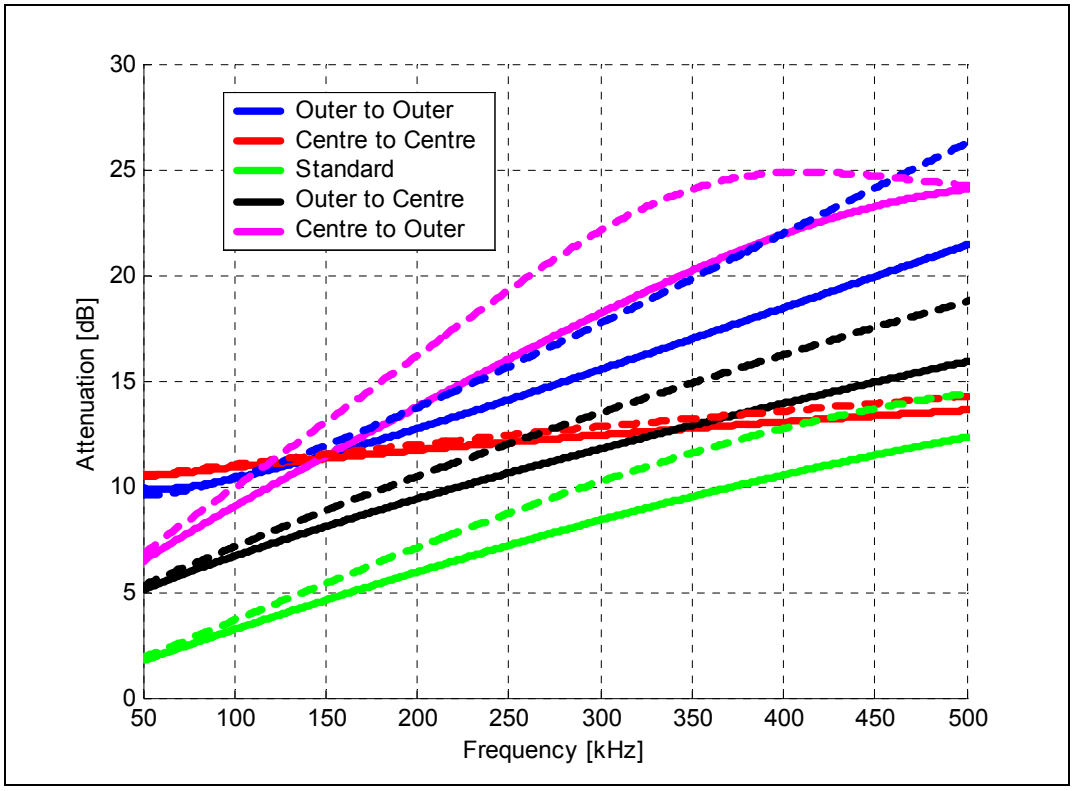

Figure 3.8 Default simulation condition for the various coupling configurations (solid line) and conductor sagged by two meters (dotted line)

However, the Outer phase to Outer phase coupling configuration again performed well as regards conductor height sensitivity and uniform variation throughout the frequency range. A more or less uniform variation is necessary in order to relate multi coupled PLC-SAG tones to each other.

Step 3: More detailed simulations on the best coupling configuration

Average conductor height simulations were done, which relate to the bold rows from Table 3.4. These simulations are shown in Figure 3.9.

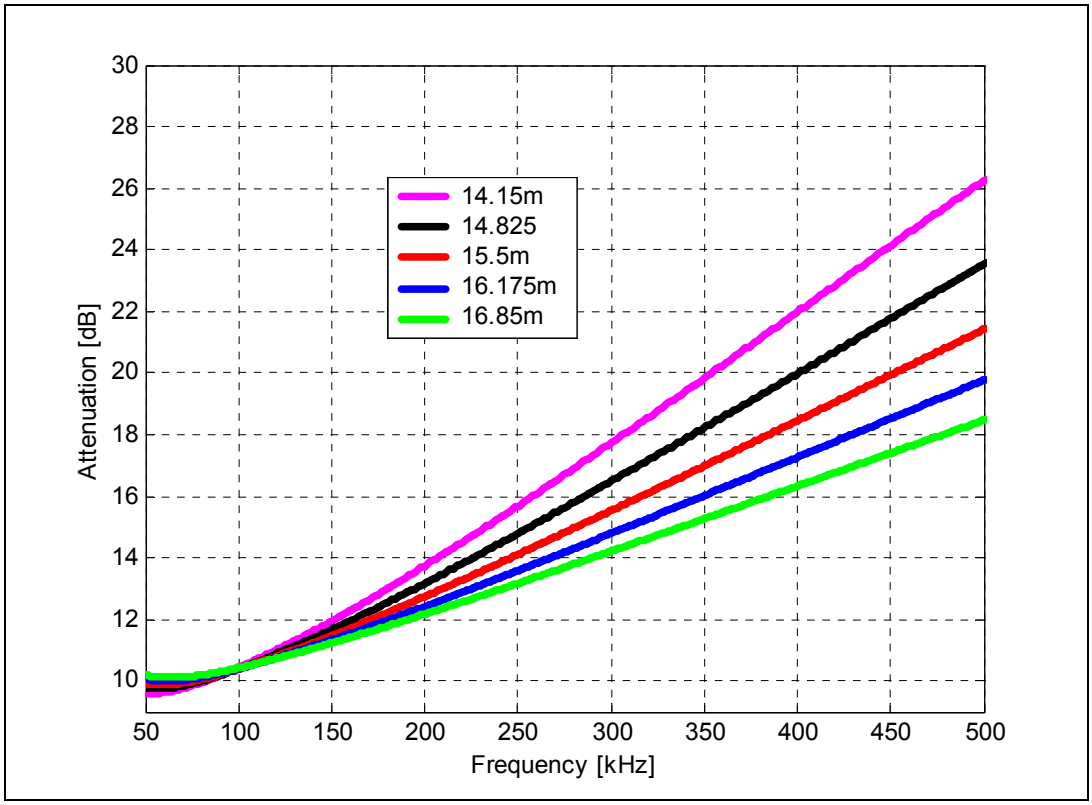

Figure 3.9 Expected PLC-SAG tone variation with average height for Outer phase (white phase at Kriel, Figure 2.9) to Outer phase (blue phase at Tutuka) coupling on Kriel-Tutuka OHTL

The sensitivity of the long, transposed KT OHTL was, surprisingly, very similar to that of the short non-transposed KA OHTL.

Thus the simulation predicted that for both case studies OHTLs had the necessary PLC-SAG sensitivity, if the PLC-SAG tones were coupled and decoupled on the Outer phases only. The following section will focus on the process of allocating PLC-SAG tone frequencies, in order to explore and verify the expected variations as simulated.

3.4 Choosing PLC-SAG tones

3.4.1 General

This section starts by addressing the question: Which frequency regions are the best for PLC-SAG tones? Then the following question will be addressed: Which frequencies are safe to use and will not interfere with the current operational PLC system?

To address the first question, simulations of both case studies indicated that the PLC-SAG sensitivity is a function of frequency. The PLC signal attenuation variation as a function of conductor height is more prominent at higher frequencies, but a phenomenon called the "tower effect", which should be avoided, is also involved.

At frequencies where the spacing between the towers is equal to half a wavelength (Equation 3.1), a phenomenon is present [2], which is not included in the presented simulations. This effect is referred to as the "tower effect".

$$0.5 \simeq \frac{fl}{c} \qquad 3.1$$

where:

f = frequency

l = tower spacing

c = Mode 1 velocity (very close to the speed of light)

The frequencies that relate to frequently repeated tower spacing according to Equation 3.1, should also be avoided. Commonly, tower spacing of ESKOM OHTLs is between 350 m and 450 m for 400 kV transmission

lines. From Equation 3.1, frequencies of 333 kHz up to 428 kHz should be avoided. With this effect, in mind and seeking high sensitivity, the only to feasible PLC-SAG frequency regions are around 300 kHz and 475 kHz (The highest frequency for a PLC system is 500 kHz). The sensitivity of the PLC-SAG system at 100 kHz is too low (Figure 3.6 and Figure 3.9).

The second question of which frequency is safe to use and will not interfere with the current operational PLC system was then addressed. The PLC-SAG system is operated on the same infrastructure as the PLC system, which occupies bandwidth at selected frequencies. To prevent conflict between the two systems, extra precautions must be taken to ensure that the correct frequencies are allocated to the PLC-SAG system.

Obtaining all the frequency allocations of nearby operational carriers is the start of the frequency location process. The nearby carriers are defined as the operational carriers that are located two busbars away from the two stations on which a PLC-SAG system will be installed. By studying the data, open frequency regions can be identified.

It is important to perform a detailed frequency scan (typical bandwidth for a detailed scan is 25 Hz), to make sure that there is no operational carrier system in the frequency regions identified as open. A selective voltmeter with a very narrowband capability is needed to perform the measurement (for example Wandel & Goltermann). Spectrum analysers normally do not have such a narrowband capability. Because carriers' frequencies are relocated or shifted as time goes by, one cannot rely completely on the frequency database of the Power Utility, which is not necessarily thoroughly updated as changes occur.

The frequency allocations of the two case studies will now be discussed.

3.4.2 Case study 1: Koeberg-Acacia

Firstly, it is necessary to determine all the neighbouring frequencies two busbars away from the relevant stations. Appendix B shows the PLC activity near the Koeberg-Acacia link. In order to double-check the frequencies, a detailed scan (20 Hz bandwidth) is performed and this is shown in Figure 3.10. Appendix B contains a larger version of Figure 3.10, with more detail about the PLC activity and how the scan was performed. Due to restrictions imposed by available instruments the duration of this detailed scan was approximately 22 hours.

Considering the allowable regions and the optimal PLC-SAG tone regions (Section 3.4.1), ten tones were selected and are tabled in Table 3.5. To illustrate the open region in which the PLC-SAG tones are located, the PLC-SAG tones are plotted in green together with the PLC frequency scans in Figure 3.10.

Table 3.5 PLC-SAG Frequency locations for Koeberg-Acacia

No	PLC-SAG tones [kHz]
1	291
2	296
3	301
4	306
5	313
6	320
7	324
8	464
9	480
10	495

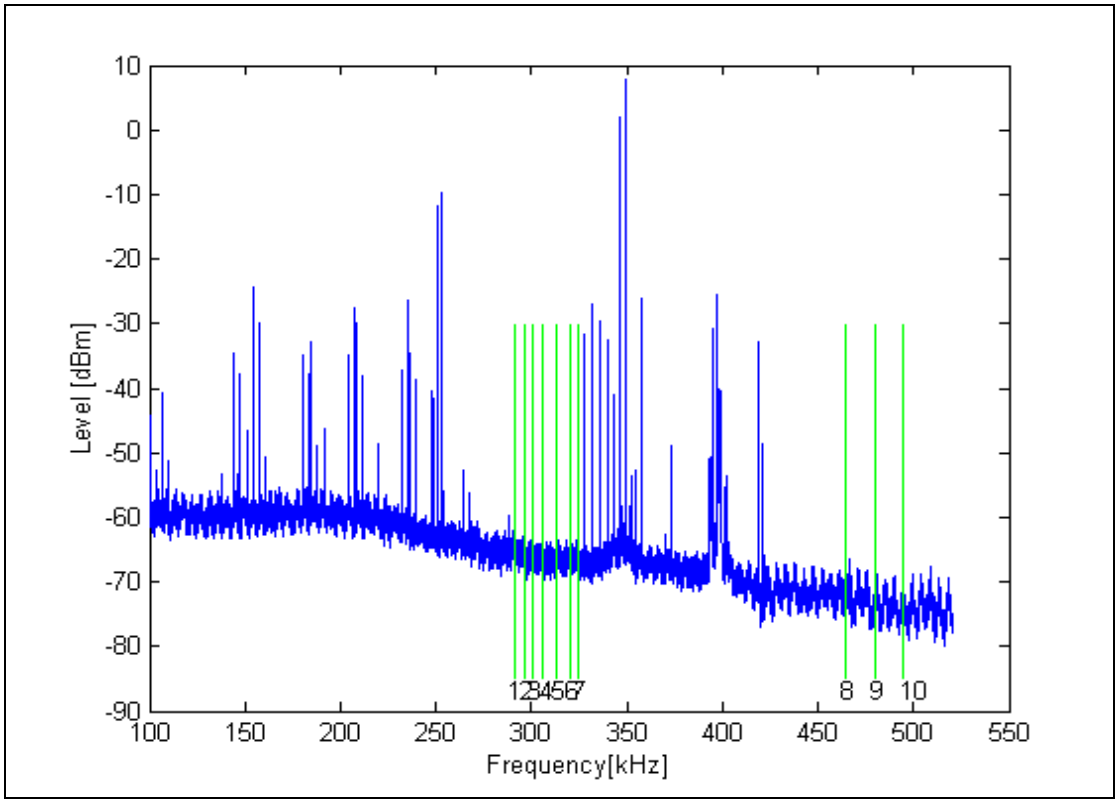

Figure 3.10 Frequency scan of the Koeberg-Acacia 400 kV OHTL performed at Acacia Sub Station

3.4.3 Case study 2: Kriel-Tutuka

The KT OHTL is located close to other power stations. This results in more PLC activity than in the KA study. Appendix B contains a table which specifies all the PLC activity near the KT OHTL. From the table, it can be confirmed that there is much more PLC activity around the KT OHTL than around the KA OHTL. The ten chosen PLC-SAG tones are tabled in Table 3.6. A detailed scan was also performed and is shown together with the ten PLC-SAG tones.

Although it may seem as if some of the located PLC-SAG tones (as indicated by green lines in Figure 3.11) conflict with existing systems, this is not the case. Better-scaled plots are given in Appendix B. Due to the

high stability of the PLC carriers and the injected PLC-SAG tones they may be separated by as little as 0.5 kHz.

Table 3.6 PLC-SAG Frequency locations for Kriel-Tutuka

No	PLC-SAG tones [kHz]
1	280
2	320
3	328
4	332
5	334
6	348.5
7	465
8	472
9	478.5
10	498

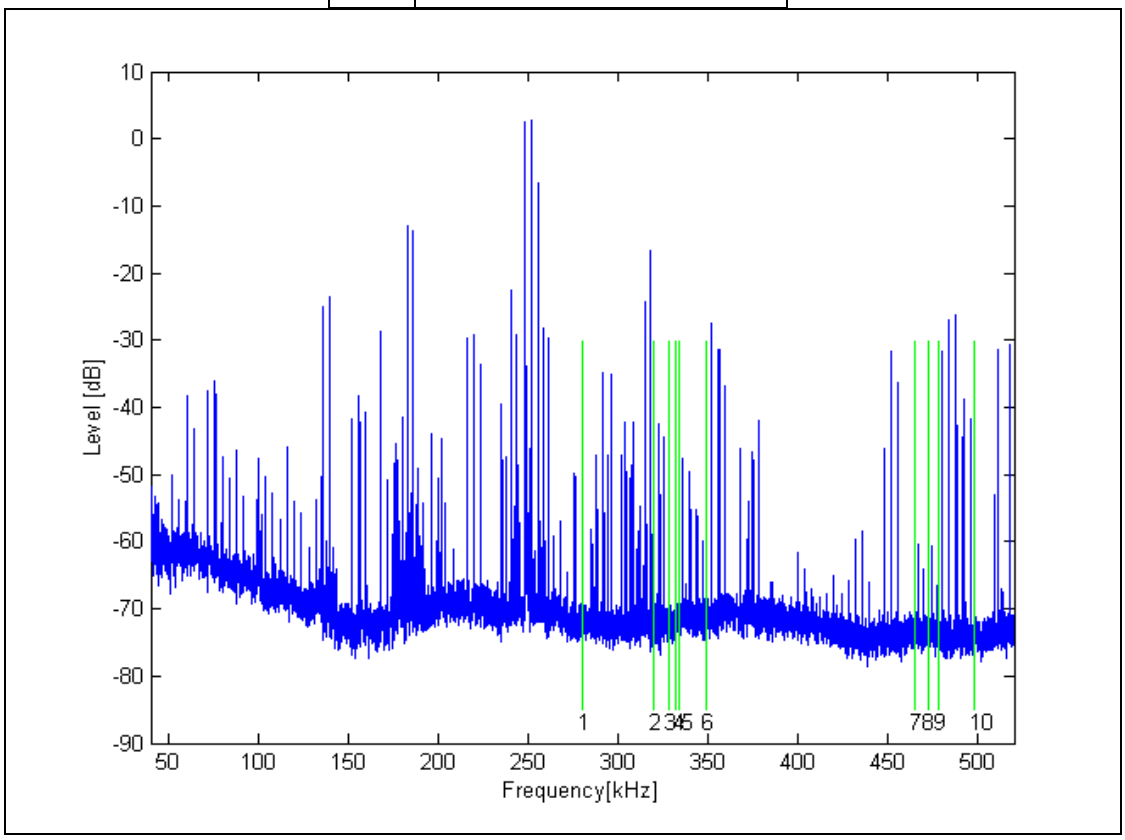

Figure 3.11 Frequency scan Kriel-Tutuka 400 kV OHTL performed at Kriel Power Station.

3.5 Conclusion

The two case studies are introduced. For the first case study, a short non-transposed standard transmission line was selected and for the second, a long transposed transmission line.

PLC signal attenuation simulations were performed on both OHTLs. The optimum coupling technique (with the adequate sensitivity) for each of the two PLC-SAG systems was found to be the outer phase to ground coupling at the local station to outer phase to ground coupling at the remote station. This coupling is also referred to as outer phase to outer phase coupling.

Two main frequency regions were identified where PLC-SAG monitoring tones could be coupled. Frequencies were allocated to the ten tones of each case study. Close co-operation was needed from the relevant power utility as the tones, called PLC-SAG monitoring tones, were coupled onto an operational PLC system.

The following chapter will discuss the hardware installations needed to realise the specially coupled multi PLC-SAG tone monitoring on the existing live system.

References:

[1] **De Villiers, W.**, *Prediction and measurement of Power Line Carrier signal attenuation and fluctuation*, MScEng Thesis, University of Stellenbosch, November 2001.

[2] **L.M. Wedepohl**, "Wave propagation in polyphase transmission systems – Resonance effect due to discretely bonded earth wires", IEE proceedings, Volume 112, No. 11, December 1965, pp. 2113-2119.

[3] **Turan Gönen**, *Electric power transmission system engineering – Analysis and Design*, John Wiley and Sons, New York, 1988.

Chapter 4

PLC-SAG experimental installations

4.1 Introduction

The hardware of the experimental PLC-SAG installations transmits and receives specially coupled PLC-SAG tones in order to measure the attenuation over a long period of time.

The PLC-SAG logging tones are specially coupled onto to the operational PLC system and decoupled at the remote station. This needs to be done without jeopardizing normal PLC operations. Ideally, the coupling should be done in such a fashion that the optimal PLC-SAG coupling configuration, as identified in the previous section, is used. The implementation of this will be discussed in Section 4.2.

There are two hardware models, a simplex PLC-SAG system (Figure 4.1) and a duplex PLC-SAG system (Figure 4.2). The simplex model was applied to the two case studies. The duplex system is recommended for a more permanent installation.

The main difference between the simplex PLC-SAG system and the duplex PLC-SAG system is, as the name indicates, that the latter system is capable of both transmitting and receiving tones at both ends. This feature increases the reliability of the system, which only needs to operate in one direction. If, however, equipment failure occurs at either the transmitter or receiver, the overall system will still be functional.

An added advantage of the duplex system is that an identical product can be developed for each side.

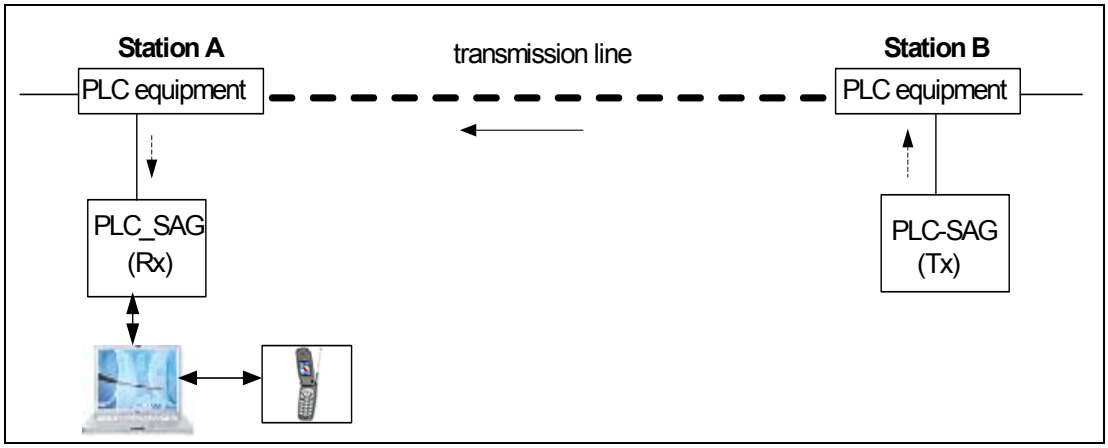

Figure 4.1 Simplex logging system. Dedicated Transmit and Receive PLC-SAG units

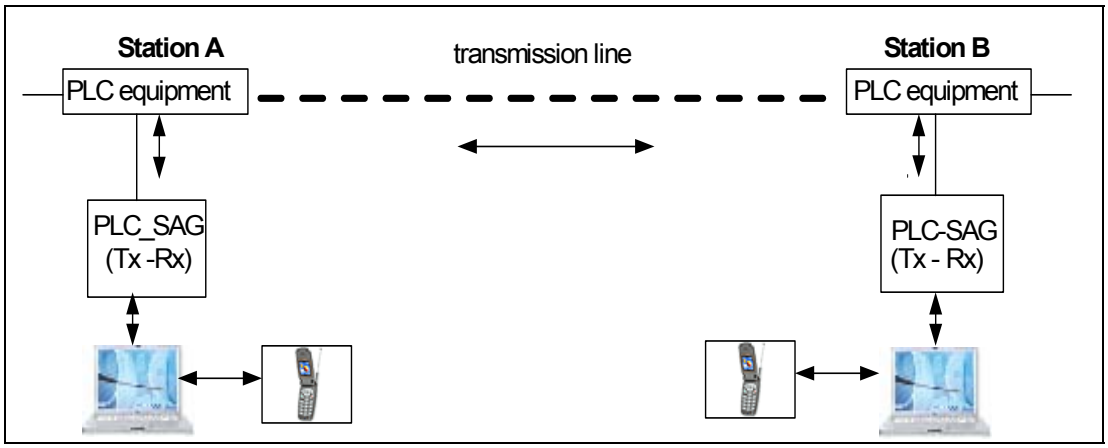

Figure 4.2 Duplex logging system. Identical Transmit and Receive PLC-SAG units

The experimental hardware installations of the two sites were similar. The first multi-tone experimental installation was on the Acacia-Koeberg transmission line and the second on the Kriel-Tutuka transmission line. Some improvements have been made since the first installation, therefore only the later installation (Kriel-Tutuka) will be discussed.

The outer phase to outer phase coupling configuration is common to both sides of the installation and to both case studies. An additional measurement hybrid is used to couple into the existing PLC system and will be discussed in Section 4.2.

The KT transmitter installation is described in Section 4.3 and the KT receiver in Section 4.4.

In [1] the author performed a preliminary experiment that coupled a single tone to the PLC system. The new experimental installation differs from original the single tone installation because more than one tone or multi tones are coupled to and decoupled from the PLC system.

4.2 Measuring Hybrid (to incorporate outer phase to outer phase coupling)

Both simulations indicated that the outer phase to ground coupling at both stations, performed the best in the context of PLC-SAG system. To physically incorporate such coupling, an additional signal entry point is needed in the existing PLC system. By inserting a supplementary measurement hybrid on the outer phase of the operational system at both stations, a signal entry point was created. Mr DC Smith, Eskom corporate Consultant: telecommunication, proposed this technique in the year 2000. In this section the installation of the supplementary measurement hybrid, the way it works and the implications for the existing PLC system will be discussed.

The normal existing hybrid in the PLC system was briefly discussed in Chapter 2 and will now be discussed in more detail.

A hybrid, as in Figure 4.3, also known as a phase combiner in PLC systems, acts mainly as a power divider/combiner. The function of the hybrid will be discussed in the framework of a standard outer phase to centre phase PLC configuration, as shown in Figure 4.3. A more detailed description will be given in Chapter 7.

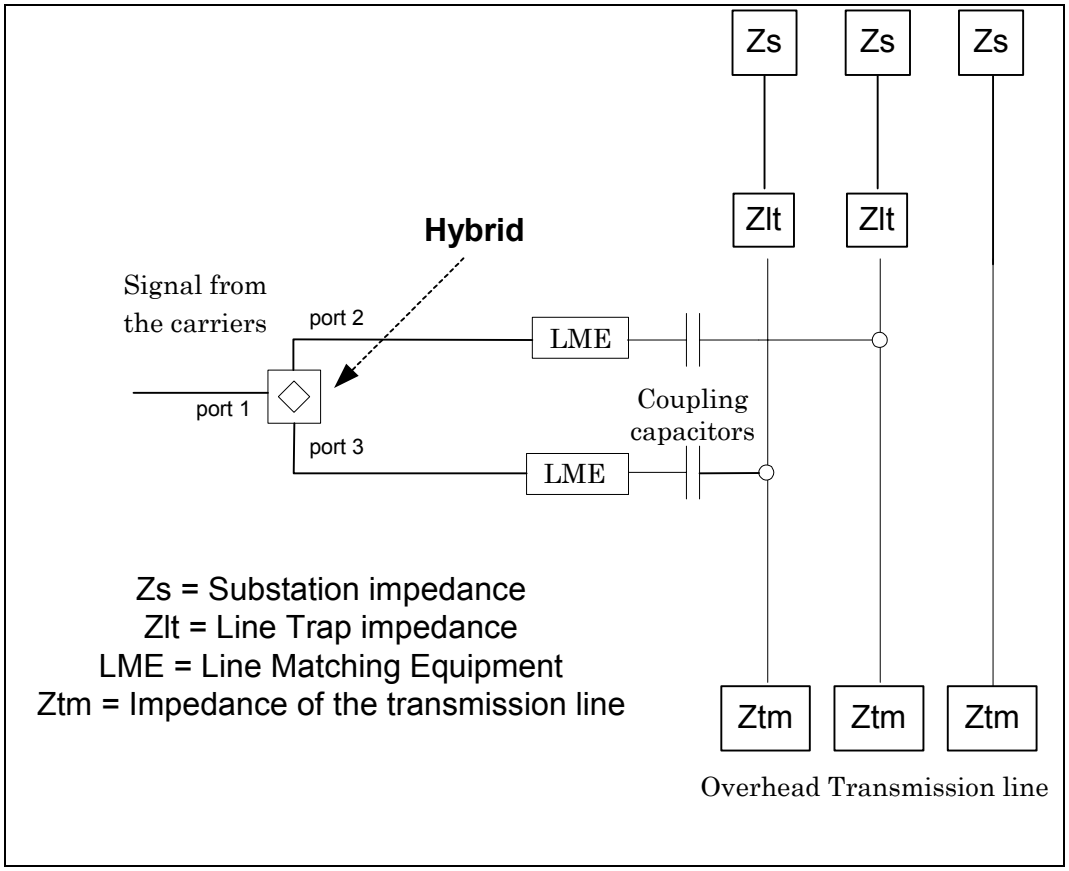

Figure 4.3 Normal PLC system with the hybrid

Ideally, and when the hybrid is used in its normal operational mode, all the terminals/ports are terminated in 75 Ω. The hybrid consists of a low insertion loss three-port transformer [7]. The hybrid is analysed in section 7.3. The transformer is wound in such a way that the power sent from the PLC carrier is divided into ports 2 and 3. On the other hand, power received at Ports 2 and 3 is combined at the hybrid and delivered to the PLC carriers.

The hybrid is normally configured in such a way that there is a 180 degrees phase shift between the voltage at Port 2 and the voltage at Port 3. Therefore, the standard differential coupling or configuration (Equation 2.4) can be realised via the standard hybrid configuration (Figure 4.3).

The special PLC-SAG outer phase to outer phase coupling can be practically implemented by inserting an additional hybrid between Port 3 of the standard hybrid and the LME of the outer phase (Figure 4.4).

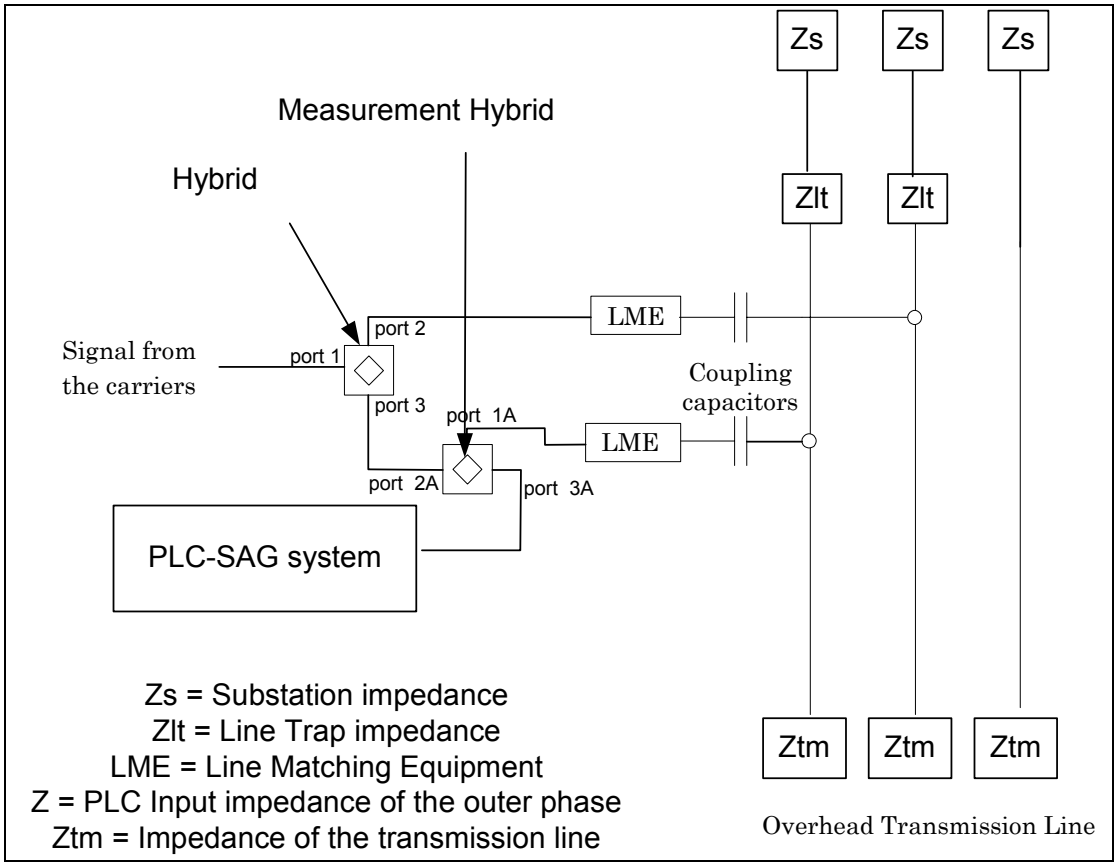

Figure 4.4 Measurement Hybrid for the PLC-SAG system

The function of the hybrid is the same as described in the previous section. The power at Port 1A is divided to Port 2A and Port 3A for a well terminated hybrid and Port 2A will be isolated from Port 3A (More detail about this in Chapter 7). The signal at Port 3A would be coupled to Port 1A with a 3 dB loss and would be isolated from Port 2A. Therefore, a

signal from the PLC-SAG is coupled and decoupled on the outer phase of the system, if the same hybrid topology is used at the remote side.

The coupling relationship between the centre phase and outer phase is also affected. The signal at Port 3, from the carrier, is attenuated by an extra 3 dB before it is coupled to the outer phase via the measurement hybrid. The effective coupling configuration for the carrier signals therefore changes from Equation 2.4 to the coupling configuration shown in Equation 4.1.

$$V_a = \begin{bmatrix} V_{p1} \\ V_{p2} \\ V_{p3} \end{bmatrix} = \begin{bmatrix} -1/\sqrt{2} \\ 1 \\ 0 \end{bmatrix} \qquad 4.1$$

It can be noted that the only difference between Equation 2.4 and Equation 4.1 is a factor $\sqrt{2}$ in the amplitude of V_{p1}. This factor is due to the power splitting characteristic of the hybrid.

In Chapter 2 the modal power distribution between the modes for the standard coupling configuration (Figure 4.3) was computed to be 75% Mode 1 (least attenuated), 25% mode 2 and 0% Mode 3. The modal power for the coupling configuration in Equation 4.1 was computed to be 81.4% mode 1, 16.7% mode 2 and 1.9% mode 3. It is clearly evident that more power is coupled to Mode 1 via the changed coupling configuration (Equation 4.1) when compared to the standard coupling configuration. Therefore, it is no surprise that more detailed simulations proved that the PLC system's reliability is not compromised by adding the measurement hybrid on the outer phase. In fact, in some cases the overall system attenuation is better, where the 3 dB loss in the outer phases due to the measurement hybrid is more than compensated for by the lesser OHTL loss, due to the more efficient coupling configuration. Photograph 4.1 shows an installed additional hybrid.

In the next section, the transmitter installation at Tutuka Power Station will be described. The transmitter was connected to Port 3A (Figure 4.4) at the sending station and the receiver, at the remote station, was also connected to Port 3A. As mentioned before, the measurement hybrid installations were similar at both stations.

Photograph 4.1 Installation of a measurement hybrid

4.3 Case 2: Transmitter at Tutuka Power Station

The main function of the Tutuka installation was to couple 10 different experimental tones sequentially on the outer phase of the OHTL. The different frequencies are given in Chapter 3.

Figure 4.5 shows the circuit diagram of the installation at Tutuka. The dotted square in the Figure contains all the apparatus in the PLC system, which was added for the experiment.

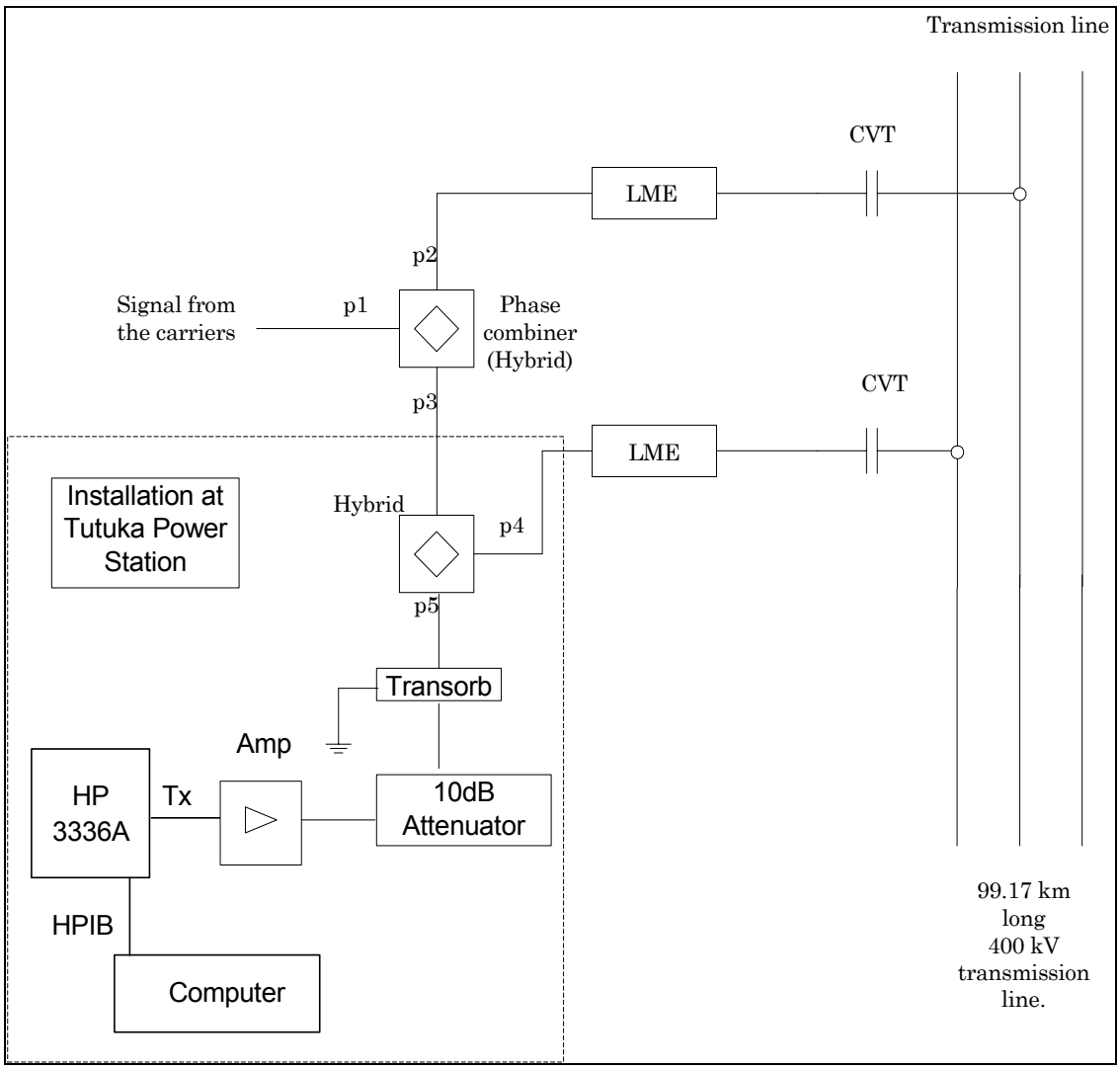

Figure 4.5 Layout of the stand-alone installation at Tutuka PS

Three main components or groups of components can be identified in the dotted square: an additional hybrid (already discussed in Section 4.2), protection devices and a signal generator under computer control.

The following protection devices were additionally installed to protect the HP 3336A transmitter from the harsh electrical environment:

- Transorb
- Amplifier
- Attenuator

4.3.1 Transorb

A Transorb is a fast acting standard protection device. The Transorb from *Clear Line* (Model 12-00109 datasheet in Appendix C) was chosen. It clamps the voltage magnitude at 5V and has a low insertion loss.

4.3.2 Amplifier

The reason for inserting an amplifier was twofold.

Firstly, the internal amplifier of signal generators in general seems to be very sensitive to incoming power. The amplifier, together with an attenuator and Transorb, was inserted between the PLC system and the signal generator. This was done to protect the signal generator from the incoming power and surges from the OHTL.

Secondly, due to the nature of the experiment, frequent relay switching occurs in the signal generator (approximately 4000 times per day). By inserting the amplifier the stress on the signal generator is reduced, since the switched power level in the signal generator is reduced.

The characteristic impedance of the amplifier is 50 Ω and it has a Voltage Standing Wave Ratio (VSWR) of 1.65 at the PLC frequencies. More detail of the amplifier is given in Appendix C.

4.3.3 Attenuator in the transmitter circuit

The main function of the attenuator in the experimental setup as shown in Figure 4.5 was to match the 50 Ω characteristic impedance of the amplifier to the 75 Ω characteristic impedance of the PLC system. A secondary function is to attenuate all power levels from the PLC system so that the amplifier's output is protected. The mathematics that relates to the matching of the amplifier will now be discussed.

Equation 4.2 shows the relationship between VSWR and the magnitude of the reflection coefficient ($|\Gamma|$)[2].

$$|\Gamma| = \frac{VSWR - 1}{VSWR + 1} \tag{4.2}$$

where

$$\Gamma = |\Gamma| e^{j\theta} \tag{4.3}$$

Applying Equation 4.2, to the worst case VSWR = 1.65 of ZHL-32A amplifier from *Mini Circuits* (Appendix C), the worst-case magnitude of the reflection coefficient is 0.245.

The impedance can now be formulated as [2]:

$$Z_L = Z_0 \frac{1 + \Gamma}{1 - \Gamma} \tag{4.4}$$

By inserting Equation 4.3 and $Z_0 = 50\Omega$ into Equation 4.4, for a range of θ, the worst-case impedance of the amplifier can be simulated. The result of the simulation is shown in Figure 4.6 (the outer red circle). It can be noted that the impedance varied from approximately 30.25 Ω to 82.5 Ω on the real axis.

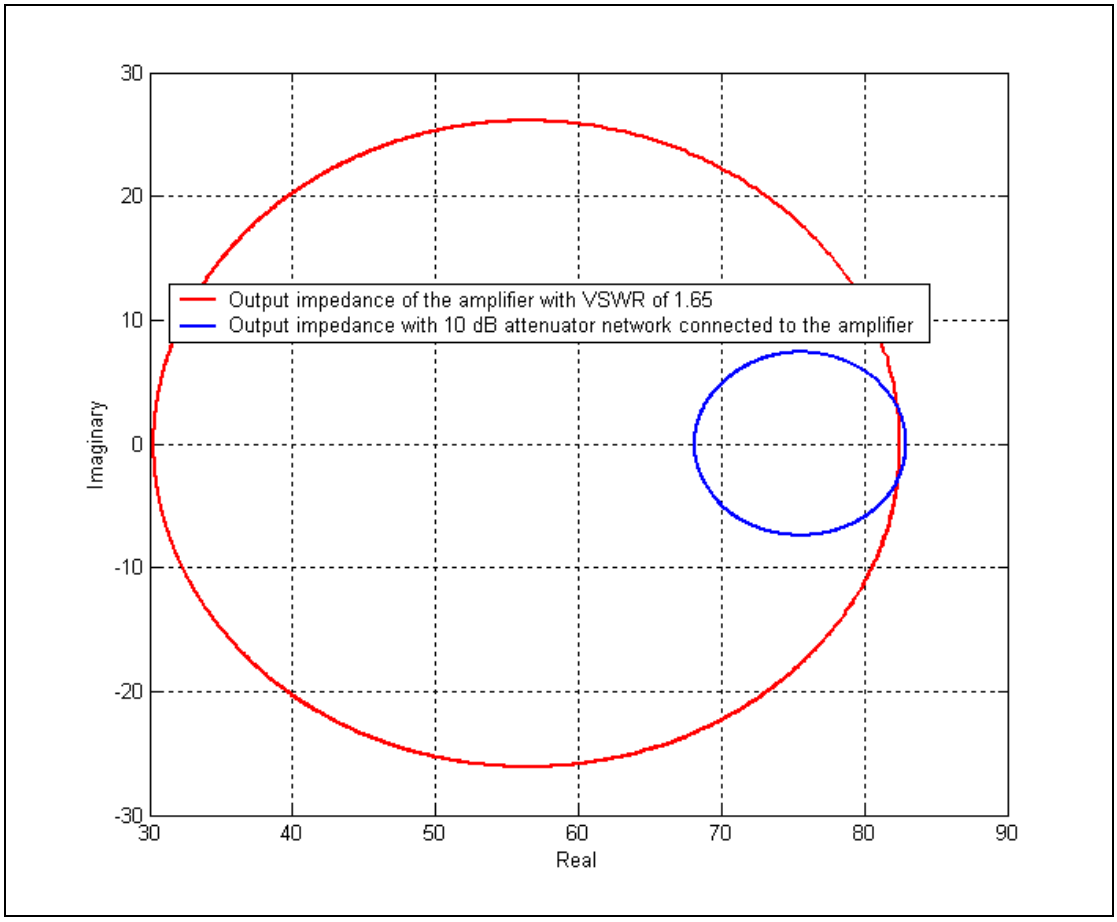

Figure 4.6 Impedance of the amplifier (red circle) and the impedance of the amplifier via a 10 dB attenuator (blue circle)

An attenuator was designed to map this relatively wide range of impedance variation of the amplifier to a smaller range of variation close to 75 Ω. Detail about the design of the attenuator can be found in Appendix C.

The small blue circle around 75 Ω represents the impedance variation of the amplifier if a 10 dB attenuator is coupled to the output of the amplifier.

The worst case Return Loss (RL) of the Amplifier with the attenuator connected in series is 23.36 dB compared to 12.2 dB without the

attenuator. This improvement is important to ensure that the additional hybrid is properly terminated.

4.3.4 Signal generator under computer control

The HP 3336A signal generator is used. This particular signal generator seems to be quite reliable when compared to previous generators used as no problems were experienced. Photograph 4.2 depicts the HP3336A and a HP85 control computer. At Tutuka PS the HP3336A is controlled via a more modern Desktop computer through the Hewlett Packard Interface Bus (HPIB).

Photograph 4.2 An HP3336A signal generator together with an HP85 computer in the Lab

The HP 3336A signal generator is controlled in such a way that tones at specified frequencies are generated sequentially. These tones are each transmitted for 22 seconds. The tone is "blanked" when the generator shifts frequency to generate the following tone. A program was written in HPVEE that controls the instrument, so that it steps through the tones via the HPIB.

4.4 Case 2: Receiver at Kriel Power Station

The installation at Kriel PS is designed to measure the attenuation of the signals transmitted from Tutuka PS in a synchronised way.
Figure 4.7 shows the components (in the dotted square) of the receiver installation. The installation consists mainly of an attenuator, 2 receivers, a computer with instrument control software and a cell phone modem.

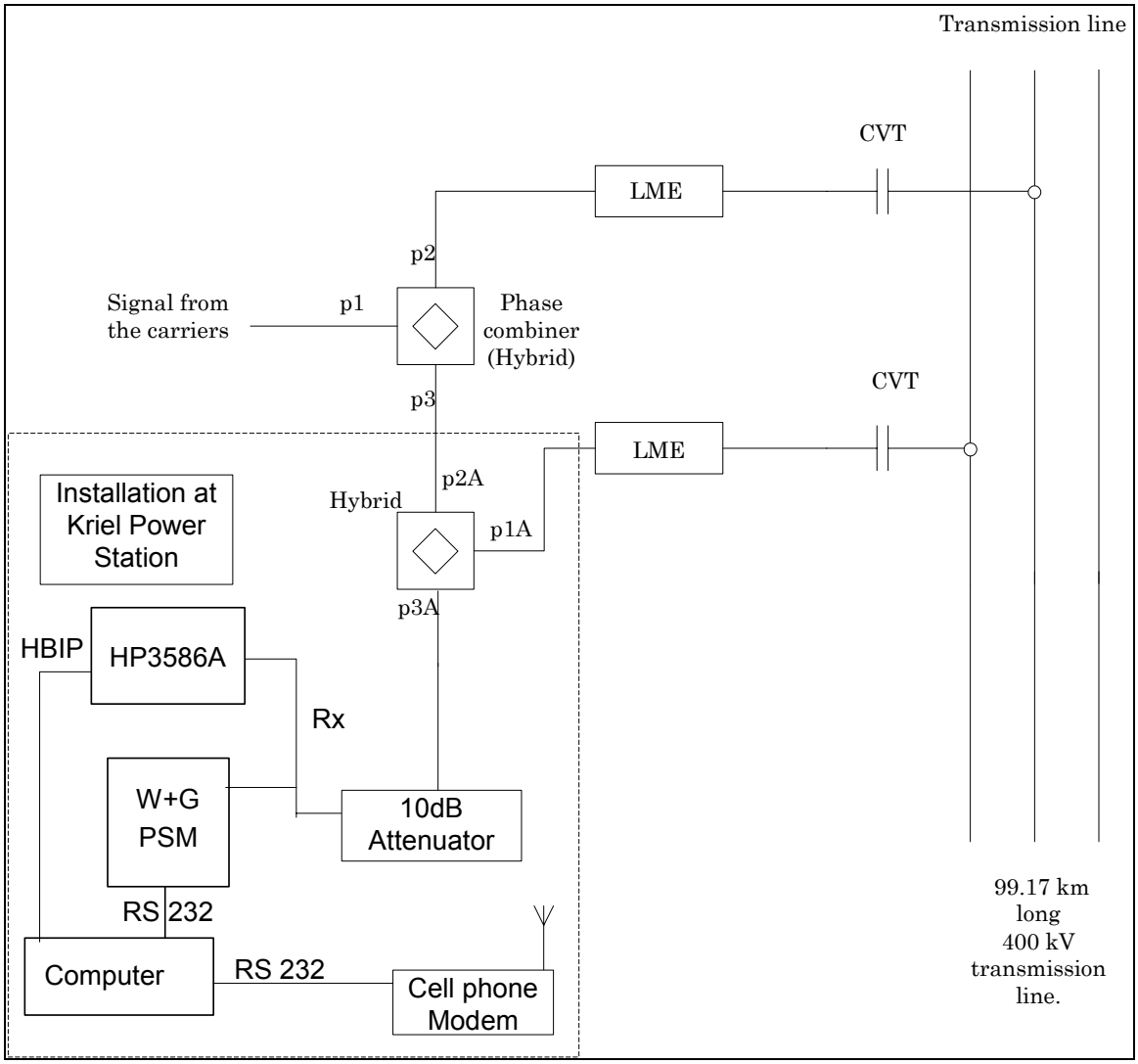

Figure 4.7 Layout of the stand-alone installation at Kriel Power Station

4.4.1 Attenuator in the receiver circuit

It is important to note that the attenuator at Kriel PS is not used as a matching device because the receiver has an impedance of 75Ω. In the receiver circuit the level of attenuation needs to be considered in more detail.

The size of the attenuator was chosen to provide adequate isolation between the local carriers and the sensitive receiver. The power level at the instrument can be calculated as:

$$PL_{In} = P_{Max\_C} - PL_{H\_S} - PL_{H\_M} - PL_{ATT} \qquad 4.5$$

where

PL_{in} = Power Level at the instrument due to the local carriers

P_{Max_c} = Maximum power of the carriers

PL_{S_H} = Power Loss due to the Standard Hybrid

PL_{M_H} = Power Loss due to the Measurement Hybrid

PL_{ATT} = Power Loss due to Attenuator

The carriers only operate for a short duration at the maximum power level when a trip signal is transmitted. At Kriel Power Station 80 Watt (P_{Max_C}) carriers are installed. The loss of the Standard Hybrid between P1 and P3 is 3 dB (PL_{H_S}) and the loss for the Measurement Hybrid between P2a and P3a is typically 25 dB (PL_{H_M}) if well terminated (Figure 4.7). Therefore, by using Equation 4.5 the Power Level at the instrument (PL_{In}) due to the local carriers is 12.67 mW for a 10 dB attenuator (PL_{ATT}). The instrument can measure up to 1W and therefore the calculated PL_{In} with the 10 dB attenuator is within specification.

4.4.2 Receivers

The direct height experimental measurement, which is the main experiment in this thesis (discussed in the following Chapter), was quite an expensive exercise due to the number of people required in the field for the measurement. It was therefore crucial that the PLC-SAG hardware was fully functional at the time of the physical direct height measurement. Due to the experimental nature of the hardware, frequency errors and failures occurred. To minimize the risk of experimental failure during the direct height measurement, two receivers were installed at Kriel Power Station. In Figure 4.7 the two receivers (selective voltmeters), Hewlett Packard (HP) HP3586A and Wandel & Goltermann (WG) PSM-137 are shown. The HP was configured to provide 75 Ω terminations and the WG measured via the high-impedance port. This was done to prevent double termination. More detail on general settings of the PSM-137 and HP 3586A are given in Appendix C.

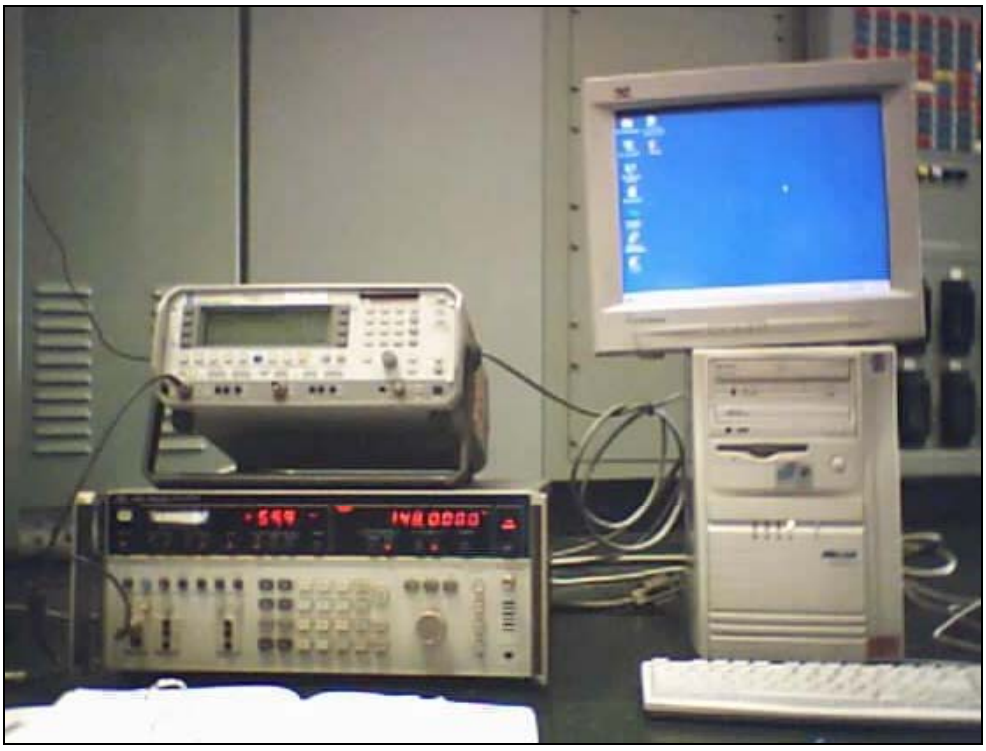

Photograph 4.3 The HP 3586A (left/bottom) and Wandel & Goltermann PSM-137 (left/top) under computer control - testing the system.

Photograph 4.3 depicts the HP 3586A and PSM-137 during system tests, before actually being installed in a cabinet.

The receiver control is more complex than the transmitter control program and will be discussed in the following section.

4.4.3 Receiver control program

The aim of the receiver is to measure the received level of the PLC-SAG monitoring tones as accurately as possible.

The frequency scan in Chapter 3 was done once at a specific time. It is possible that there could be non-continuous 'noise' or impulsive noise from other systems in the identified bands, which the frequency scans failed to identify. To establish whether or not there is noise, a noise measurement in each band was done before the PLC-SAG tone was activated and measured. If no unwanted signals had been detected for a period of time, the system could be changed to monitor only the received levels of the PLC-SAG tones. The reason for changing the system is to get the maximum number of measurements of a specific tone in the 22 seconds that it is transmitted. The individual measurements can then be 'stacked' to improve the signal to noise ratio and to produce a better reading than a single measurement would give.

These two measurement procedures can be alternated via software change only. First the combined noise and tone measurement procedure will be discussed and then the procedure for the tone measurement only.

<u>The combined noise and tone software</u>

The receivers were programmed (using HPVEE) in such a way that they would automatically synchronize with the transmitter using the transmitter signals. Therefore, no additional communication between the transmitter and receiver was necessary. Steps A to F in Figure 4.8 are the basic steps in the measurement cycle (number of cycles equals the number of tones).

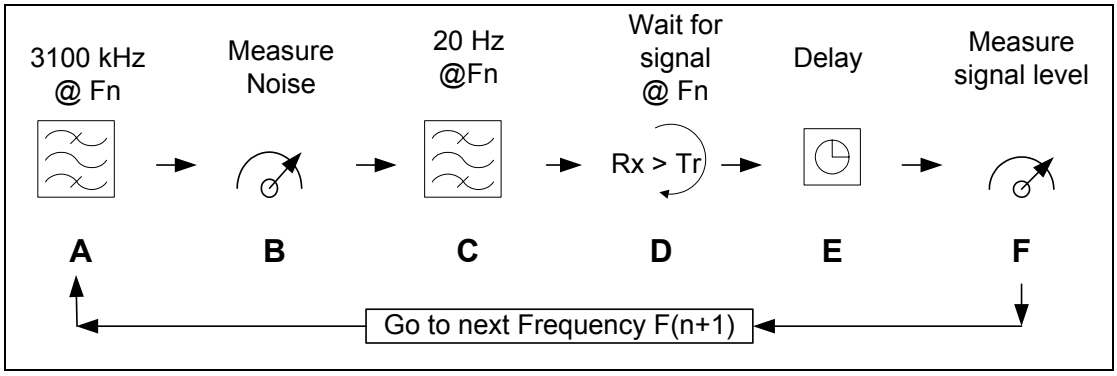

Figure 4.8 Steps in the measurement cycle, which measure noise and the received level.

The steps in Figure 4.8 explain the receiver's activities and modes. The cycle of the transmitter is also included for clarity in the following explanation:

A – Transmitter: Signal is transmitted at the previous frequency (F_{n-1})[3] in the cycle.
Receiver: Change the centre frequency of the noise filter to F_n.

B – Transmitter: Signal is transmitted at the previous frequency (F_{n-1}) in the cycle.
Receiver: Measure the noise at frequency F_n with the 3.1 kHz filter.

[3] F_n is the n^{th} frequency and $n \in [1,2,3...10]$

C – Transmitter: Signal is transmitted at the previous frequency in the cycle.
Receiver: Change the type of filter to the 20 Hz/25 Hz selective filter.

D- Transmitter: Change frequency to F_n with a soft blanked action.
Receiver: Test the received signal level each second. If the level of the received signal is more than the threshold of -45 dBm then it will step to E.

E- Transmitter: Signal is transmitted at F_n.
Receiver: Cycle is delayed by 1 second. The reason for this delay is the fact that the transmitter is soft blanked. The level of the transmitter could be greater than the threshold, and therefore detected in step D, but not yet at full power.

F- Transmitter: Signal is transmitted at F_n.
Receiver: Measures the received signal level at F_n.

While the transmitter is still activated at F_n the receiver goes back to step A to measure the noise at $F_{(n+1)}$. The transmitter tone will be delayed for long enough (22 seconds between tones) for the receiver to perform steps A to D and wait (at step D) for the next tone. This loop will continue to measure the noise and signal levels for the duration of the experiment.

<u>Tone measurement only</u>

Measurement results for both case studies proved that the frequency regions had been well identified. No unexpected noise occurred in those frequency regions.

Eliminating steps A and B changed the measurement cycle as shown in Figure 4.8. The time gained by skipping steps A and B was utilised by repeating step F five times. Thus the PLC-SAG tone results obtained in the main experiment, discussed in the following Chapters, were the raw data average from 5 repeated measurements (Step F) of the relevant tone.

The last hardware component in the receiver is the industrial cell phone, which will now be discussed.

4.4.4 Industrial cell phone

The control program (In HPVEE) stored the measured levels in a data file. This file size becomes larger as more and more measurements accumulate.

The main power supply of the computer is connected to a timer. The timer switches the computer off once a week, for approximately 10 minutes at midnight. As the computer program restarts, a new set of data files is generated.

These files were then downloaded via the cell phone, which was convenient, as downloading could be performed at any time and place.

The remote computer (with the external cell phone connected) and the local computer interface were controlled by a software package called *PCAnyWhere*. The software needs to be installed on both computers. In this KT case study the remote computer was at the Kriel Power Station together with the rest of the PLC-SAG receive system. The local computer was in Stellenbosch most of the time. The local computer communicates with the remote computer to enable data download or PLC-SAG software updates.

4.5 Conclusions

For both case studies, a simplex logging methodology was used as explained by Figure 4.1.

Due to the nature of the hardware (equipment designed to work in laboratories) frequent hardware failures occurred. Adding extra protective devices to the system, additional to the standard PLC protection devices, improved the robustness of the experimental installations. Two receivers were installed at Kriel Power Station to increase the reliability of the installations.

Both experimental installations of the two case studies were fully operational during the direct height measurement, which was essential. The direct height measurement will be discussed in the following chapter. The results from the logging stations will be presented in Chapter 6, as they will be compared to the simulations and the direct height measurements.

References:

[1] **De Villiers, W.**, *Prediction and measurement of Power Line Carrier signal attenuation and fluctuation*, MScEng Thesis, University of Stellenbosch, November 2001.
[2] **R.E. Ziemer** and **W.H. Tranter**, *Principles of Communications*, Fourth Edition, John Wiley & Sons, 1988.

Chapter 5

Direct height measurements

5.1 Introduction

This chapter focuses on measuring the average conductor height of the whole OHTL. The average height variation of the conductor above the ground is estimated by taking the average of three direct height measurements of well-spaced spans.

The measurement commenced by selecting an appropriate instrument. Four instruments were tested on a live OHTL trial. These tests and the associated finding will be discussed in Section 5.2.

The average height measurement methodology will be introduced in Section 5.3. The methodology comprises i) selecting appropriate sites, ii) marking the specific measuring points with pegs, iii) surveying the span and iv) performing continuous direct conductor height measurements. The four steps will be further discussed, as applied to each case study, in Section 5.4 to Section 5.7.

The transformation of the individual height measurements to the average height of the OHTL is discussed in Section 5.8.

5.2 Different instruments considered for the direct height measurements

The four measurement devices shown in Photograph 5.1 were tested to determine which type of instrument would be used for the planned conductor height measurements. The devices represent three different technologies.

Photograph 5.1 Four instruments (from left to right) Theodolite, Laser meter (Disto), Laser meter (Trimble) and Ultrasonic meter (Suparuler).

The Theodolite measures angles optically. From these angles, the height of the conductor can be computed. The laser meters determine distance directly via reflections from the object, obtained by illuminating the object with a class 2 laser. The principal of the Ultrasonic meter is the same as that of the laser, but uses reflections from ultrasonic sound waves.

The live OHTL conductor height measurement will now be discussed.

5.2.1 Setup for the direct height measurement

The height variation of the conductor between towers 2 and 3 of the 400 kV transmission line between Acacia Substation and Koeberg Power Station was measured. Measurement stations were placed underneath the outer conductor of the phase bundle. In total, three measurement stations were defined. Two of the stations were directly beneath the outer conductor of the transmission line's phase bundle, and the third station was approximately 30 m to the side of the outer bundle of the OHTL. Photograph 5.2 shows the three measuring stations on the yellow tripods. The stations were named, from left to right, Station A, B and C.

Photograph 5.2 Three measurement stations

5.2.2 Measurements

During the execution of the measurements the following was noted. The theodolite was difficult to set up, especially in the sandy environment of the KA OHTL. Both the theodolite and the laser meters were difficult to operate in windy conditions.

Figure 5.1 shows the results from the four different measurement devices, all referred to measurement Station A. Five measurement results can be noted in Figure 5.1 obtained from the two fixed lasers at stations A and B (which were on tripods), the theodolite (also on a tripod) at measurement station C and the handheld ultrasonic meter at stations A and B.

It can be noted that all the data have not continuous. Measurements from the ultrasonic instrument indicated the most interruption; the reason is uncertain, but the instrument gave frequent errors. The laser meter at station A (Trimble) did not produce any readings between 7:15 and 8:00. At that stage, some level of moisture affected all the instruments. After the moisture evaporated the instruments seemed to work correctly. A strong wind appeared at 15:30. The Disto laser at Station A was unable to measure the conductor height in the strong windy conditions (around 17:00). Due to a difficult setup procedure, the theodolite was only operational from midday onwards.

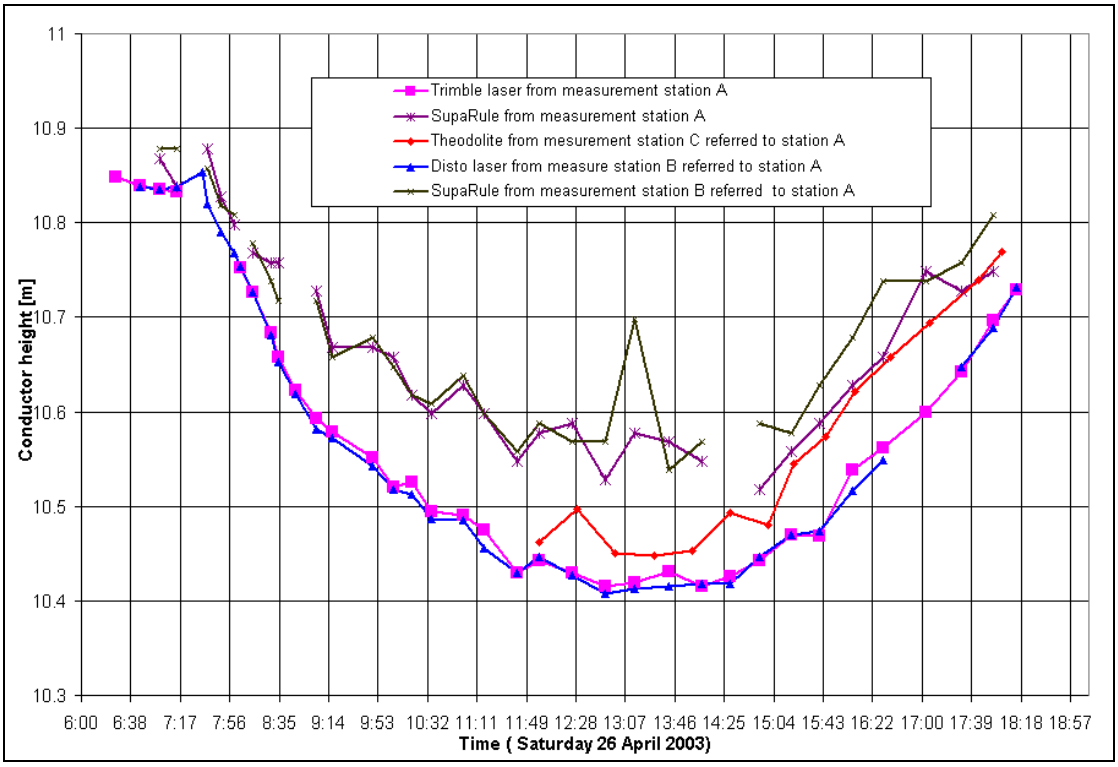

Figure 5.1 Conductor heights, measured on Saturday 26 April 2003, via the four different instruments

From Figure 5.1, it can be seen that the two laser instruments correlate the best with each other. The correlation between the ultrasonic measurement and the lasers was close during the early morning. The variation between subsequent measurements was greatest for the ultrasonic measurements. Although the device was not mounted on a tripod (as were the other instruments), great care was taken to position it accurately for the measurements. Results from the theodolite and the lasers showed a relatively small average difference of approximately 5 cm between 12:00 and 15:00. After the wind strengthened the difference increased.

5.2.3 Conclusion of the OHTL conductor height measurement trial

It was concluded that the laser devices were the best, considering accuracy, cost, robustness, reliability and operational simplicity. More specifically a *'Disto™ pro'* laser was chosen which is manufactured by Leica Geosystems.

The only concern when using the laser meter was the fact that unreliable measurement occurred during windy conditions. It was later found that the laser instrument could be purchased with an additional telescopic viewer, which enabled the laser operator to 'track' the conductor in windy conditions. This worked well, as the direct height measured data presented later in this thesis are uninterrupted, unlike the data presented in Figure 5.1.

Photograph 5.3 shows the laser meter with the telescopic viewer. Three lasers (all the same make and model - *'Disto™ pro'*), with telescopic viewers, were used from then onwards in the research to measure the height of the OHTL conductor.

Photograph 5.3 *'Disto™ pro'* laser with telescopic viewer

5.3 The measurement methodology

The following are steps in the methodology used to measure the average height of the OHTL for the two case studies.

Step 1) Select three OHTL spans that are relatively long, easily accessible and well spaced from one other.

Step 2) Determine more or less the centre point of the span and then find an easily identifiable point on the conductor itself to be measured. This easily identifiable point is called the upper 'fixed' point, which cannot move in the direction of the transmission line. The conductor spacer keeps the individual conductors of a bundle conductor in place. It is ideal to choose the phase combiner as the upper 'fixed' point on the conductor. Mark the location directly underneath the upper fixed point with a peg. Now there are two 'fixed' points, the upper located on the conductor itself and the lower being the peg on the ground. The height movement of the upper point relative to the peg can now be measured. If the experiment is repeated on a different day, using the same 'fixed'

measurement points minimizes the setup differences between the two days.

Step 3) Survey the site to refer all the dimensions of the span to the newly planted survey peg of step 2.

Step 4) Perform 3 uninterrupted height measurements (to obtain an average height measurement) at three sites simultaneously, every 5 minutes for two days. The two days on which measurements were taken were not consecutive, since the three teams (2 people per measuring site) were exhausted after the first day. The three consecutive measurements every 5 minutes are documented and time stamped. GPS time was used to eliminate time related errors.

The data harvested via the above procedure can be transformed into the average height variation of that specific span. The height data sets from the three sites are then averaged to get a good estimation of the average height variation of the whole transmission line. This methodology will be discussed in more detail when applied to the two case studies.

5.4 Step 1: Site selection

The two transmission lines (case studies) were introduced to the reader in Chapter 3. Detailed maps of the transmission lines are provided in Figure 3.1 and Figure 3.2. Referring to Figure 3.1 and Figure 3.2, waypoints CA1, CA2 and CA3 represent the three calibration locations along the OHTL. "CA1" is an abbreviation that stands for **CA**libration site **1**.

The measurement sites are referred to as "calibration" sites because the results of the height experiment will be used to calibrate the PLC-SAG system. In an operational PLC-SAG system the experimental height measurement procedure, which is discussed in this chapter, forms part of the calibration procedure of the system.

The following factors need to be considered when locating the sites:

- Preferably close to a road and easily accessible. It can be noted, in studying Figure 3.1 and Figure 3.2, that all six CA sites were located close to a nearby road.
- Sites should be well spaced from each other, but must represent the whole transmission line.
- The span on which height measurements are to be made has to be relatively long, since this increases the measurement sensitivity.

5.4.1 Case 1: Koeberg-Acacia (KA)

In Figure 5.2 the calibration sites are plotted next to each other as a function of distance along the length of the OHTL. From Figure 5.2, it can be seen that the sites are well spaced. The span lengths of the relevant spans are given, also indicated in Figure 5.2. The span lengths of CA1 and CA3 are longer than the ruling span (347.36m, as computed in Chapter 3 for the simulation) and the CA2 span is 2.2m shorter. The tower number in the figure is shown as KA X, which represents Koeberg-Acacia tower number X. The towers are numbered from Acacia to Koeberg and not from Koeberg to Acacia as one might have deduced from the sequence of the 'K' and the 'A'.

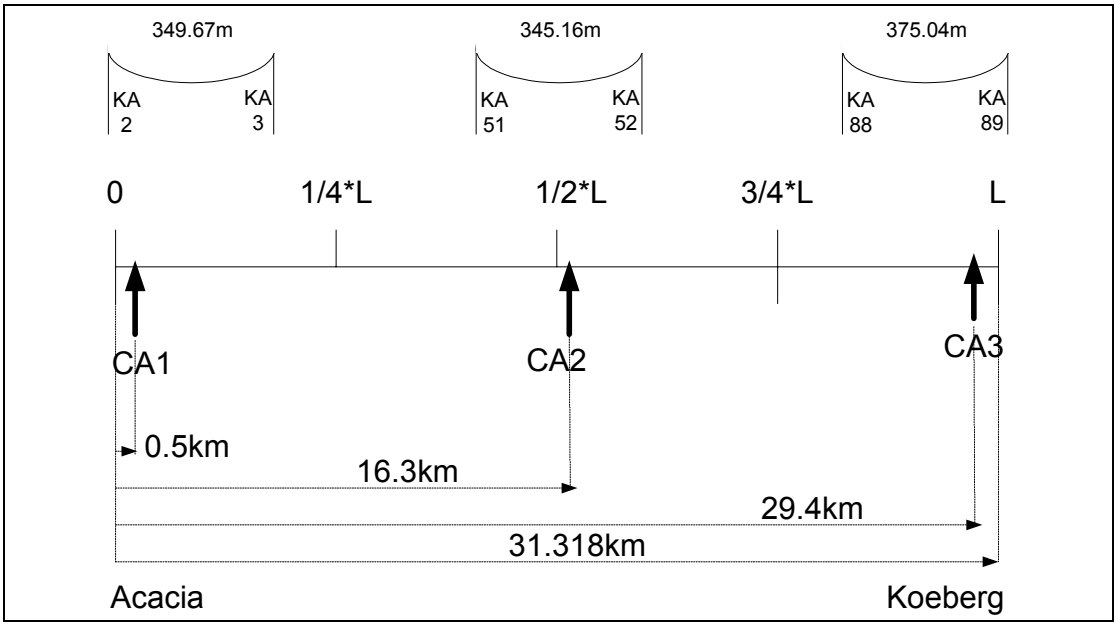

Figure 5.2 Locations of the calibration points on the 400 kV Koeberg-Acacia transmission line as a function of length.

5.4.2 Case 2: Kriel-Tutuka (KT)

The KT OHTL is 99.5 km long and is therefore approximately three times longer than the KA OHTL. Figure 5.3 shows the locations of the different CA sites. All the spans are longer than the ruling span (404.157m) of the OHTL.

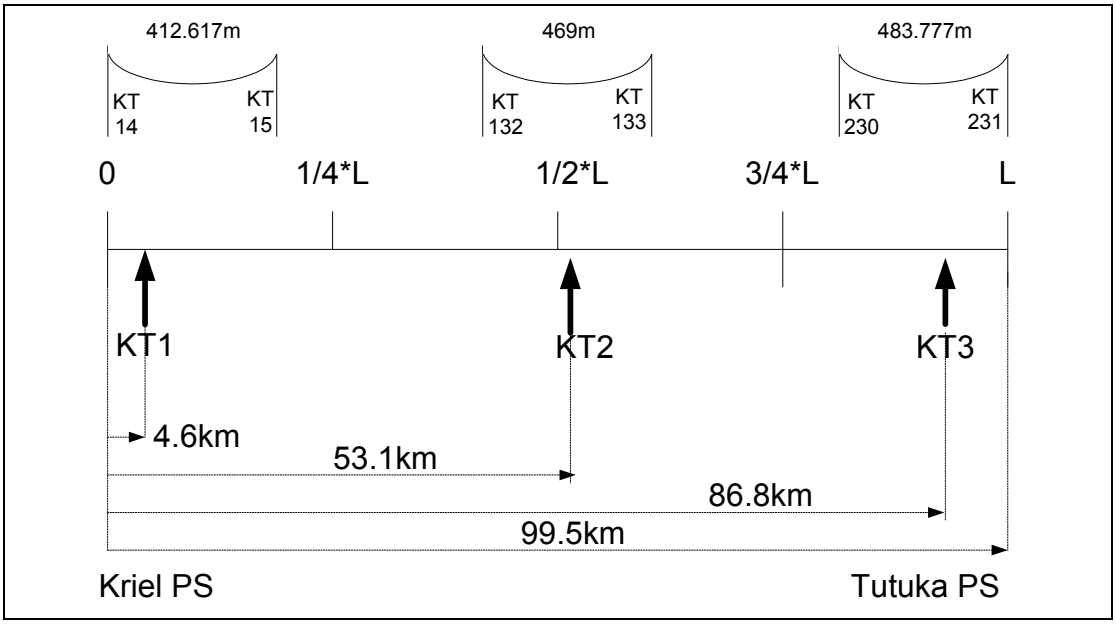

Figure 5.3 Locations of the calibration points on the 400 kV Kriel-Tutuka transmission line.

The following step in the average height measurement methodology will now be discussed.

5.5 Step 2: Marking measurement points at selected sites

Once the CA site is selected, the upper and lower 'fixed' points need to be established by locating the approximate centre of the span. The spans are in the order of 450 m long and one cannot rely on a naked eye judgement. Photograph 5.4 depicts an instrument (Bushnell Range Finder), which can assist in obtaining an indication of the centre point of the span.

Photograph 5.4 Bushnell range finder

After the centre of the span is identified, the closest bundle combiner needs to be located. Directly under the conductor spacer, a peg can be planted. The selection of the peg depends on the type of soil. Photograph 5.5 depicts the peg that was used in the KT OHTL's hard muddy type of soil. At KA, the soil is sandier; therefore longer thinner pegs were used. The top of the peg was marked with red paint for easy identification.

Photograph 5.5 Showing a peg made of railway sleeper (used as the lower 'fixed' point) together with the laser meter

The laser meter can then be set up above the peg for measurements. The laser meter is aimed at the conductor spacer (the upper fixed point) Photograph 5.6 depicts the red laser dot of the instrument aimed at the conductor where the phase combiner is located.

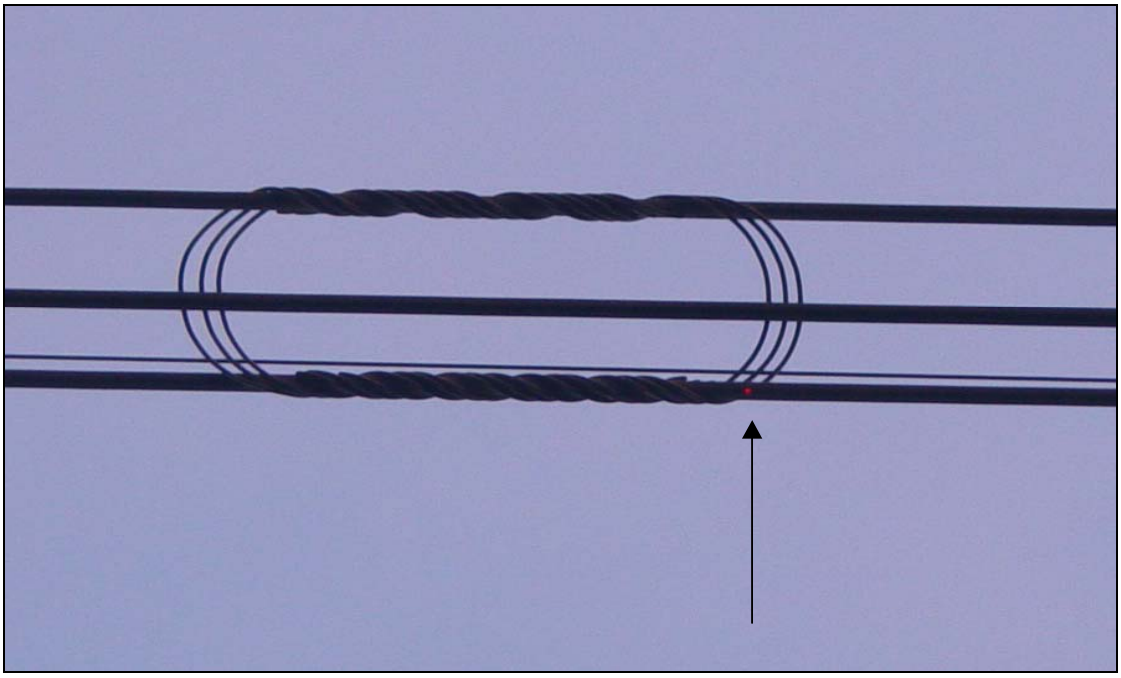

Photograph 5.6 Location where the conductor height was measured – the red dot on the outer phase of the conductor. (Used as the upper 'fixed' point)

5.6 Step 3: Measurement site survey

In the Tables in Appendix A, details of the spans are given. It is difficult to apply all the span detail available to the newly planted peg. Therefore a site survey was conducted to obtain accurate data, which is correctly referred to the newly planted survey pegs.

At the first sites measured (CA1-CA3 at KT) a level meter (dumpy-meter), laser meter and a "range finder" were used. It took one day to measure two

sites because the range of the dumpy level meter is only approximately 70 m. During the second set of survey measurements for KA, a "total station" was used which can measure longer distances. Using the 'total station' all three sites can easily be surveyed in one day. Figure 5.4 shows all the relevant lengths (A-D) to be measured during the survey. E is the height difference between the upper and lower 'fixed' points, which is measured to compute the average height variation.

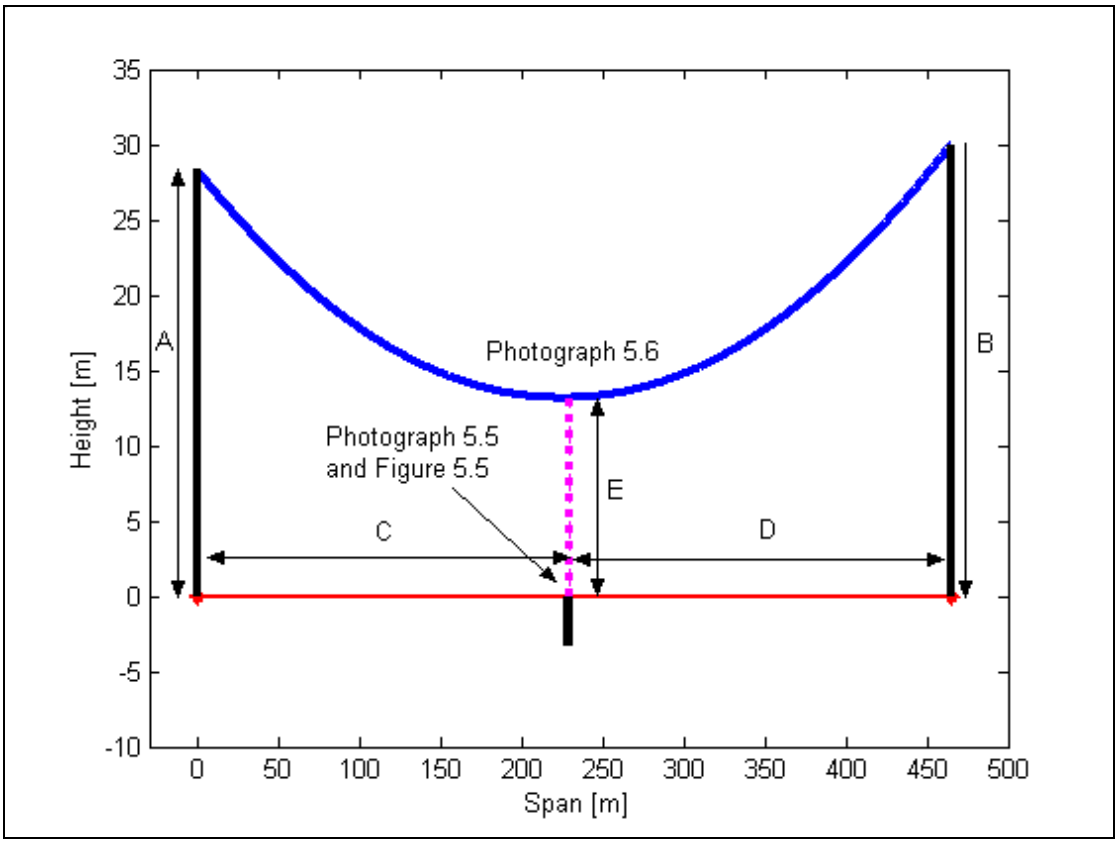

Figure 5.4 Dimensions of a typical span

The results of the surveys are tabled in Table 5.1

Table 5.1 Dimensions of the various sites

Length as Figure 4.3 shows	A	B	C	D	Length of Tower A	Length of Tower B
KA - CA1	18.1085	21.1085	180	164	25	28.2
KA - CA2	16.729	25.101	169	174	19.9	22.95
KA - CA3	23.163	17.616	237	139	27.9	25.8
KT - CA1	20.2	26.827	206	208	19.86	25.86
KT - CA2	28.345	29.891	230	236	27	29.5
KT - CA3	27.733	29.981	214	271	19.86	28.86

It can be noted that the summation of C and D does not correlate precisely with the ESKOM data in Appendix A. Lengths A and B cannot be compared with the attachment heights in Appendix A as all the heights in Table 5.1 refer to the newly planted location pegs of each span.

5.7 Step 4: Performing the direct height measurement

The direct height measurement can now be performed. Photograph 5.3 and Photograph 5.5 show the laser mounted on the tripod. It is very important to document the setup height between the bottom of the laser meter and the location peg (Figure 5.5) before the measurements are initiated.

The teams at the calibration sites take three measurements every 5 minutes. All the measurements are written down, each with its exact associated time. Photograph 5.7 shows a team member writing down the results as the laser meter operator calls them out. The instrument operator can easily spot the red dot on the conductor (Photograph 5.6) at night, but it becomes more difficult at midday and in windy conditions. In those conditions the additional telescopic viewer is great help in

measuring accurately. The measured results from the two case studies will now be discussed.

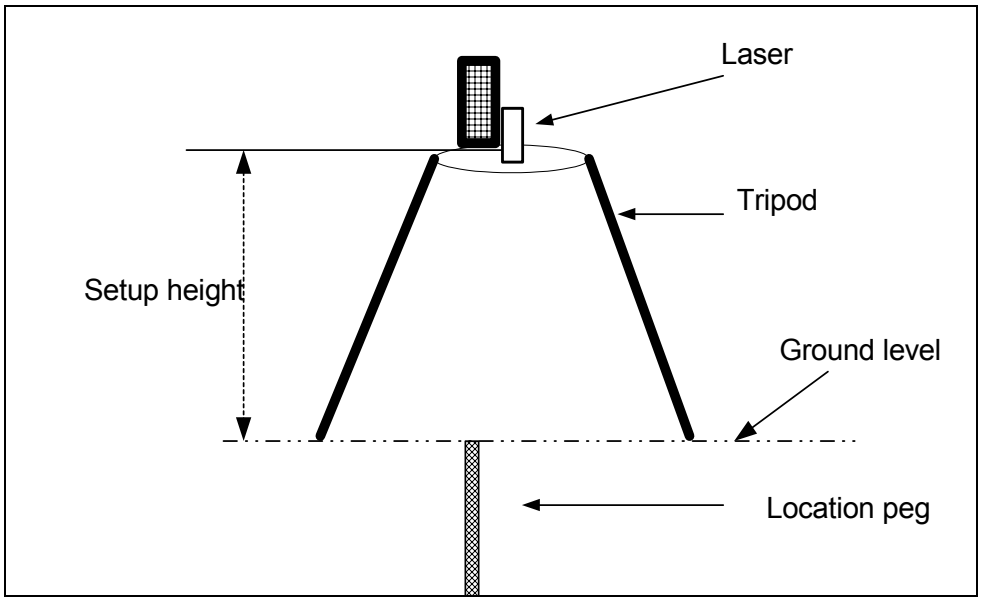

Figure 5.5 Measurement set-up at a site

Photograph 5.7 Mr P Pretorius recording the measurements at KT CA2 with the GPS located on the table for GPS time.

5.7.1Case study: KA (Direct height measurement above peg)

The three CA points on the KA OHTL were measured during two days, 5th and 12th October 2004, from early morning till mid afternoon. The results are plotted in Figure 5.6. The height variations above the pegs cannot be compared directly, due to the different span lengths and measurement points. Generally, it can be noted that the conductor sagged to its maximum on 5th October around 11:30 in the morning. During the next day of measurements the maximum sag occurred noticeably at 11:30, only this time at CA3. The other sites had not sagged to their maximum before the experiment was stopped. This highlights the fact that measuring only one site's height variation could have been misleading in the framework of this study.

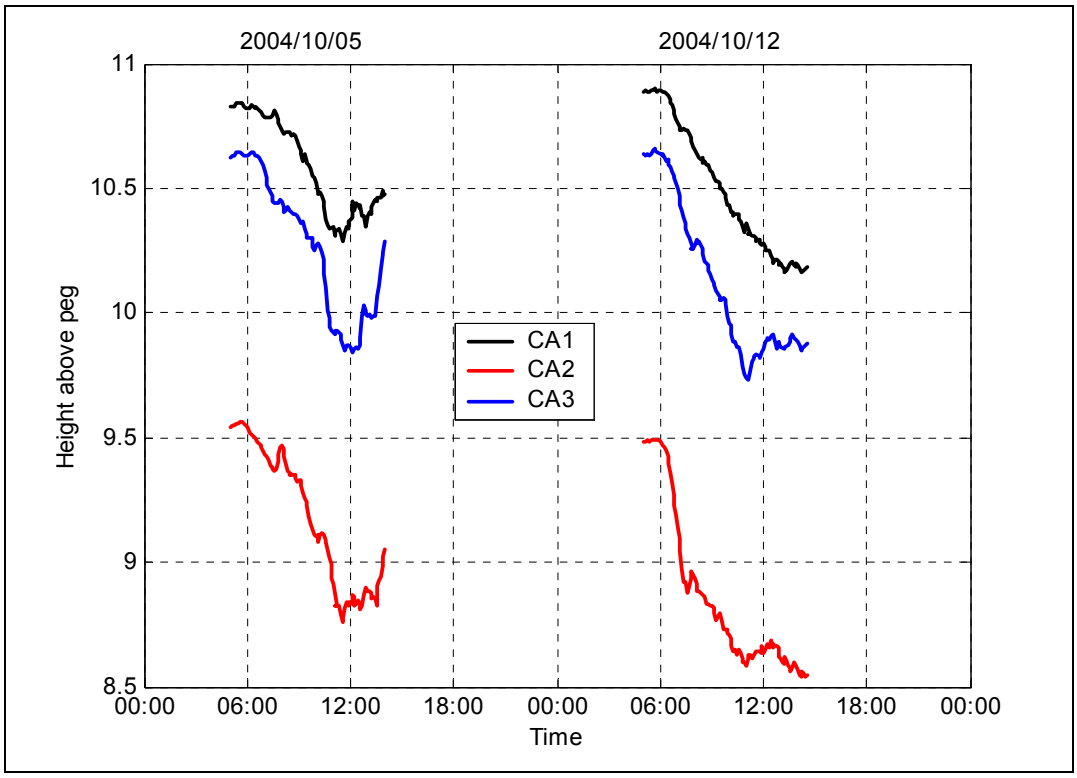

Figure 5.6 Direct height measurement above the pegs of KA

5.7.2 Case study: KT (Direct height measurement above peg)

Figure 5.7 shows the height variation above the three pegs during 4th May and 6th May 2004 for the KT OHTL. Logistics in the KT case study allowed the teams to measure for longer than in the KA case study. Again, relatively big differences can be noted between the times of maximum sag at the different CA points, especially for the second day of measurement.

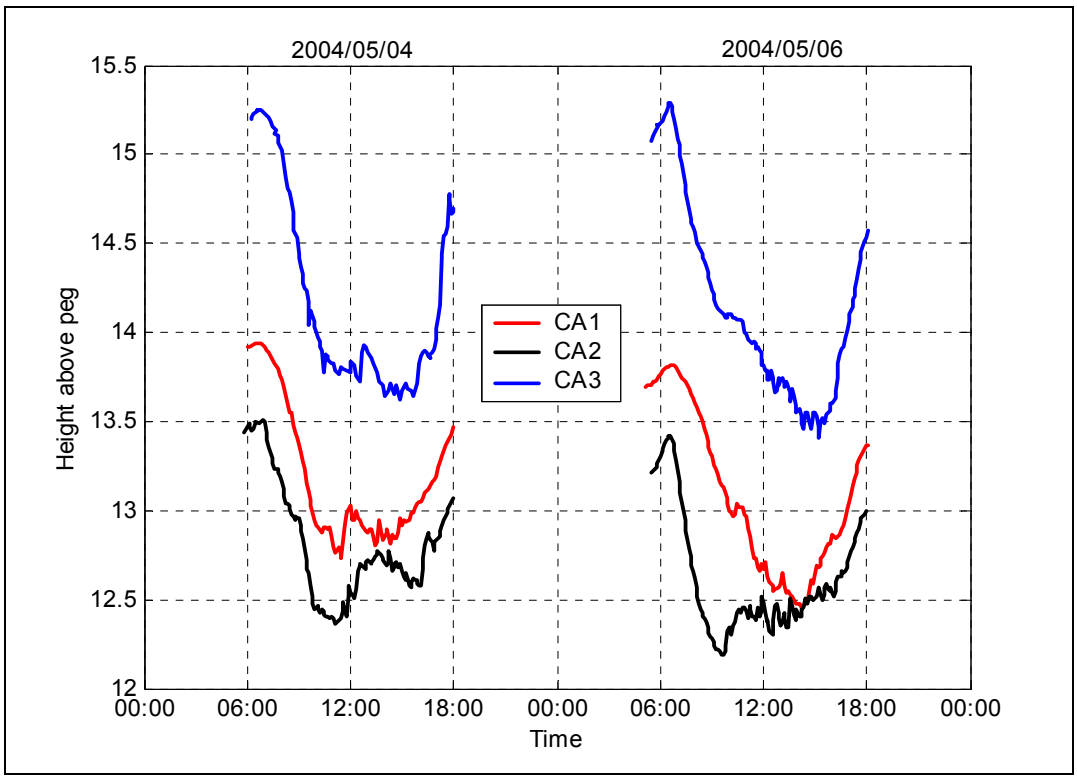

Figure 5.7 Measured height variation at the three KT calibration sites (2004/05/04) and (2004/05/06)

The transformation of the presented results to an average height will be discussed in the next section.

5.8 Transforming to the average height

In order to explain this section, the focus will be on KA CA1 (Figure 5.8). The dotted vertical line in the middle of the graph represents the location where the OHTL conductor height movement was observed. The OHTL conductor is plotted for a range of different heights in Figure 5.8. If the observation point moves, the results of the direct height measurement will be correspondingly different, for the same range of conductor heights. Therefore, the direct height measurements at the sites need to be transformed to the average height measurement of the span.

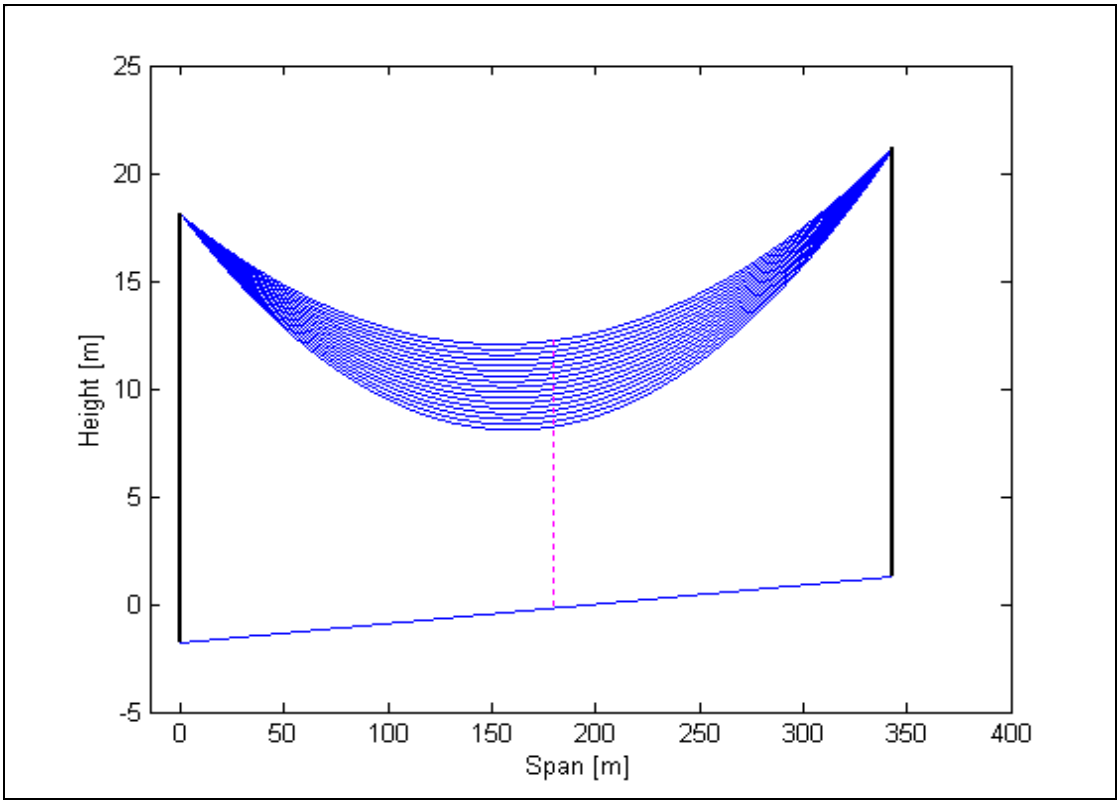

Figure 5.8 Layout of KA - CA1 and measurement point

A program (in MatLab) was written to produce a transformation graph. In the graph the measured data at a specific location along the span (x-axis) is transformed to the average height variation of the span (y-axis). The program is based on typical sag formulas, as described in [1] and needs all

the relevant dimensions as described in Figure 5.4. Figure 5.9 shows the transformation graph for KA CA1. The graph can be used as a lookup table. For example: if the direct height measurement is 9 m (measured 180 m from tower 2) the average height of the span is 12.75 m above an ideal ground plane (an ideal ground plane is a straight line between the two bases of the relevant towers as drawn in Figure 5.8).

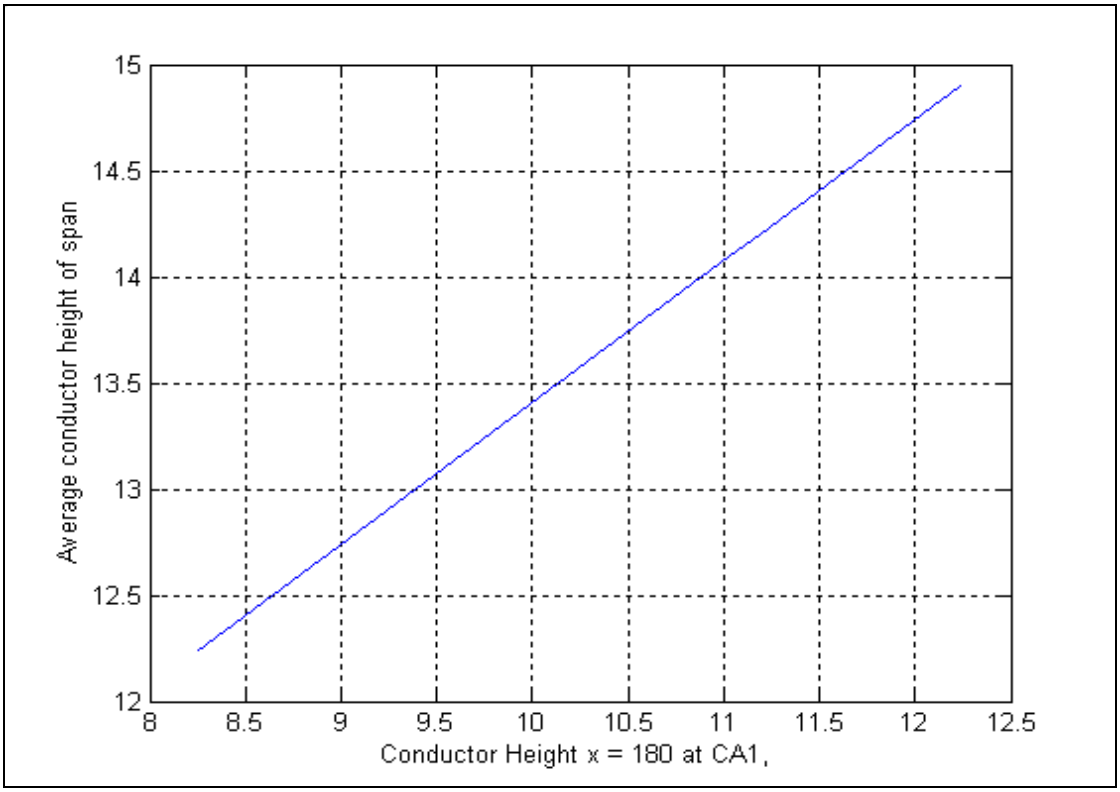

Figure 5.9 Average height movement of the conductor above a perfect ground plane for the calibration point KA - CA1

The three average height data sets for a case study are added and then divided by three to get an estimation of the average height of the whole transmission line. Figure 5.10 and Figure 5.11 shows the estimated average height for the two case studies via three direct height measurement sites per case study. Comparing the two sets of results, it can be noted that there was a greater variation present in the second case study, KT OHTL. From the results it was also evident that the average height of the conductor at KT OHTL was greater than that of the KA

OHTL. It has been confirmed that ESKOM re-tensioned the KT OHTL to a higher rating, due to the importance of the line. This also implies that the average conductor height is higher after the line had been re-tensioned.

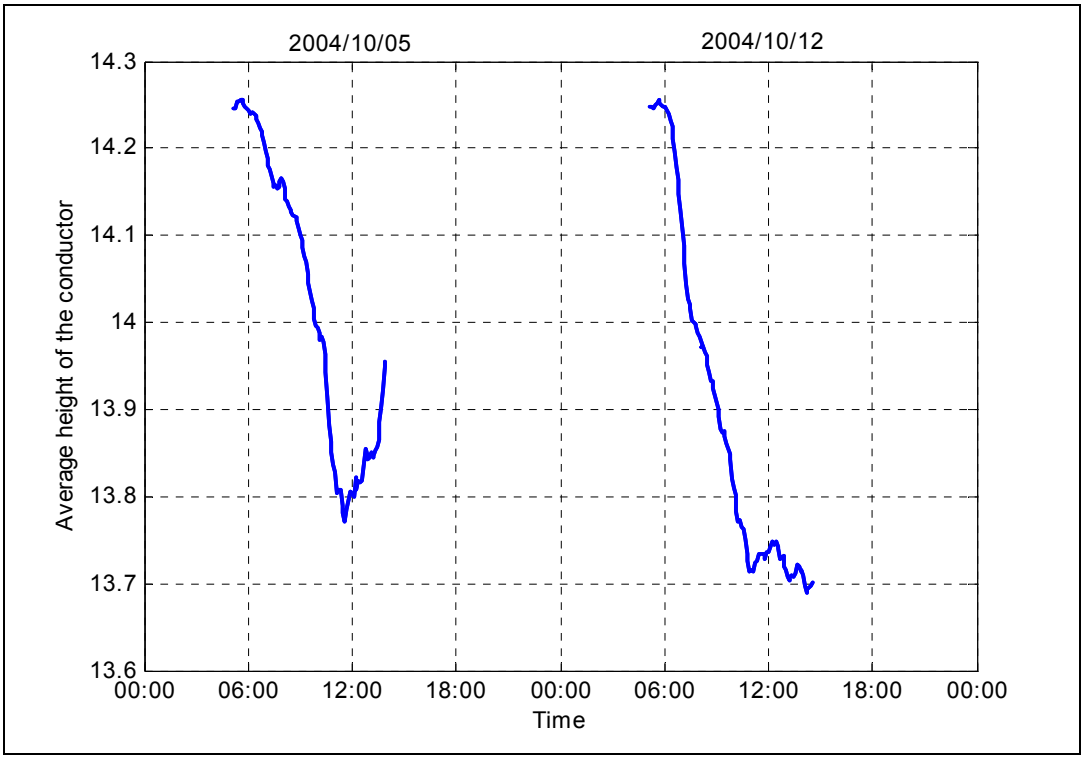

Figure 5.10 Estimated average height variation of the KA OHTL (Case study 1)

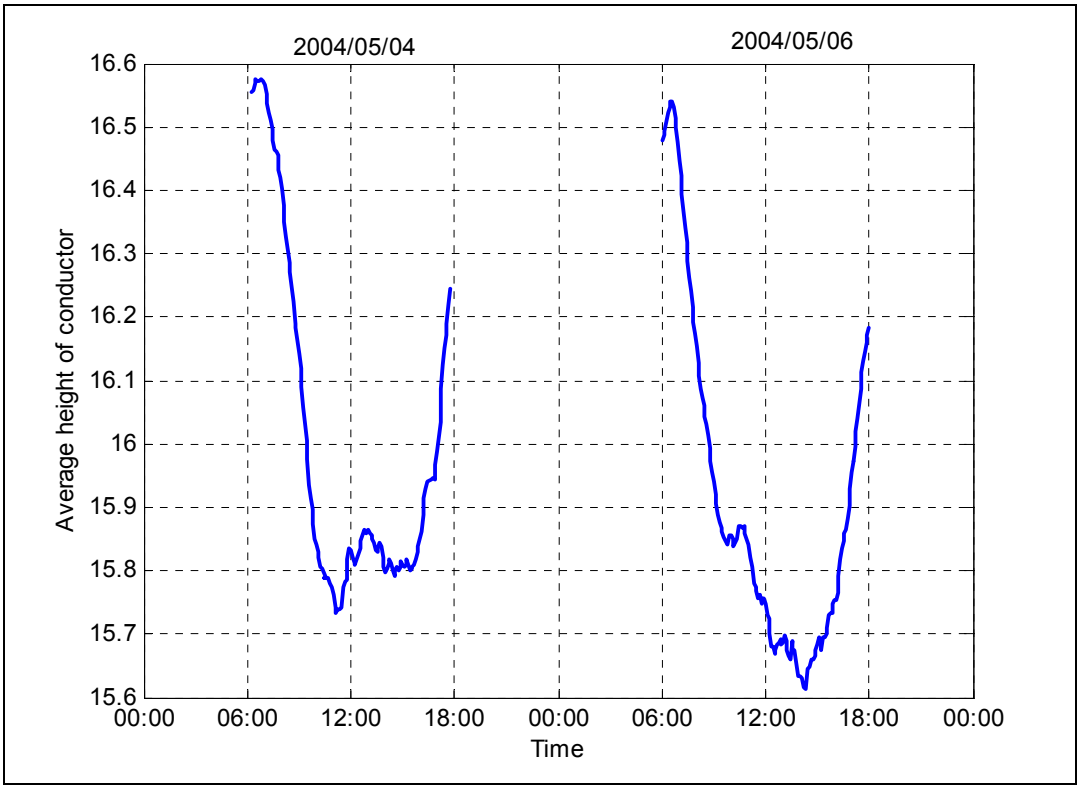

Figure 5.11 Estimated average height variation of the KT OHTL (Case study 2)

The data presented in Figure 5.10 and Figure 5.11 will be frequently referred to as the 'measured average height' of the two case studies. The two PLC-SAG experimental systems were operational during the time of direct height measurement. The following chapter will study the capability of the PLC-SAG system in measuring the average height of the OHTL and the system will be tested against these data sets.

5.9 Conclusions

A laser meter with a telescopic viewer was identified as the most suitable instrument to measure the direct height of the OHTL conductor.

The measurement methodology is discussed step by step, as applied to the two case studies. The methodology can be summarised as determining the site, establishing the specific calibration location at the site, surveying the site and, lastly, measuring the conductor height continuously for a period of approximately 7 to 8 hours on two separate occasions.

The direct height measurements above the peg were transformed to the average height. The data presented in Figure 5.10 and Figure 5.11 will be used in the following chapter and will be compared with the data produced by the PLC-SAG system.

References:

[1] **Turan Gönen**, *Electric power transmission system engineering – Analysis and Design*, John Wiley and Sons, New York, 1988.

Chapter 6

PLC-SAG system evaluation and calibration

6.1 Introduction

This chapter addresses the main focus of the study undertaken by disclosing whether the PLC-SAG system tracks the average height of an OHTL conductor above ground and, if it does, with what accuracy.

In Chapter 3 two case studies were chosen on which the PLC-SAG system could be evaluated. The first case study can be classified as a typical configuration and the second case study as a non-standard scenario, as it is transposed and comprises 7 different sections (Chapter 3). The latter case is considered the ultimate test. Simulations created the expectation that the level of the specially coupled PLC-SAG tones would vary as the conductor sagged, in both case studies. Chapter 4 focused on the tasks and challenges associated with the implementation of two PLC-SAG systems on KA and KT to produce the logged values of the level of the PLC-SAG tones. Chapter 5, on the other hand, discussed the coordinated effort of measuring the average conductor height of the OHTLs via three simultaneous direct measurements.

Chapter 6 will now show the comparison of those results as discussed in Chapter 3 (Simulations), Chapter 4 (Logged results from the PLC-SAG

hardware) and Chapter 5 (Direct height measurements) to study the PLC-SAG technique.

In this thesis no advanced Digital Signal Processing (DSP) techniques were used to improve the quality of the data.

This chapter starts by discussing the first case study. The logged data will be shown and discussed with emphasis on signal level variations. The attenuation simulations from Chapter 3, for the specially coupled PLC-SAG tones, are redrawn as a function of height. The simulation and logged PLC-SAG tones are compared. These tones are correlated with the direct height measurement as discussed in Chapter 5. From the correlation, the best tones were identified and combined to get the Principal PLC-SAG tone. At this point the abovementioned process was repeated for the second case study.

The Principal PLC-SAG tone level for each of the two case studies was then calibrated. The calibration technique will be discussed. After the calibration the Principal PLC tone will be called the PLC-SAG Average Height Signal (AHS) and is given in meters. PLC-SAG AHS is then plotted with the direct height measurements and the level of accuracy will be determined.

6.2 Case study 1 (Koeberg-Acacia) logged tones

6.2.1 Logged PLC-SAG monitoring tones

Figure 6.1 shows the logged data set from the PLC-SAG experimental system. The red squares in the data sets represent the segment of the data that will be used in the correlation, as it is at the same time intervals as those used in the first and second day of direct height measurements. The

red squared days are labelled as 'Day 1' and 'Day 2' of height measurement, which represent the 5th and 12th October 2004 respectively.

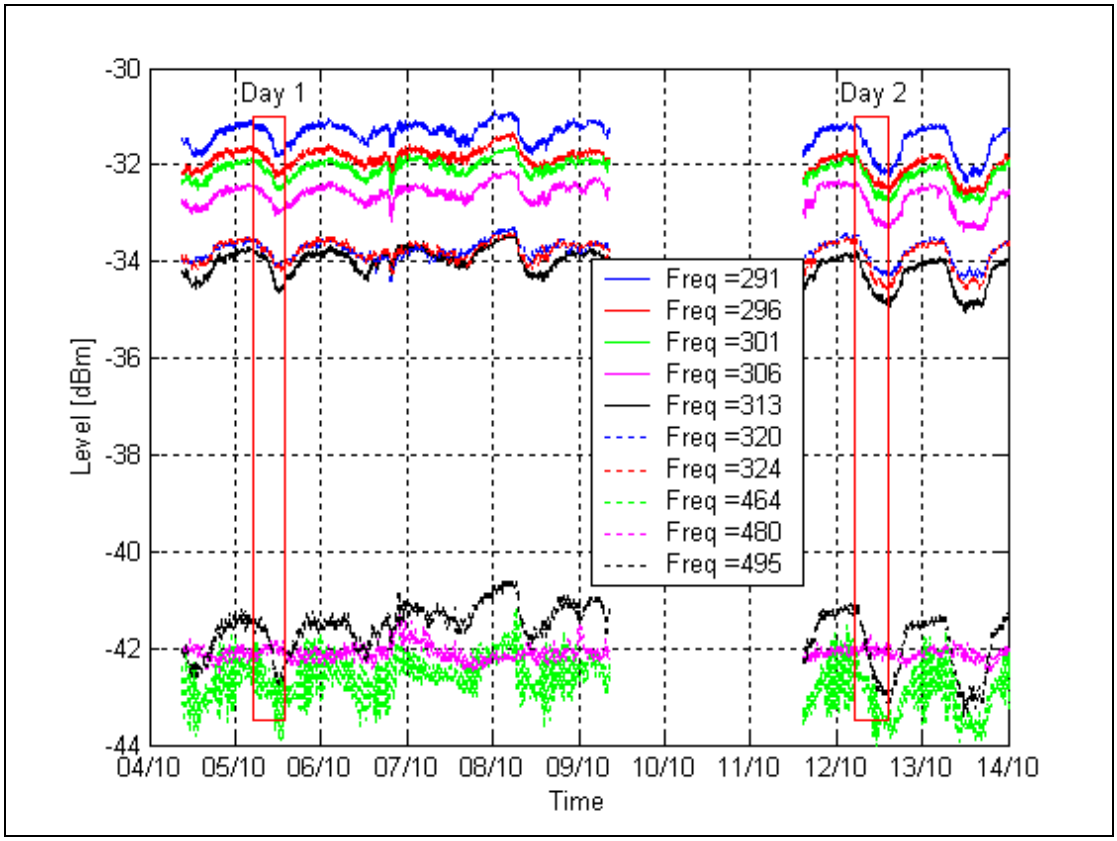

Figure 6.1 Attenuation variation of all ten tones on KA PLC-SAG system. Measurement days 1 and 2 are indicated by the red squares in the data (Specific configuration is specified in Appendix C).

6.2.2 General comments about the logged data

A day-night variation can be noted between the tones - as the simulations predicted, except for Tone 9 (Frequency of 480 kHz). More noise can also be noted on Tone 8 (Frequency of 464 kHz) compared to the other tones. The physical explanation of the behaviour of Tones 8 and 9 is unknown, as they do not act as predicted. Due to the harsh environment of the PLC system, it was expected that there would be evidence of some interference from neighbouring equipment. At the time of the experiment, the author

was informed by the Station Operator of Acacia (where the receiver (selective Voltmeter) is located) that a protection relay (called P40) was giving problems. The operating frequency of the P40 protection relay is 468 kHz to 476 kHz, which is located between tone 8 and tone 9.

Frequent problems occurred due to the experimental nature of the hardware. The absence of data during the 9-10 October 2004 is due to logger related problems.

6.2.3 Levels of the received PLC-SAG tones

Various insertion loss experiments and measurements were performed on this specific OHTL [1]. They will not be repeated, although an analysis will be done to see whether the received level from the experiment is close to the expected level. The frequency of PLC-SAG monitoring Tone 3 is 301 kHz and this will be used in this discussion, as it is close to the centre of the PLC frequency band (100-500 kHz).

The level of the logged Tone 3 (Frequency 301 kHz) varies around –32 dBm (refer to Figure 6.1).

The total attenuation of a PLC-SAG monitoring tone can be expressed as:

$$Att_{PLC-SAG} = \text{TxPower} - (2 \cdot CL + 2 \cdot MHL + AA + SLL) \qquad 6.1$$

where
TxPower = Transmit power
CL = Coupling Loss
MHL = Measurement Hybrid Loss
AA = Attenuation of Attenuator
SLL = Simulated Line Loss

Commonly, the Coupling Loss (CL) that includes coaxial losses is approximately 3 dB per station[4]. This value was confirmed via simulations. There is an uncertainty about this approximated value, because the insertion loss due to the coupling depends on the station impedance, which is unknown. This subject will be addressed again later.

The theoretical Measuring Hybrid Loss (MHL) is 1.25 dB per side (if ideally terminated). A 13 dB attenuator is used as protection for the receiver at Acacia and the transmit level is 0 dBm at Koeberg Power Station.

From the simulations done in Chapter 3 it can be seen that the expected line attenuation for the KA, for a range of heights, is between 9 and 13.5 dB for 301 kHz.

Therefore, by substituting the mentioned values in Equation 6.1, estimated levels of between -30.5 dBm and –35 dBm can be calculated. The observed level of tone 3 is approximately in the centre of the expected range.

It can also be noted from the KA OHTL line attenuation simulations from Chapter 3 that as the frequency increases the attenuation also increases. By studying Figure 6.1 it can be noted that the highest tone's average attenuation is not the greatest. This seemed strange at first, but it later appeared that the station impedance varies considerably with frequency. Therefore the offset of the received tone depends on the station impedance at that frequency. More simulations and analysis concerning the station impedance uncertainty will be done in Chapter 7.

---

[4] Personal communication with Mr DC Smith, ESKOM Corporate Consultant: Telecommunications, dated 2004-11-12

6.2.4 Variation of the received PLC-SAG tones compared with the simulations

As mentioned before, the simulation model as presented in Chapter 2 was tested against instantaneous PLC system insertion loss measurements across the frequency band [1]. For the first time ever (to the knowledge of the author) the dynamic variation of the PLC signal attenuation, as noted in Figure 6.1, will be tested against the theory as presented in Chapter 2.

By focusing on Tones 3 and 10, the signal level variation can be studied in the mid PLC frequency region and the upper frequency region. The relationship between attenuation and average conductor height is simulated in Chapter 3. For easier interpretation the same simulation will be plotted in Figure 6.2 for only the two tones under investigation, with the average conductor height on the x-axis.

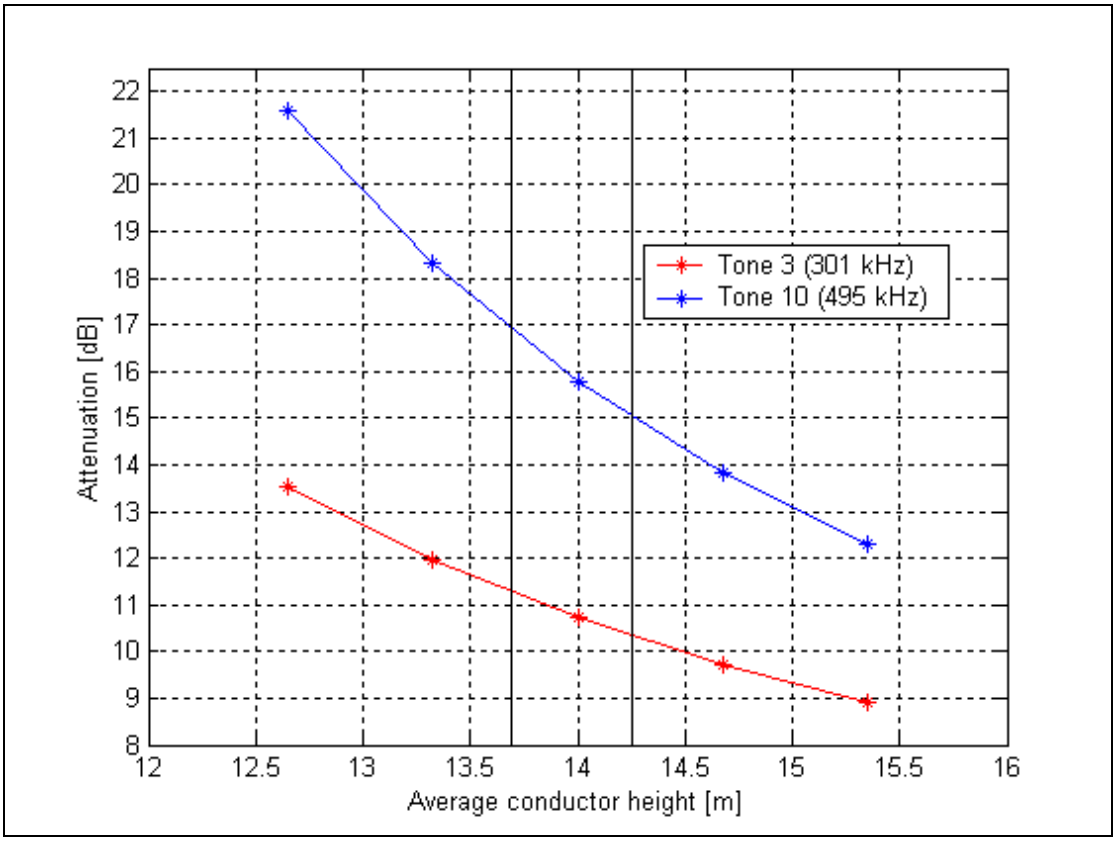

Figure 6.2 KA OHTL attenuation simulation as a function of average conductor height for Tone 3 and Tone 10.

The two black vertical lines represent the lowest and highest average conductor height measured (Chapter 5); more detail is given in Table 6.1. This measured height variation (vertical black lines) is in the centre of the simulated range, which is based on the default simulation condition as specified in Chapter 3.

Table 6.1 Lowest and highest average height levels observed on the KA OHTL via direct height measurement

From the direct height measurement in Chapter 5		
Condition	Average height	Time
Lowest height observed	13.688	2004/10/12 14:10
Highest height observed	14.256	2004/10/12 05:40

The difference between the two conditions from the direct height measurement in Table 6.1 is 0.568 m. The expected variation from the simulations can be seen in Figure 6.2 and for clarity it is tabled in Table 6.2.

Table 6.2 Simulated attenuation variation for Lowest and highest average height on KA OHTL

PLC –SAG tone attenuation from the simulations in Figure 6.2		
Condition	Attenuation at 301 kHz [dB]	Attenuation at 495 kHz [dB]
Lowest measured height	11.257	16.90
Highest measured height	10.423	15.194
Difference between two conditions	**0.834**	**1.706**

It can be noted from Table 6.2 that the expected variation at the higher frequency is more than double that at the lower.

The logged attenuation variation from Figure 6.1 will now be compared with the expected variation as tabled in Table 6.2. The logged attenuation

values are tabled in Table 6.3 at the same time as highest and lowest conditions were observed via the direct height measurement.

Table 6.3 Logged variation at the time of the lowest and highest average height on KA OHTL

PLC-SAG tone attenuation from the measurement in Figure 6.1		
Condition	Level at 301 kHz [dBm]	Level at 495 kHz [dBm]
Level at the time of the lowest height	-32.691	-43.03
Level at the time of the highest height	-31.852	-41.263
Difference between two conditions	**0.839**	**1.767**

The variation as predicted and simulated are very close, if the last rows of Table 6.2 and Table 6.3 are compared.

The following section will focus on more detail regarding the comparison between the logged attenuation of the tones and the direct height measurements.

6.2.5 Correlation between direct height measurement and the logged attenuation values for KA

The correlation between the height measurements and PLC-SAG monitoring tones is determined. The correlation coefficient is computed by dividing the covariance of two data sets with the product of their individual standard deviations [2]. This formula is shown in Equation 6.2

$$\rho_{xy} = \frac{\mu_{xy}}{\sigma_x \sigma_y} \qquad 6.2$$

where

μ_{xy} = covariance of x and y
σ_x = standard deviation of x
σ_y = standard deviation of y

Table 6.4 shows the correlations, as computed by Equation 6.2, between the direct height measurements (Data as plotted in Figure 5.10) and the individual tones (Data as plotted in Figure 6.1).

Table 6.4 Correlation table between measured average height and the PLC-SAG monitoring tones for KA

	Correlation Day 1	Correlation Day 2
Tone 1	0.97032	0.9845 (5)
Tone 2	**0.98484 (1)**	0.99151 (2)
Tone 3	0.9749 (5)	0.99068 (3)
Tone 4	0.98375 (2)	0.98454 (4)
Tone 5	0.97982 (3)	**0.99506 (1)**
Tone 6	0.96777	0.98876
Tone 7	0.97089	0.98293
Tone 8	0.74964	0.89366
Tone 9	-0.6019	0.08153
Tone 10	0.97709 (4)	0.98264

A remarkably high correlation can be noted in Table 6.4. The 5 best-correlated tones are ranked for each day and ranking are indicated in brackets after the correlation. Tone 2 shows the best correlation of 98.84% for the first day of height measurement and tone 5 shows the best correlation of 99.50% for the second day of height measurement. Tone 9 is the most uncorrelated tone, as expected from Figure 6.1.

Due to superior correlations tabled in Table 6.4, it is proven that the height of the conductor can be tracked via the PLC-SAG system for this case study. The best-correlated tones are Tones 2 to 5, as they are the

intersection of the two groups of best-correlated tones. Equation 6.3 formulates this more mathematically as:

$$\begin{aligned} BestTones &= BestTonesDay1 \cap BestTonesDay2 \\ (T2,T3,T4,T5) &= (T2,T3,T4,T5,T10) \cap (T1,T2,T3,T4,T5) \end{aligned} \qquad 6.3$$

where

TN = Tone number N

Figure 6.3 is a magnification of Figure 6.1, which shows only the best-correlated tones as identified by Equation 6.3.

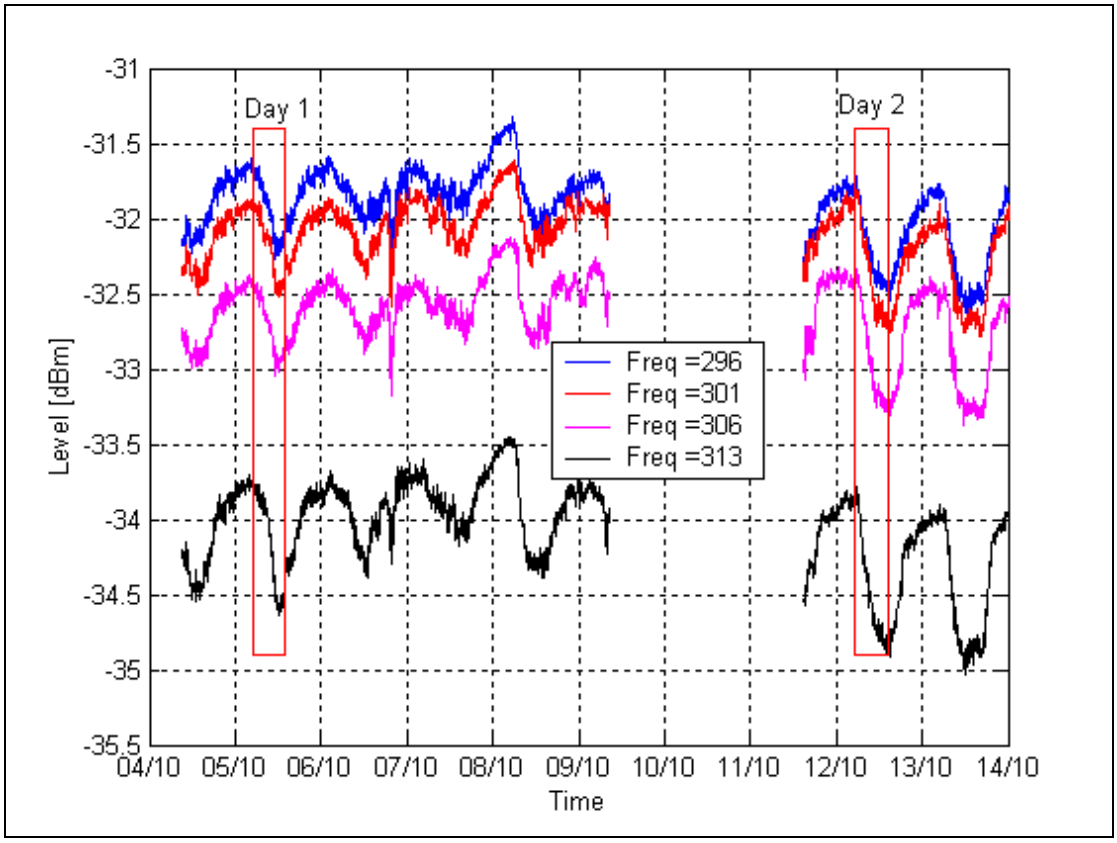

Figure 6.3 Best correlated tones for KA PLC-SAG system

The average of best-correlated tones can be used to calibrate the PLC-SAG system. This average will be referred to as the principal PLC-SAG tone. The principal PLC-SAG tone is plotted in Figure 6.4 for same time duration as the direct height measurement (Figure 5.10).

After the PLC-SAG system is calibrated, the direct height measurement as shown in Figure 5.10 will be plotted on the same graph. But first, the correlation between the direct height measurement and PLC-SAG monitoring tones for the second case study will be analysed.

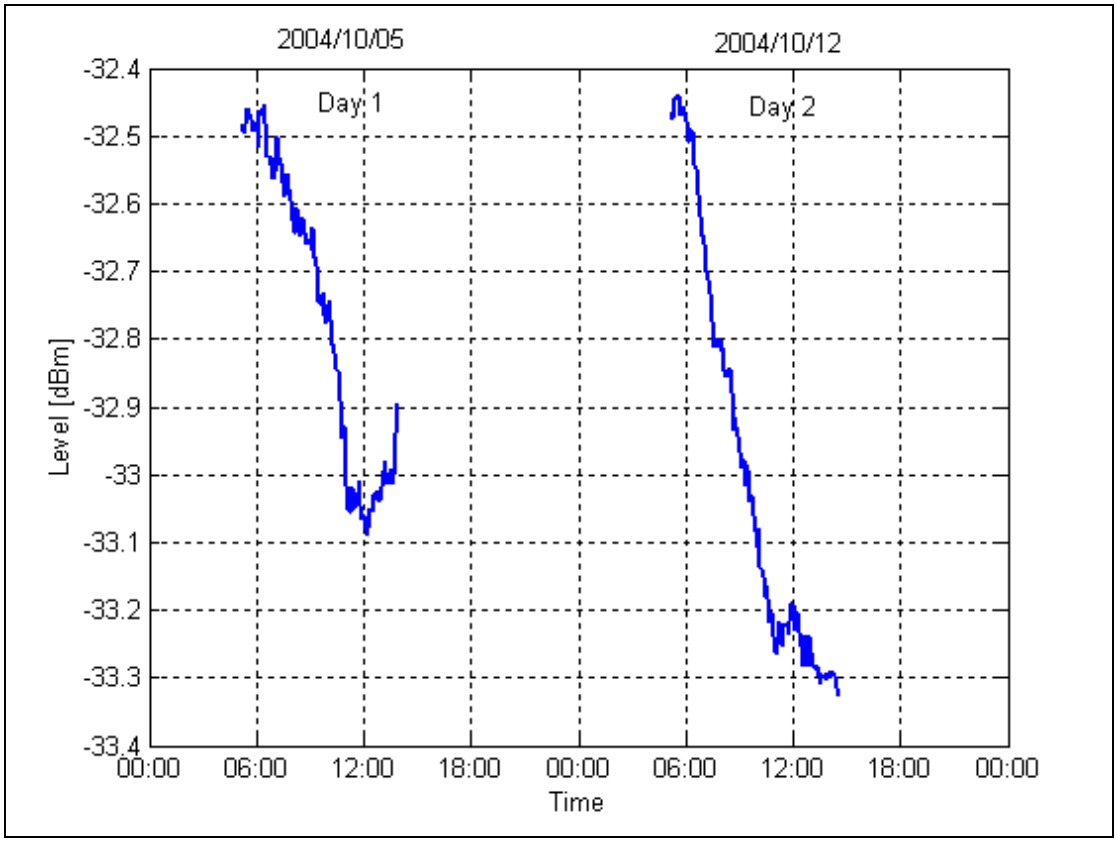

Figure 6.4 The principal PLC-SAG tones for the KA system

6.3 Case study 2 (Kriel-Tutuka) logged tones

6.3.1 Logged PLC-SAG monitoring tones

Figure 6.5 shows the logged levels of the ten PLC-SAG tones transmitted from Tutuka Power Station and received at Kriel Power Station. A more prominent day-night cycle is noticeable in the data.

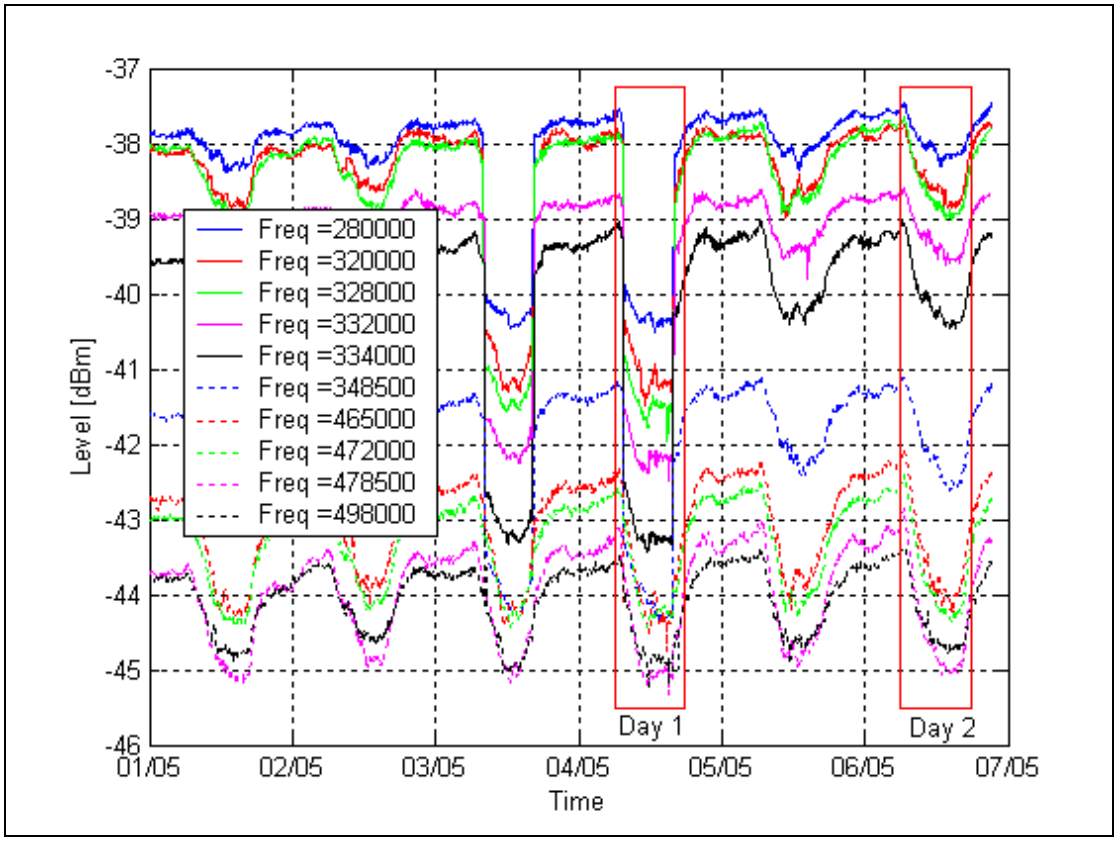

Figure 6.5 Signal level variation of all ten tones on KT PLC-SAG system. Measurement days 1 and 2 are indicated by the red squares (Measured with Wandel & Goltermann selective voltmeter)

The red square shows the part of the data that will be correlated with the direct height measurement, similar to the previous case study. 'Day 1' in the graph represents the first day of height measurements done on 4th May 2004 and Day 2 presents the second day of height measurements done on 6th May 2004.

6.3.2 General comments about the logged data

Two line outages occurred on 3rd and 4th May 2005, of which the author was unaware until the direct height measurements had been performed. The effects of the outage on the PLC system were prominent, since a step change can be noted during those two days. It can also be noted that the

tones with lower frequencies are affected more than the tones with the higher frequencies. Normally, when an outage occurs, an operator earths the OHTL on the station side of the coupling equipment. This action changes the impedance of the PLC system and, as a result, a step change in the signal levels occurs. This does not affect the propagation characteristics of the coupled signals and the PLC system is still operational.

The data of 4th May 2004 had to be reconstructed, as the synchronized direct height measurements were performed on that day. The best way to reconstruct the data is to add a constant value during the time of the outage to the affected regions. Appendix D shows the details of the tones before and after reconstruction. Only five tones (Tones 3-6 and 9) could be reconstructed successfully by following this unsophisticated approach.

6.3.3 Levels of the received PLC-SAG tones

The received level of the PLC-SAG tone 2 (Frequency = 320 kHz) varies around -38.2 dBm (Figure 6.1).

According to the simulations in Chapter 3, the line attenuation at that frequency is between 15 dB and 19 dB. The transmit level of the tone is 0.5 dBm at Tutuka Power Station. A 10 dB attenuator is used in this case study (Chapter 4). Adding these losses together with the coupling losses and losses associated with the measurement hybrid (similar to Equation 6.1) the expected attenuation can be computed to be between –34 dBm and –38 dBm. The received level is not in the centre of the expected range, as in the first case study, but it is close to the predicted range.

6.3.4 Variation of the received PLC-SAG tones compared to the simulations

Tone 3 and Tone 9 were chosen for the analysis as they represent the 300 kHz and 475 kHz regions. The attenuation simulation done in Chapter 3 for the KT case study was re-plotted in Figure 6.6 for these two tones as a function of average conductor height.

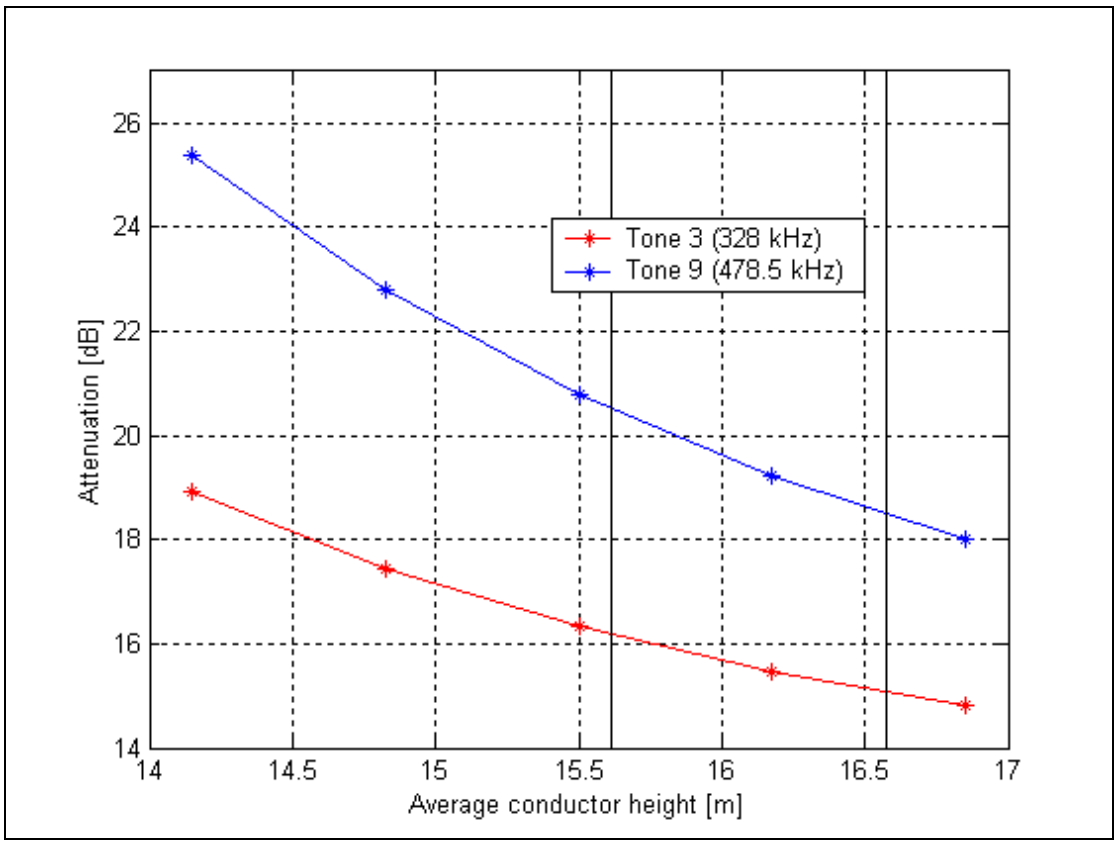

Figure 6.6 KT OHTL attenuation simulation as a function of average conductor height for Tone 3 and Tone 10.

Details about the highest and lowest observed average conductor height are tabled in Table 6.5 and are shown as vertical black lines in Figure 6.6. It can be noted that the variation also occurred in the simulated region, although the average height of the conductor is generally greater than initially expected. It was confirmed with ESKOM that this transmission

line had been re-tensioned, which would result in a higher average conductor height.

Table 6.5 Lowest and highest average height levels observed on the KT OHTL via the direct height measurement

From the direct height measurement in Chapter 5		
Condition	Average height	Time
Lowest height	15.613	2004/05/06 14:20
Highest height	16.575	2004/05/04 06:50

From the direct height measurement data in Table 6.5 it can be seen that the average height difference between the two conditions is 0.962 m. This is greater than in the previous case. The associated expected variation in two PLC-SAG tones are tabled in Table 6.6

Table 6.6 Simulated attenuation variation for lowest and highest average height on KT OHTL

Attenuation levels from the simulations in Figure 6.6		
Condition	Attenuation at 325 kHz [dB]	Attenuation at 475 kHz [dB]
Lowest height	16.201	20.535
Highest height	15.078	18.516
Difference between two conditions	**1.123**	**2.019**

The logged received levels for these conditions are summarised in Table 6.7

Table 6.7 Logged variation at the time of the lowest and highest average height on KA OHTL

From the measurement in Figure 6.5		
Condition	Level at 328 kHz [dBm]	Level at 478.5 kHz [dBm]
Level at the time of the Lowest height	-38.936	-45.023
Level at the time of the Highest height	-37.889	-43.121
Difference between two conditions	**1.047**	**1.902**

The level of variation (last row in Table 6.5 and Table 6.6) of the simulation and the logged signal levels compare well, taking into consideration that this is a 100 km long transposed transmission line.

6.3.5 Correlation between direct height measurement and the logged attenuation values for KT

Table 6.8 shows the correlation between the logged PLC-SAG monitoring tones and the direct height measurement (Figure 5.11) for the second case study.

Table 6.8 Correlation table between measured average height and the PLC-SAG monitoring tones for KT

	Correlation Day 1	Correlation Day 2
Tone 1	-	0.9813287(5)
Tone 2	-	0.9684792
Tone 3	0.9666195 (4)	0.9866302 (2)
Tone 4	0.9804030 (2)	0.9766517
Tone 5	0.9741615 (3)	0.9844968 (3)
Tone 6	0.8969064 (5)	0.9633970
Tone 7	-	0.9796565
Tone 8	-	0.9818151(4)
Tone 9	**0.9857411 (1)**	**0.9866542 (1)**
Tone 10	-	0.9711523

Due to the outage only five recovered tones (Appendix D) are used in the correlation calculation. Again, remarkably high correlations can be noted. What is even more significant is the fact that there is not one 'bad' correlated tone, since the worst correlation (89.69%) is between Tone 6 and the height measurement of the first day.

In order to be consistent, the same methodology is used as in the first case study: to identify the best tones for the PLC-SAG calibration. Therefore Equation 6.3 can be rewritten as

$$\begin{aligned} &BestTones = TonesDay1 \cap BestTonesDay2 \\ &(T3, T5, T9) = (T3, T4, T5, T6, T9) \cap (T1, T3, T5, T8, T9) \end{aligned} \qquad 6.4$$

These tones are plotted in Figure 6.7. There is a distinct improvement in the signal to noise ratio in Figure 6.7, compared to Figure 6.3. This is due to the quality of the Wandel & Goltermann receiver itself. The correction in the tones (due to the outage on 4th May 2005) can be noted, as the step effect is not present in data for 4th May on this graph.

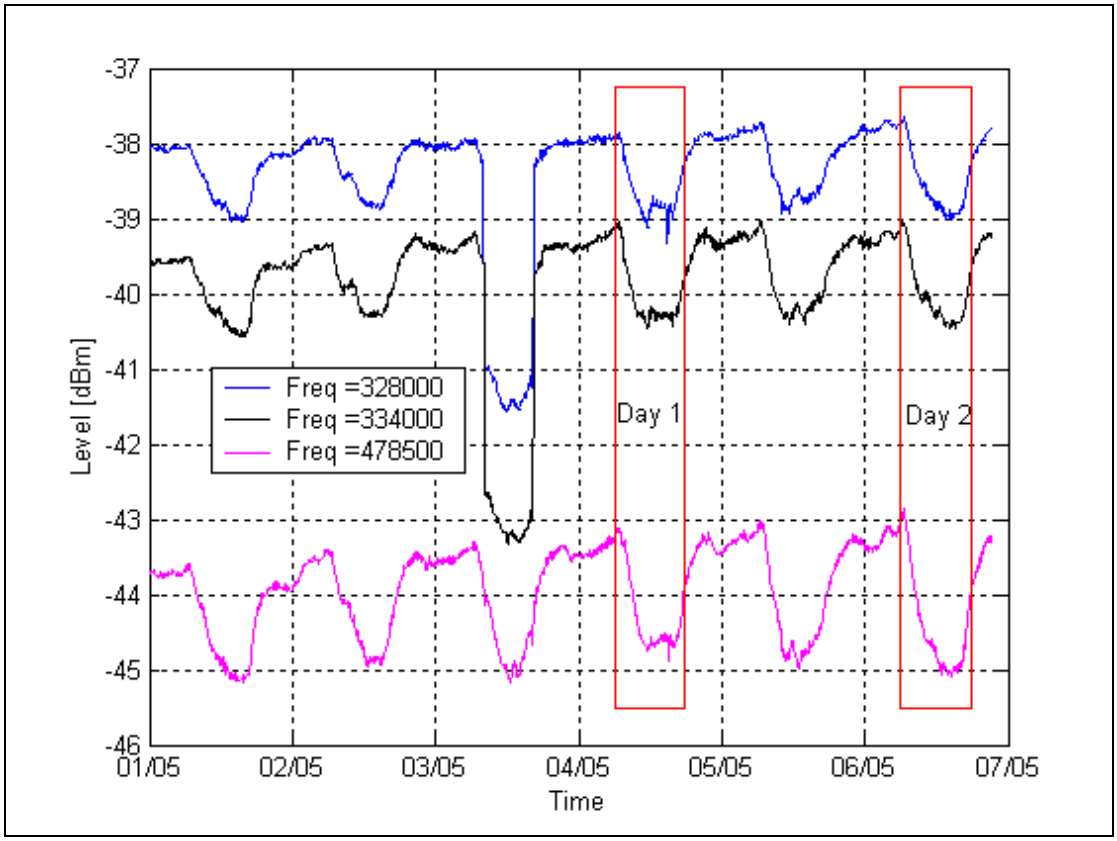

Figure 6.7 Best 3 correlated tones for KT PLC-SAG system measured with the W&G receiver

The average of the best-correlated tones are plotted in Figure 6.8. This tone in Figure 6.8 is called the principal PLC-SAG tone for the KT system. Note that the two relevant days' data, as indicated by red squares, are plotted next to each other in Figure 6.8, although there is a day in-between.

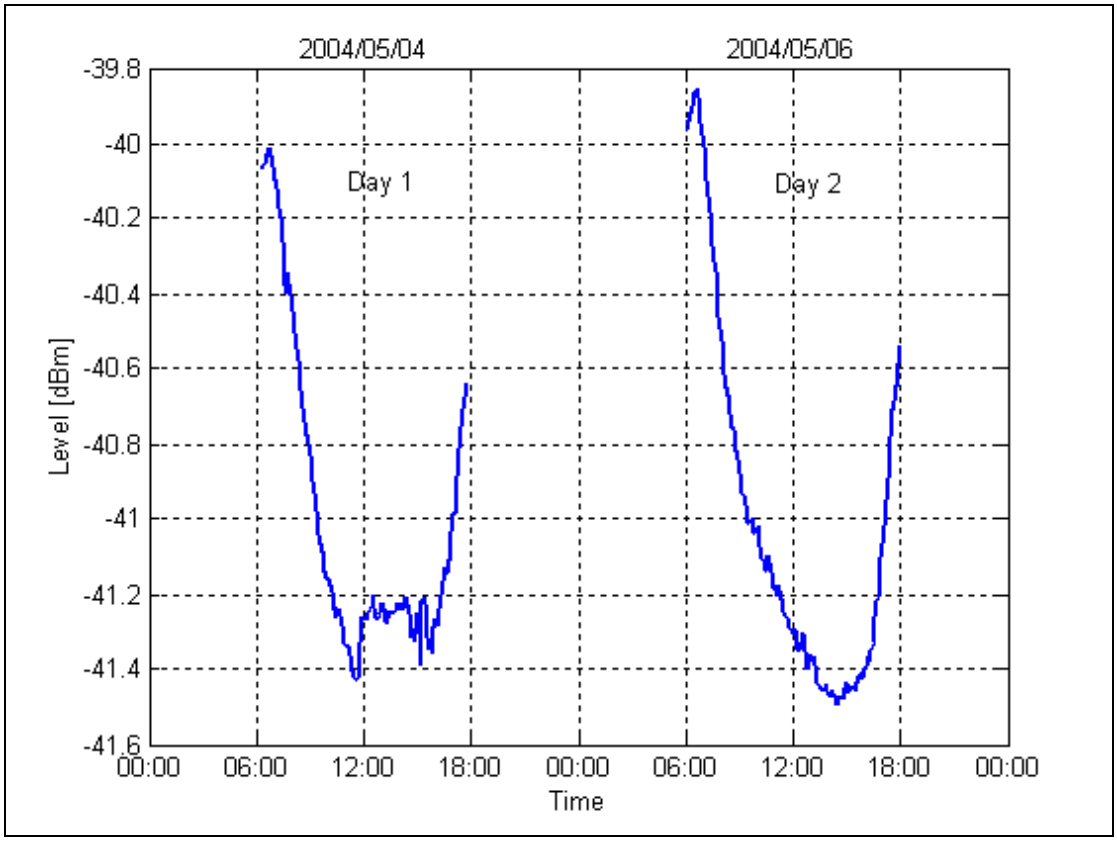

Figure 6.8 The principal PLC-SAG tone for KT (Average of the 3 best correlated KT PLC-SAG tones)

The data represented in Figure 6.4 and Figure 6.8 will be used in the following section to calibrate the PLC-SAG system for the two case studies.

6.4 Calibration of the PLC-SAG system

The goal of the calibration is to transform the level of the PLC-SAG monitoring tones (which is in dBm) into the average conductor height of the transmission line (which is in meters). Theoretical transfer curves (Figure 6.2 and Figure 6.6), which relate the average conductor height and signal attenuation, can be used as a lookup table to utilize a calibration function.

More specifically, the average of the best-correlated tones (called the principal PLC-SAG tone as shown in Figure 6.4 and Figure 6.8) will be calibrated to compare it with the measured average height of the two case studies.

6.4.1 Case study 1 (Koeberg-Acacia)

The theoretical relationship between average height and signal attenuation is computed by using the simulation program. The principal PLC-SAG tone for KA was identified in Section 6.2.5 as the combination of Tones 2,3,4 and 5. The theoretical transfer function for the principal PLC-SAG tone is plotted in Figure 6.9 as the red stars. All the signal losses as specified in Equation 6.1 are included in the presented simulation. It can also be noted that the axes are differently defined - to compute the Average height for a given signal level.

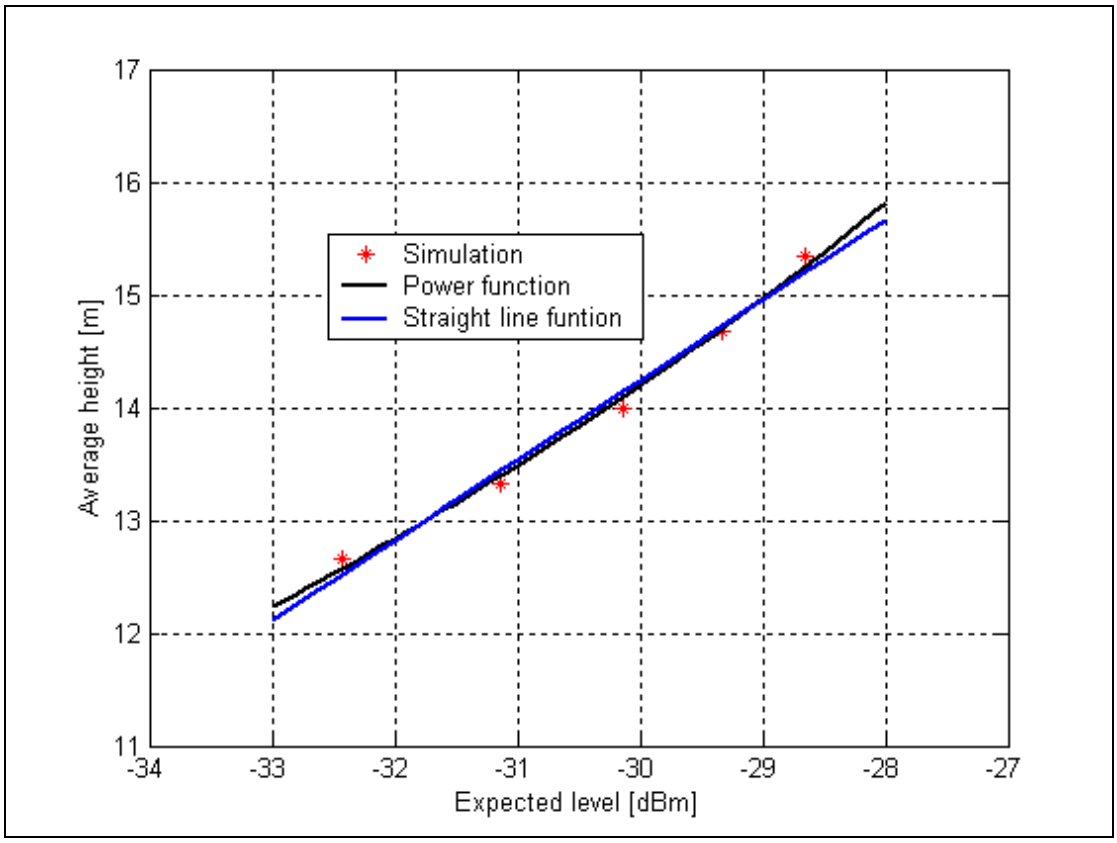

Figure 6.9 Theoretical calibration curve for the principal PLC-SAG tone for the KA OHTL.

Two additional functions were also plotted on Figure 6.9 together with the simulated data, a normal line and a more complex function, on Figure 6.9.

A Least Squares based curve-fitting algorithm called ('polyfit') from Matlab was used to characterize the two functions. The specific functions as plotted in Figure 6.9 can be described by the following parameters:

The line:

$$y = mx + c \tag{6.5}$$

where

m = 0.710 (The slope)

c = 35.544 (Offset value)

The more complex function:

$$y = \left| e^{a} x^{b} \right| \tag{6.6}$$

where

a = 7.96 + 4.902i

b = -1.56

By studying Figure 6.9 it can be noted that in the framework of the simulated range, the complex function best fits the data, especially at 12.25 m and 15.75 m. For the range between 13.7 m and 14.3 m there is a small difference between the two curves. Therefore, from the theory, one expects linear behaviour in the region of the measured height variation. This is remarkable, since this implies that the principal PLC-SAG tone can be calibrated in the required region by using a linear transformation.

The two data sets, namely the height measurement for two days (Figure 5.10) and the average of the best-correlated PLC-SAG tones (Figure 6.4), will now be incorporated to compute the empirical calibration curve in the form of a straight line (Equation 6.5). To get the best parameters for

Equation 6.5, the calibration curve knowns as the 'Least Squares' method will be used again.

The Least Squares method [3] finds optimum values for m and c that will minimize the error shown in Equation 6.7 between two data sets (X and Y).

$$error = NORM\left(\begin{bmatrix} X_1 & 1 \\ X_2 & 1 \\ & 1 \\ X_N & 1 \end{bmatrix}\begin{bmatrix} m \\ c \end{bmatrix} - \begin{bmatrix} Y_1, Y_2, ...Y_N \end{bmatrix}\right) \qquad 6.7$$

where

X = Principal PLC-SAG tone

Y = Measured average height

The following calibration parameter values were computed by using Equation 6.7: m = 0.672 and c = 36.078. The slope (m) and the offset (c) parameters compare well to the theoretically determined calibration curve.

The empirical calibration function can be used to compute the PLC-SAG AHS (Average Height Signal) in meters. This PLC-SAG AHS is plotted in Figure 6.10 together with the measured height levels.

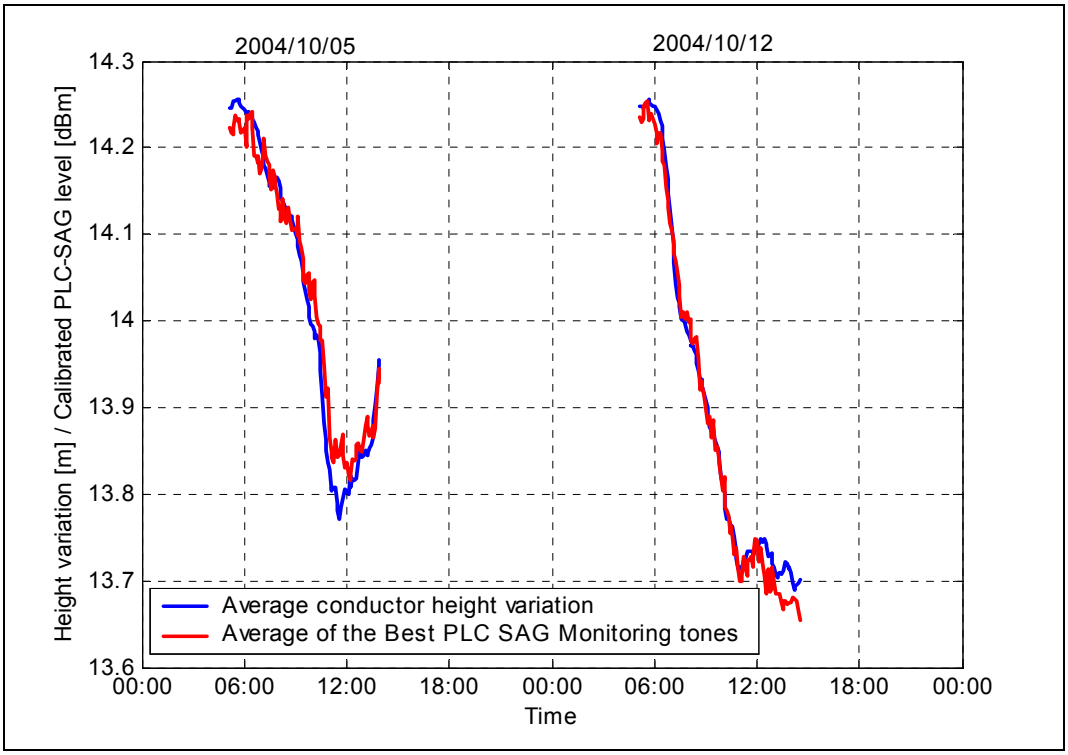

Figure 6.10 Calibrated PLC-SAG signal and the measured average height of the conductor for KA (Correlation = 99.02%)

The two data sets, presented in Figure 6.10, have a correlation of 99.02 %. This is a truly an outstanding result. Very small errors between the data sets can be noted, which are much smaller than 75 mm. It can be noted that, according to Eskom specialists, an error of up to 500 mm is commonly allowable for this type of conductor height tracking system.

From a different viewpoint, Figure 6.10 shows a PLC-SAG AHS, which presents the average height of the whole OHTL by utilising the existing PLC infrastructure in an innovative way. The measured average height obtained (by monitoring three spans) correlates nearly perfectly with the PLC-SAG AHS. This is without doubt proof that very accurate height measurement can be done via the PLC-SAG system.

The calibration of case study two (KT OHTL) will now be discussed.

6.4.2 Case study 2 (Kriel-Tutuka)

A similar methodology to that employed in the previous case study is followed. The theoretical calibration curve for the principal PLC-SAG tone, together with the Line and complex functions, are plotted in Figure 6.11. The principal PLC-SAG tone is a combination of Tones 3,5, and 9.

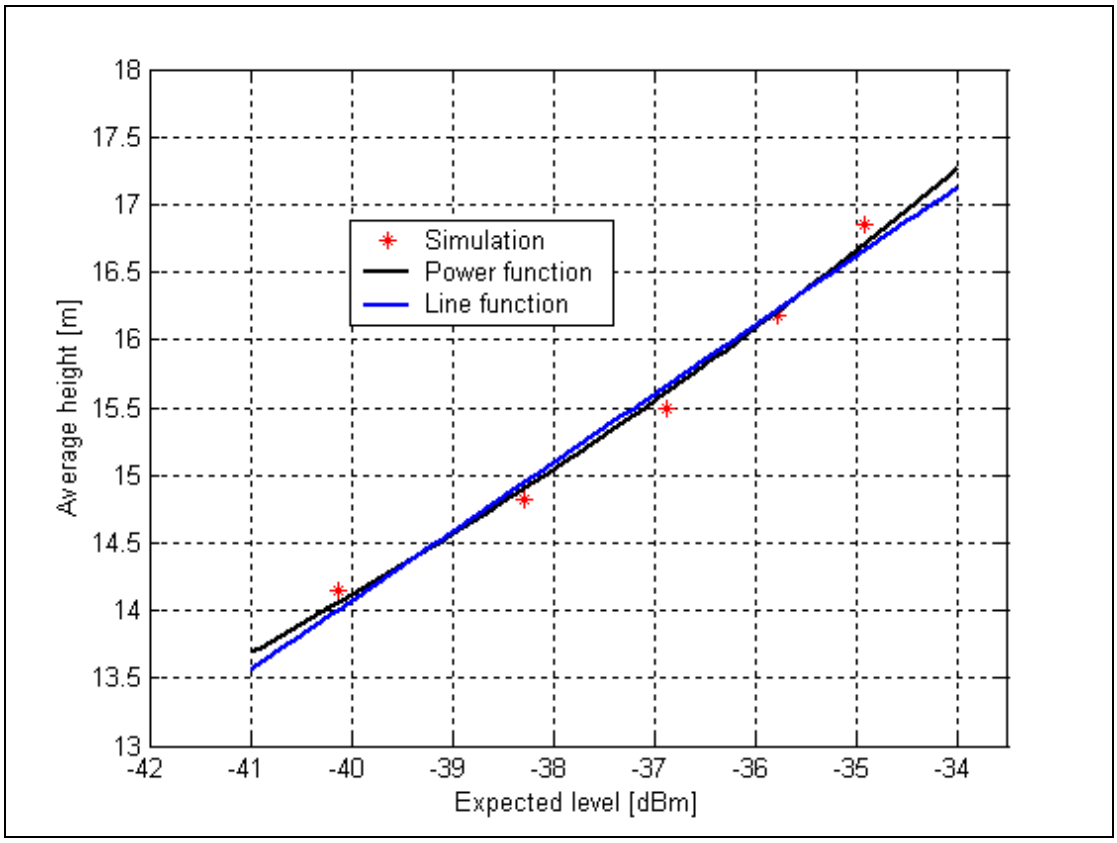

Figure 6.11 Theoretical calibration curve for the principal PLC-SAG tone for the KT OHTL.

A very strong linear behaviour in the simulation data can be noted especially in the region of 15.1m to 16.2m. The parameters describing the line and the Power function are tabled in Table 6.9.

The KT PLC-SAG system is calibrated (in a similar manner to the KA) by using the measured data. The principal PLC-SAG tone (as shown in Figure 6.8) and the measured average height (as shown in Figure 5.11)

can be applied to Equation 6.7. The results of the empirical calibration are also tabled in Table 6.9.

Table 6.9 Calibration curves for KT OHTL

Line fitted to the simulation	
m = 0.509	c = 34.45
Complex Function fitted to the simulation (Equation 6.6)	
a = 7.228 + 3.901i	b = -1.241
Calibration line using the measured data sets	
m = 0.581	c = 39.793

A bigger difference can be noted between the theoretical calibration line and the empirical determined line. The coupling loss seems greater than was predicted. The station impedance, which is an unknown factor, influences the coupling loss. Simulations will be performed in the next chapter to address the subject of station impedance.

The calibrated principal PLC-SAG tone, which is called the PLC SAG AHS, together with the measured height, is plotted in Figure 6.12. The correlation between the two data sets is 97.38%.

The difference between the two data sets is less than 75 mm. This result proves that the PLC-SAG system is practical and feasible, with very big potential, as it has performed well on a long, complex and transposed OHTL.

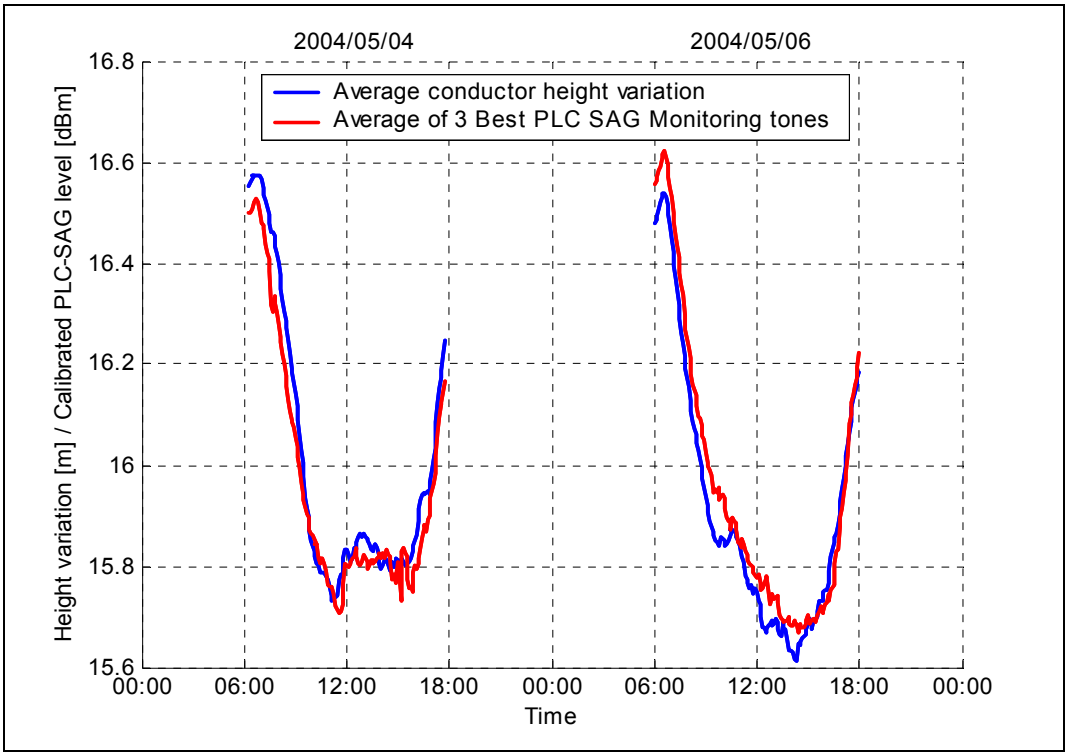

Figure 6.12 PLC-SAG AHS and the measured average height of the conductor (Correlation = 97,38%) for KT

6.5 Conclusions

The computations in this chapter have proved that the average height of an OHTL conductor could be tracked via a PLC-SAG system exceptionally accurately to within 75 mm on a day-to-day time scale.

The average height of an OHTL conductor can be tracked accurately on a day-to-day time scale. But how stable is the PLC-SAG system over longer periods of time? This question will be addressed in the following chapter.

References:

[1] **De Villiers, W.**, *Prediction and measurement of Power Line Carrier signal attenuation and fluctuation*, MScEng Thesis, University of Stellenbosch, November 2001.

[2] **R.E. Ziemer** and **W.H. Tranter**, *Principles of Communications*, Fourth Edition, John Wiley & Sons, 1988.

[3] **J.G. Proakis and D.G. Manolakis,** *Digital signal processing principles, algorithms and applications,* Third Edition. Prentice-hall international, 1996.

Chapter 7

PLC-SAG impedance monitoring system

7.1 Introduction

A strong relationship between the average conductor height and the PLC-SAG tone level was documented in the previous chapter. This phenomenon seemed very stable in the timeframe of the experiments. The data produced from the installations were analysed to see whether any other events or phenomena in the system would have an impact on the PLC-SAG method.

Logged data were studied and an unexpected step change was seen to occur in the received levels of the PLC-SAG monitoring tones. Initially, this effect was not alarming, but after analysis it became apparent that it is indeed problematic for the PLC-SAG system. An explanation is given in Section 7.2 regarding this PLC-SAG monitoring tone step effect and the associated implications.

An innovative and practical solution was discovered during the process of solving the PLC-SAG step problem, which primarily involves a PLC hybrid (Chapter 2 and Chapter 4). In order to fully understand the proposed solution, the theory of a hybrid will be disused in more depth in Section 7.3. In Section 7.4 the isolation of the hybrid is discussed and the fact that it was discovered that the hybrid could be utilised as a complex impedance-monitoring device. By monitoring the complex impedance of

the PLC system the problem of unwanted step-like variations in the signal level of the PLC-SAG monitoring can be compensated for.

Two practical PLC impedance monitoring systems are discussed in Section 7.5. To conclude this chapter, Section 7.6 defines all transmission line and system impedances, which may be expected to influence the PLC system impedance. An initial experiment proves that this new solution has the necessary sensitivity in the harsh HV environment.

Longer-term performance studies cannot be performed without an incorporated and fully functional impedance monitoring system.

7.2 Logged received levels with unexpected step effect in data

A step change in signal level of the received PLC-SAG tones was noted in the logged data of the KA experiment and is shown in Figure 7.1.

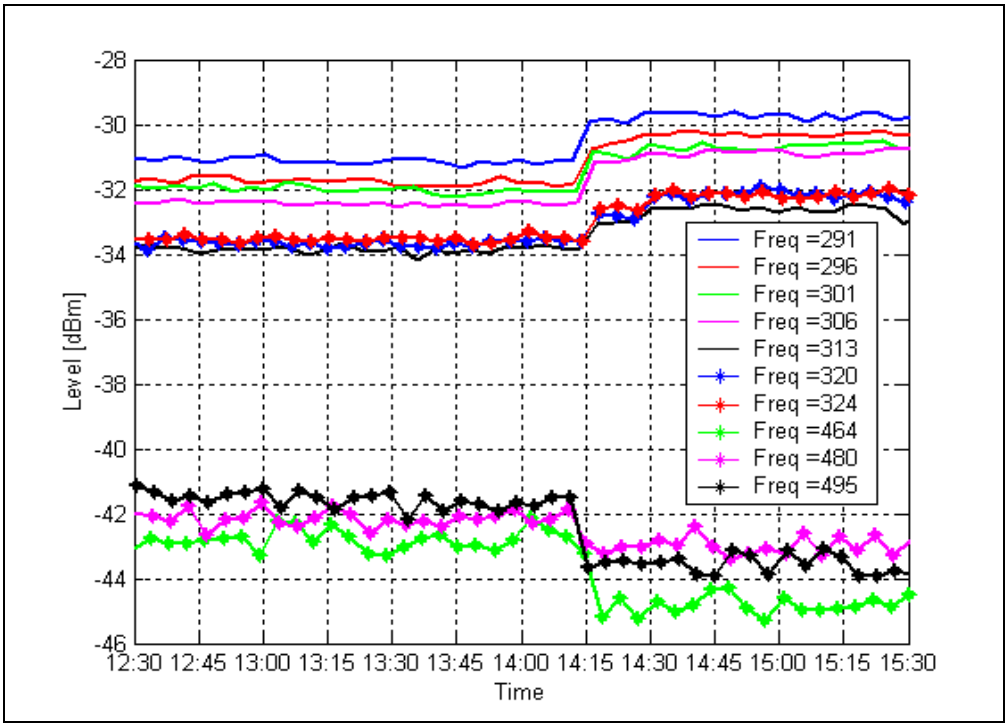

Figure 7.1 Logged KA PLC-SAG tones during 2004/09/17

Step changes in the received levels of PLC tones were of no big concern initially, because they had been noted before during an outage (Figure 6.5). The explanation was that maintenance had been done on the system and the change influenced the system temporarily. For example, there was an outage and while the maintenance was being done the OHTL was grounded temporarily. The same explanation does not explain the step change in the PLC-SAG tone received levels in Figure 7.1, because there had not been a line outage.

Table 7.1 shows the logged events from the ESKOM Supervisory Control and Data Acquisition (SCADA) system at the time of the step shown in Figure 7.1. From the SCADA data, the step change in the PLC-SAG tone levels occurred because a 500 MVA transformer breaker was operated.

Table 7.1 Logged events on the ESKOM SCADA system

Date	Time	Internal Code	Station	Description
17-Sep-04	14:00:11	A6	ACACIA	BB_CX_2_BKR_UNHEALT NORMAL
17-Sep-04	14:14:13	*6	ACACIA	TR12_SIS ALARM
17-Sep-04	14:14:39	*4	ACACIA	TR12_132_BKR TRIP
17-Sep-04	14:15:08	*4	ACACIA	TR12_400_BKR TRIP
17-Sep-04	14:15:09	*6	ACACIA	TR12_TRFR_UNHEALTHY ALARM
17-Sep-04	14:18:32	L4	ACACIA	TR12_132_MAL2 OPEN

The electrical drawing of Acacia Sub Station is shown in Figure 7.2 to help understand the trip event as tabled in Table 7.1. The transformer 12 (TR12 as shown in Figure 7.2 and Table 7.1) connects the 400 kV busbar with the 132 kV busbar. Two breakers on both sides of the transformer were operated (tripped) and this therefore isolated the transformer from the rest of the network. The reason for isolating the transformer is not known and in the framework of this study it is irrelevant.

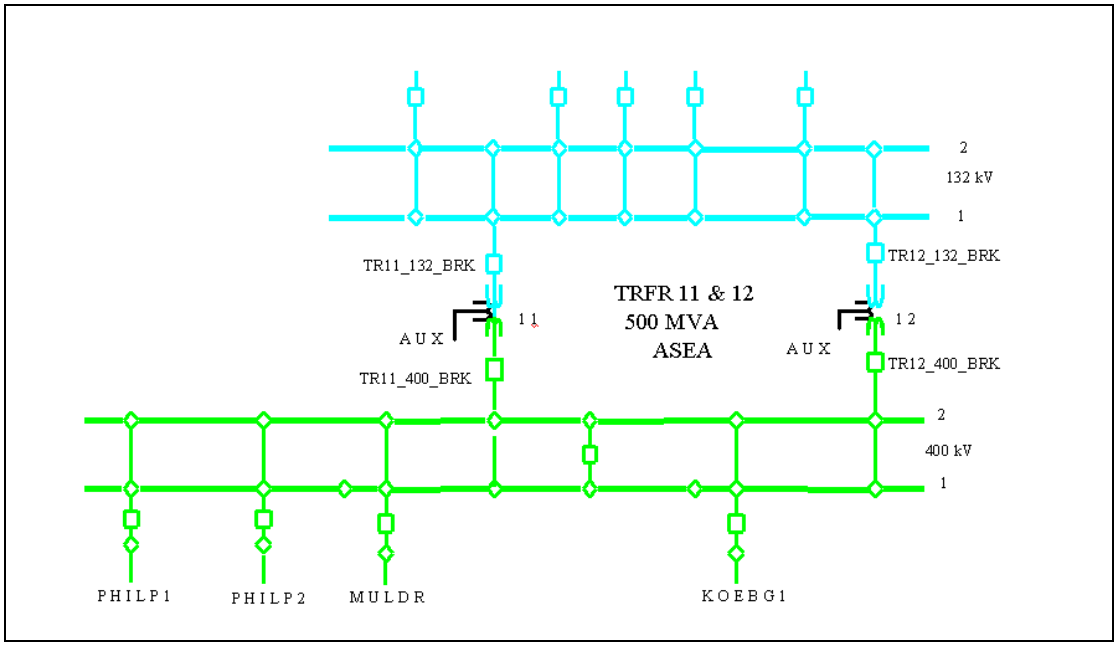

Figure 7.2 Simplistic electrical diagram showing the two 500 MVA transformers at Acacia Sub Station

The influences of this transformer isolation event on the PLC system will now be discussed. The power network change resulted in a station impedance change at PLC frequencies. The Line Trap's (LT) function is to minimize the effect of the station impedance variation on the PLC system (Chapter 2). Ideally, the LT totally isolates the PLC system from the station impedance variations. Simulations need to be performed to quantify the level of isolation which a non-ideal LT actually provides. The discovered step effect in Figure 7.1 could be due to a faulty line trap or it could be within the realistic performance expectation of a fully functional LT.

In previous simulations, shown in Chapter 2 and 3, a value of 1000 Ω was used for the station impedance (Z_s) due to the lack of more detailed information. Using the simulation program as described in Chapter 2 the effect of station impedance (Z_s) variations on the PLC signal attenuation was simulated. The result of the simulations is shown in Figure 7.3.

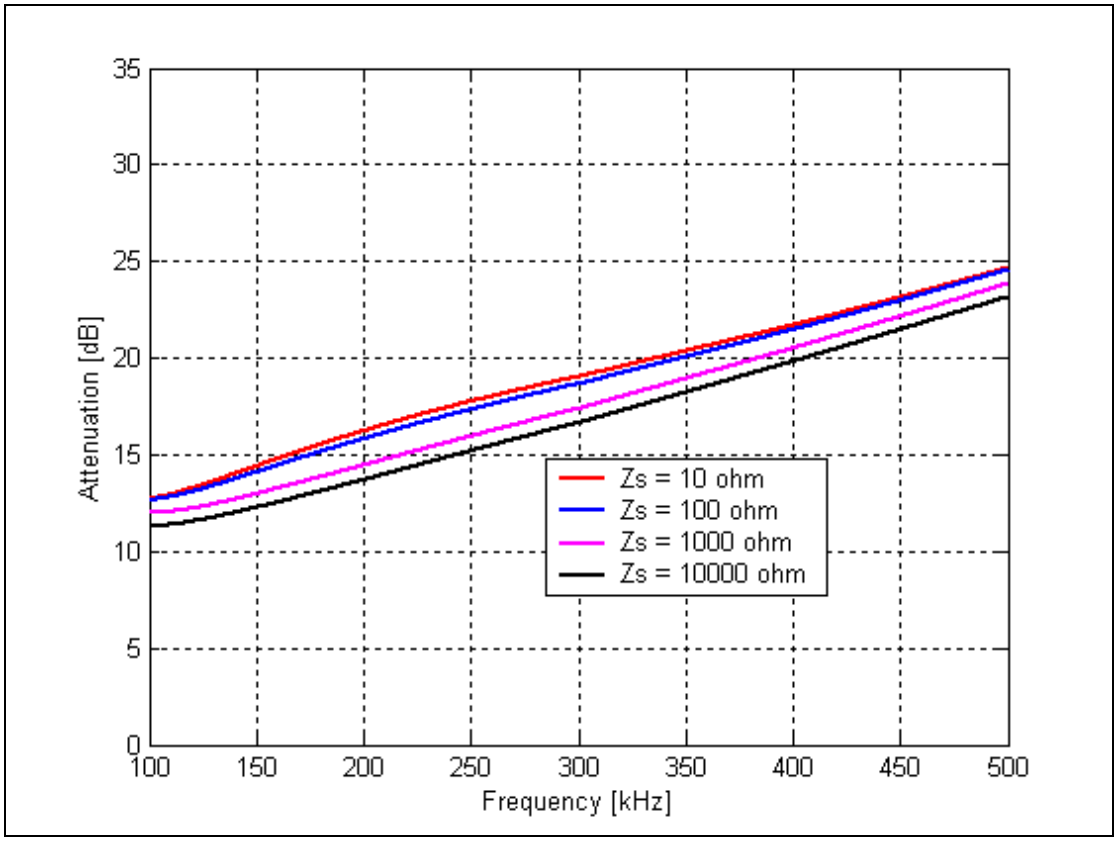

Figure 7.3 Effect on signal level due to variation in station impedance (Outer phase to Outer phase coupling on KA system)

In the simulations shown in Figure 7.3 the station impedance was changed at one station while keeping it fixed at the other station. A maximum change in the order of 3 dB can be noted. The simulation is done only for real values of impedance. The indicated impedances are constant over the simulated frequency range.

This simulation has therefore indicated that a step effect of a few dB in signal levels is indeed realistic. It can also be noted from Figure 7.1 that the step change of lower frequency levels was increased, while that of the higher frequency levels decreased. From the simulations this implies that the impedance change on the live system is not constant throughout the PLC frequency range.

The operational PLC system is built to be fully functioning in the event of station impedance changes. The PLC-SAG system, on the other hand, needs to be calibrated very accurately and a step change (as noted in Figure 7.1) would result in incorrect height monitoring levels.

This was very quickly singled out as the biggest problem that needed to be overcome to make the PLC-SAG system robust and practical.

An innovative solution was found to address this problem. In order to understand the proposed solution, the characteristics of the hybrid will be discussed in the following section.

7.3 Background theory of hybrid applied to the PLC System

In [1] a similar hybrid to that used by the PLC system is used in a vacuum tube amplifier. The equations and theory that relate directly to the hybrid itself in this section are similar to those in [1], but as applied to the PLC system. Figure 7.4 shows an electrical circuit of a hybrid or specially configured two-winding transformer. When driven at Port 1, as depicted, a properly designed hybrid serves as a differential mode power splitter.

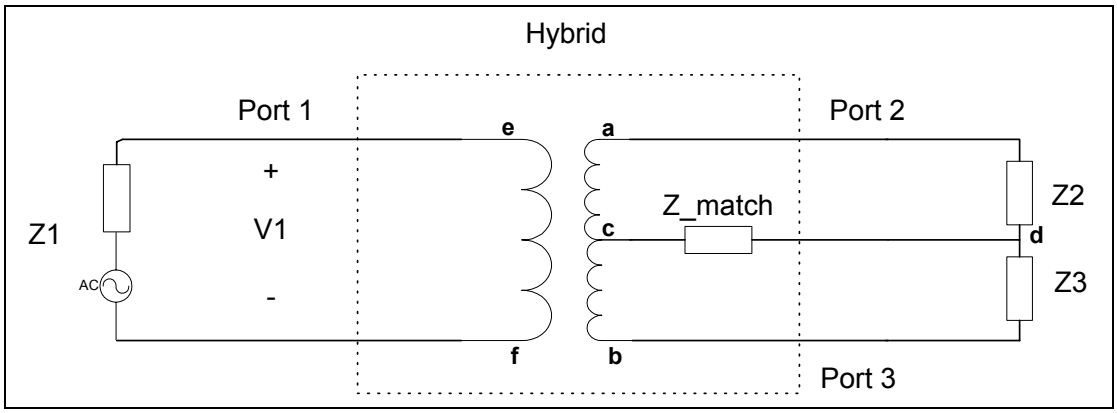

Figure 7.4 Circuit diagram of a hybrid

In a normal hybrid installation, Z1 (Figure 7.4) would represent the impedance of the carrier. A carrier has a 4 kHz transmit band and an adjacent 4 kHz receive band. The impedance over this operational frequency band of 8 kHz is 75 ohms. The carrier provides high impedance for frequencies below and above its design band of operation. This out of band high impedance of the first carrier makes it possible to connect another carrier (with a different operational frequency band). It can be connected in parallel with the first one, without double termination. Therefore, a couple of carriers can be connected in parallel. Z2 and Z3 represent the two PLC impedances looking into the LME's coupled to each phase. Line Matching Equipment (LME) transforms all the impedances beyond the LME ideally to 75 ohms via an impedance matching transformer. Let us assume, for the following analysis, that all the ports are perfectly matched. Thus Z1, Z2 and Z3 are all equal to 75 Ω, the characteristic impedance of the PLC system.

The main function of the hybrid used in the PLC system is to equally split and combine power, passively and with minimal losses. All the ports of the hybrid need to be matched to the characteristic impedance. In transmit mode the power presented to Port 1 has to be divided equally and out of phase between Port 2 and Port 3. In receive mode the power received at Port 2 and Port 3 needs to be combined in-phase at Port 1. In order to comply with these design conditions, two values need to be computed i.e., the windings relationship and the matching impedance Z_{Match}.

Winding ratio of the hybrid:

Let n_1 represent the number of turns on winding *ef* and n_2 the number of windings on *ab*. Since Z2 is equal to Z3, which is also equal to the characteristic impedance (Zo), the load of coil *ab* will be 2Zo. The impedance of Port 1 needs to be matched to Zo. This is the first matching condition.

$$Z_1 = \left(\frac{n_1}{n_2}\right)^2 2Z_0 = Z_0 \qquad 7.1$$

Equation 7.1 can now be rewritten in terms of the winding ratio, as Equation 7.2 shows

$$\frac{n_1}{n_2} = \sqrt{\frac{Z_0}{2Z_0}} = \sqrt{\frac{1}{2}} \qquad 7.2$$

The hybrid is made in such way that the number of turns on coil *ac* is equal to the number of turns on coil *cb,* the summation of which is equal to n_2 (number of turns for coil *ab*).

Common hybrid impedance:

Now assume that Port 2 is driven by a generator with impedance Zo and that Ports 1 and 3 are passively terminated also with Zo.

The impedance of Port 2 or Z_{ad} can be formulated in general as:

$$Z_{ad} = Z_{ac} + \frac{Z_{Match}\left(Z_{cb} + Z_3\right)}{Z_{Match} + Z_{cb} + Z_3} \qquad 7.3$$

Assume next that Port 3 is isolated. Thus V_{ab} = 0, and Z_3 is effectively disconnected. Thus Equation 7.3 reduces to Equation 7.4. This is the isolation condition.

$$Z_{ad} = Z_{ac} + Z_{Matxh} \qquad 7.4$$

But Z_{ad} needs to be equal to Z_0, with Port 1 correctly terminated, Z_{ac} can be computed as follows in Equation 7.5.

$$Z_{ac} = \left(\frac{\left(\frac{n_2}{2} \right)}{n_1} \right)^2 Z_0 = \frac{1}{4} \left(\frac{n_2}{n_1} \right)^2 Z_0 = \frac{Z_0}{2} \qquad 7.5$$

By substituting Equation 7.5 into Equation 7.4 with Z_{ad} = Zo, Z_{Match} can be computed to be $\frac{Z_0}{2}$.

The current flowing in coil *ac* (in an ideal transformer) would produce a voltage in coil *cb* that would be equal to the voltage produced in coil *ac*. Thus

$$V_{ac} = V_{cb} \qquad 7.6$$

but, with Port 1 terminated in Zo

$$V_{ac} = V_{cd} \qquad 7.7$$

Therefore, the voltage between *b* and *d* (or at Port 3) will be zero. In fact it makes no difference if Z_3 is connected or not and our assumption that Z_3 is disconnected does not have an impact on the deduction made [1].

7.4 Isolation of a hybrid

The following section will extend the theoretical discussion of a hybrid. The analysis, as discussed from this point onwards, is unique in the framework of PLC system impedances and the monitoring thereof.

In Subsection 7.4.1 the isolation between Port 2 and Port 3 of the hybrid will be examined. The isolation characteristics are then further explored

via simulations (Subsection 7.4.2) and a laboratory experiment (Subsection 7.4.3).

7.4.1 Isolation

The isolation between Port 2 and Port 3 will now be discussed. Assume Port 2 is driven by a generator V_g with impedance Zo and Port 3 is terminated in Zo. Then isolation between the two ports can be defined in Equation 7.8 as:

$$Isolation = 20\log\left|\frac{V_{ad}}{V_{db}}\right| \tag{7.8}$$

From the previous analysis, it has become clear that if the hybrid is correctly terminated in Zo at all three ports, the isolation is perfect, in the ideal case. The reason for this ideal isolation is due to zero voltage at Port 3, as previously discussed.

Let us assume that we do not know the value of the impedance at Port 1. The isolation can be defined as a function of Z_1.

The voltage relationship of Port 2 and Port 3 can be expressed as:

$$\frac{V_{ad}}{V_{db}} = \frac{Z_0 + 3Z_1}{Z_0 - Z_1} \tag{7.9}$$

An odd mode excitation (Figure 7.5) and even mode excitation (Figure 7.6) analysis can be done to derive Equation 7.9 [2]. All the currents and voltages for the two modes can be derived and then superimposed to obtain Equation 7.9. A key assumption is that the transformer is ideal.

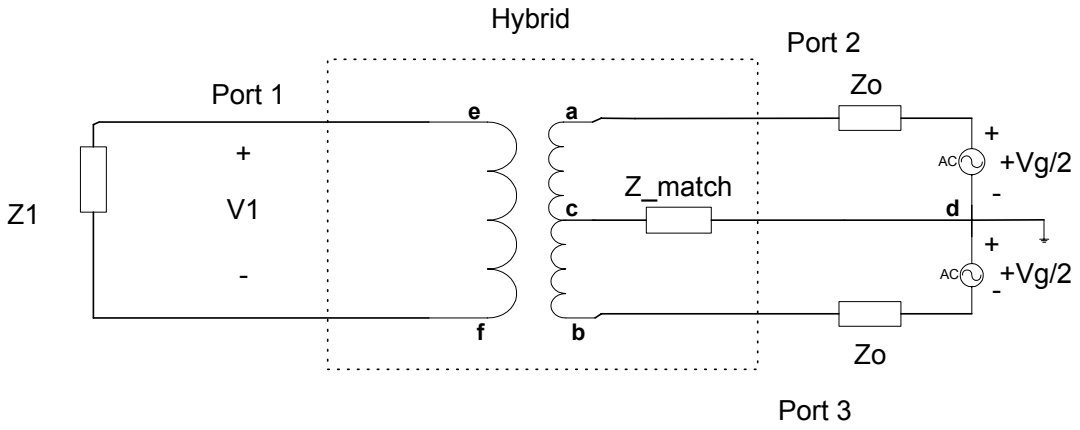

Figure 7.5 Odd mode excitation of hybrid

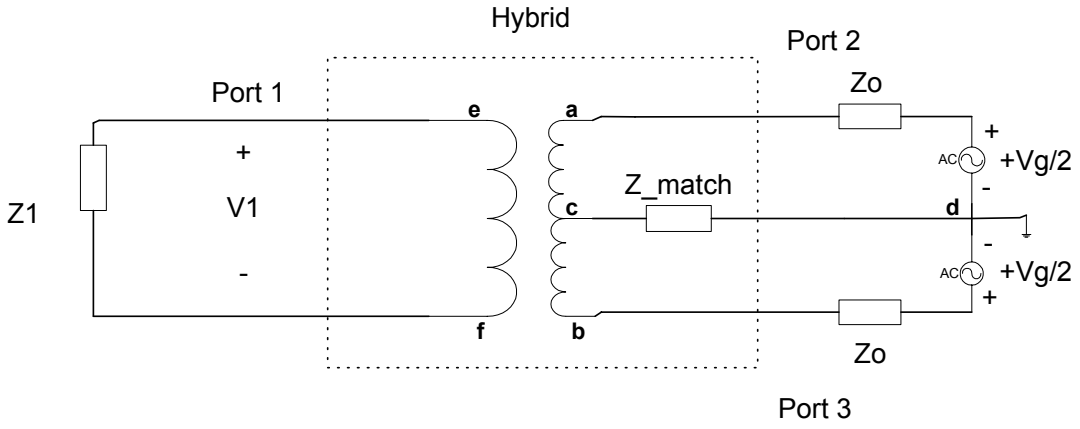

Figure 7.6 Even mode excitation of hybrid

For this specific hybrid we know that the characteristic impedance (Zo) is equal to 75 Ω. The isolation, as defined in Equation 7.8, can then be defined as:

$$Isolation = 20\log\left|\frac{75+3Z_1}{75-Z_1}\right| \qquad 7.10$$

with Z_1 an arbitrary complex impedance connected to Port 1.

The complex isolation ratio is defined as V2/V3, which is commonly expressed as

$$Complex\_isolation\_ratio = \frac{V_2}{V_3} = \left|\frac{V_2}{V_3}\right| e^{j(\phi v2 - \phi v3)} \qquad 7.11$$

The magnitude of the complex isolation will be equal to the Equation 7.8. The isolation and complex isolation characteristics of the hybrid will now be further explored in the following section via simulations.

7.4.2 Simulations

Matlab was used to simulate the isolation (Equation 7.8) for a range of real values of impedance Z_1 and the result of the simulation is plotted in Figure 7.7.

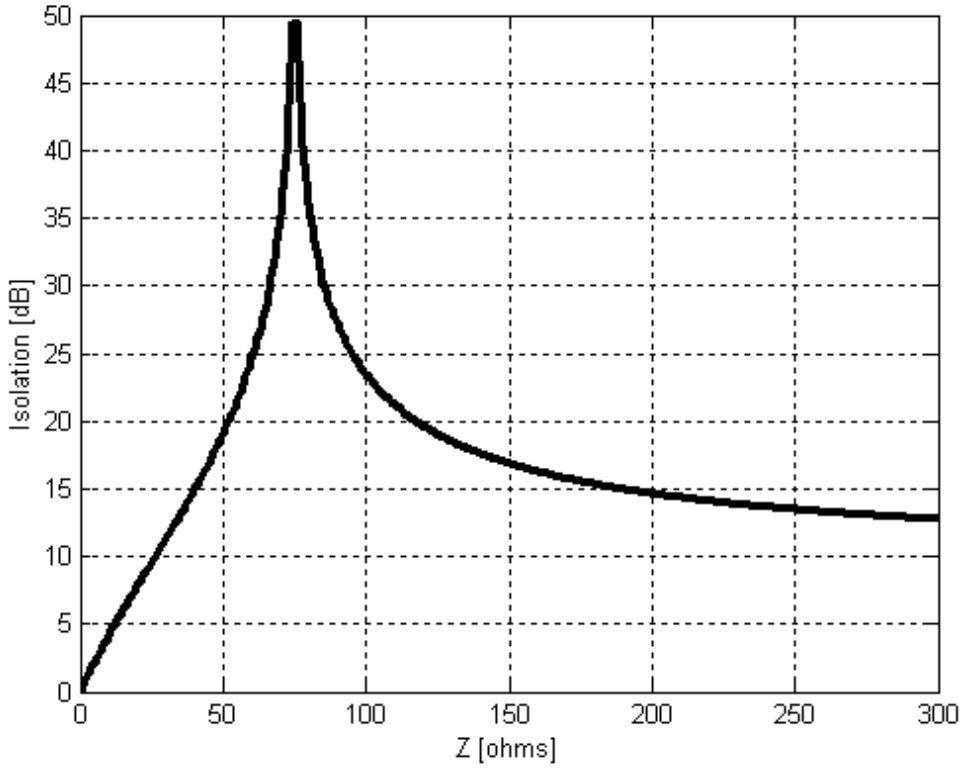

Figure 7.7 Isolation between Port 2 and Port 3 as a function of resistance for an ideal hybrid

From Figure 7.7, it may be seen that the isolation tends towards infinity when the impedance at Port 1 (Z1) is close to 75 ohms. It can also be noted that the change in isolation increases as the value of resistance approaches 75 ohm from both sides. Therefore, even if the isolation could be measured, the value of resistance cannot be determined uniquely. The complex isolation will now be discussed.

The real part of the complex isolation is plotted in Figure 7.8 and the imaginary part in Figure 7.9. By studying the graphs in these figures, it is clearly evident that the complex isolation changes rapidly as the impedance at Port 1 approaches 75 Ω. If the real part of the complex isolation could be measured, together with the imaginary part, then the complex impedance could be uniquely determined.

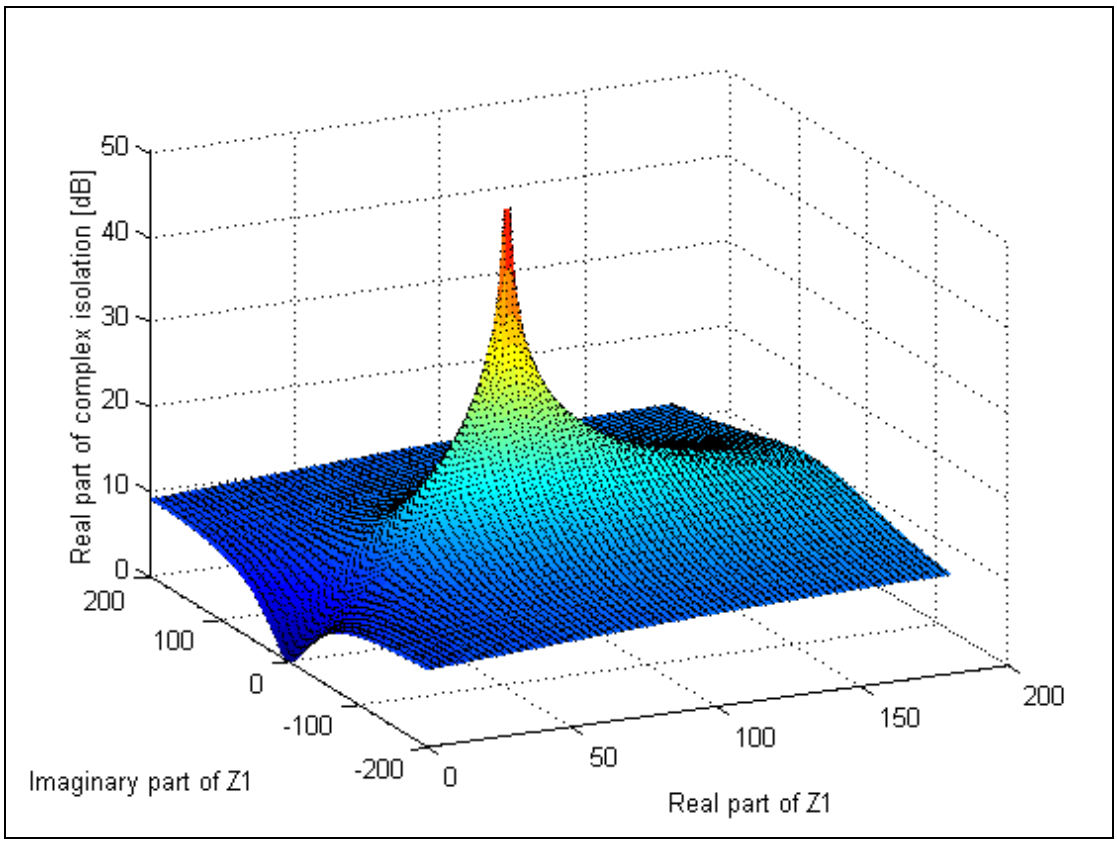

Figure 7.8 Real part of the complex isolation for a complex Z1 for an ideal hybrid

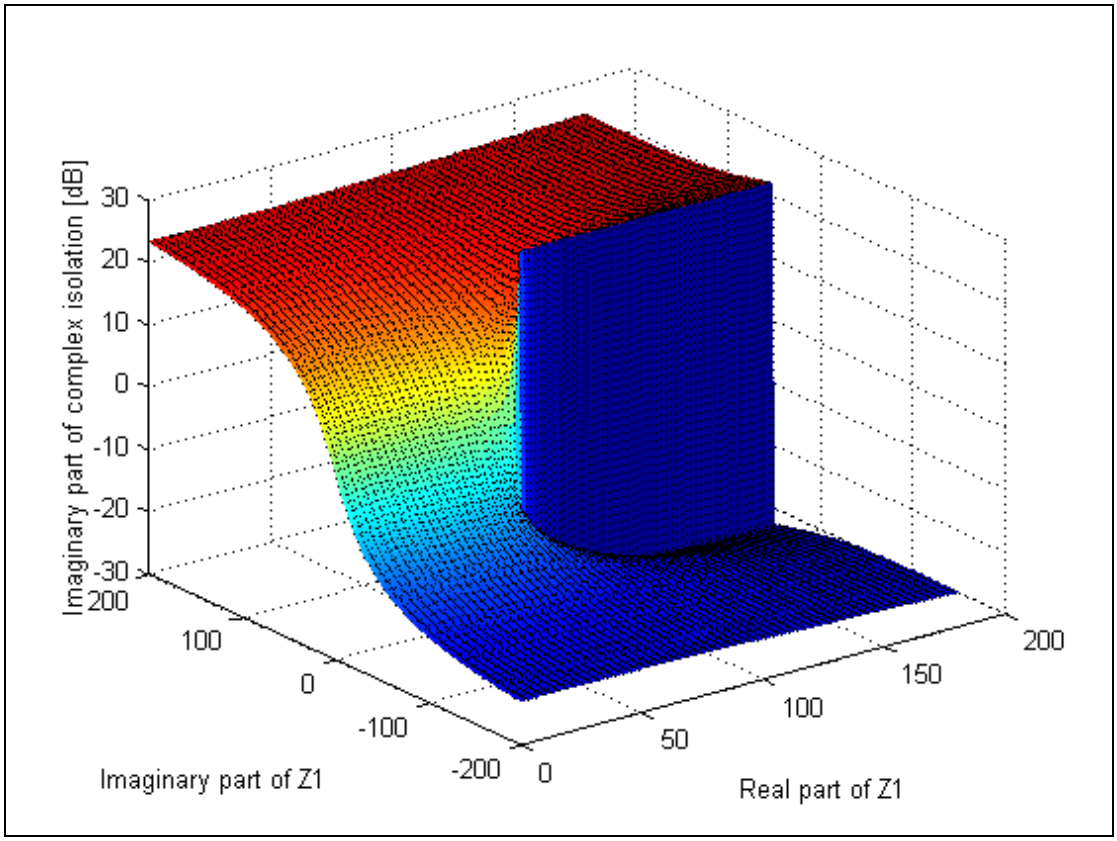

Figure 7.9 Imaginary part of the complex isolation for a complex Z1 for an ideal hybrid

7.4.3 Insertion loss laboratory experiment

A laboratory experiment was performed to verify the simulations and theory.

A hybrid, type A9BM manufactured by ABB Powertech [3], was used to perform the experiment. Photograph 4.1 depicts this type of Hybrid, which is commonly used in ESKOM PLC systems.

Port 2 of the hybrid was driven by a Wandel & Goltermann signal generator (PS-3), configured with a 75 Ω output impedance. A Tektronix TDS 220 oscilloscope was connected to Port 3 and Port 2, while port 3 is terminated in 75 Ω. This experiment was done at 250 kHz. Different resistors were then applied to Port 1 and the isolation was measured

between Port 2 and Port 3 via the oscilloscope. The result of the experiment, together with the simulated graph, is plotted in Figure 7.10.

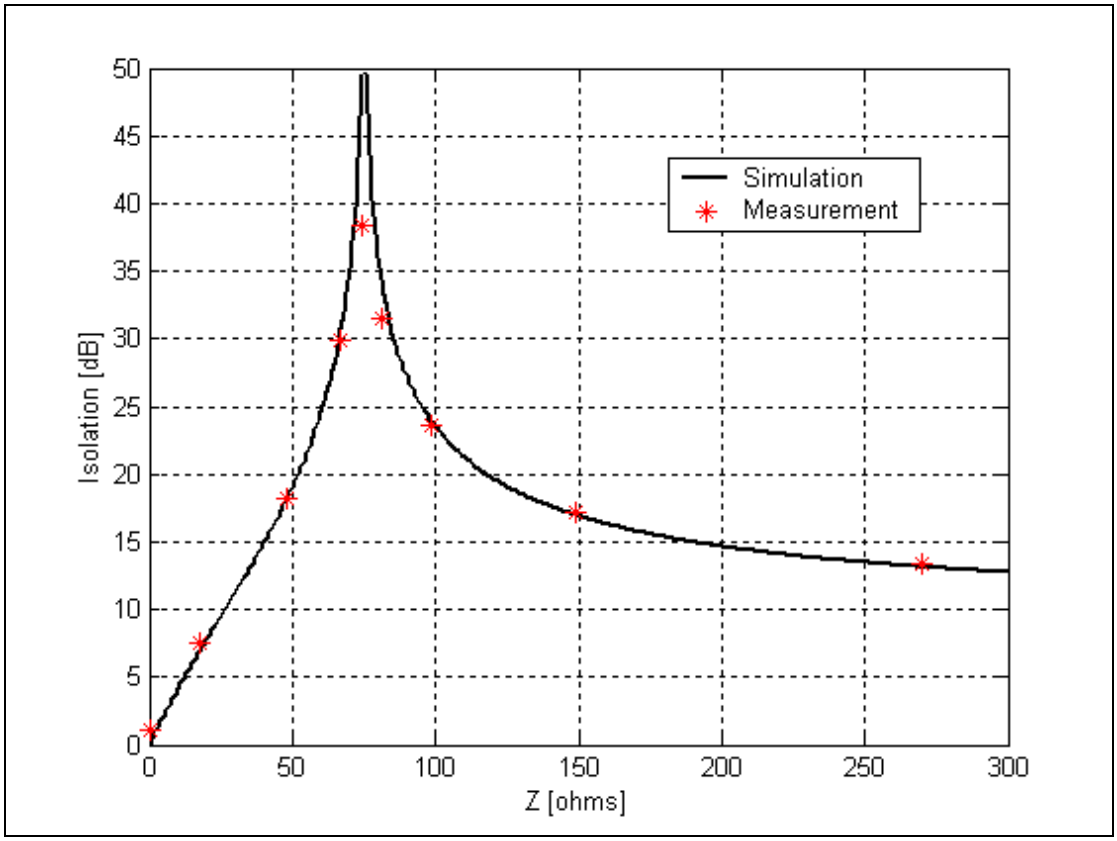

Figure 7.10 Experimental results and simulations of isolation for different values of resistance at Port 1 at 250 kHz. The exact resistance values are 17.7, 47.7, 67, 74.3, 81.15, 98.4, 149 and 270 ohms as measured on a bridge.

The black graph represents a simulation for the ideal case, as shown in Figure 7.7. The red asterisks show the measured values. The experiment indicates that the simulation model and the measurements correlate well for a wide range of resistance values. When Port 1 is open-circuited the simulated value is 9.5 dB and measurement value is 9.71 dB (Not shown in Figure 7.10). The measured isolation for the 74.7 Ω resistor is lower than the simulated value because the noise floor of the oscilloscope limits the measurement accuracy.

7.5 PLC impedance (PLC-IMP) monitoring system

From the isolation analysis in Section 7.4 it became clear that the hybrid could be used to measure the impedance at Port 1 near 75 Ω. In practice when performing such a measurement Port 2 and Port 3 need to be well terminated. The hybrid needs to be driven at either Port 2 or Port 3 and the complex ratio between Port 2 and Port 3 needs to be measured very accurately to determine the complex impedance at Port 1. The impedance measurement technique is only sensitive at impedances close to 75 Ω.

All the conditions mentioned appear to be reachable, with the goal of realizing an impedance measurement system in the current PLC-SAG hybrid setup (Chapter 4) without any additional hardware change to the current PLC system attained. This is truly exceptional. The technique described here is distinct from the usual impedance bridge technique used in the PLC environment, as described in [4]. The new technique is called PLC-IMP.

Two potential PLC impedance measurement setups will now be discussed. The first setup will enable measurement of the PLC-system impedances at carrier frequencies. The second measurement setup will address PLC-SAG tone impedance measurements.

7.5.1 Monitoring the PLC impedance at the carrier frequency

By inserting a Measurement Hybrid between Port 3 of the existing hybrid and the LMU the phase impedance of the PLC system can be monitored in real-time. This is exactly the same hybrid configuration as discussed in Chapter 4. The impact of the measurement hybrid on the existing PLC system is therefore the same as discussed in Chapter 4.

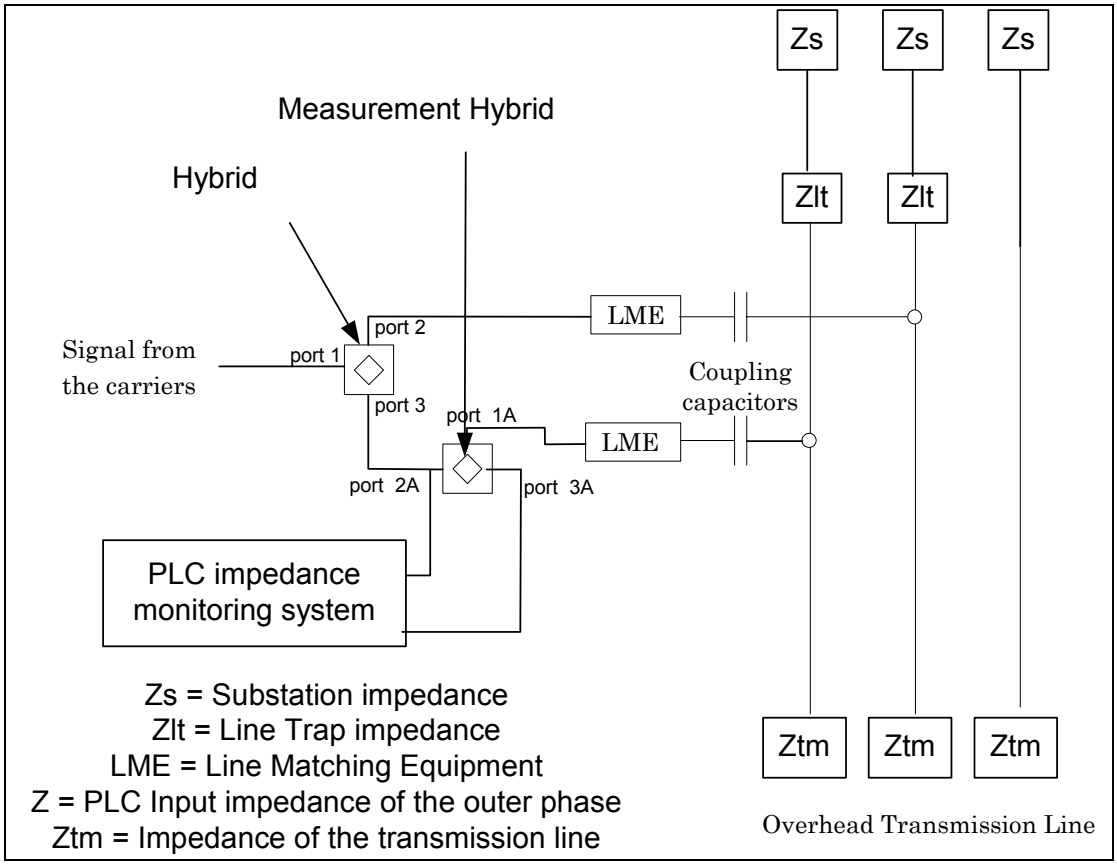

Figure 7.11 Measurement Hybrid which monitors the PLC impedance on the outer phase at carrier frequencies.

Port 2A and Port 3A of the measurement hybrid are well terminated in the system characteristic impedance via the PLC carrier system and the impedance monitoring system respectively. (Variations in the phase impedance presented at Port 2 of the PLC hybrid do not cause significant system impedance variations at Port 3 of the PLC hybrid, due to its intrinsic isolation.) Port 1A of the additional hybrid is connected to the rest of the PLC system.

The carrier system generates a high power tone. At the hybrid the power of the tone is divided between Port 2 and Port 3. Focusing only on the outer phase, the energy leaving Port 3 enters Port 2A of the Measurement Hybrid, which in turn is coupled to the outer phase of the OHTL via Port 1A.

From equations in Section 7.4 it is evident that the terminating impedance of Port 1A can be observed by measuring the relative amplitude and phase of the complex voltages at Port 2A and Port 3A.

The Logging Device samples/measures the instantaneous voltages at Port 2A and Port 3A, and uses standard techniques (such as I and Q component decomposition) to determine the relative amplitude and relative phase of V3A / V2A to measure the complex isolation. From this the impedance at the carrier frequencies can be computed. Sampling cards are available with 90 dB dynamic ranges at the required frequencies. This type of equipment makes this a practical and economical technique.

7.5.2 Monitoring the PLC impedance at different frequencies

A tone at the required frequency is generated. The tone is transmitted in a same way than the PLC-SAG system via the Port 3a of the measurement hybrid (Figure 7.12). By knowing the transmitted and received signals phase and amplitude the complex isolation can then computed, as in the previous case, to determine the PLC system impedance.

Therefore, by monitoring the complex isolation of the Measurement Hybrid the impedances of the PLC phase impedance can be monitored while the PLC system is fully operational.

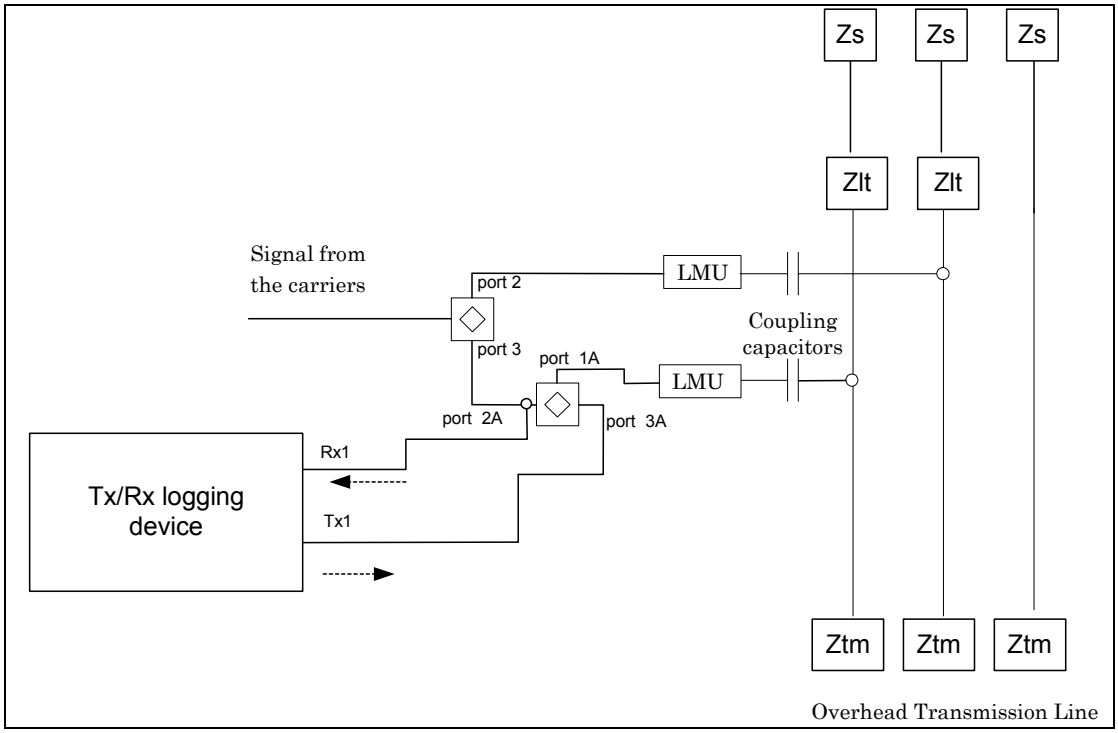

Figure 7.12 Logging complex isolation at the Measurement Hybrid at any frequency in the PLC band

7.6 Transmission line and station impedance

In Section 7.2, a PLC attenuation step change problem in the PLC-SAG tones was discovered and discussed. Section 7.3 provided background on the hybrid and Section 7.4 and 7.5 showed that a hybrid could be utilised to measure impedance very accurately in the vicinity of 75 Ω

The following section focuses more on the problem at hand. This section contains the following subsections to address the feasibility of the PLC-IMP system:

- Identifying the PLC related impedances
- PLC-IMP sensitivity analysis

- Preliminary impedance monitoring experiment on a live 400 kV system

7.6.1 Identifying PLC related impedances

The phase on which the impedance monitoring system is installed in Figure 7.11 and Figure 7.12 can be redrawn as shown in Figure 7.13. At the carrier frequencies, the coupling capacitor can be simplified as a short. It provides a low impedance path for the signals to be coupled to the OHTL. The LME is also simplified in Figure 7.13 and only the matching transformer is taken into consideration.

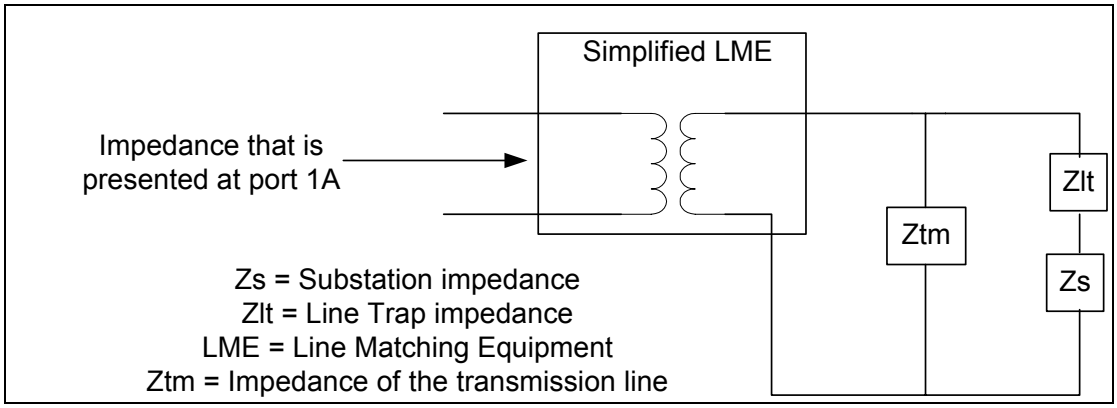

Figure 7.13 Impedance variations in the PLC system

In a normal operating PLC system only two major impedances can vary, namely the impedance of the transmission line (Ztm) and the impedance of the Power/Sub Station (Zs). The impedance of the Line Trap (Zlt) is fixed and should not vary under normal operating conditions unless it is damaged.

The Impedance of the transmission line (Ztm) normally varies with a day-night cycle, as the geometry of the conductor changes. This is primarily due to sag. The Power Station impedance variations are commonly more

dramatic, as station equipment (such as transformers) is switched on and off. Therefore it has a more step-like nature, but does not occur very often.

Variations in those impedances are transformed via the LME to be close to 75 ohm. Section 7.4 showed that the impedance monitoring technique is most sensitive at 75 ohm and therefore the slightest changes in transmission line impedance or power station impedance can be observed.

If the station impedance changes, the level of change will be known via the PLC-IMP system and the level changes of the PLC-SAG tones can be compensated for.

To obtain a more practical view of the proposed technique a sensitivity analysis will be done, followed by a preliminary experiment on the live KA OHTL.

7.6.2 PLC-IMP sensitivity analysis

The Koeberg-Acacia (KA) system will be used as basis for the following discussion. For simplification of the analysis let us assume that all the impedances are real.

The LME can be differently configured to match the impedance on the line side to the characteristic impedance of the PLC system. The LME at Acacia is strapped to match $390\,\Omega$ to $75\,\Omega$. From this, the winding ratio of the matching transformer can be easily computed as:

$$\frac{n_1}{n_2} = \sqrt{\frac{75}{390}} \qquad 7.12$$

The impedance of the transmission line (Ztm) can be simulated for three different heights at 250 kHz. The simulation default condition (as defined in Chapter 3) was used to compute Ztm. Three simulations were done for three different average heights (Table 7.2).

Table 7.2 OHTL Impedance of the KA OHTL

Average height [m]	Absolute value of the OHTL impedance [ohm]
13	333.7
14	336
15	338

Let's assume the Line trap impedance of $400\,\Omega$ at 250 kHz

Since the station impedance (Z_s) is unknown, an analysis will be done where $Z_s = \infty$ (open circuit) and $Z_s = 0$ (short circuit). With all the above information we can redraw Figure 7.13 as Figure 7.14.

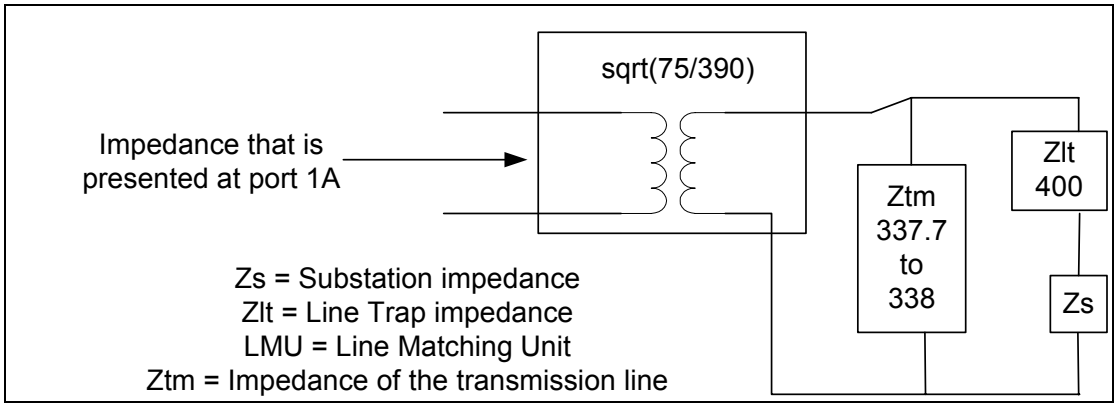

Figure 7.14 Impedances at Acacia's outer phase

Assume $Z_s = 0$ then

$$Z_{port1\_13m} = \left(\frac{75}{390}\right)\left(\frac{333.7 \cdot 400}{333.7 + 400}\right) = 37.81\ \Omega$$
$$Z_{port1\_15m} = \left(\frac{75}{390}\right)\left(\frac{338 \cdot 400}{338 + 400}\right) = 37.6\ \Omega \qquad 7.13$$

Further assume $Z_s = \infty$ then

$$Z_{port1\_13m} = \left(\frac{75}{390}\right)(333,7) = 64.17\ \Omega$$
$$Z_{port1\_15m} = \left(\frac{75}{390}\right)(338) = 65\ \Omega \qquad 7.14$$

If these impedances were measured via the PLC-IMP monitoring system the following results would be predicted by using the simulation done in Figure 7.7.

For the scenario where $Z_s = 0$

$$F_h\left(Z_{port1\_13m}\right) = 14.09dB$$
$$F_h\left(Z_{port1\_15m}\right) = 14.01dB \qquad 7.15$$

For the scenario where $Z_s = \infty$

$$F_h\left(Z_{port1\_13m}\right) = 22.178dB$$
$$F_h\left(Z_{port1\_15m}\right) = 22.922dB \qquad 7.16$$

where F_h is the transfer function of the isolation (Equation 7.10) as a function of the impedance presented at Port 1 (Z_1).

The technique therefore provides a range of at least 8 dB to monitor the station impedance (Z_s) as described in this particular case. The sensitivity

would be further analysed via preliminary live line impedance experiment on the KA system.

7.6.3 Preliminary impedance monitoring experiment

Due to the fact that no hardware change was needed for the PLC-IMP system, the hybrid already installed at Acacia and used by the PLC-SAG system could be utilised to perform the initial trial of the impedance monitoring technique.

Referring to Figure 7.11, the local carrier tone (349.4 kHz) energised Port 2A of the measuring hybrid. The magnitude of the power at Port 3A of the measurement hybrid was logged over a period of one week at a local carrier frequency. The local carrier's transmit level is very reliable and constant under normal operating conditions. The results of the logged data at Port 3A are shown in Figure 7.15.

A very clear day-night variation in the impedance can be noted. The magnitude variation in the carrier signal level measured at Port 3A (Figure 7.11) is in the order of 0.4 dB. This implies that the impedance monitoring technique is sensitive enough to detect fractional variations of ohms (Equation 7.15 and 7.16). The impedance variations of the station can thus be monitored very accurately.

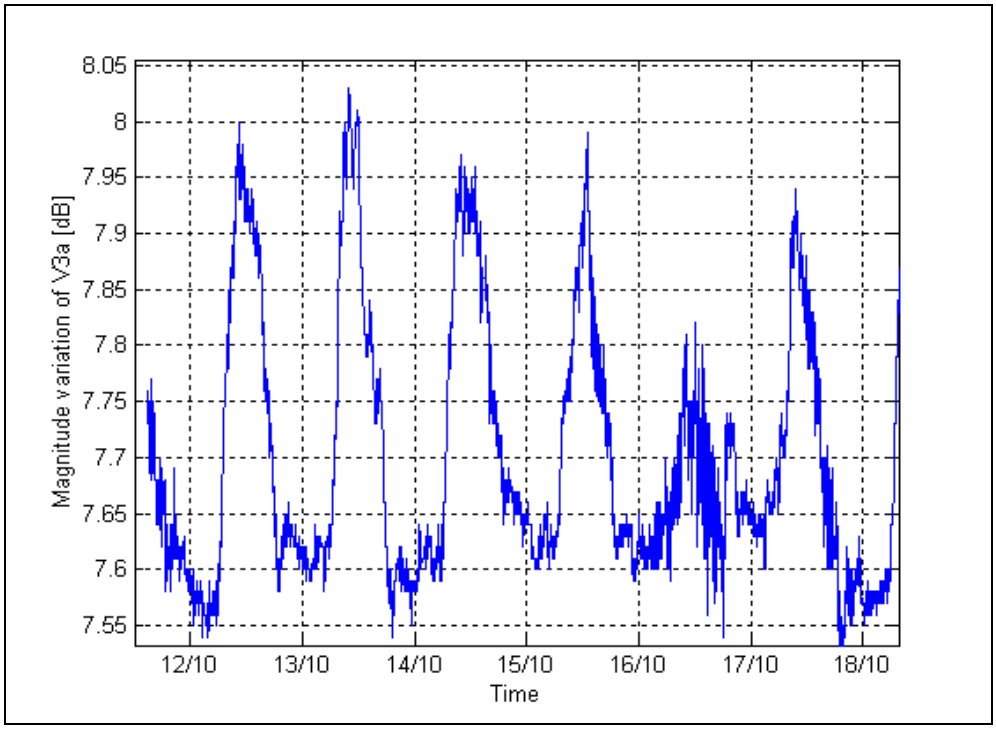

Figure 7.15 Measured variations in the magnitude of the insertion loss over a period of one week on the KA OHTL

7.7 Conclusion

A step change in the logged data at Acacia Substation led to the reliability of the PLC-SAG technique being questioned. This was alarming, since it was unclear whether the problem could be overcome.

After a demanding period of time, a unique solution was found. By exploring the complex isolation characteristics of the hybrid, it was found that the hybrid could be employed to measure the PLC impedance. This technique proved to have the required sensitivity to measure the changes in impedance. In the event of unexpected impedance change the PLC-SAG calibration can be adjusted. Details of the PLC-IMP monitoring technique and the interaction with the PLC-SAG system have still to be researched.

The new technique also could be used for real-time condition monitoring of PLC hardware.

References:

[1] **Everitt, W. L,** *Communication Engineering*, Second Edition, McGraw-Hill, New York, 1937, page 318.

[2] **JH Cloete,** Personal communication, University of Stellenbosch, September 2005.

[3]] **Brown Boveri** (BBC) application sheet for **A9BM**, Carrier combiner Unit used for Phase to Phase Coupling, BBC stock no. henf 105 169 R1, edition 1981.

[4] **Funk, H.**, Wandel & Goltermann Operation manual **"**LevelPRO /LevelPRO NT Control and Evaluation Software for SPM/PSM – 37..139", Edition: 02/99.09 (V3.0), 1999, page 4.4.

Chapter 8

Conclusions and Recommendations

8.1 Conclusions

This thesis has proved experimentally, by two independent case studies, that the PLC system can be utilised to measure the average conductor height variation of an OHTL very accurately. The technique of "tracking" the OHTL conductor height is called the PLC-SAG technique or system.

The procedure of installing the PLC-SAG system is streamlined with the simulation program as discussed in Chapter 3. A simulation methodology was defined together with a criterion to select the PLC-SAG monitoring tones' frequencies.

Two experimental PLC-SAG installations were successfully made on live 400 kV transmission systems without interrupting the power supply (Chapter 4).

The PLC-SAG calibration process was discussed, which involves direct height measurements (Chapter 5 and 6). Once the measurements had been performed the PLC-SAG system could be calibrated.

A PLC-SAG calibration problem was discovered which threatened the practicality of the PLC-SAG technique (Chapter 7).

An innovative solution was found to address this PLC-SAG calibration problem. The new system, called PLC-IMP, tracks the impedance of the PLC system by taking advantage of all the characteristics of the measurement hybrid.

One of the exceptional advantages of the PLC-IMP solution in the framework of this research is that it uses the same measurement hybrid as the PLC-SAG system. A single system integrating the PLC-SAG and the PLC-IMP can now be proposed and will be discussed in the following section.

The reason why the impedance monitoring technique was given its own entity, PLC-IMP, and not incorporated into the PLC-SAG entity, was that there is a potential market for a PLC-IMP product alone. The PLC-IMP system can be implemented as a condition monitoring system of the PLC infrastructure. The PLC-SAG system cannot operate independently without the PLC-IMP system.

The lifetime of an Ampacity system is in the order of 2-3 years, as the power system is upgraded. Therefore the ability to quickly install a system without major changes to the existing system is very important. In this regard the PLC-SAG & PLC-IMP systems can be quickly installed and calibrated, which makes this a highly competitive technique.

8.2 Recommendations

From the above study, measurable PLC-SAG tone level variations are noted due to conductor sag and impedance changes in the system. Major station impedance has a very low frequency of occurrence, which is noticeably different to the day-to-day variations due to OHTL conductor sag. In order to monitor the PLC-SAG tones efficiently it is very important to distinguish between the two phenomena and to correctly compensate for station impedance variations.

Development needs to be done on an integrated PLC-SAG & PLC-IMP system. The following system is proposed as a starting point of this future research.

At each monitoring station one PLC-SAG & PLC-IMP unit needs to be installed. The PLC-SAG & PLC-IMP units comprise the following:

1) Generator 1: 75 ohm generator
2) Channel 1: High impedance voltage measurement in the time domain
3) Channel 2: High impedance voltage measurement in the time domain

The PLC-SAG & PLC-IMP units need to be connected to the existing PLC system, as shown in Figure 8.1. The measurement hybrid does not influence the PLC system significantly, as has been discussed in Chapter 4.

Table 8.1 Modes of operation for the PLC-SAG&PLC-IMP system

Mode	PLC-SAG & PLC-IMP UNIT A	PLC-SAG & PLC-IMP UNIT B
1) PLC-IMP at Station A	GEN 1, CH 1 and CH 2	-
2) PLC-SAG A to B	GEN 1	CH 2
3) PLC-IMP at Station B	-	GEN 1, CH 1 and CH 2
4) PLC-SAG B to A	CH 2	GEN 1

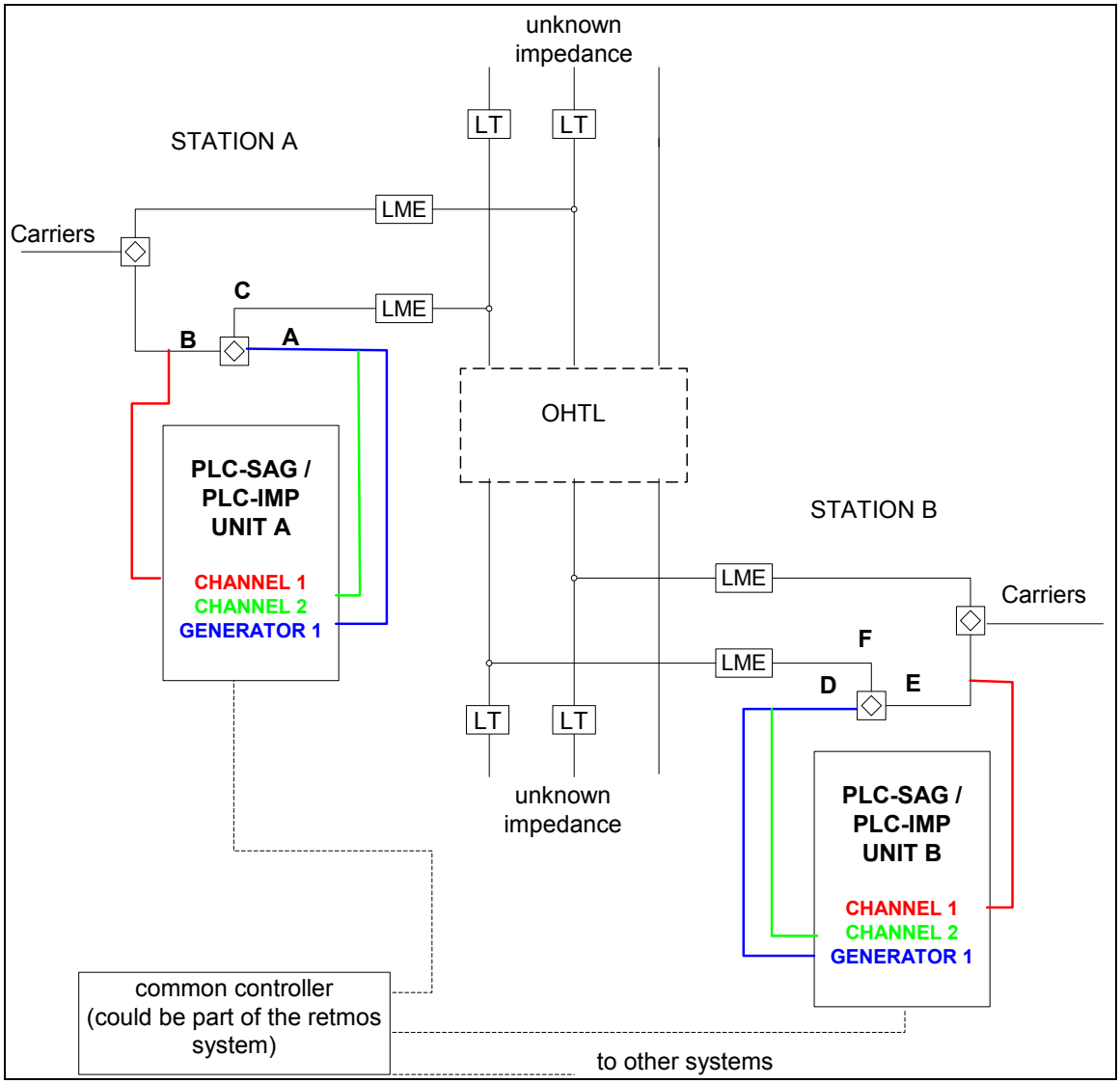

Figure 8.1 Proposed setup for newly designed prototype units (Coupling Capacitors not shown)

The operational modes of the proposed system can be summarized in column 1 in Table 8.1. Columns 2 and 3 table the active components for each mode of the PLC-SAG & PLC-IMP units A and B respectively.

Only modes 1 and 2 will now be further discussed, as they are functionally identical to modes 3 and mode 4.

8.2.1 Mode 1: PLC-IMP at Station A

In this mode the PLC impedance at point C in Figure 8.1 is measured. Significant impedance variations, which influence the PLC-SAG system, can be tracked by using the monitoring hybrid as a sensitive impedance-monitoring device (Chapter 7). By tracing the PLC impedance, the PLC-SAG calibration values can be compensated for in the event of an impedance change.

8.2.2 Mode 2: PLC-SAG A to B

In this mode the PLC-SAG tones are transmitted at station A and logged at Station B. As proved in this thesis, by a straightforward action of transmitting and receiving specially coupled tones, the average conductor height can be tracked very accurately. Mode 2 and Mode 4 form part of the duplex logging system as described in Chapter 4.

Appendix A

OHTL and PLC system details for the two case studies

A.1 Introduction

This Appendix contains detailed information about the two case studies.

First, the Koeberg-Acacia OHTL (Case study 1) is described in Section A.2. Figure A.1 shows the database information used for the simulation program. Table A.1 shows the tower and span details of Koeberg Acacia OHTL from the ESKOM GIS database. Section A.3 gives more detail about the PLC system on the Koeberg-Acacia OHTL.

Section A.4 describes the Kriel-Tutuka OHTL (Case study 2). As the line is introduced in Chapter 3, seven different sections can be noted. The seven different sections need to be individually specified for the simulations. The details of the section are given in Figure A.3 to Figure A.9. The simulation program automatically integrates the sections, to simulate the whole transmission line. The Appendix is concluded with PLC system information of the Kriel-Tutuka system in Section A.5

A.2 Koeberg-Acacia OHTL

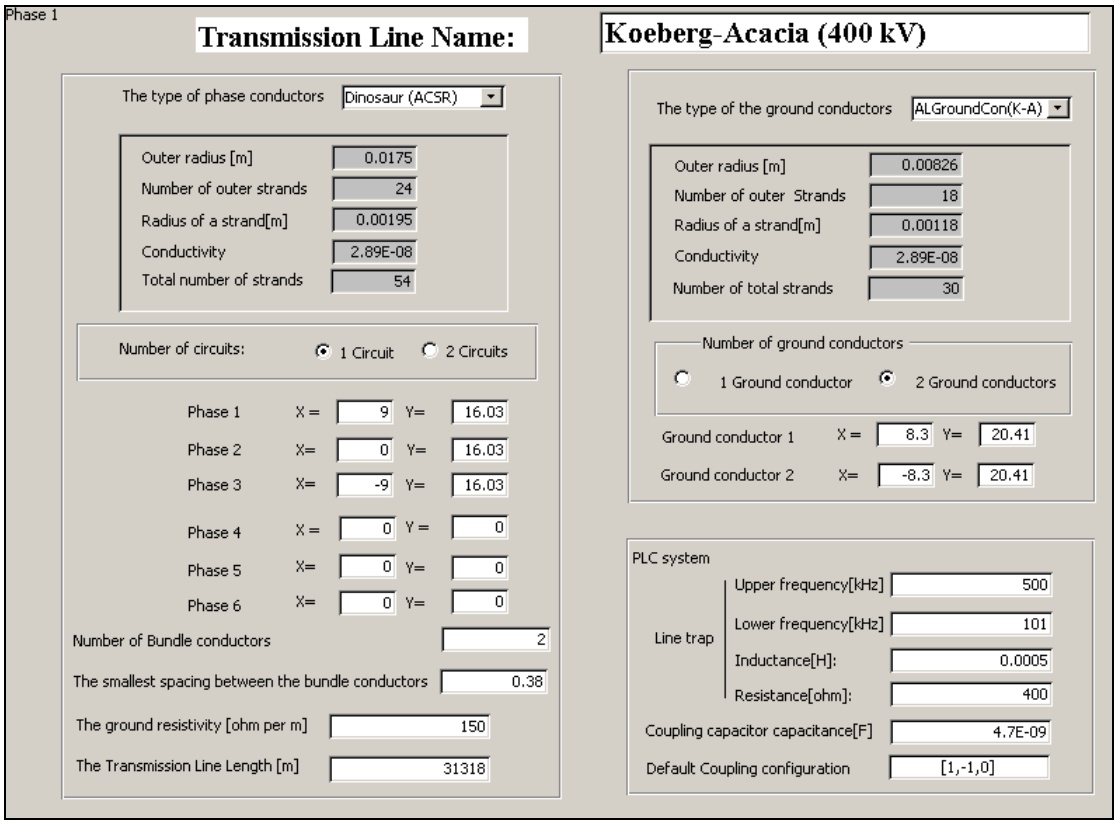

Figure A.1 OHTL details of Koeberg-Acacia

Table A.1 Tower and span details of the Koeberg-Acacia OHTL

TWR_PREF	TWR_NO	COND_ATT	HEIGHT	TWR_START	TWR_END	LENGTH	Calibration points
1AC/KO	1	19.9	22.6	1	2	343.225	
1AC/KO	2	19.9	25	**2**	**3**	**349.672**	**CA 1**
1AC/KO	3	19.9	28.2	3	4	356.372	
1AC/KO	4	19.9	30.4	4	5	334.354	
1AC/KO	5	22.95	34.2	5	6	305.32	
1AC/KO	6	19.9	37.8	6	7	318.33	
1AC/KO	7	19.9	41.5	7	8	313.324	
1AC/KO	8	22.95	46.1	8	9	296.308	
1AC/KO	9	19.9	50.4	9	10	159.166	
1AC/KO	10	19.9	52.3	10	11	296.025	
1AC/KO	11	19.9	54.2	11	12	251.009	
1AC/KO	12	19.9	54.2	12	13	358.033	
1AC/KO	13	19.9	56.4	13	14	330.149	
1AC/KO	14	19.9	56	14	15	317.14	
1AC/KO	15	19.9	55.6	15	16	297.128	
1AC/KO	16	19.9	58	16	17	321.147	

1AC/KO	17	19.9	59.1	17	18	341.148	
1AC/KO	18	19.9	61.5	18	19	300.13	
1AC/KO	19	19.9	63.5	19	20	312.259	
1AC/KO	20	19.9	60.1	20	21	310.267	
1AC/KO	21	19.9	56.9	21	22	392.325	
1AC/KO	22	26	55.1	22	23	400.328	
1AC/KO	23	19.9	55	23	24	273.232	
1AC/KO	24	19.9	51.7	24	25	361.324	
1AC/KO	25	22.95	49	25	26	379.353	
1AC/KO	26	19.9	45.6	26	27	354.328	
1AC/KO	27	19.9	41.6	27	28	301.274	
1AC/KO	28	19.9	35.8	28	29	345.382	
1AC/KO	29	22.95	26.7	29	30	389.427	
1AC/KO	30	19.9	15.8	30	31	240.267	
1AC/KO	31	19.9	12.8	31	32	217.359	
1AC/KO	32	19.9	11.2	32	33	242.392	
1AC/KO	33	19.9	9.8	33	34	302.045	
1AC/KO	34	26	5.4	34	35	467.069	
1AC/KO	35	22.95	11.2	35	36	344.053	
1AC/KO	36	19.9	7.7	36	37	333.047	
1AC/KO	37	19.9	9.3	37	38	397.063	
1AC/KO	38	26	10.3	38	39	404.042	
1AC/KO	39	19.9	17.7	39	40	292.093	
1AC/KO	40	19.9	22.4	40	41	313.087	
1AC/KO	41	19.9	27.1	41	42	313.086	
1AC/KO	42	19.9	32.6	42	43	316.08	
1AC/KO	43	19.9	36	43	44	301.079	
1AC/KO	44	19.9	40.3	44	45	362.1	
1AC/KO	45	19.9	44.1	45	46	329.085	
1AC/KO	46	19.9	50.6	46	47	332.079	
1AC/KO	47	19.9	54.3	47	48	334.087	
1AC/KO	48	19.9	58.8	48	49	334.086	
1AC/KO	49	19.9	64	49	50	302.03	
1AC/KO	50	19.9	69.1	50	51	289.019	
1AC/KO	51	19.9	73.6	**51**	**52**	**345.161**	**CA 2**
1AC/KO	52	22.95	78.8	52	53	369.182	
1AC/KO	53	22.95	87.6	53	54	347.164	
1AC/KO	54	19.9	97.3	54	55	349.16	
1AC/KO	55	19.9	104.6	55	56	362.167	
1AC/KO	56	19.9	114.5	56	57	354.171	
1AC/KO	57	19.9	125.8	57	58	338.153	
1AC/KO	58	19.9	134.7	58	59	326.146	
1AC/KO	59	19.9	144.2	59	60	251.404	
1AC/KO	60	19.86	150.1	60	61	422.121	
1AC/KO	61	25.86	139.3	61	62	432.127	
1AC/KO	62	22.86	123.8	62	63	374.106	

1AC/KO	63	19.86	112.1	63	64	390.115	
1AC/KO	64	19.86	106.2	64	65	349.093	
1AC/KO	65	19.86	107.3	65	66	307.087	
1AC/KO	66	19.86	107.8	66	67	367.103	
1AC/KO	67	22.86	112	67	68	323.09	
1AC/KO	68	19.86	117	68	69	257.076	
1AC/KO	69	22.86	104	69	70	414.11	
1AC/KO	70	19.86	87.8	70	71	342.116	
1AC/KO	71	19.86	82	71	72	380.131	
1AC/KO	72	22.86	73.6	72	73	392.129	
1AC/KO	73	19.86	72.1	73	74	292.098	
1AC/KO	74	19.86	64.3	74	75	364.113	
1AC/KO	75	22.86	51.9	75	76	403.133	
1AC/KO	76	22.86	35.9	76	77	409.131	
1AC/KO	77	22.86	27.9	77	78	262.084	
1AC/KO	78	19.86	28.8	78	79	361.12	
1AC/KO	79	19.86	27.3	79	80	360.119	
1AC/KO	80	22.86	28.2	80	81	360.112	
1AC/KO	81	19.86	29.1	81	82	376.111	
1AC/KO	82	22.86	29.1	82	83	372.108	
1AC/KO	83	19.86	30.4	83	84	338.108	
1AC/KO	84	22.86	28.9	84	85	379.119	
1AC/KO	85	19.86	28.4	85	86	356.097	
1AC/KO	86	19.86	29.8	86	87	352.109	
1AC/KO	87	19.86	29.4	87	88	296.029	
1AC/KO	88	22.86	27.9	**88**	**89**	**376.035**	**CA 3**
1AC/KO	89	19.86	25.8	89	90	244.021	
1AC/KO	90	19.86	24.5	90	91	379.036	
1AC/KO	91	22.86	21.3	91	92	404.024	
1AC/KO	92	19.86	23.3	92	93	302.04	
1AC/KO	93	25.86	15.5	93	94	365.722	
1AC/KO	94	19.86	14				

A.3 Koeberg-Acacia PLC system

Line Trap inductance: 0.5mH;

Bandwidth of Line Trap: 101-500 kHz

Capacitance of CVT: 4600 pf

LME Strapping of an “Electrisk Bureau” (EB):

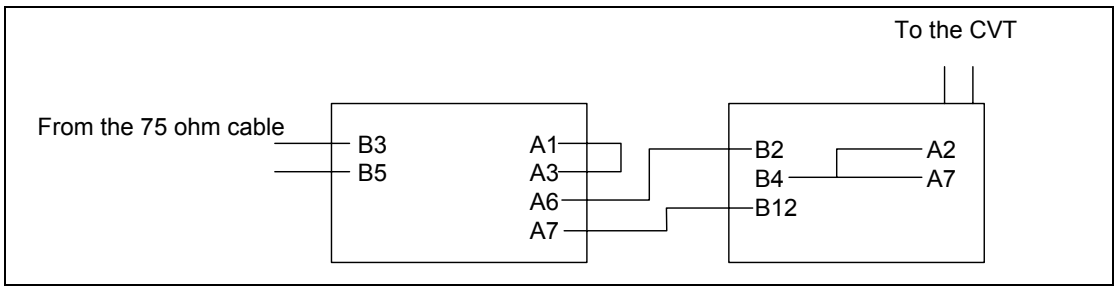

Figure A.2 LME strapping at Koeberg and Acacia for a standard ("Electrisk Bureau" LME)

A.4 Kriel-Tutuka OHTL

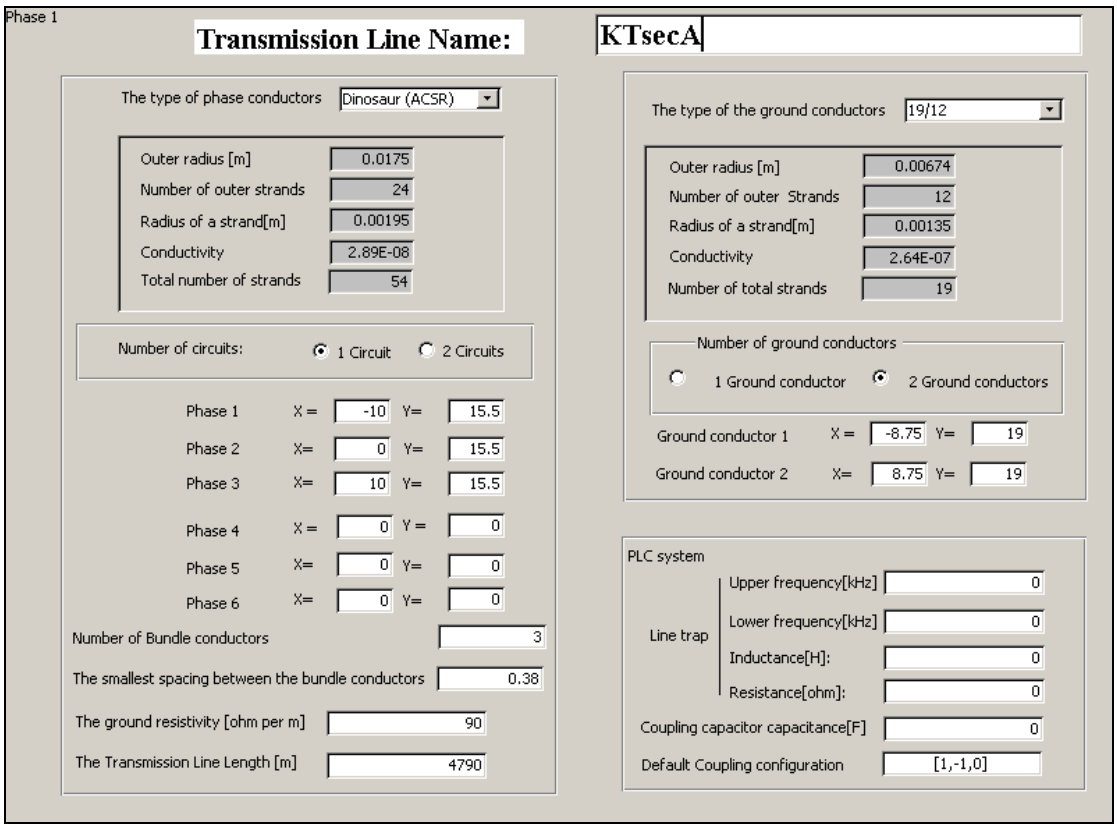

Figure A.3 Section A of KT

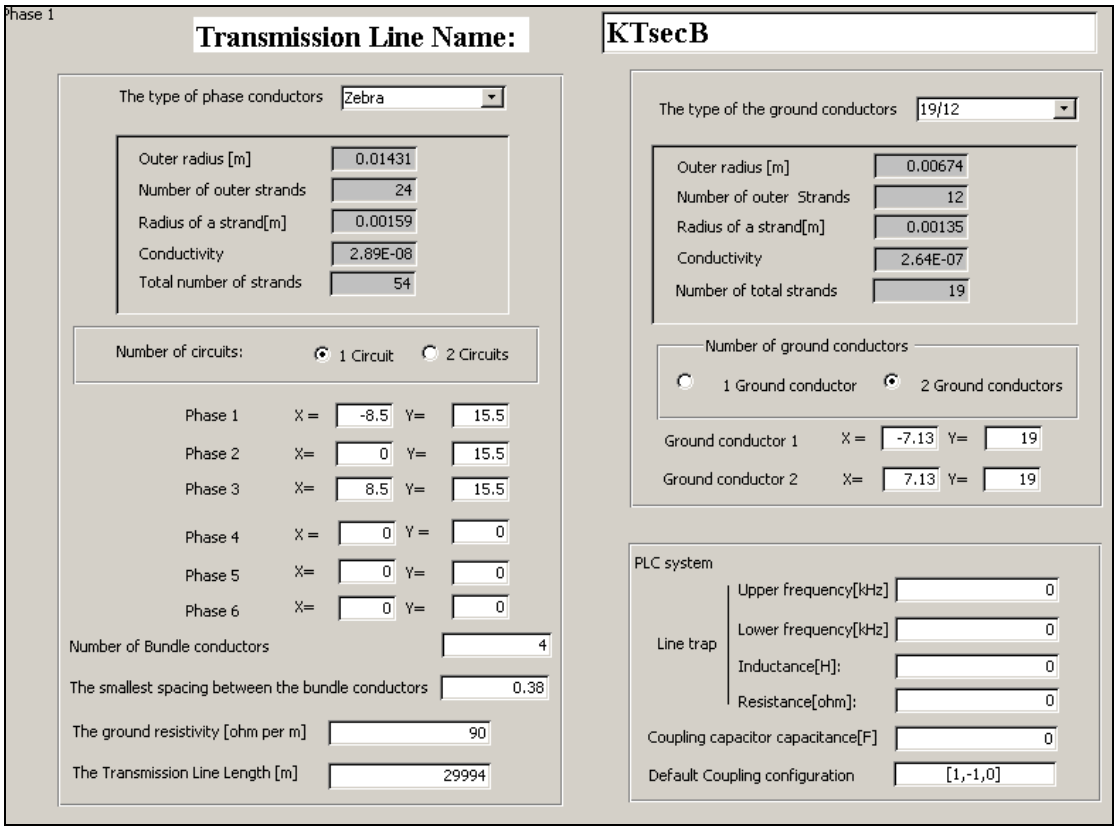

Figure A.4 Section B of KT

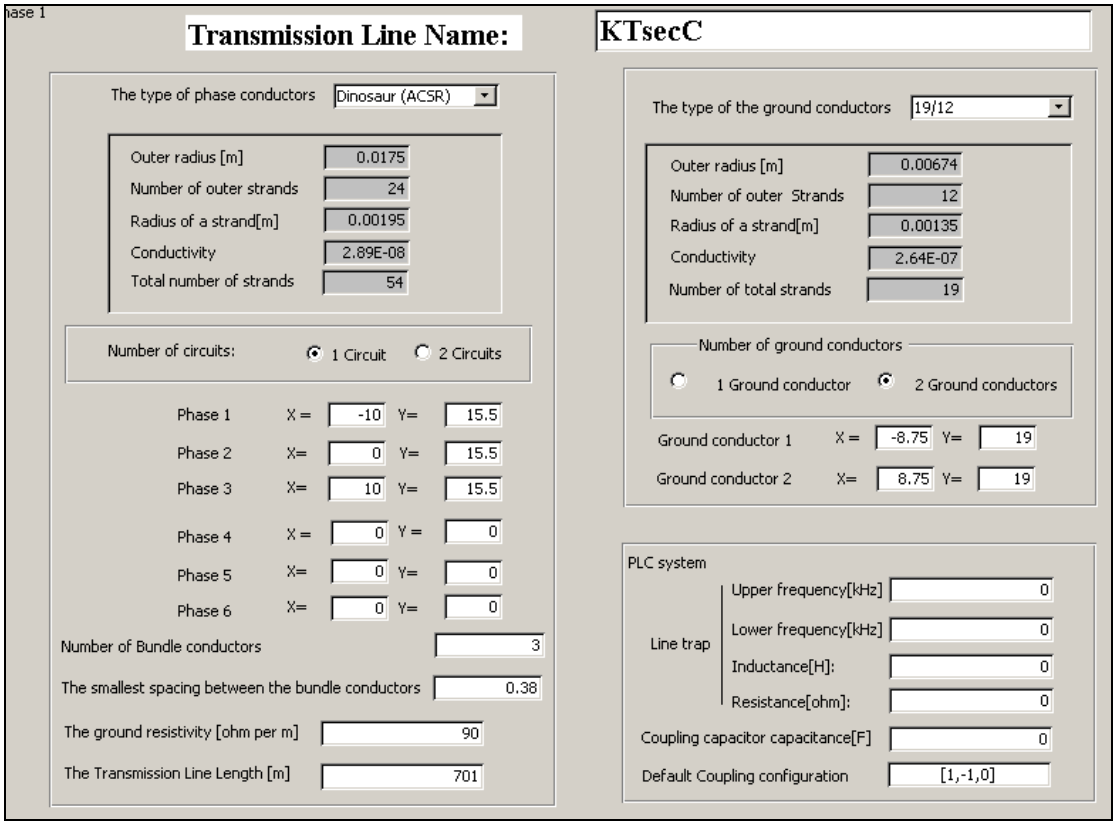

Figure A.5 Section C of KT

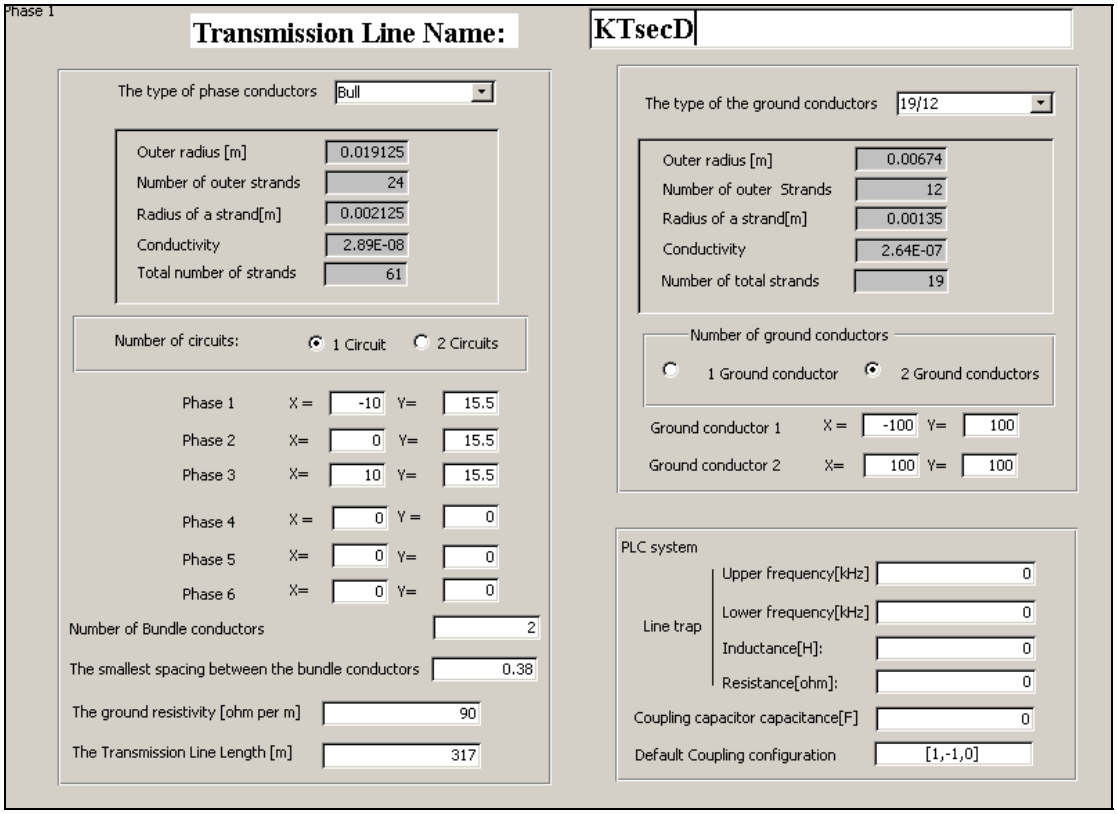

Figure A.6 Section D of KT

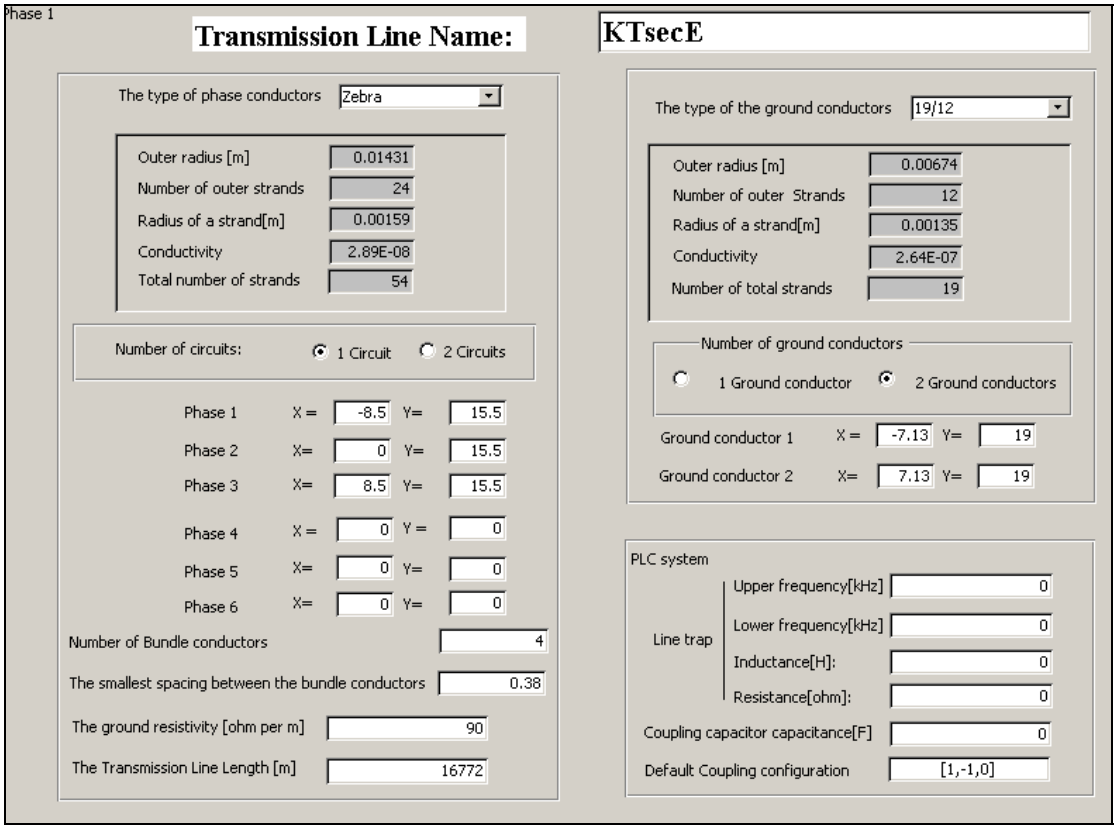

Figure A.7 Section E of KT

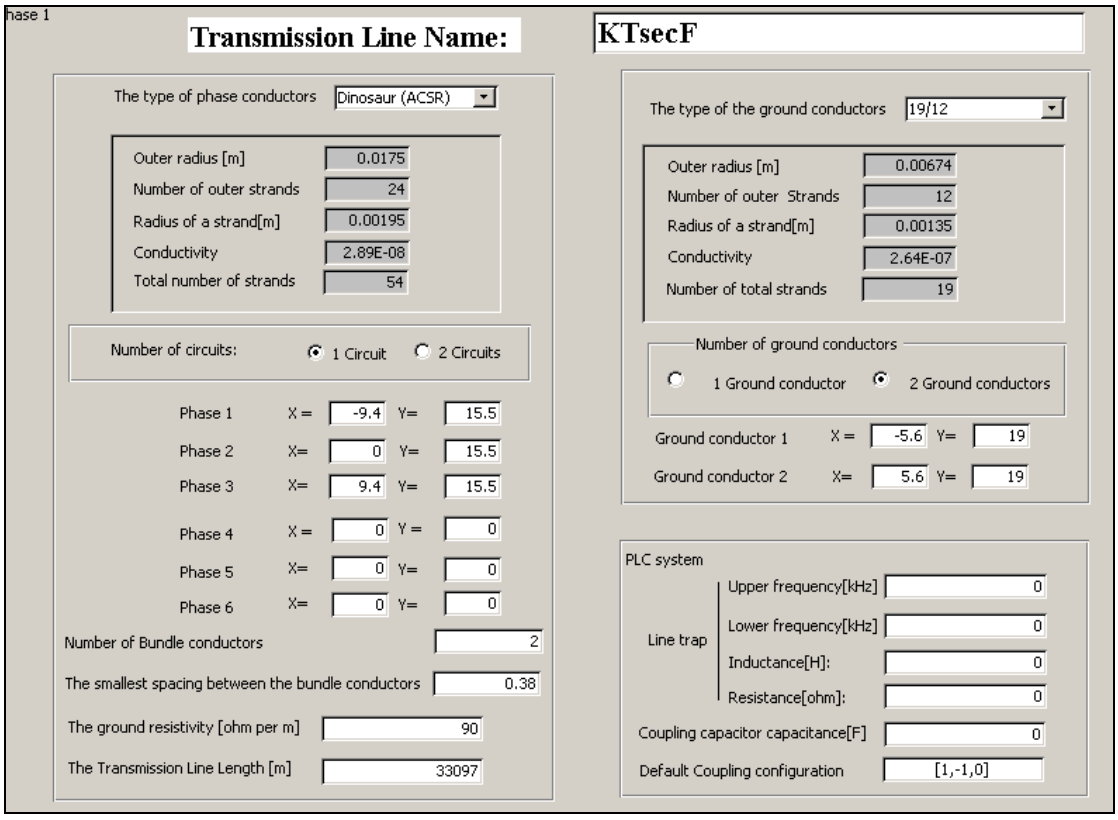

Figure A.8 Section F of KT

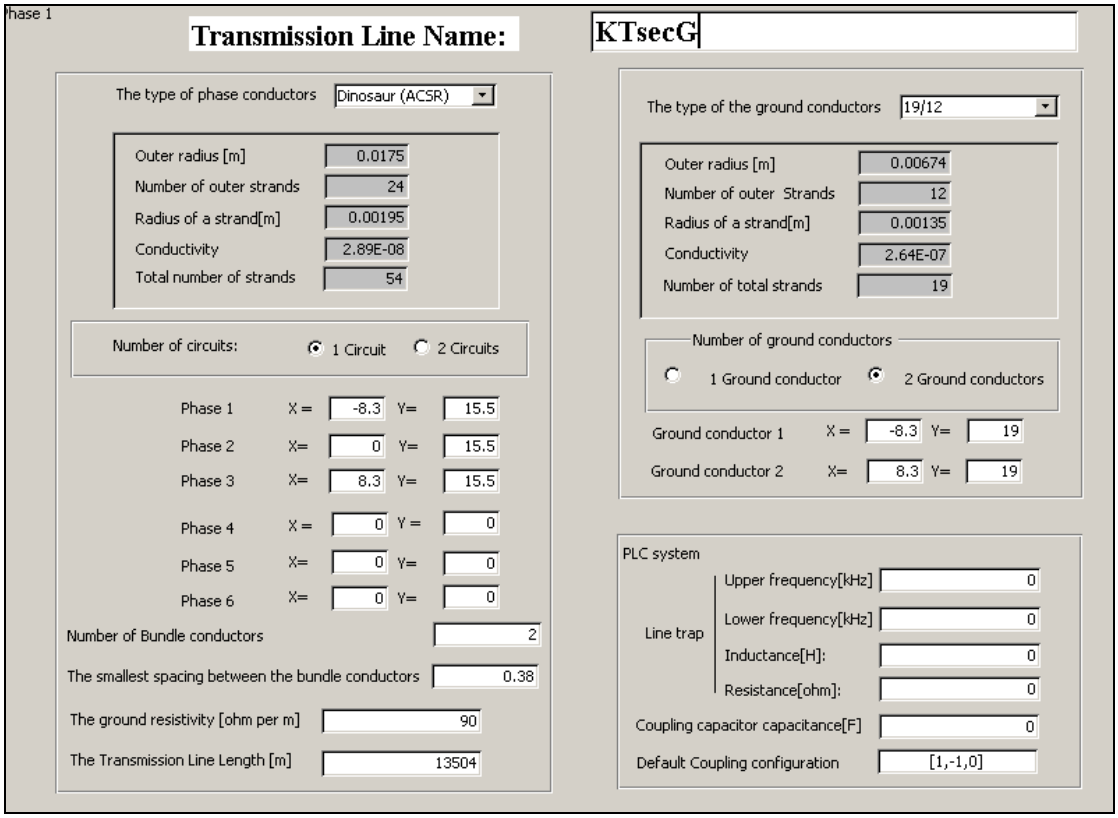

Figure A.9 Section G of KT

Table A.2 Tower and span details of the Kriel-Tutuka OHTL

TWR_PREF	TWR_NO	COND_ATT	HEIGHT	TWR_START	TWR_END	LENGTH	Calibration points
--------	----	---------	---------	----	----	---------	
1KR/TU	1	19.86	1621.5	1	2	213.84	
1KR/TU	2	25.86	1616.7	2	3	225.819	
1KR/TU	3	19.86	1613.8	3	4	202.842	
1KR/TU	4	19.86	1610.6	4	5	412.04	
1KR/TU	5	25.86	1619.1	5	6	358.029	
1KR/TU	6	19.86	1616.8	6	7	346.023	
1KR/TU	7	19.86	1614.7	7	8	335.036	
1KR/TU	8	19.86	1612.5	8	9	326.027	
1KR/TU	9	19.86	1612.1	9	10	342.005	
1KR/TU	10	19.86	1609.6	10	11	311	
1KR/TU	11	25.86	1601.9	11	12	481.012	
1KR/TU	12	25.86	1604.1	12	13	222.001	
1KR/TU	13	19.86	1617	13	14	196.928	
1KR/TU	14	19.86	1616.5	**14**	**15**	**412.617**	**CA 1**
1KR/TU	15	25.86	1617.9	15	16	408.622	
1KR/TU	16	22.5	1622.2	16	17	333.35	
1KR/TU	17	25.5	1622	17	18	278.205	
1KR/TU	18	24	1611.2	18	19	357.882	
1KR/TU	19	27	1597	19	20	533.833	

1KR/TU	20	27	1603.4	20	21	453.852	
1KR/TU	21	27	1592.9	21	22	399.867	
1KR/TU	22	25.5	1588	22	23	502.838	
1KR/TU	23	25.5	1595.6	23	24	403.874	
1KR/TU	24	24	1606.8	24	25	471.853	
1KR/TU	25	28.5	1616.9	25	26	256.113	
1KR/TU	26	27	1623.5	26	27	343.103	
1KR/TU	27	22.5	1626.6	27	28	460.925	
1KR/TU	28	31.5	1619.4	28	29	514.918	
1KR/TU	29	30	1612.2	29	30	483.92	
1KR/TU	30	28.5	1611.5	30	31	503.925	
1KR/TU	31	31.5	1603.4	31	32	495.912	
1KR/TU	32	30	1589	32	33	497.927	
1KR/TU	33	25.5	1576.8	33	34	311.246	
1KR/TU	34	22.5	1581.8	34	35	413.769	
1KR/TU	35	27	1587.2	35	36	471.732	
1KR/TU	36	27	1569.5	36	37	450.743	
1KR/TU	37	25.5	1572.6	37	38	451.749	
1KR/TU	38	25.5	1578.5	38	39	394.775	
1KR/TU	39	21	1581	39	40	362.493	
1KR/TU	40	19.5	1584.8	40	41	265.477	
1KR/TU	41	25.5	1587.4	41	42	466.316	
1KR/TU	42	33	1595.1	42	43	498.374	
1KR/TU	43	25	1599.8	43	44	348.77	
1KR/TU	44	18	1608	44	45	324.061	
1KR/TU	45	22.5	1599.8	45	46	424.78	
1KR/TU	46	27	1616.5	46	47	467.764	
1KR/TU	47	27	1620.1	47	48	457.769	
1KR/TU	48	25.5	1631.2	48	49	433.781	
1KR/TU	49	27	1639.9	49	50	486.75	
1KR/TU	50	28.5	1642.5	50	51	476.751	
1KR/TU	51	28.5	1645.5	51	52	447.976	
1KR/TU	52	22.5	1646.5	52	53	479.038	
1KR/TU	53	31.5	1660.7	53	54	483.04	
1KR/TU	54	30	1659.3	54	55	515.037	
1KR/TU	55	31.5	1664	55	56	485.046	
1KR/TU	56	28.5	1665	56	57	446.431	
1KR/TU	57	27.5	1680.1	57	58	370.119	
1KR/TU	58	28.5	1664.5	58	59	535.158	
1KR/TU	59	27	1658.5	59	60	496.254	
1KR/TU	60	30.5	1663.4	60	61	441.988	
1KR/TU	61	33	1655.4	61	62	510.981	
1KR/TU	62	24	1648	62	63	488.977	
1KR/TU	63	43	1638.3	63	64	408.987	
1KR/TU	64	33	1644.5	64	65	507.979	
1KR/TU	65	30	1648.1	65	66	489.984	

1KR/TU	66	31.5	1647	66	67	486.984	
1KR/TU	67	28.5	1629.5	67	68	497.98	
1KR/TU	68	31.5	1624.4	68	69	477.98	
1KR/TU	69	30	1615.5	69	70	470.992	
1KR/TU	70	28.5	1594.5	70	71	398.181	
1KR/TU	71	22.5	1598.3	71	72	442.746	
1KR/TU	72	28.5	1606.6	72	73	461.733	
1KR/TU	73	29.5	1611.5	73	74	301.119	
1KR/TU	74	22.5	1616	74	75	253.686	
1KR/TU	75	18	1620	75	76	279.254	
1KR/TU	76	19.5	1621.2	76	77	399.916	
1KR/TU	77	25.5	1612.7	77	78	491.89	
1KR/TU	78	31.5	1606.4	78	79	509.887	
1KR/TU	79	31.5	1606.8	79	80	466.899	
1KR/TU	80	30	1607	80	81	530.883	
1KR/TU	81	28.5	1589	81	82	394.213	
1KR/TU	82	22.5	1583.7	82	83	234.86	
1KR/TU	83	18	1575.7	83	84	322.8	
1KR/TU	84	28.5	1569	84	85	402.55	
1KR/TU	85	19	1567.5	85	86	262.903	
1KR/TU	86	19.86	1566.1	86	87	373.862	
1KR/TU	87	19.86	1565.8	87	88	327.929	
1KR/TU	88	11.8	0	88	89	69.347	
1KR/TU	89	11.8	0	89	90	82.109	
1KR/TU	90	11.8	0	90	91	90.252	
1KR/TU	91	11.8	0	91	92	30.583	
1KR/TU	92	8.8	0	92	93	44.078	
1KR/TU	93	11.8	0	93	94	362.326	
1KR/TU	94	27	1575	94	95	449.32	
1KR/TU	95	28.5	1575.9	95	96	477.6	
1KR/TU	96	31.5	1577.9	96	97	519.236	
1KR/TU	97	28	1581.9	97	98	232.659	
1KR/TU	98	33.5	1582.7	98	99	550.256	
1KR/TU	99	47	1591.3	99	100	550.813	
1KR/TU	100	22	1597.6	100	101	466.263	
1KR/TU	101	31.5	1604.1	101	102	533.253	
1KR/TU	102	31.5	1604.1	102	103	450.943	
1KR/TU	103	22	1600.7	103	104	425.477	
1KR/TU	104	22	1607.5	104	105	334.082	
1KR/TU	105	19.5	1601.9	105	106	455.192	
1KR/TU	106	27	1586.5	106	107	473.202	
1KR/TU	107	27	1587.1	107	108	416.932	
1KR/TU	108	24	1593.2	108	109	474.942	
1KR/TU	109	27	1600.9	109	110	434.002	
1KR/TU	110	28.5	1613.2	110	111	402.682	
1KR/TU	111	25	1617.7	111	112	439.126	

1KR/TU	112	30	1621.4	112	113	406.796	
1KR/TU	113	28.5	1636.8	113	114	472.779	
1KR/TU	114	30	1634.6	114	115	448.327	
1KR/TU	115	18	1626.9	115	116	380.81	
1KR/TU	116	18	1629.7	116	117	327.608	
1KR/TU	117	24	1612.5	117	118	507.363	
1KR/TU	118	25.5	1589.7	118	119	483.992	
1KR/TU	119	25.5	1603.7	119	120	460.482	
1KR/TU	120	30	1612.8	120	121	519.326	
1KR/TU	121	25.5	1606.5	121	122	391.296	
1KR/TU	122	19.5	1595.9	122	123	362.119	
1KR/TU	123	18	1582.7	123	124	335.822	
1KR/TU	124	18	1586.2	124	125	400.92	
1KR/TU	125	30	1595.8	125	126	475.856	
1KR/TU	126	25.5	1608	126	127	500.708	
1KR/TU	127	27	1594.5	127	128	470.255	
1KR/TU	128	22.5	1593.1	128	129	311.803	
1KR/TU	129	18	1603	129	130	106.424	
1KR/TU	130	18	1607	130	131	408.766	
1KR/TU	131	33	1616.1	131	132	350.923	
1KR/TU	132	27	1622.5	**132**	**133**	**464.967**	**CA2**
1KR/TU	133	29.5	1621.2	133	134	98.159	
1KR/TU	134	19.9	1624.7	134	135	343.572	
1KR/TU	135	19.9	1627	135	136	321.003	
1KR/TU	136	19.9	1624.6	136	137	374.053	
1KR/TU	137	19.9	1618.5	137	138	287.166	
1KR/TU	138	19.9	1605.4	138	139	349.362	
1KR/TU	139	19.9	1590.4	139	140	309.111	
1KR/TU	140	19.9	1577.9	140	141	353.024	
1KR/TU	141	19.9	1568.9	141	142	348.136	
1KR/TU	142	19.9	1567.3	142	143	365.213	
1KR/TU	143	19.9	1568.8	143	144	355.448	
1KR/TU	144	19.9	1573.7	144	145	340.211	
1KR/TU	145	19.9	1576.1	145	146	397.153	
1KR/TU	146	22.95	1579.8	146	147	367.858	
1KR/TU	147	19.9	1579.2	147	148	355.966	
1KR/TU	148	19.9	1580.4	148	149	356.559	
1KR/TU	149	19.9	1580.9	149	150	381.256	
1KR/TU	150	22.95	1581.3	150	151	382.757	
1KR/TU	151	19.9	1582.5	151	152	410.26	
1KR/TU	152	19.9	1595.3	152	153	341.954	
1KR/TU	153	19.9	1602	153	154	342.566	
1KR/TU	154	19.9	1602.3	154	155	360.957	
1KR/TU	155	19.9	1599.9	155	156	338.864	
1KR/TU	156	19.9	1605.4	156	157	368.159	
1KR/TU	157	19.9	1613.9	157	158	317.567	

1KR/TU	158	19.9	1614.2	158	159	357.154	
1KR/TU	159	19.9	1606.9	159	160	337.667	
1KR/TU	160	19.9	1600.8	160	161	352.657	
1KR/TU	161	19.9	1595.9	161	162	319.67	
1KR/TU	162	19.9	1593.8	162	163	374.558	
1KR/TU	163	19.9	1598.7	163	164	309.76	
1KR/TU	164	19.9	1599.3	164	165	429.758	
1KR/TU	165	19.9	1597.4	165	166	325.766	
1KR/TU	166	19.9	1602.6	166	167	319.951	
1KR/TU	167	19.9	1603.5	167	168	319.971	
1KR/TU	168	19.9	1603.8	168	169	342.265	
1KR/TU	169	19.9	1596.5	169	170	402.253	
1KR/TU	170	19.9	1592.9	170	171	362.062	
1KR/TU	171	19.9	1596.2	171	172	316.059	
1KR/TU	172	19.9	1601.7	172	173	337.968	
1KR/TU	173	19.9	1601.1	173	174	355.152	
1KR/TU	174	19.9	1606.9	174	175	340.171	
1KR/TU	175	19.9	1607.8	175	176	363.259	
1KR/TU	176	19.9	1610.2	176	177	356.561	
1KR/TU	177	19.9	1609.6	177	178	370.252	
1KR/TU	178	19.9	1612.9	178	179	353.864	
1KR/TU	179	19.9	1619.4	179	180	354.758	
1KR/TU	180	19.9	1624.6	180	181	336.158	
1KR/TU	181	19.9	1622.4	181	182	436.951	
1KR/TU	182	19.9	1619.4	182	183	346.861	
1KR/TU	183	19.9	1622.4	183	184	343.471	
1KR/TU	184	19.9	1622	184	185	355.363	
1KR/TU	185	19.9	1616	185	186	341.36	
1KR/TU	186	19.9	1607.5	186	187	359.647	
1KR/TU	187	19.9	1597.1	187	188	363.27	
1KR/TU	188	19.9	1590.7	188	189	415.351	
1KR/TU	189	22.95	1588.3	189	190	373.953	
1KR/TU	190	22.95	1598.4	190	191	397.756	
1KR/TU	191	22.95	1601.7	191	192	313.564	
1KR/TU	192	19.9	1601.4	192	193	365.765	
1KR/TU	193	19.9	1598.4	193	194	380.352	
1KR/TU	194	19.9	1604.1	194	195	337.668	
1KR/TU	195	19.9	1605.9	195	196	367.857	
1KR/TU	196	19.9	1606.9	196	197	366.651	
1KR/TU	197	22.95	1605.7	197	198	314.569	
1KR/TU	198	19.9	1614.5	198	199	304.166	
1KR/TU	199	19.9	1609.9	199	200	344.368	
1KR/TU	200	19.9	1610.5	200	201	351.761	
1KR/TU	201	19.9	1604.5	201	202	360.261	
1KR/TU	202	19.9	1605.7	202	203	350.162	
1KR/TU	203	19.9	1609	203	204	336.158	

1KR/TU	204	19.9	1613.3	204	205	375.463	
1KR/TU	205	19.9	1618.2	205	206	356.551	
1KR/TU	206	19.9	1623	206	207	354.165	
1KR/TU	207	22.95	1622.7	207	208	392.555	
1KR/TU	208	19.9	1619.7	208	209	357.455	
1KR/TU	209	19.9	1623.4	209	210	380.956	
1KR/TU	210	19.9	1633.4	210	211	351.369	
1KR/TU	211	19.9	1641	211	212	342.556	
1KR/TU	212	19.9	1642.9	212	213	349.266	
1KR/TU	213	19.9	1637.7	213	214	384.659	
1KR/TU	214	22.95	1631.3	214	215	362.655	
1KR/TU	215	19.9	1625.5	215	216	274.269	
1KR/TU	216	19.9	1619.9	216	217	301.964	
1KR/TU	217	19.9	1616.9	217	218	302.376	
1KR/TU	218	19.9	1615.7	218	219	386.95	
1KR/TU	219	19.9	1613.9	219	220	370.956	
1KR/TU	220	19.9	1610.9	220	221	355.966	
1KR/TU	221	19.9	1606.9	221	222	312.657	
1KR/TU	222	19.9	1603.5	222	223	379.769	
1KR/TU	223	22.95	1601.7	223	224	289.559	
1KR/TU	224	19.9	1600.5	224	225	407.757	
1KR/TU	225	19.9	1598.9	225	226	335.856	
1KR/TU	226	19.9	1599.3	226	227	312.677	
1KR/TU	227	19.9	1605.1	227	228	325.958	
1KR/TU	228	19.86	1615.2	228	229	345.835	
1KR/TU	229	19.86	1610.9	229	230	269.591	
1KR/TU	230	19.86	1600.2	**230**	**231**	**483.777**	**CA 3**
1KR/TU	231	28.86	1592.8	231	232	450.797	
1KR/TU	232	25.86	1602.7	232	233	423.803	
1KR/TU	233	25.86	1608	233	234	387.83	
1KR/TU	234	19.86	1612	234	235	340.839	
1KR/TU	235	19.86	1611.9	235	236	359.835	
1KR/TU	236	19.86	1610.9	236	237	362.842	
1KR/TU	237	19.86	1611.1	237	238	366.829	
1KR/TU	238	19.86	1617	238	239	357.843	
1KR/TU	239	19.86	1624.1	239	240	353.839	
1KR/TU	240	19.86	1621.7	240	241	359.835	
1KR/TU	241	19.86	1619.9	241	242	359.835	
1KR/TU	242	19.86	1618.1	242	243	349.999	
1KR/TU	243	19.86	1619.7	243	244	296.982	
1KR/TU	244	19.86	1617.6	244	245	364.993	
1KR/TU	245	19.86	1625	245	246	343.998	
1KR/TU	246	19.86	1631.5	246	247	326.985	
1KR/TU	247	19.86	1633.1	247	248	350.991	
1KR/TU	248	19.86	1631.3	248	249	340.991	
1KR/TU	249	19.86	1631.4	249	250	369.992	

1KR/TU	250	28.86	1641.3	250	251	476.993	
1KR/TU	251	31.86	1631.4	251	252	470.985	
1KR/TU	252	19.86	1619.7	252	253	348.985	
1KR/TU	253	19.86	1626.1	253	254	353.998	
1KR/TU	254	19.86	1633	254	255	268.983	
1KR/TU	255	19.86	1628.5	255	256	375.541	
1KR/TU	256	19.86	1617.5	256	257	368.519	
1KR/TU	257	19.86	1608.9	257	258	433.775	
1KR/TU	258	19.86	1611	258	259	332.357	
1KR/TU	259	19.86	1612.7	259	260	384.575	
1KR/TU	260	19.86	1608.3	260	261	411.682	
1KR/TU	261	19.86	1606.7	261	262	318.303	
1KR/TU	262	19.86	1614.7	262	263	335.375	
1KR/TU	263	19.86	1619	263	264	324.333	
1KR/TU	264	19.86	1611.8	264	265	331.355	
1KR/TU	265	19.86	1619.5				

A.5 Kriel-Tutuka PLC System

Line Trap inductance: 0.5mH;

Bandwidth of Line Trap at Kriel: 104-500 kHz

Bandwidth of Line Trap at Tutuka: 101-500 kHz

Capacitance of CVT at Kriel: 4700 pF

Capacitance of CVT at Tutuka: 7000 pF

LME Strapping of an “Electrisk Bureau” (EB):

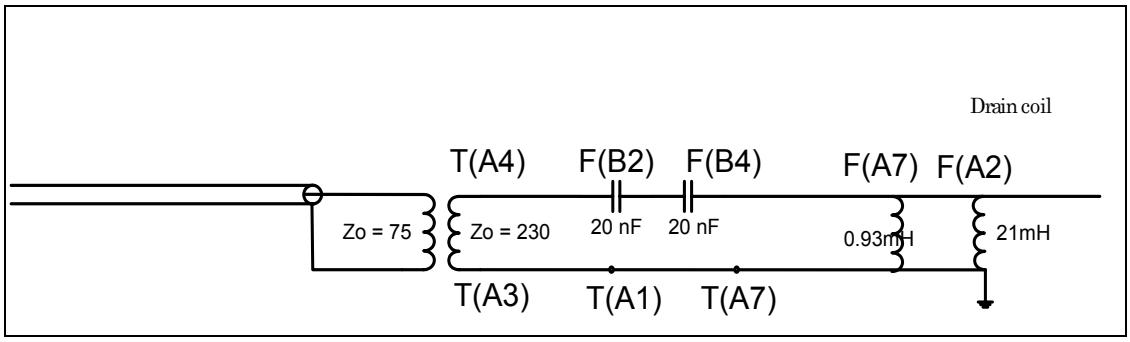

Figure A.10 LME strapping at Kriel and Tutuka

Appendix B

Additional information about Koeberg-Acacia and Kriel-Tutuka operational PLCs

B.1 Introduction

This Appendix primarily gives more information about the neighbouring systems in the PLC frequency range (50-500 kHz). This information is needed in order to allocate the frequencies for the PLC-SAG monitoring tones.

Acacia-Koeberg (Case study 1):

Section B.2 contains a table with all the neighbouring carrier frequencies. Section B.3 shows a map with aviation beacon frequencies. An enlarged version of the frequency scan is given in Section B.4 and shown in Figure B.2. The neighbouring carriers (letter as specified in Table B.1) and the aviation frequencies (short black lines) are indicated on this frequency scan. The measurement bandwidth of the frequency scan was 20 Hz and the sweep rate = 22 hours. The scan was done with a HP 3586A selective level meter, which was controlled by a desktop computer.

Kriel-Tutuka (Case study 2):

Section B.5 contains a table with the neighbouring PLC system frequencies for the Kriel-Tutuka PLC link. The table contains information of neighbouring carriers: 1 busbar away (black) from Kriel and Tutuka PS; 2 busbars away (grey) and 3 busbars away (light grey). The rows between Kriel and Tutuka Power Station are filled with light grey, for reference purposes. The columns that are filled from top to bottom in grey indicate frequencies, which are occupied by an open wire Telkom carrier systems. These frequencies are avoided to prevent interference with the Telkom carrier circuits. The red indicates an overlapping scenario were two same frequency band is occupied by two different systems.

In Section B.6, the results of the KT frequency scan is shown. The scan was preformed with a HP 3586 A selective voltmeter. The narrowest bandwidth, 20 Hz, was used and the sweep time was approximately 22 hours which is similar to case study 1. Due to their great number, it was not possible to identify all the carriers on the graph, as was done in the previous case. There was no aviation beacon information in this area. Studying Figure B.3, it may seem that some of the frequencies are overlapping. Zoomed in figures are also given to show the frequency separation between the PLC-SAG tones and the neighbouring systems. .

Mr Piet Lubbe, Eskom Transmission, gathered and processed all the information required to create the two frequency tables in Section B.2 and in Section B.4.

B.2 Acacia-Koeberg neighbouring PLC frequencies

Table B.1 Names and locations of existing and neighbouring PLCs of the Koeberg-Acacia link

Symbol in Figure B.2	Locations existing Power Line Carrier's		Frequency [kHz]	
	Subsation / Power Station	Substation / Power Station	Start	Stop
a	Koeberg	Muldersvlei	152	160
b	Koeberg	Aurora	180	188
c	Koeberg (132kV KAS)	Acacia (132kV KAS)	204	212
d	Acacia	Plattekloof	216	224
e	Koeberg (132kV KAS)	Acacia (132kV KAS)	232	240
f	Acacia	Philippi	248	256
*g	Koeberg	Muldersvlei	312	320
h	Acacia	Muldersvlei	328	336
i	Koeberg	Aurora	336	404
j	Acacia / Koeberg	Koeberg / Acacia	344	352
k	Koeberg	Muldersvlei	352	360
l	Acacia	Philippi	368	376
*m	Koeberg	Muldersvlei	376	384
n	Acacia	Philippi	392	400
*o	Acacia	Muldersvlei	400	408
p	Koeberg	Dassenberg	416	424
q	Acacia	Philippi	416	424
r	P40 Phase comparison equipment for Acacia / Philippi		452	460
s	P40 Phase comparison equipment for Acacia / Philippi		468	476
*Carrier is decommissioned and is not shown in the figure 4.2				

B.3 Navigational Radio Beacon Frequencies (053/1839)

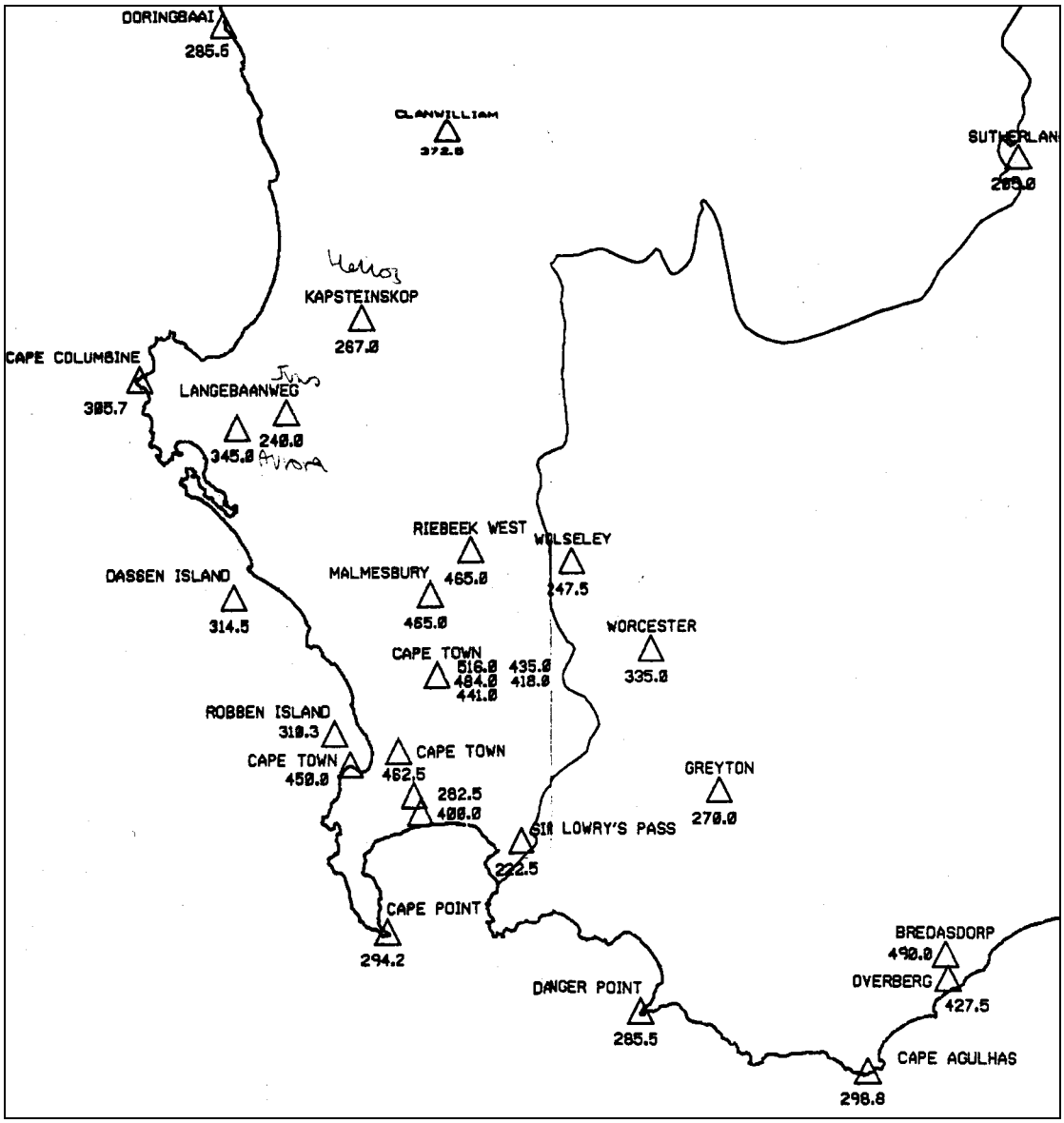

Figure B.1 Part (Western Cape) of the Navigational Radio Beacon Frequencies map in South Africa (053/1839)

B.4 Koeberg-Acacia frequency scan

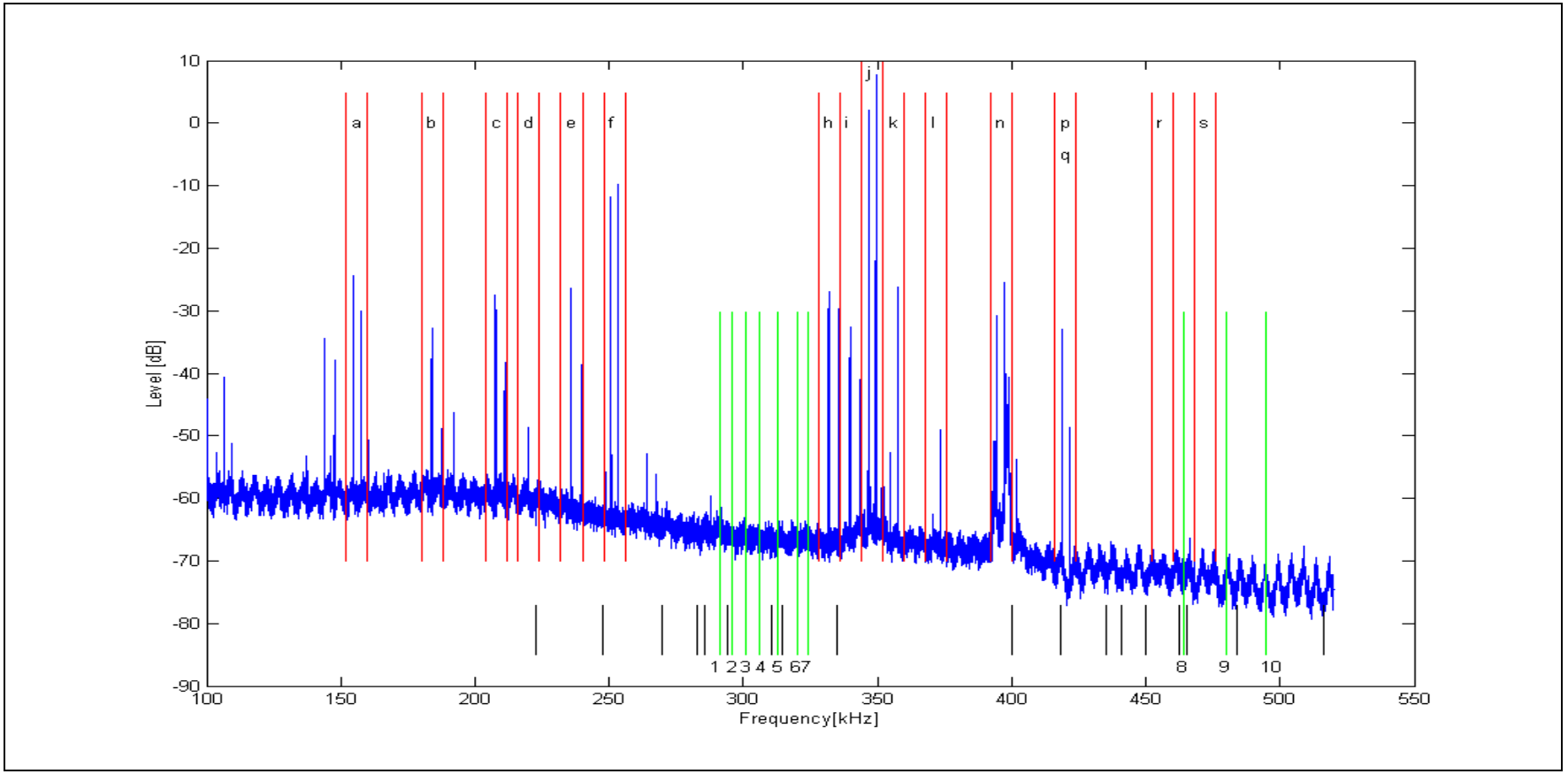

Figure B.2 100-520 kHz wideband measurement at Acacia Sub Station (2004/03/18-2004/03/19). See Table B.1 and Figure B.1 for symbol definition.

B.5 Kriel-Tutuka neighbouring PLC frequencies (See paragraph B.1 for colour definitions)

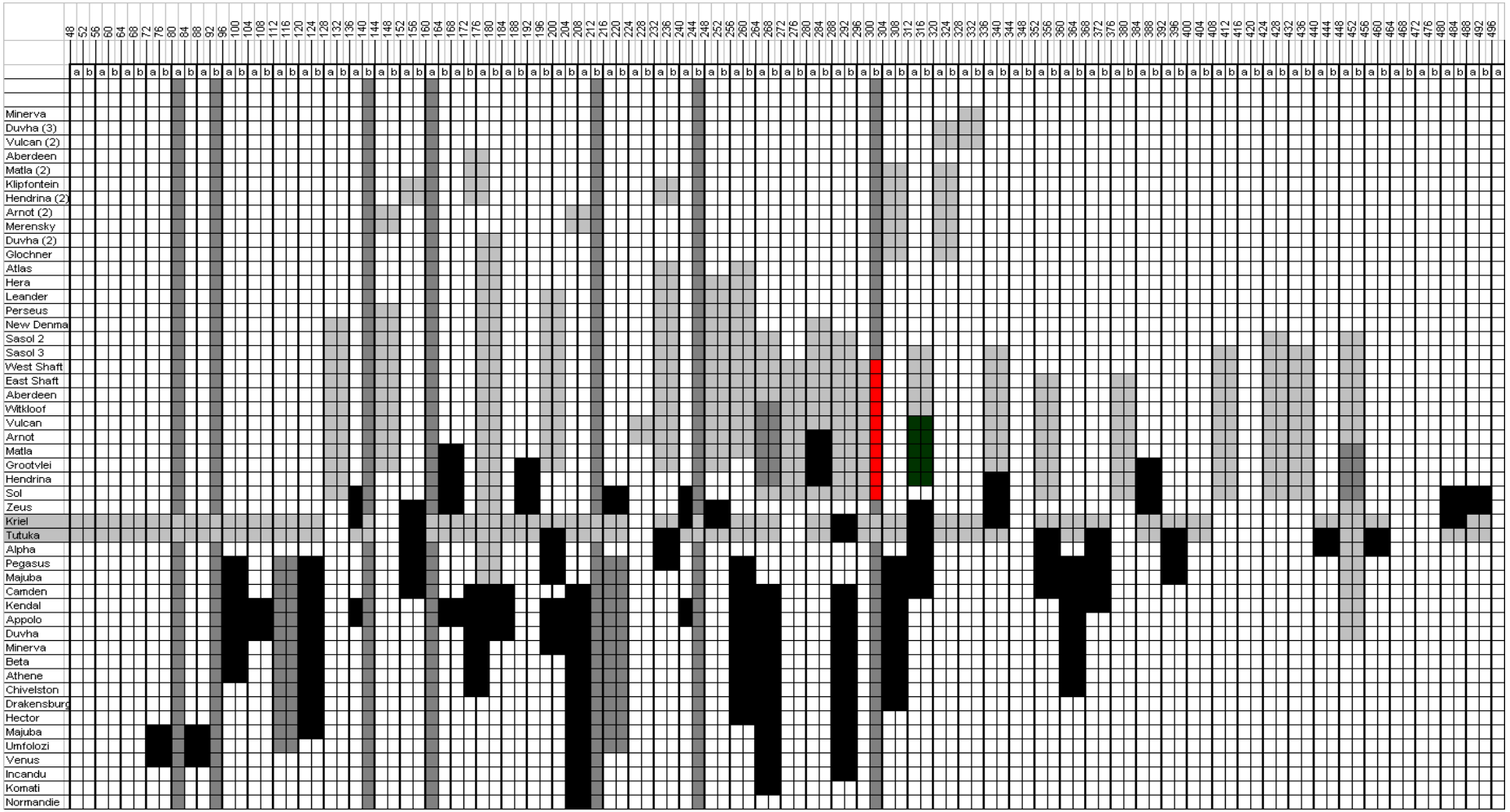

B.6 Kriel-Tutuka frequency scan

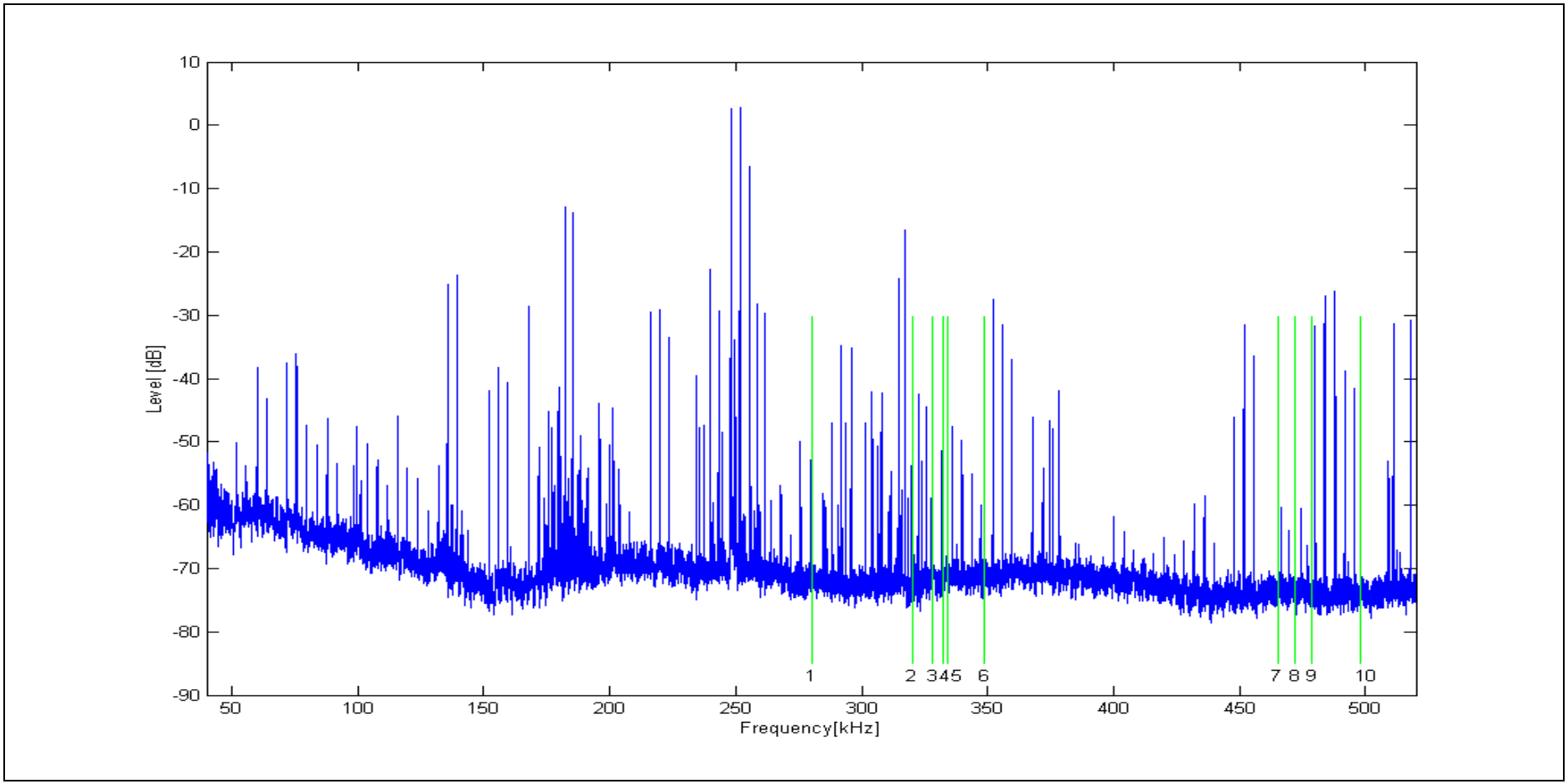

Figure B.3 40-520 kHz wideband measurement at Kriel PS (2004/03/19-2004/03/20)

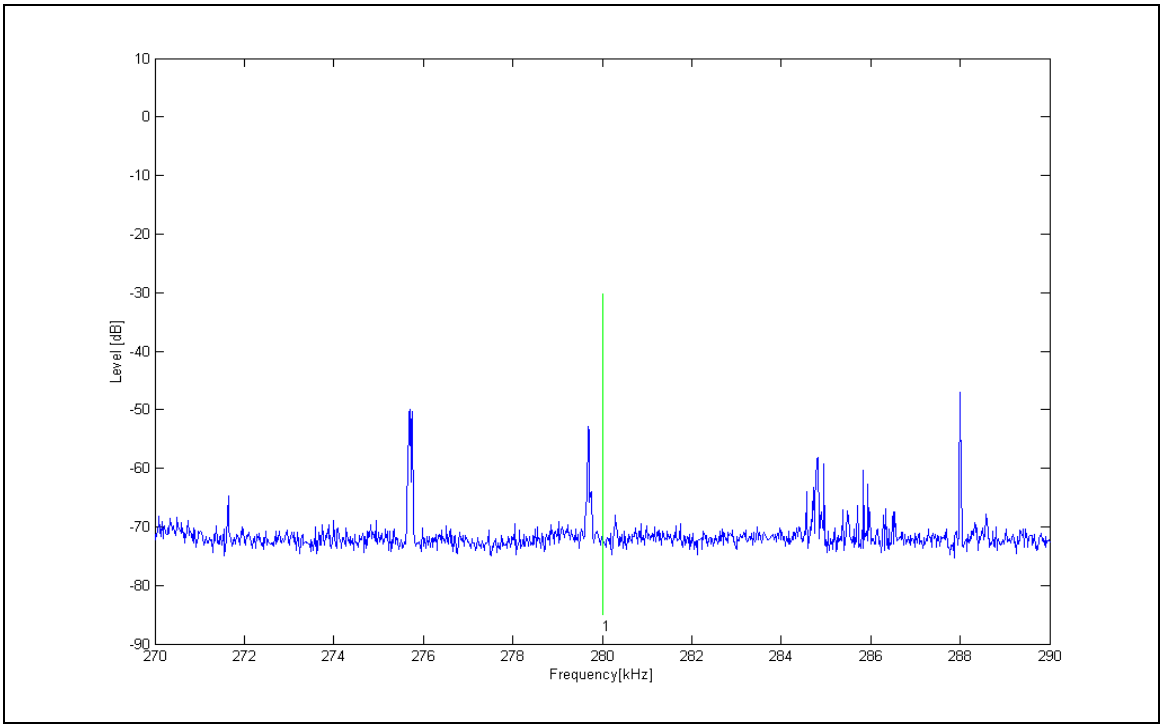

Figure B.4 Zoomed frequency scan of the Kriel-Tutuka 400 kV PLC link (270 kHz – 290 kHz) (Tone 1)

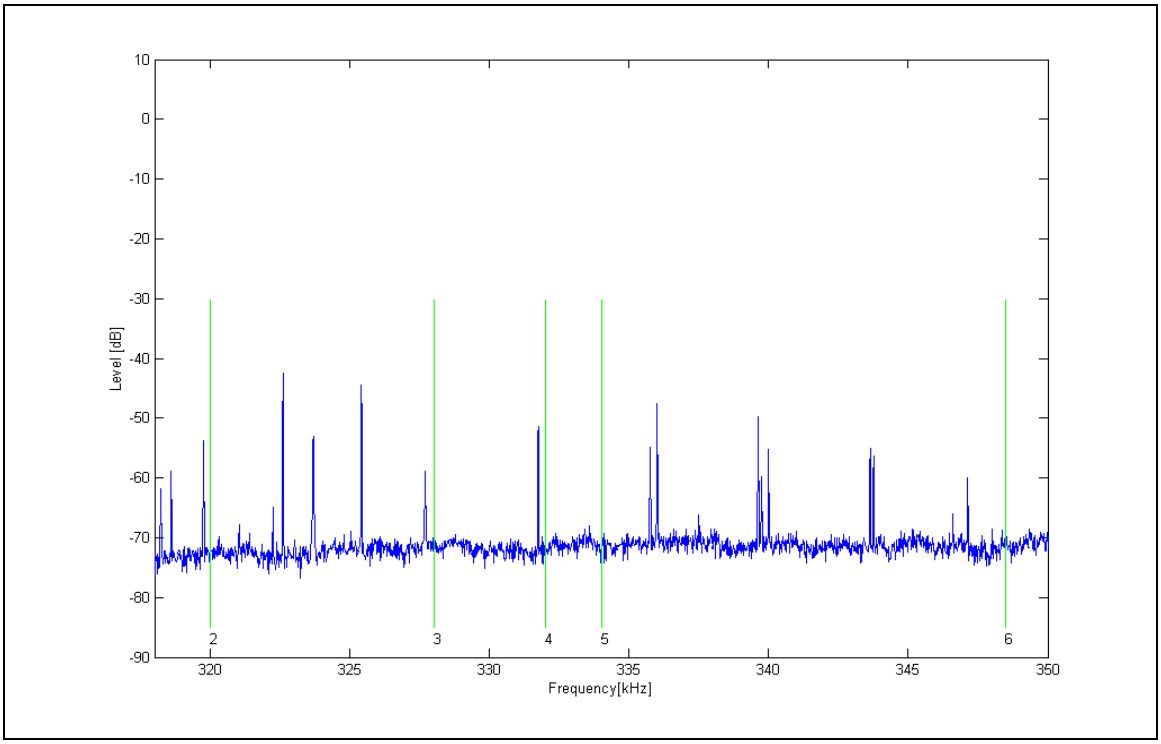

Figure B.5 Zoomed frequency scan of the Kriel-Tutuka 400 kV PLC link (318 kHz – 350 kHz) (Tones 2-6)

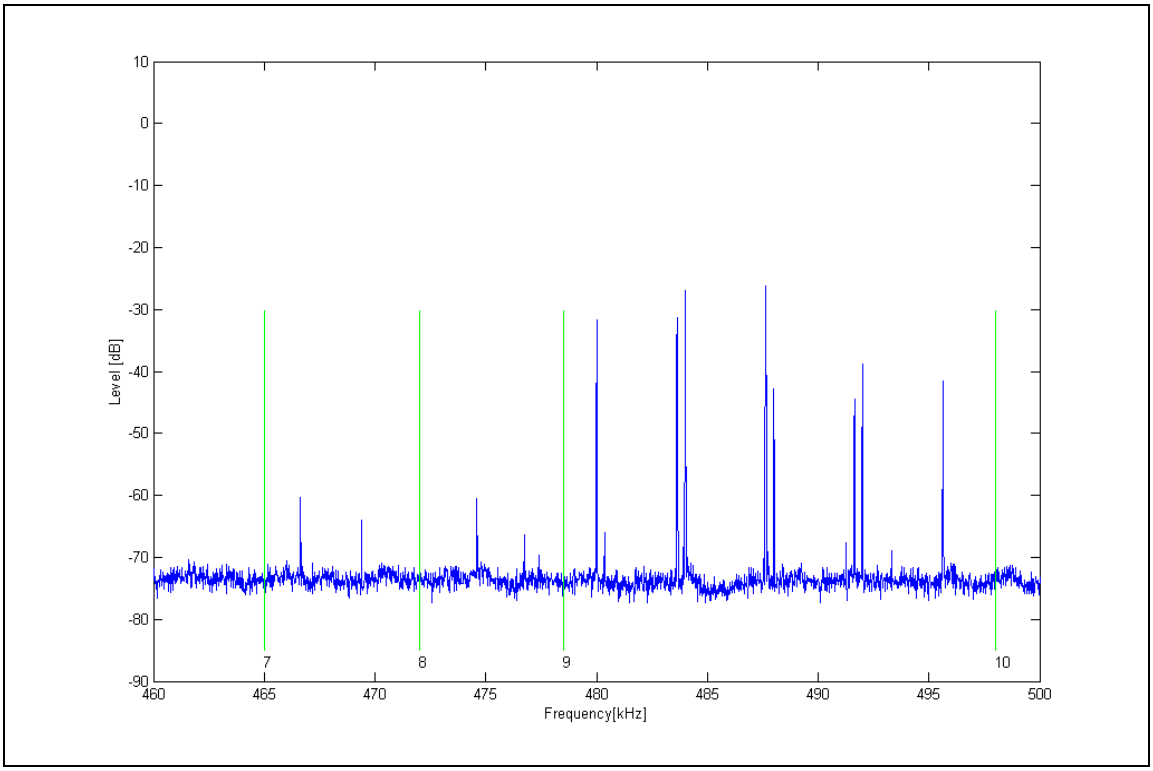

Figure B.6 Zoomed frequency scan of the Kriel-Tutuka 400 kV PLC link (460 kHz – 500 kHz) (Tones 7-10)

Appendix C

Additional information about the experimental transmitter and receiver installations

C.1 Introduction

More information is given on the Transorb (Section C.2) and the amplifier (Section C.3) used in the PLC-SAG hardware installations.

The design of the attenuator, which also has an impedance matching function, is given in Section C.4.

The normal setting of receivers will be given in Section C.5.

C.2 Transorb datasheet

Photograph C.1 Transorb from Clear Line (Model 12-00109)

Table C.1 Data sheet of the Transorb (Model 12-00109)

Max. operating voltage	**+/- 5V dc**	+/- 24V dc	+/- 5V dc
Max. operating current	**0.3A**	0.3A	0.3A
Max. discharge current ismax differential mode (8/20)	**10kA**	10kA	10kA
Max. discharge current ismax common mode (8/20)	**10kA**	10kA	10kA
Residual voltage differential mode at 5kA (8/20)	**Approx. 40V**	Approx. 40V	Approx. 40V
Residual voltage common mode at 5kA (8/20)	**Approx. 120V**	Approx. 120V	Approx. 120V
Insertion loss at 10MHz	**0.08 dB**	0.08 dB	0.08 dB
Connectors	**BNC**	BNC	N-type
Temperature range	**-10°C to + 70°C**	-10°C to + 70°C	-10°C to + 70°C
Application	**Cheapernet 10 Base 2**	Arcnet, CCTV	Ethernet 10 Base 5
Order Code	**12-00109**	**12-00112**	**12-00049**

C.3 Amplifier

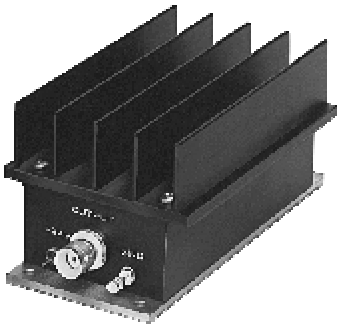

Photograph C.2 Amplifier from *Mini-Circuits* (model ZHL-32A)

Table C.2 Data sheet of the Amplifier (model ZHL-32A)

FREQ (MHz)	Gain (dB)			Directivity (dB)			VSWR		N.F. (dB)	Pout(dBm) (@1dB COMPR)
	23V	24V	24.5V	23V	24V	24.5V	IN	OUT		
0.05	26.65	26.67	26.69	15.1	15.1	15.1	1.02	2.00	-	32.21
0.14	27.27	27.30	27.31	13.8	13.8	13.8	1.03	1.65	-	32.68
0.68	27.41	27.44	27.45	13.5	13.5	13.4	1.04	1.58	-	32.83
3.2	27.57	27.60	27.63	13.1	13.1	13.2	1.08	1.62	-	32.99
15.3	27.45	27.48	27.49	13.3	13.2	13.2	1.20	1.61	5.85	32.76
46.7	27.12	27.16	27.18	13.5	13.5	13.4	1.38	1.52	6.00	31.88
56.7	27.18	27.21	27.24	13.4	13.5	13.4	1.39	1.56	6.04	31.83
66.7	27.35	27.38	27.40	13.2	13.3	13.3	1.36	1.56	6.04	31.43
73.4	27.55	27.59	27.60	13.0	13.1	13.1	1.33	1.57	6.02	31.30
80.0	27.76	27.81	27.83	13.0	13.0	12.9	1.30	1.56	5.99	31.33
90.0	28.00	28.04	28.06	12.9	12.7	12.8	1.28	1.50	6.00	30.98
100.0	27.97		28.05		12.9		1.29		6.08	30.47
110.0		27.80		13.2		13.2	1.32		6.19	
120.0	27.32		27.40		13.6		1.36	1.19		30.17
130.0		26.71		14.2	14.2	14.2	1.43		6.45	

C.4 Impedance matching network and attenuator

The specifications for the design are the following:

a) Input impedance of port 1 must be 50 ohm (to match the spectrum analyser with the system)
b) Input impedance of port 2 must be 75 ohm (to terminate the additional symmetrical hybrid correctly)
c) 10 dB attenuation.

Figure C.1 demonstrates these design criteria.

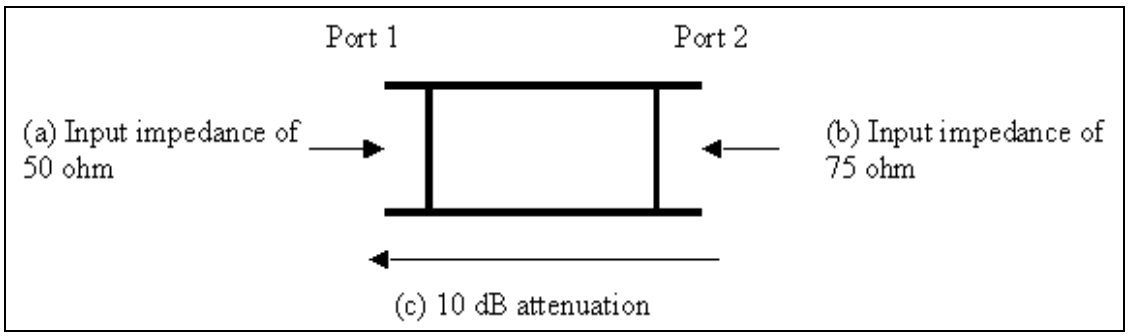

Figure C.1 Impedance matching network (and 10 dB attenuator) illustrating the design criteria.

Figure C.2 shows the proposed circuit layout with x, y and z as the unknown resistors.

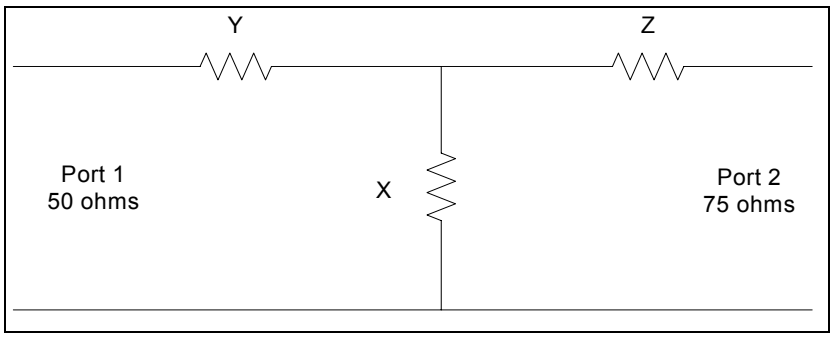

Figure C.2 Circuit layout of the impedance matching circuit

From the first two design criteria the following equation can be derived.

$$50 = \left[\frac{(75+z)x}{75+z+x}\right] + y$$

$$75 = \left[\frac{(50+y)x}{50+y+x}\right] + z$$

Assuming port 2 is connected to a matched (75 ohm) source, which produces 1V rms over the terminals of port 2. Then the power delivered by the 1 V supply at port 2 is

$$P_{port2} = \frac{V_2^{\,2}}{75} = 0.0133$$

Design criterion *c* specifies a 10 dB attenuation. Therefore the power at port 1 must be 10 dB less than port 1. The following equation incorporates this design criterion

$$10dB = 10\log\left(\frac{P_{port2}}{P_{port1}}\right)$$

P_{port1} can be calculated as 0.001333 and consequently V_1 as 0.25819 RMS. The final design equation can be formulated as the ratio of $\frac{V_1}{V_2}$.

Solving the equations simultaneously produced the following results: $x = 43.3$, $y = 18.1$ and $z = 48.6$.

High wattage resistors (25± W) are used with the following combinations: $x = 33 + 10$, $y = 18$ and $z = 39 + 10$.

The matching circuit was tested after it was built. If port 1 was terminated into 50 ohms, then the input resistance of Port 2 was 75.5 ohms. On the other hand, terminating Port 2 provides an input resistance of 50.1 ohms at Port 1. The attenuation of the circuit was measured to be 9.7 dB.

C.5 Receiver settings for PLC-SAG tone monitoring

HP 3586A at Acacia Sub Station

- 50 ohm impedance (the attenuator also match the 50 ohm to the 75 ohm characteristic impedance)
- 20 Hz selective filter
- Average on
- Unit setting dBm

HP 3586A at Kriel Power Station

- 75 ohm - high impedance setting
- 20 Hz selective filter
- Average on
- Unit setting dBm

PSM 37 Wandel & Goltermann at Kriel Power Station

- 75 ohm – high impedance setting
- 25 Hz selective filter
- Average on
- Unit setting dBm
- Battery standby function: off

Appendix D

PLC tone during the outage on the KT OHTL dated 2004/05/04

D.1 Introduction

Appendix D describes how the signals were amended to compensate for the outage on 2004/05/04. The black graph in the following figures represents the compensated attenuation. The red dots highlight the signal level just before and after the line was switched off and on. The blue graph shows the actual recorded signal level.

Adding a constant value of attenuation to the signal in the region of the outage made the compensation. The exact level in each case is given in the titles of the relevant figure.

D.2 The 5 relevant tones

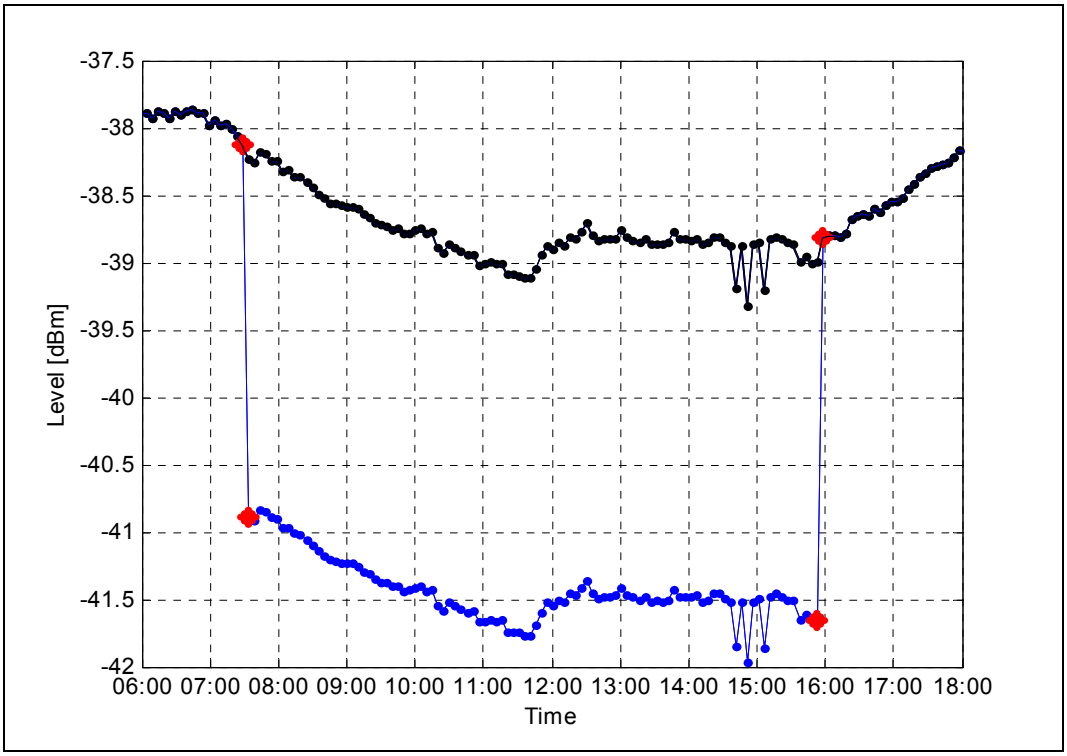

Figure D.1 Tone 3 - 2.653 dB added during the period of the outage

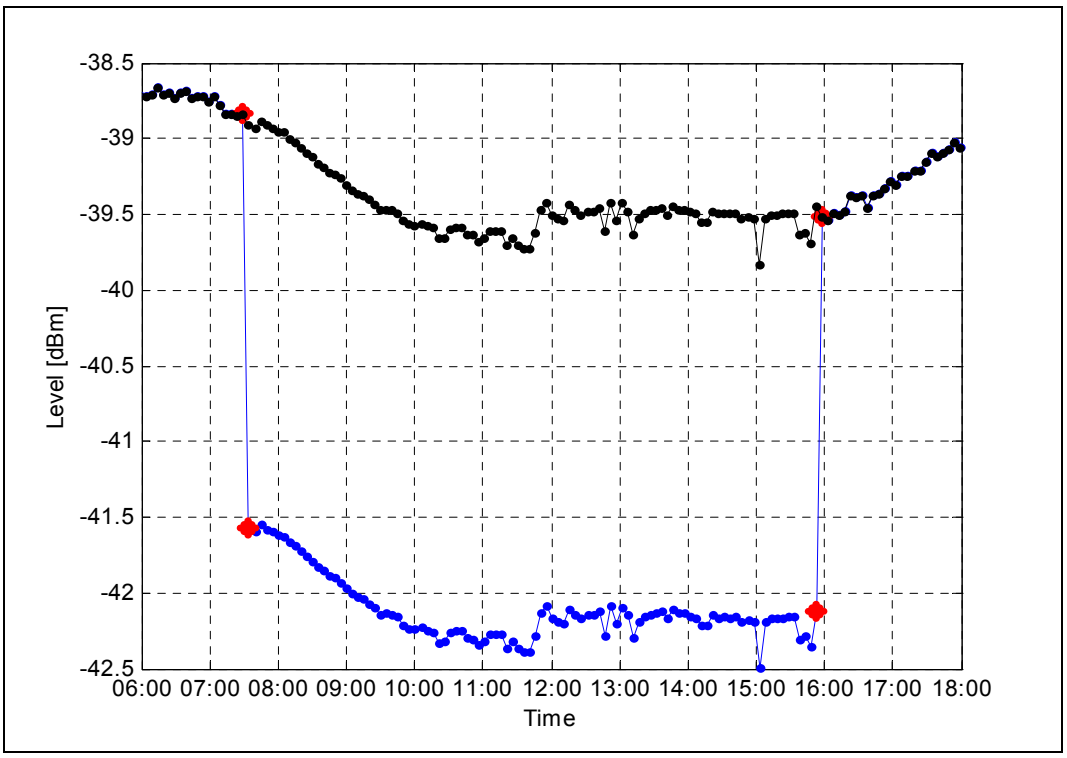

Figure D.2 Tone 4 - 2.671 dB added during the period of the outage

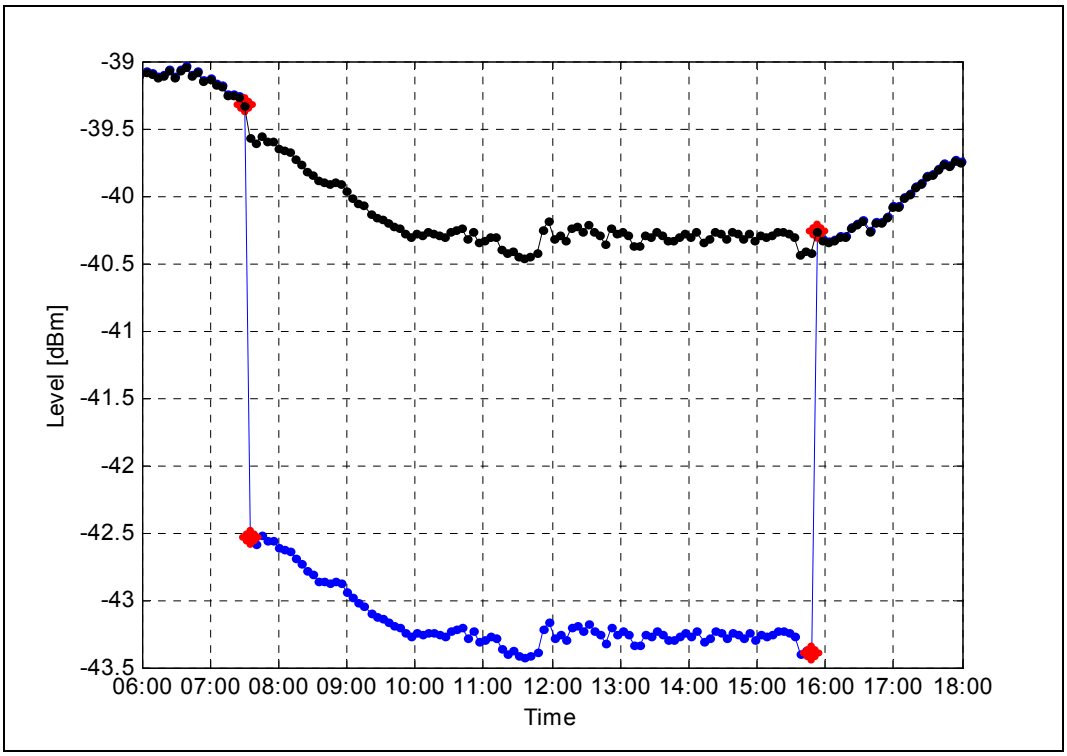

Figure D.3 Tone 5 - 2.975 dB added during the period of the outage

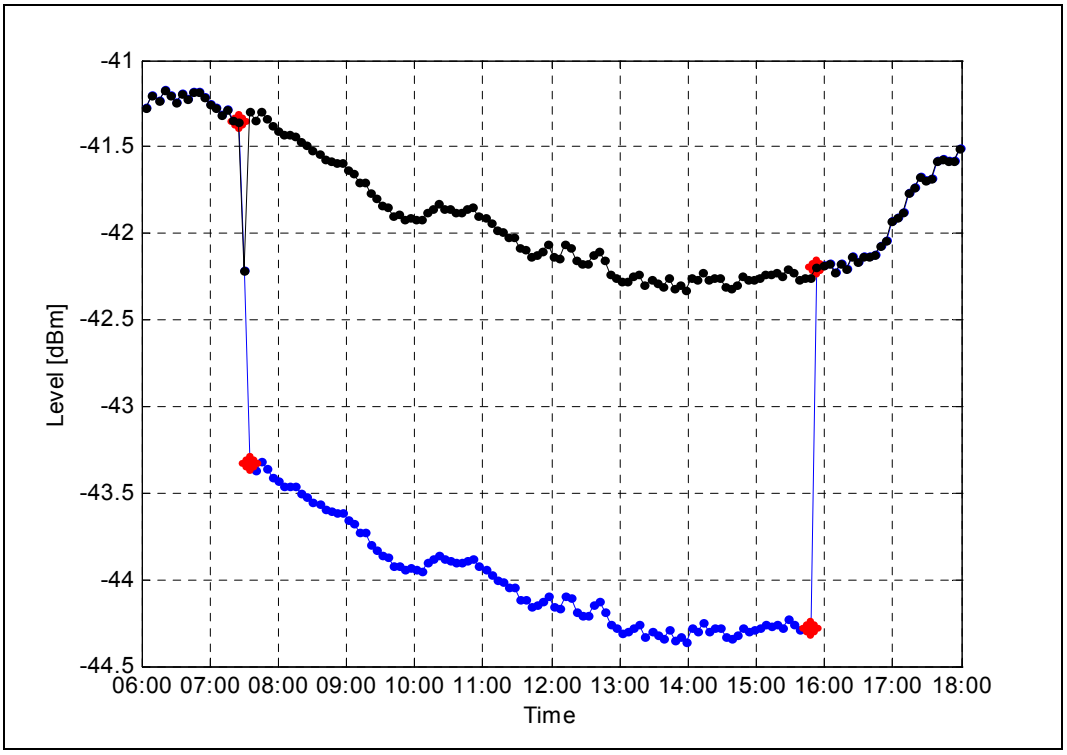

Figure D.4 Tone 6 - 2.031 dB added during the period of the outage

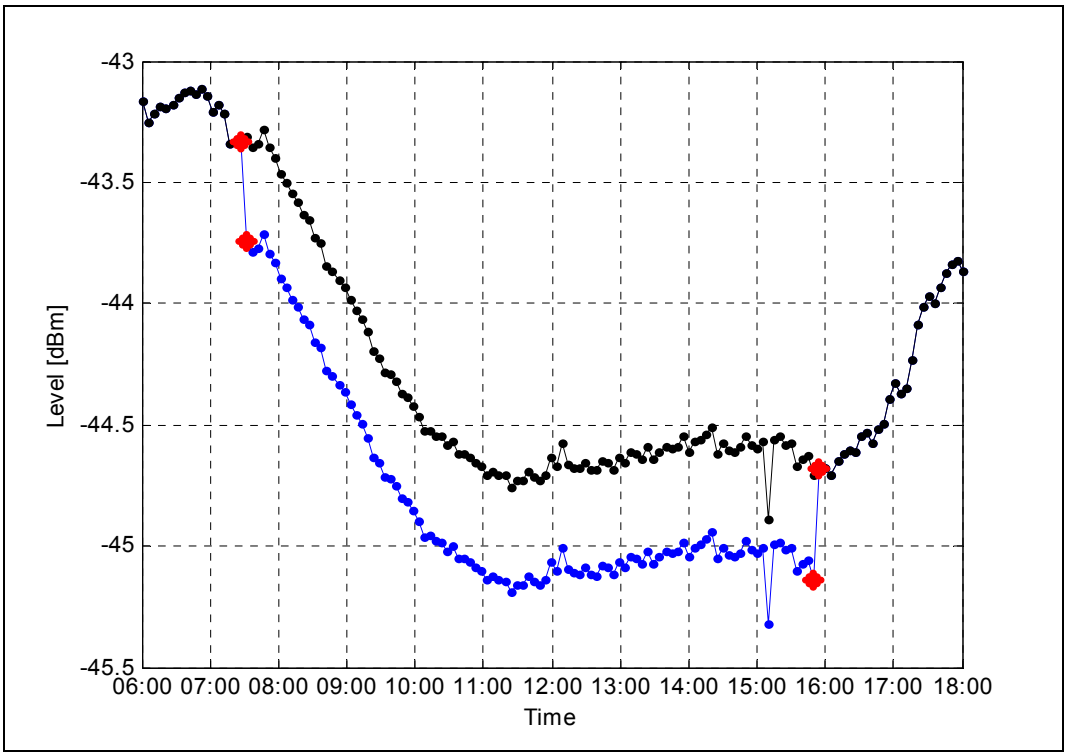

Figure D.5 Tone 9 - 0.4325 dB added during the period of the outage